TRANSPORT PHENOMENA AT ELEVATED TEMPERATURES - STUDIES RELATED TO DIRECT POLYMETALLIC SMELTING

by

ROBERT KEITH HANNA

A thesis submitted to the
Faculty of Engineering
of the
University of Birmingham
for the degree of
DOCTOR OF PHILOSOPHY

School of Chemical
Engineering,
University of Birmingham,
P.O. Box 363,
Birmingham,
B15 2TT
England.

February 1990

ABSTRACT

The modelling of two key areas of transport phenomena in a new polymetallic smelter has been achieved by using both mathematical and physical models to investigate optimum operating conditions.

A study of oxygen mass transfer caused by multiple top-blown, subsonic gas jets contacting water flowing in a full-scale channel model of the smelter converting hearth has been carried out. A liquid phase solute mass transfer model that incorporates a flowing liquid phase has been developed. It has been used to compare mass transfer for both open-packed and close-packed multiple lance arrays of 2.26 mm, 4.95 mm, 10.95 mm and 24.40 mm nozzles delivering the same quantity of gas. It was found that for fewer lances of the larger nozzle diameters, up to a 75% reduction in liquid phase mass transfer occurred especially for the close-packed configurations. This restriction of mass transfer will result in reduced metal losses in the analogous smelter situation.Over a wide range of channel flowrates the mass transfer coefficient was found to be independent of water velocity.

A computer model that predicts the amount of fog formation in the zinc vacuum condenser of the smelter for binary vapour/gas mixtures has identified operating conditions most susceptible to vapour fogging and subsequent metal losses. A fog problem is most likely to occur in condensable mixtures with high vapour concentrations and low initial quantities of superheat, and at low cooling wall temperatures as well as at high total pressures. Any lead in a $Pb/Zn/N_2$ condensable mixture will fog heterogeneously at least $400^{o}C$ before zinc droplets form and act as condensation nuclei for the zinc vapour. An engineering approach to estimating quantities of homogeneous fog formation has been developed and is used to analyse the performance of the Imperial Smelting Furnace zinc condenser and the Port Pirie Vacuum Dezincing Unit.

ACKNOWLEDGEMENTS

The author wishes to extend his gratitude to Professor N.A. Warner for his supervision and guidance during the course of this project.

Thanks are due to Mr. P. Hinton and the Minerals Engineering Workshop for their help in constructing the experimental rigs. The author is grateful to Mr. S. Clabon for the fabrication of the glass models and lances used in the testwork. The photographs by Dr. J. Anderson, the advice from Mr. G. Titmus and the typing by Miss C. Green are all very much appreciated. The assistance of Mr. A. Roberts during the development of the computer program is also gratefully recognized.

The author is indebted to Mr. P. Partington of Broken Hill Associated Smelters, Port Pirie, South Australia, Mr. R. Knight of Britannia Refined Metals, Northfleet, Kent and Mr. M. Gammon of Commonwealth Smelting Limited, Avonmouth for access to samples from their zinc condensers and their ready provision of technical information. The criticism of this work and the technical comments offered by the following people are all very much appreciated:

Dr. T. Jones,	British Steel's Teesside Research Laboratories, Grangetown, Middlesbrough.
Dr. E.R. Buckle,	Department of Metallurgy, University of Sheffield.
and Mr. D.E. Steinmeyer,	Monsanto Company, St. Louis, Missouri, U.S.A.

The Department of Education for Northern Ireland is acknowledged for providing financial support during the term of this venture.

To

Betty and Kenneth

"Some men see things as they
are and ask 'Why?'
I dream of things that never were
and ask 'Why not?' "

JOHN F. KENNEDY

CONTENTS

LIST OF FIGURES

LIST OF TABLES

LIST OF PHOTOGRAPHIC PLATES

CHAPTER 1: INTRODUCTION

1.1 PYROMETALLURGY: ITS RELATIONSHIP TO CHEMICAL ENGINEERING

Pyrometallurgy involves heating and processing operations whereby metallic ores or concentrates are treated, usually in several stages, to yield a product metal. The extraction of metals requires both chemical reactions and physical processes such as the transfer of heat, mass and momentum (transport phenomena). At a process level pyrometallurgy involves the analysis of processes, the synthesis of new processes and the building of control schemes for processes. Thus pyrometallurgy, and extractive metallurgy generally, clearly falls within the ambit of chemical engineering (Rankin, 1984). In the past pyrometallurgy used large, inefficient and slow reverbatory type furnaces (Themelis, 1987). Over the last 20 years there has been a drive towards the development and continuous improvement of high-intensity smelters with fast-acting processes that require information on the transport phenomena within the furnace and between the furnace and the outside world.

Extractive metallurgy processes are not simply chemical engineering processes conducted at high temperatures. Metallurgical extraction and refining processes have particular problems and difficulties not found in standard chemical engineering processes:

i) The attainment of a high temperature poses special problems.

ii) Heat transfer by radiation is often a major mechanism.

iii) High temperatures cause containment problems such as refractory attack and wear.

iv) Mechanical stirring, a standard chemical engineering approach to promote mass transfer, is rarely possible due to the materials problem at high temperatures. Stirring by gas injection is much more common.

v) Because of the high temperatures, temperature gradients within phases can be very large.

vi) The variable nature of ore feeds to metallurgical processes introduces special problems such as

   a) an ore usually has more than one metal of economic significance; it may also contain elements that lead to technical problems hence economic penalties,

   b) most of the principal, valuable metal usually occurs as one mineral though small but significant proportions may occur in different minerals,

   c) crystallographic inhomogeneities like grain size distributions and grain associations introduce separation problems,

   d) mineral grains are chemically impure and in physically different forms within the ore,

   e) non uniform physical and chemical properties as a consequence of impure mineral grains.

Most important of all is the fact that each of characteristics (a) to (e) may vary along the length, breadth and depth of an ore body. Because of this variability in raw materials the composition of crude metal produced is variable also. Since the specifications for metals are usually quite tight refining is frequently done on a batch basis.

vii) The variation in ore feed and its complex nature ensures complex chemistry.

viii) The products of metallurgical processes tend to have complicated separation steps.

ix) Metallurgical processes are frequently equilibrium limited rather than rate limited.

1.2 SCOPE AND AIMS OF THIS INVESTIGATION

The work presented in this thesis was undertaken with the aim of investigating the fundamental aspects of two high temperature transport phenomena related to polymetallic smelting. A novel new smelter currently being commissioned in the Minerals Engineering Section of the School of Chemical Engineering in the University of Birmingham and designed to treat complex sulphide ore bodies has been the driving force behind this work (Warner; 1989, 1985, 1983).

At an early stage of development of the smelter two key areas of the smelting operation were identified as requiring optimisation. These were the vacuum condensation of metal vapours and liquid phase solute mass transfer during the smelting of metallic sulphides via top-blown gas jets. The top-blowing problem had previously been investigated by Jones (1987, 1986) in this school and this work extends his study to the industrial situation of complex multiple lance configurations top-blowing onto a moving liquid phase.

During the vacuum condensation of metallic vapours it is known that there is a strong propensity for certain metals to form as a fog in the gas phase rather than as a condensate (Warner, 1970). This will result in downstream treatment problems as well as potential vapour loss and subsequent low recovery efficiencies. It is desirable to be able to predict the point at which metallic vapour fogs will form and the extent of fog formation. A mathematical model of the coupled heat and mass transfer equations for vapour fog formation during forced cooling is needed to gain such an insight. Moreover, a low temperature physical model of the vacuum condenser is necessary to highlight condensation and fog formation

characteristics in an analogue to the high temperature situation.

In order to elucidate multiple lance top-blowing mass transfer, physical modelling studies are necessary. These involve investigating liquid phase mass transfer within a flowing liquid phase in a full-scale water model of the converting hearth of the pilot-scale smelter. Primarily this is used to determine the effect of a flowing liquid phase on a comprehensive mass transfer correlation developed by Jones (1987) for subsonic gas jets contacting stationary baths of various liquids. The effect of different close-packed and open-packed cellular lance configurations (for a range of nozzle sizes) on liquid phase mass transfer also needed to be examined.

1.3 MATHEMATICAL AND PHYSICAL MODELLING IN PYRO-METALLURGY

Modelling techniques are now used extensively in the pyro-metallurgical industries (both ferrous and non-ferrous) to elucidate both the functioning of a process and its operation. Physical models date back to the early 1960s whereas mathematical models have only recently come of age, i.e. mid 1970s (Guthrie, 1987).

Brimacombe and Gray (1985) outline five basic process analysis tools open to the extraction metallurgist to improve existing processes and to develop new ones that remove some of the guesswork that may otherwise surround a process development project:

i) Mathematical Models
ii) Physical Models
iii) Pilot plants
iv) Laboratory Measurements
v) In-Plant Trials Including Plant Measurements .

It is a combination of these five techniques together with a basic knowledge of a process that provides the most powerful approach to process development.

Mathematical Models

Mathematical models are useful in establishing criteria for the adjustment of process parameters to effect optimum process operation. Evans (1987) notes that mathematical models provide a means of understanding the behaviour of processes. Mathematical precision is sought after but is second to realism and utility, i.e. knowledge is more

important than numbers. He points out that compared to the chemical industry, metallurgical operations are far more complex and the principal expectation, at present, is that mathematical models of metallurgical processes will provide knowledge (or at least insight). He cites areas where mathematical modelling is best avoided:

a) When the mathematical model is more expensive to develop than any benefits to be gained from it.

b) When the physico-chemical phenomena of a process are not understood in a quantitative sense or are not amenable to straightforward experimental measurement.

Mathematical models usually involve detailed numerical analysis of momentum, mass and heat balances, reaction kinetics and reaction chemistry of a process over finite changes within a reactor. Semi-empirical relations, too, are often required to describe macroscopic phenomena; e.g. flame geometry, heat and mass transfer rates (Rankin and Batterham, 1984). The solution of these complex, sometimes 3-dimensional equations requires the use of sophisticated computer software packages now increasingly available at a reasonable cost (Guthrie, 1987).

These models usually involve basic assumptions such as plug flow, steady state etc. inherent in their development. Mathematical models highlight trends that will exist at high temperatures and provide a means of predicting sensitivity to change necessary for design work. They must always be verified by comparing them with pilot plant, laboratory and in-plant measurements to check their validity.

Guthrie confidently predicts that metallurgical processes will be designed more and more from the 'ground-up' so that new processing operations can be 'pre-optimised' and costly 'retrofits' become a thing of the

past. The great strength of mathematical models is that, once the model has been carefully validated on small-scale systems, it can be applied with a reasonable degree of confidence to full-scale plant where a hostile environment may preclude almost any measurement. The procedure for validating a mathematical model is outlined in Figure 1.3.1 given by Rankin and Batterham (1984). Moreover, a validated mathematical model is extremely useful as a means of establishing process control strategies. In some instances mathematical models can be adapted to run on process control computers to provide plant operators and management with predicted information on the real, and otherwise immeasurable, state of the process on a time scale relevant to plant operations. Usually, however, it is almost inevitable that model predictions fail to match real-world measurements in metallurgical processes.

Physical Models

Physical models or low temperature models of high temperature processes involve constructing scale models (usually of a clear substance such as perspex) to study fluid flow, mass transfer and mixing effects. Such relationships are not easily established from plant trials because measurements in high temperature, hostile and sometimes confined environments are expensive, difficult and frequently inconclusive. Moreover, there is understandably great reluctance from plant operators to make significant changes for test purposes if a loss of productivity or other problem could result.

Physical models will permit visual observation of mixing and fluid flow patterns with the added ability to photograph or video phenomena. There are important limitations to physical modelling such as the inability to

FIGURE 1.3.1 METHODOLOGY OF THE DEVELOPMENT AND VALIDATION OF A 'RESEARCH TYPE MATHEMATICAL MODEL'
(Rankin and Batterham, 1984)

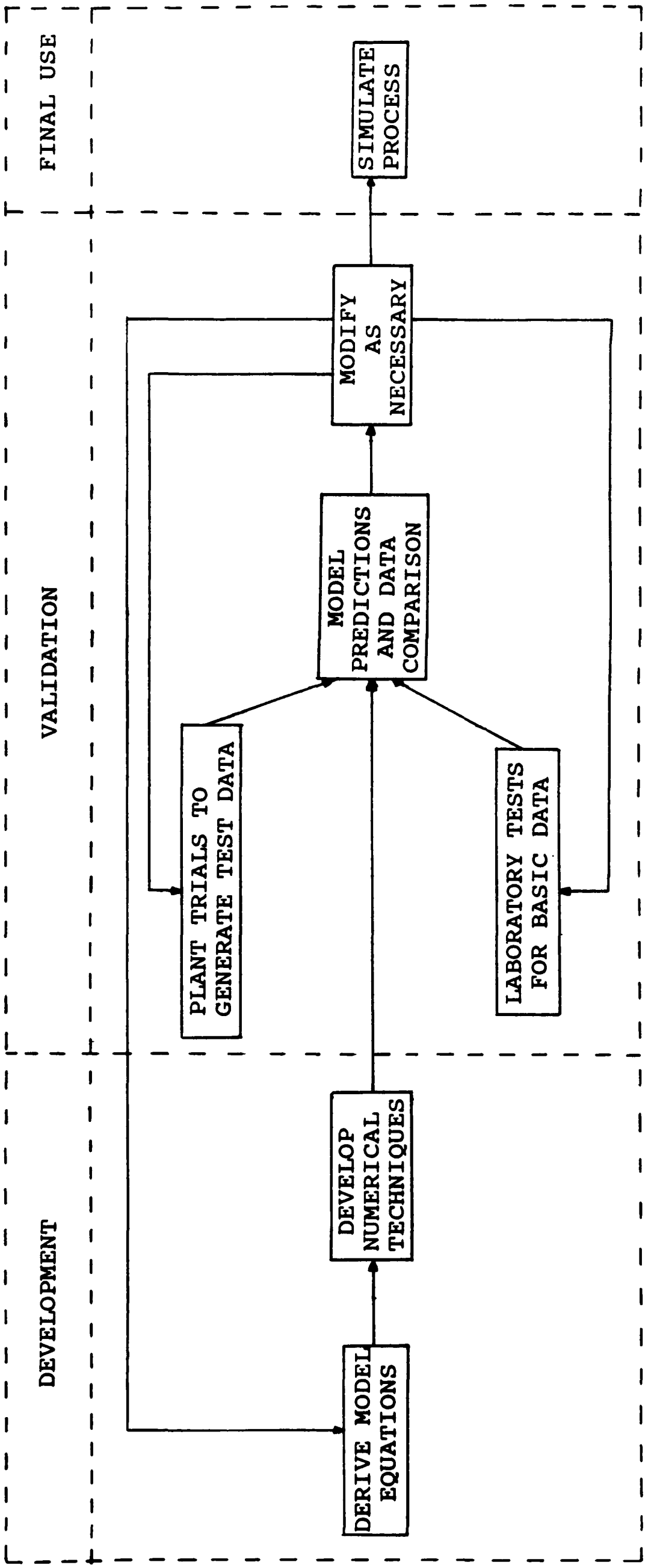

provide data on temperature distribution in the high temperature plant under consideration. Because models are isothermal, care must be taken in correcting for nonisothermal fluid flow effects present in high temperature prototypes but missing in models, e.g. cold gases injected into a hot environment.

Richardson (1973) cautions on the extrapolation of water model results, in which there are no significant temperature gradients, to high temperature systems. With high temperature processes there is always some natural convection arising from thermal gradients in addition to the forced convection that a low temperature model will simulate. It is always prudent to evaluate the relative significance of each convection term to assess if a change in the forced convection component will affect the overall convection term significantly.

Physical modelling provides data against which mathematical fluid flow and mass transfer models may be verified or modified. Predictions can then be used to aid in the understanding and further development of full scale processes. Prolonged plant tests must be used to confirm the design changes a physical model may suggest.

Hydrodynamic similarity is a key criterion as far as low temperature scale models of high temperature processes are concerned. Models are normally based on equivalence of Froude (convective/potential) and Reynolds (convective/viscous) Numbers (Holmes and Thring, 1960; Holden and Hogg, 1960; Brimacombe and Gray, 1985; Guthrie, 1987). In the polymetallic smelter connected with this work the kinematic viscosity of the molten copper matte phase at 1300^{o}C is 1.92×10^{-6} m/s compared to a typical water value of 1.36×10^{-6} m/s. Since these values are of the same order of magnitude dynamic similarity and physical modelling suitability is thus ensured.

1.4 DIRECT POLYMETALLIC SMELTING

The innovative direct polymetallic smelter currently undergoing commissioning trials in this School is a radical new approach to the treatment of complex sulphide ore feeds notably the lead/zinc/copper type. The smelter is being developed primarily to treat a massive 227,000,000 tonne zinc deposit near McArthur River in Northern Australia (9.2% Zn, 4.1% Pb, 41 g/t Ag) (Croxford and Jephcott, 1972). It is one of the world's largest, undeveloped, high-grade, near-surface sulphide ore bodies. At present it is uneconomic to treat the ore by conventional processing techniques due to low metal recoveries resulting from the fine grain structure and intimate intergrowths of the economic sphalerite and galena minerals with non-economic dolomite and pyrite.

The smelter itself essentially consists of two reverbatory type hearths sitting side-by-side and linked by a weir at one end and RH vessel snorkel legs the other (Figure 1.4.1). The key to the smelter lies with the forced circulation of the smelter contents (matte) induced by inert gas injection into the snorkel upleg. The melt itself, at 1250^{o}C, is subjected to chemical changes as it passes through an oxidation zone in the converting branch of the smelter when it is top-blown by multiple lance oxygen enriched air. This produces elemental blister copper by the following gas phase diffusion control reaction and it collects in the furnace hearth:

$$Cu_2 S_{(l)} + O_{2\,(g)} = 2Cu_{(l)} + SO_{2(g)} \qquad (1.4.1)$$

As the copper-saturated matte is exposed to the RH vessel and subjected to a moderately high vacuum pure metals of high volatility, e.g.

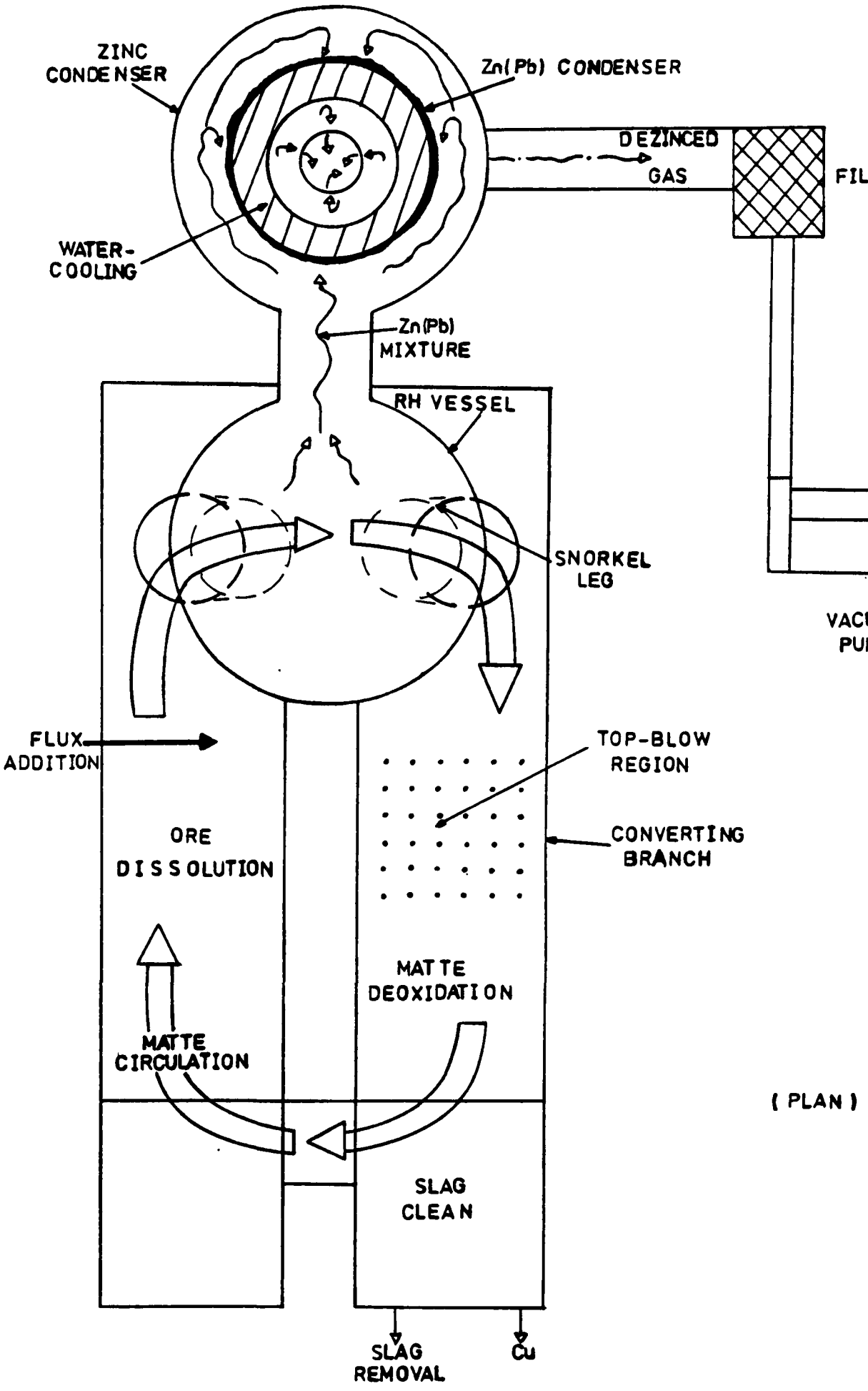

FIGURE 1.4.1 : SCHEMATIC LAYOUT OF THE WARNER SMELTER

zinc and lead, are flashed off by the following reactions:

$$ZnS + 2Cu = Cu_2S + Zn_{(g)} \qquad (1.4.2)$$

$$PbS + 2Cu = Cu_2S + Pb_{(g)} \qquad (1.4.3)$$

Some lead sulphide is also flashed off. The vapours at around 1200°C plus any inert gases from the RH vessel are cooled in an adjacent water-cooled barrel condenser (Figure 1.4.2). Equations 1.4.2 and 1.4.3 reveal that the copper matte is effectively regenerated by this method. As the gases cool the PbS will form as a fog and other equilibrium changes to be expected in the cross-over between the RH vessel and the condenser include the following:

$$PbS_{(l,s)} + Zn_{(g)} = ZnS_{(s)} + Pb_{(l)} \qquad (1.4.4)$$

$$SO_2 + 3Zn_{(g)} = 2ZnO + ZnS \qquad (1.4.5)$$

These will produce a profusion of gas phase particulates that ultimately will end up as a sulphide/oxide dross in the condenser sump. Both zinc and lead will be collected (probably by direct zinc contact or possibly using liquid lead, though at present a cooling wall is used) as molten zinc or as a lead/zinc alloy.

Thermodynamic calculations on the vacuum dezincing (VDZ) of matte (Warner, 1983) have indicated that the equilibrium partial pressure of zinc vapour in the RH vessel will be in the region of 60 mm Hg compared to the

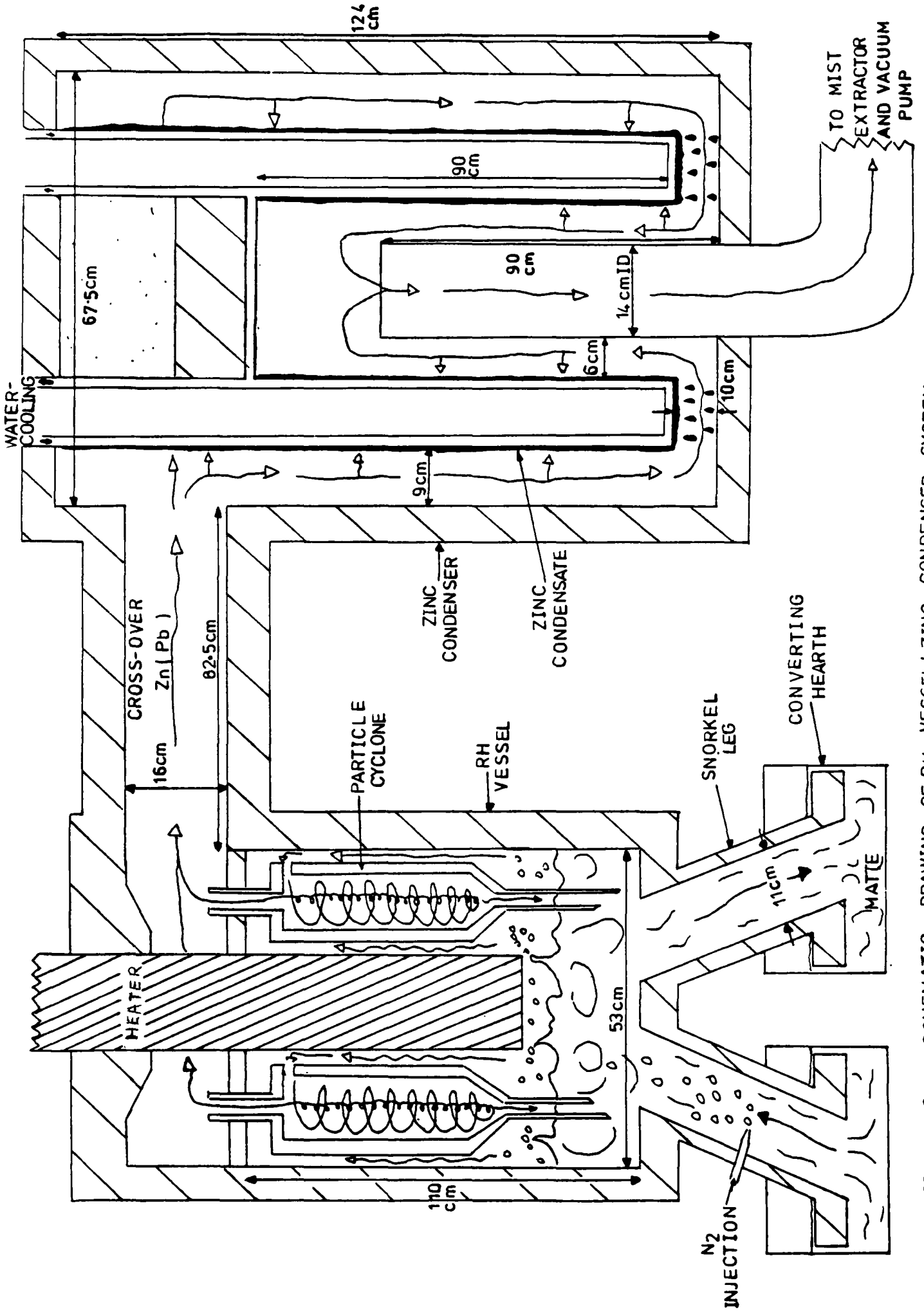

FIGURE 1.4.2 : SCHEMATIC DRAWING OF RH VESSEL/ ZINC CONDENSER SYSTEM

practical 1-2 mm Hg reported (Herbertson and Warner, 1974) for VDZ of lead in the Imperial Smelting Process. The significance of this is that VDZ of matte in the presently considered smelter is kinetically much more favourable than VDZ of lead. However, the mode of circulation in the Warner smelter whereby inert gas lift is utilised will ensure a higher inert gas concentration in the feed to the condenser compared to the relatively low residual inert gas concentrations associated with VDZ of lead. A typical matte feed should yield RH vessel partial pressures for elemental lead and PbS around 3.2 mm and 1.5 mm respectively. The exhaust gas flow (inert gases and SO_2) pulled back at the vacuum pump may be as high as 10 mm Hg (Warner, 1989). Calculations have also shown that a typical condensable mixture to be treated in the condenser will have a greater than 90% zinc vapour content.

In the top-blow region of the smelter, normal submerged tuyère iron slagging reactions would not work as they would result in excessive zinc and lead losses to slag as oxides. A method of enhancing the gas phase mass transfer process that supplies oxygen for the reaction stoichiometry whilst at the same time inhibiting liquid phase oxygen diffusion is used. This involves a multiple lance array of top-blowing subsonic gas jets impinging upon the matte surface relatively gently so no splashing occurs. The maximum loss of zinc and lead species to the slag cannot exceed the rate of liquid phase transport of these species from the bulk of the matte to the surface. Once the zinc and the lead enters the slag phase they are lost from the smelter and overall metal recoveries will fall. For oxygen blowing under probable gas phase diffusion control, the surface layers of matte in the immediate impact area under the top-blow lances can be expected to approach equilibrium in terms of dissolved oxygen. The matte can then be

expected to pick up dissolved oxygen corresponding to the liquid phase diffusion rate. A major portion of this dissolved oxygen has to be removed before the matte is exposed to the reduced pressure inside the RH vessel because every mole of dissolved oxygen ends up as one mole of SO_2. This in turn will cause 3 moles of zinc to revert to the oxide and sulphide by equation 1.4.5. This ZnO/ZnS dross would have to be recirculated to the front end of the smelter. Matte would also have to be deoxidised by chemical reation with appropriate reductants such as coal char, coke or natural gas. This problem may not be that significant as it is likely that reaction 1.4.5 has slow reaction kinetics at reduced pressure.

A slag of a few millimetres thickness will be generated and quickly blown away from the top-blow region by the force of the jets, as demonstrated by Rottmann and Wuth (1975). Because forced matte circulation will continuously remove slag from the top-blow zone, the jet impact area will consist of a network of surface depressions all essentially free of slag with direct contact between the oxidising gas and the matte.This gentle blowing will also prevent excessive over-oxidation and magnetite formation. Once the slag is moving away in a thin layer from the top-blow region, in-situ slag cleaning can be effected by contacting with solid reductants to reduce any magnetite and revert any copper from the slag back into the matte phase. The discard slag will be tapped periodically from the lower end of the converting hearth of the smelter (that has a built-in 1^{o} slope). Excess copper surplus to that necessary for the production of zinc and lead will also be a product from the smelter.

Depending on the material being smelted, the effectiveness of the vacuum in removing zinc and lead and the mass transfer intensity in the top-blow region, steady state and self-regulating conditions will tend to be

established within the matte circuit. A minimum matte circulation rate of 90 litres/minute is dictated by the thermal requirements and the temperature range over which matte can reasonably be handled. Matte circulation rate can be varied by control of the amount of lift gas admitted to the RH upleg. The rate at which solids are assimilated into the melt will reflect smelting intensity for a given physical size of plant.

The polymetallic smelter has inherent advantages over competing processes:

i) Three metals are produced simultaneously in one vessel in a fully continuous process.

ii) High overall metals recovery compared to alternative hydrometallurgical and minerals processing operations.

iii) It will accept directly certain crushed ore feeds or pelletised feeds.

iv) Forced circulation under a closed loop ensures rapid heat and mass transport via forced convection processes that

  a) prevent back-mixing

  b) allow for countercurrent contact

  c) permit sequential processing of the melt

  d) allow for oxidising and reducing conditions in different areas of the loop

  e) provide a mechanism for direct recovery of heat from exothermic slagging and converting reactions as well as fuel combustion, and its transference as sensible heat to sites of endothermic chemical reaction, charge assimilation, volatilisation and slag cleaning

and f) permit the smelting intensity to be very much under the control of the process designer/operator.

v) Zinc metal is produced directly from zinc sulphide without going through the oxide phase and the requirement of a carbonaceous reducing agent is thus eliminated.

vi) The oxygen requirements are provided by a number of subsonic, top-blown lances operating in a controlled, non-splash mode rather than submerged tuyère oxygen injection or a top-blown supersonic jet.

vii) A steady state slag layer of a few millimetres thickness is formed and easily cleared by the force of the jets. This can be compared with typical converter slags tens of centimetres thick.

CHAPTER 2: LITERATURE SURVEY AND THEORETICAL BACKGROUND

2.1 TOP-BLOWING THEORY

2.1.1 The Scope of Published High and Low Temperature Investigations

2.1.1.1 High Temperature Top-Blowing Experiments

There have been relatively few published studies on high temperature, subsonic top-blowing systems. This is probably due to the high cost of constructing small scale versions of top-blowing smelters and converters. Extensive fundamental research into the field of subsonic oxygen jets impinging on molten silver at 1000^{o}C has been carried out. Work by Wakelin (1966), Chatterjee (1970, 1972), Baker (1977) and Herbertson (1978) using ostensibly the same experimental rig have set the precedent for elucidating mass transfer mechanisms. These authors have studied the effect of physical variables such as lance height and nozzle diameter on the rate of mass transfer. The Japanese workers, Mori and Sana (1974), have also utilised silver in top-blowing experiments.

Experimental pilot-scale steel converters of up to 1800 kg capacity have been used by Flinn and coworkers (1967). They used supersonic oxygen jets to study the depth of jet penetration into a melt during top-blowing tests as well as observing the resultant flow circulation patterns. Recently, Koria and Lange (1987) have studied depth of jet penetration during the interaction of a single nozzle oxygen lance and a multiple nozzle oxygen lance with a molten steel bath. In these small scale tests, 10 cm diameter quartz crucibles and 1.2 mm nozzles were used.

Several experiments on the copper deoxidation system have been reported by Rottmann and Wuth (1975) and by Schmitt and Wuth (1981). This is more analogous to the Warner smelter connected with this work. In Schmitt and Wuth's paper they blew various supersonic reducing gas jets singly onto a copper/oxygen melt. They found that the deoxidation reaction was gas phase transport controlled for oxygen-in-copper concentrations down to 0.5%. Below this figure liquid phase resistance becomes important. In the work carried out by Rottmann and Wuth a supersonic oxygen jet was top-blown onto copper matte in a small scale laboratory converter. Both pure and diluted oxygen jets were employed to establish the fact that the reaction was gas phase diffusion controlled. Under the jet momenta used it was possible to keep the impingement zone free from slag, the conversion reaction being confined to the depression. The authors concluded that the induced circulation field in the bath must be a semisphere with diameter three times that of the depression so as to prevent the formation of concentration gradients in the bulk matte. Recently, Baker and Rajakumar (1983) have also studied impinging jet deoxidation of a copper/oxygen melt.

The industrial problem of cleaning copper smelter slags that have a high copper content has been tacked by Chaudhuri et al (1980). They developed a pilot plant that included a top-blown reactor where up to six water-cooled lances (blowing subsonic and supersonic jets) directed a reducing gas/oxygen mixture onto the melt. They noted that the induced slag circulation patterns were similar to those previously reported for metallurgical systems. The authors also found that there was a limit to the circulation pattern associated with each lance. Hence, to achieve the required degree of mass transfer in the slag several lances in series were used.

2.1.1.2 Top-Blowing Physical Modelling Studies

To exactly simulate the complex physical and chemical effects of top-blowing in a furnace with low temperature, scaled water models is almost impossible; a fact echoed by Holden and Hogg (1960), Davenport et al (1966) and Baker (1977). However, as far as flow visualisation, mixing and rates of mass transfer are concerned, low temperature analogues will show trends that will also exist at high temperature.

Problems, such as the inevitable formation of chemical reaction products as gas bubbles evolving from a melt are hard to model at low temperature as indeed is the simulation of slag formation. Moreover, the physical formation of bubbles may enhance liquid phase mass transfer. Indeed, a strongly reactive jetting medium in a smelter may induce or affect strongly splashing in the liquid phase. Alternatively, studies have shown that product bubbles from metallurgical reactions are small and disperse over the bath surface considerably decreasing the extent of splashing (Wright and Morrison, 1985).

Holden and Hogg (1960) in their low temperature model of a steel converter simulated the formation of carbon monoxide bubbles in the melt. They fitted a felt base to the bottom of the tank so the liquid phase could be aerated. Though imperfect in terms of similarity it did provide the indication that the bubbles did not affect the shape or size of the depression caused by an impinging air jet. They observed that the bubbles were deflected such that they burst through the surface near the centre of the crater. Van Langen (1966) has also studied gas evolution in a model of an L-D converter. He blew dry HCl gas onto $NaHCO_3$ solution with a layer of oil on top simulating

the slag phase. He assessed the extent of the reaction by using methyl orange indicator. His qualitative results showed that stirring within the $NaHCO_3$ solution was enhanced by:

a) Using a thinner oil film

b) Increasing the impinging jet momentum flux, and

c) Reducing the lance height or the bath depth.

Dubrawka (1961) has used CO_2 gas jets blowing onto NaOH(aq) through 3.2 mm nozzles. He discovered that the rate of CO_2 absorption increased as baths of larger diameter were used. Wakelin (1966) as part of his work studied the absorption of CO_2 into tap water as did Bradshaw and Chatterjee (1971). They showed that the mass transfer model for this system was best characterised by considering a bulk liquid surface renewal motion.

Jones (1986) here at Birmingham University has studied various gas/liquid systems in his extensive research. He used NH_3 gas jets blowing onto water and HCl as well as O_2 jets blowing onto water and PVA solutions. Several unpublished undergraduate reports have also been produced within this School e.g. by Malakfam and Malone (1983). These preliminary studies utilised CO_2 jets blowing onto water over a variety of blowing parameters.

For this top-blowing study the mass transfer system utilised has been the desorption of oxygen from water into nitrogen and air jets. This was chosen because of the relatively low solubility of oxygen in water. This ensures that all resistance to mass transfer will lie in the liquid phase. Hence it is a comparable mass transfer analogue to oxygen diffusion into the melt in the high temperature polymetallic smelter related to this work. So, despite the large temperature differences between room temperature

models and the smelter at 1300^{o}C the fundamental mass transport mechanism is essentially the same. Low temperature trends can then be expected to occur at high temperature.

2.1.2 Structure and Properties of a Turbulent Gas Jet

All the gas jets employed in the present work were turbulent and subsonic in nature, as indeed virtually all of the experimental investigations in this field have been. Jet behaviour has been well documented in the various textbooks such as the in-depth Abramovich (1963) which gives extensive background theory. Since experimental jet studies tend to vary from system to system numerous empirical as well as theoretical correlations have been developed.

Figure 2.1.2.1 illustrates the main characteristics of a 'free' turbulent jet. Such a jet has a nozzle Reynolds Number greater than 2000 and its cross-sectional flow area is less than one fifth of the total cross-sectional flow area of the region through which it is flowing.

A free jet discharging from a nozzle will entrain the surrounding fluid and expand (Tuve, 1953; Perry, 1984). The momentum of the jet is conserved as it entrains the surrounding fluid. As well as momentum both mass and heat transfer will occur due to eddy diffusion. A "jet boundary layer" forms due to the shear between the jet fluid and the surroundings.

The free jet is characterised by four zones:

ZONE 1

A region of flow establishment of between 2 and 6 nozzle diameters in length (Tuve, 1953) including the so-called potential core - a central zone unaffected by diffusion of eddies. Within this core the velocity remains steady at the nozzle outlet value, U_0.

ZONE 2

As the jet moves further downstream it decelerates (whilst accelerating the surrounding medium and increasing entrainment of that fluid). This

FIGURE 2.1.2.1 : STRUCTURE OF A FREE TURBULENT GAS JET

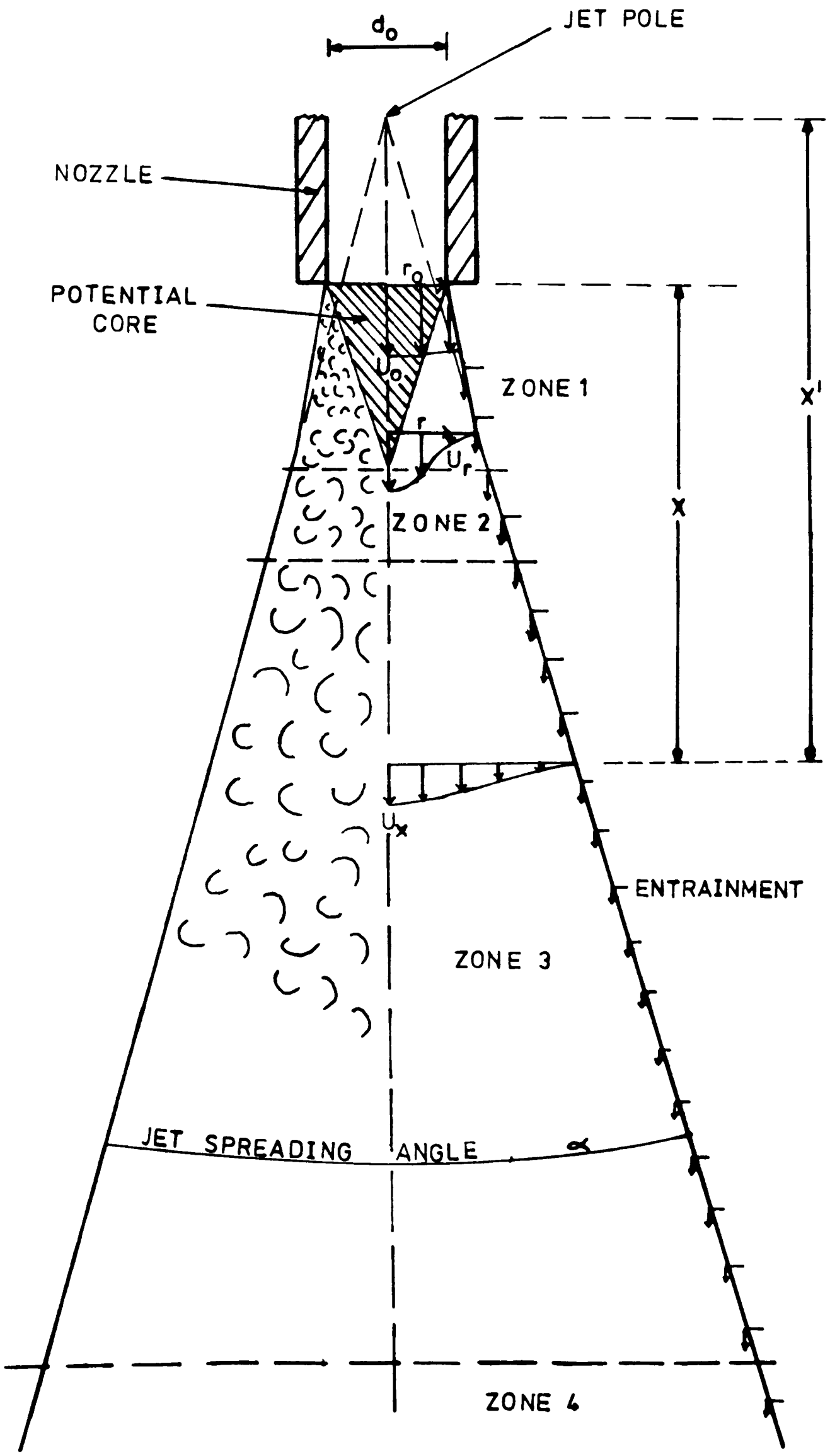

transition zone extends to about 8 to 10 nozzle diameters.

ZONE 3

A region of established fully-developed flow - the principal region of the jet extending to about 100 nozzle diameters.

ZONE 4

A terminal region where the residual centerline or maximum velocity reduces rapidly within a short distance. For air jets, the residual velocity will reduce to less than 0.3 m/s; this is usually regarded as still air.

2.1.2.1 Velocity of the Gas Jet

i) Longitudinal Distribution of Centre Line Velocity (U_x)

As the gas jet effuses from the nozzle its longitudinal centre line velocity decays due to viscous drag between it and the surrounding fluid such that it results in mass entrainment. The axial velocity components of the turbulent jet vary both with radial distance, r, and downstream distance, x, from the nozzle orifice.

Various researchers have been able to relate the reduction of jet centre line velocity, U_x, to nozzle diameter, d_0, and distance from the jet pole, x.

The general relationship is of the form:

$$U_x/U_0 = K1 \cdot d_0/x \qquad (2.1.1)$$

where K1 is called the jet momentum constant for a given system. It is best determined by direct measurement of the variables. Numerous investigators have produced correlations of this form, the more reliable of

which are shown in Table 2.1.2.1 with the limiting restrictions applicable to each. It can be seen that K1 can take values in the range 5.0 to 8.6 dependent upon system parameters. The present work has utilised lance systems with x/d_o ratios of up to 100.

ii) Radial Distribution of Longitudinal Velocity (U_r)

Various investigators (Albertson et al, 1950; Tuve, 1953) have produced correlations for the radial distribution of velocity across the jet at any point.

Tuve gives:

$$\frac{U_r}{U_x} = \exp\left(-40\left(r/x\right)^2\right) \quad \text{for } 7 < x/d_o < 100 \qquad (2.1.2)$$

Wakelin (1966) and Davenport et al (1966) report:

$$\frac{U_r}{U_x} = \exp\left(-80\left(r/x\right)^2\right) \quad \text{for } U_o = 52.4 \text{ m/s} \quad \left(Re = 8 \times 10^3\right) \qquad (2.1.3)$$

and

$$\frac{U_r}{U_x} = \exp\left(-100\left(r/x\right)^2\right) \quad \text{for } U_o = 133 \text{ m/s} \quad \left(Re = 3 \times 10^4\right) \qquad (2.1.4)$$

Giralt (1977) found that in the potential core region of a jet ($x/d_o < 5.6$)

TABLE 2.1.2.1: SUMMARY OF CENTRE LINE VELOCITY EQUATIONS

AUTHOR	EQUATION	LIMITATIONS AND RESTRICTIONS
Albertson et al (1950)	$U_x/U_o = 6.2\ d_o/x$	x/d_o = 7-250
Baines (1950)*	$U_x/U_o = 6.90\ d_o/x$	$Re = 2.1 \times 10^4$ } $x/d_o < 60$
	$U_x/U_o = 5.76\ d_o/x$	$Re = 7.0 \times 10^4$ }
Tuve (1953)	$U_x/U_o = 5\ d_o/x$	U_o = 2.5-5.0 m/s } $7 < x/d_o < 100$
	$U_x/U_o = 6.2\ d_o/x$	U_o = 10-50 m/s }
Wakelin (1966)	$U_x/U_o = 6.2\ d_o/x$	$Re = 8 \times 10^3$ $x/d_o > 30$
	$U_x/U_o = 8.6\ d_o/x$	$Re = 5.1 \times 10^4$ $9 < x/d_o < 30$
Davenport et al (1966)	$U_x/U_o = 6.2\ d_o/x$	$Re = 8 \times 10^3$ $10 < x/d_o < 300$
	$U_x/U_o = 7.0\ d_o/x$	$Re = 1.9 \times 10^4$ $10 < x/d_o < 300$
	$U_x/U_o = 7.8\ d_o/x$	$Re = 3.2 \times 10^4$ $10 < x/d_o < 300$
	$U_x/U_o = 8.6\ d_o/x$	$Re = 5.1 \times 10^4$ $10 < x/d_o < 300$
Lohe (1966)	$U_x/U_o = 1/(0.37 + 0.106\ x/d_o)$	$x/d_o < 20$
Beltaos et al (1974)	$U_x/U_o = 6.3\ d_o/x$	$x/d_o < 17$
	$U_x/U_o = 6.8\ d_o/x$	$17 < x/d_o < 53$
Giralt et al (1977)	$U_x/U_o = 6.8/(0.72 + x/d_o)$	$x/d_o > 8.6$
	$U_x/U_o = 1.39 - 0.077\ (x/d_o)$	$8.6 \geq x/d_o \geq 5.4$
	$U_x/U_o = 1.0 - 0.0048\ (x/d_o)$	$x/d_o < 5.4$

* Baines contributes to the discussion of Albertson et al's paper.

$$r_{1/2} = 0.5 + 0.006 \,.\, (x/d_o) \qquad (2.1.5)$$

where $r_{1/2}$ is the radius at which $U_r = U_x/2$

and

$$r_{1/2}/d_o = 0.081 \quad (1 + x/d_o) \qquad (2.1.6)$$

Forestall and Gaylord (1955) and Beltaos et al (1974) expressed the velocity change with radial distance across the jet as:

$$\frac{U_r}{U_x} = \exp\left(0.694 \left(r/r_{1/2}\right)^2 \right) \qquad (2.1.7)$$

Lohe (1966) gives:

$$\frac{U_r}{U_x} = \exp\left(- 0.69 \left(r/r_{1/2}\right)^2 \right) \qquad (2.1.8)$$

iii) Entrainment of Surrounding Fluid into the Gas Jet

The expressions describing mass entrainment into the jet take the same form as velocity change in the jet. A typical equation given by Albertson et al (1950) and Tuve (1953) to calculate the increase in mass flowrate with distance, x, downstream of the nozzle is:

$$\dot{m}_x/\dot{m}_o = (2/K2) \cdot (x/d_o) \quad \text{for } 7 < x/d_o < 100 \qquad (2.1.9)$$

where $\dot{m}_x$ is the mass flowrate at distance x and $\dot{m}_o$ is the mass flowrate at the nozzle. K2 is the jet constant for mass entrainment. The above equation applies for gas jets discharging into an environment of ostensibly the same gas.

Ricou and Spalding (1961) have produced a modified equation for the case where the environment is a different gas to that of the jetting medium.

$$\frac{\dot{m}_x}{\dot{m}_o} = (2/K2)\frac{x}{d_o}\left(\frac{\rho_1}{\rho_o}\right)^{1/2} \qquad (2.1.10)$$

where ρ_1 = density of the environmental gas

and ρ_o = density of the gas in the jet.

They found that for Re > 2.5 x 10^4, K2 = 6.25. This same value of K2 has also been reported by Albertson et al (1950), Tuve (1953) and Davenport et al (1966).

iv) <u>Jet Spreading Angle, α</u>

Although the jet boundary is not entirely discrete due to eddy entrainment it has been useful for many investigators to approximate the jet spreading angle, α. In line with Lohe (1966), Wakelin (1966), Davenport et al (1966) and Jones (1986) this study uses a figure of 21^o as a uniform value for gas jets at room temperature. Tuve notes that for a jet where α = 21^o it is restricted to the range $x/d_o < 100$. Abramovich et al (1966) have

produced evidence to show that the jet spreading angle is different for a cold jet entering a hot environment (the probable smelter case) compared to the isothermal expansion of a jet at room temperature (the water model situation). Their work provides photographs that show smaller spreading angles for the former rather than the latter. No quantitative data on jet spreading angles are offered. Clearly, this effect will have to be taken into account for the polymetallic smelter situation in terms of the geometry of the multiple lance top-blowing array to be utilised.

2.1.3 The Interaction of a Top-Blown Gas Jet With Liquid Surfaces in Stationary Baths

2.1.3.1 Deformation of the Liquid Surface

When a relatively turbulent, high velocity gas jet strikes a liquid vertically a cavity or depression is formed on the surface. The jet is deflected back from the surface of the crater. The depth of the depression depends on the jet velocity and the distance of the nozzle from the surface as well as the surface tension.

For a gas jet impinging on a liquid surface three main modes of interaction can be defined (Mathieu, 1962; Rosler et al, 1968; Molloy, 1970) - See Figure 2.1.3.1:

a) Stable Indention or 'Dimpling' Mode

If a gas jet is blown very gently onto a liquid surface ($U_H < 3\ ms^{-1}$) the surface will not be disturbed and it will resemble a flat plate. As the velocity is increased (or if a high velocity at a large nozzle height is employed) a classical wall jet pattern is formed with a slight surface depression (Figure 2.1.3.1(a)). Ripples or waves are formed in the central disturbed zone; they move radially outwards and the depression itself is seen to oscillate both laterally and vertically.

b) Unstable and Oscillating Indention or 'Splashing' Mode

If the jet velocity is increased further or the lance height decreased the depression gets deeper until a point is reached where vigorous oscillation of the indention disperses bubbles of gas into the liquid. At slightly higher velocities there is a dispersion of liquid droplets into the gas phase due to

FIGURE 2.1.3.1 : COMPARATIVE GEOMETRY OF JETTING FLOW MODES

a) DIMPLING

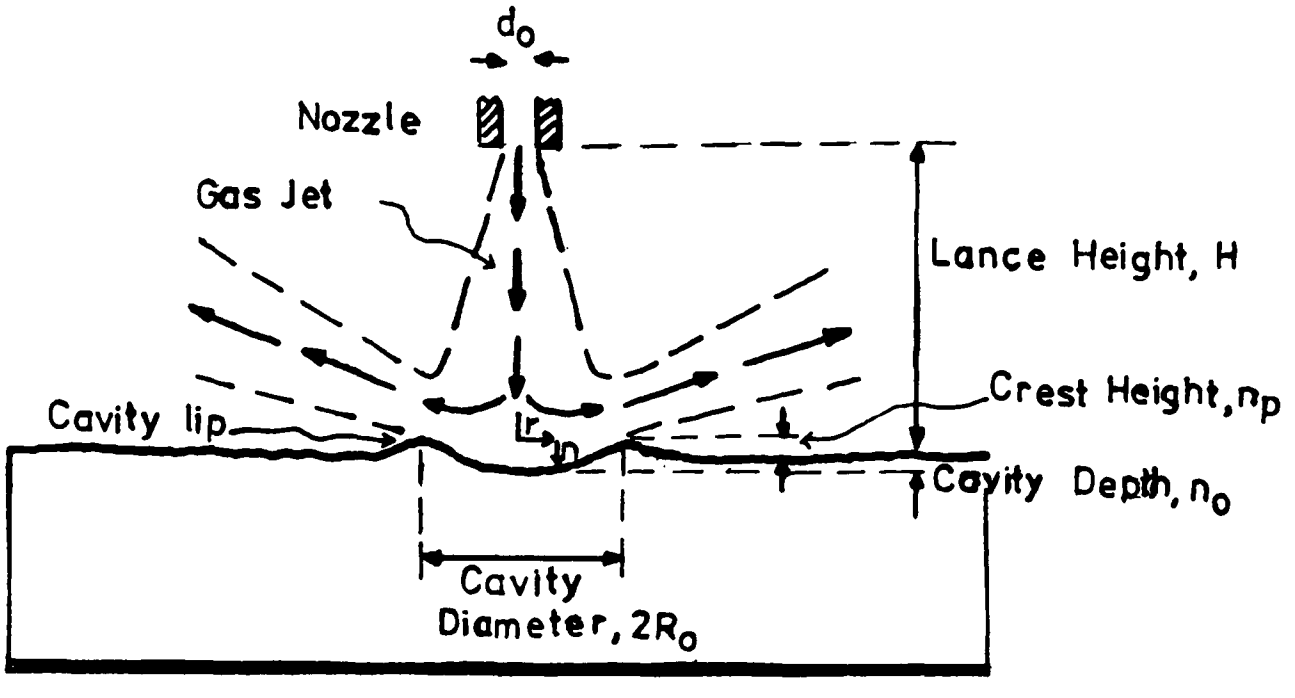

b) SPLASHING

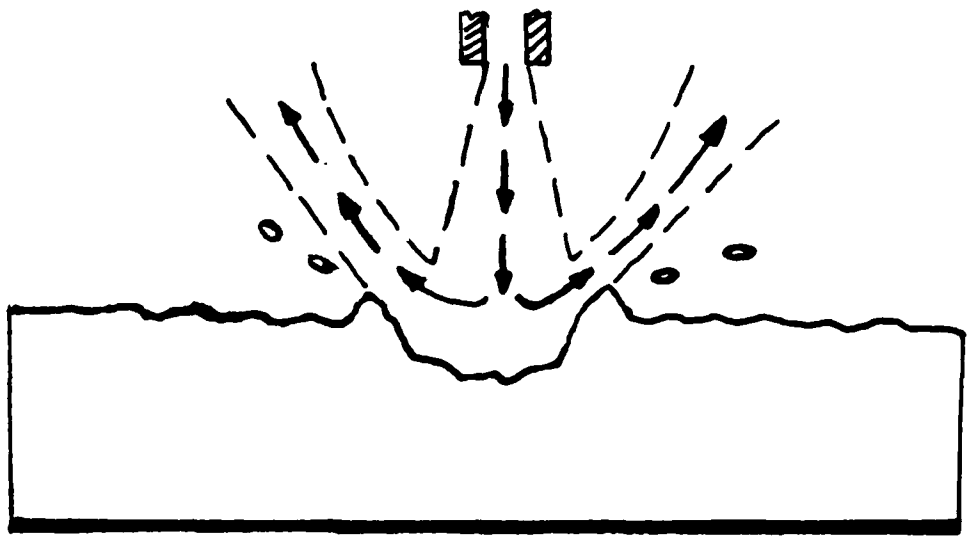

c) PENETRATION

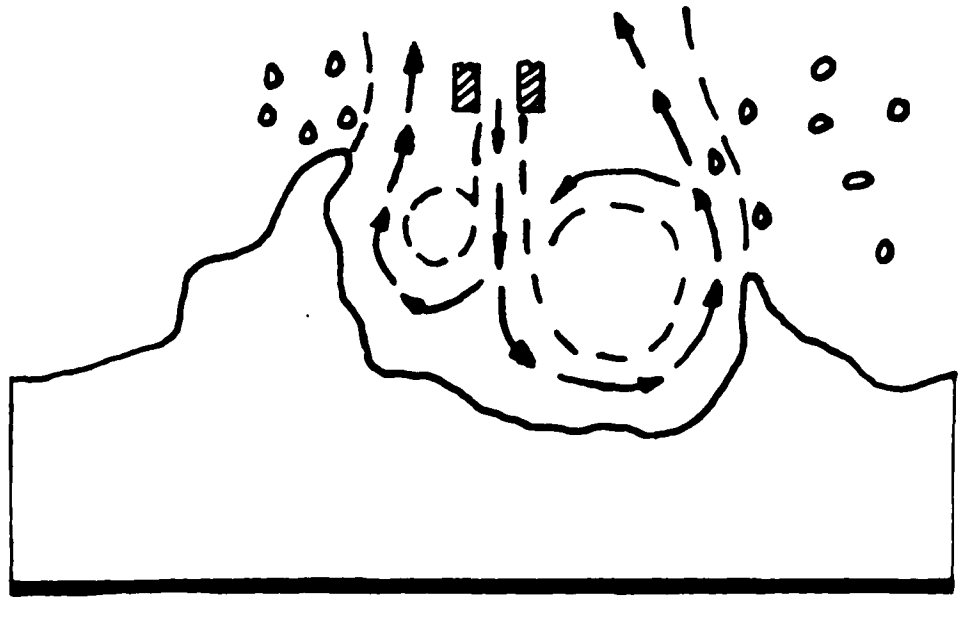

the shearing action of the gas tending to remove the tips of the waves as droplets. This phenomenon is known as sputtering or splashing. The droplets are thrown out from the cavity with the gas stream. The cavity bottom tends to oscillate vertically and the sides laterally (Struck, 1965).

c) Dispersion or 'Penetration' Mode

With a further increase in velocity and/or reduced nozzle height, much deeper penetration of the bath takes place accompanied by an apparent reduction in the amount of outwardly directed splash. The jet energy is used up in causing very pronounced stretching, bending and rotation of the cavity about the jet axis (Rosler and Stewart, 1968). The normal paraboloid shape of the depression becomes a steep-sided 'U'. Very pronounced surface waves are also created (Mathieu, 1962). This sort of interaction is very common in an LD converter (Flinn et al, 1967) where the jet is supersonic and may even penetrate all the way to the bottom of the vessel.

2.1.3.2 Depth, Diameter and Profile of the Liquid Depression

There has been an extensive array of correlations produced by dimensional analysis techniques to predict the depth of the depression especially in the dimpling mode of jetting. Most take the form:

$$\frac{n_o}{H} = \text{function}\left(\frac{\dot{M}}{\rho_L\, g\, H^3}\right) \qquad (2.1.11)$$

Table 2.1.3.1 is a summary table of all the equations derived by various

TABLE 2.1.3.1: DIMENSIONLESS CORRELATIONS FOR DEPTH OF DEPRESSION

AUTHOR	CORRELATION
Collins and Lubanska (1954)	$\frac{\dot{M}}{\rho_L g H^3} = \frac{1}{53}\left(\frac{n_o}{H}\right)\left[1 + 19\left(\frac{\dot{M}}{\rho_L g H^3}\right)^{2/3}\right]$
Banks and Chandrasekhara (1963)	$\left(\frac{n_o}{H}\right)^2 = \left(1 + \frac{1000\sigma_L}{\rho_L g H^2}\right)\left(\frac{\pi}{2K1^2}\right)\left(\frac{\dot{M}}{\rho_L g\, n_o^3}\right)$
Wakelin (1966)	$\frac{\dot{M}}{\rho_L g H^3} = \left(\frac{\pi}{115}\right)\left(\frac{n_o}{H}\right)\left(1 + \frac{n_o}{H}\right)^2\left(1 + \frac{2\sigma_L}{\rho_L g R_o n_o}\right)$
Davenport et al (1966)	$\frac{\dot{M}}{\rho_L g H^3} = \left(\frac{\pi}{115}\right)\left(\frac{n_o}{H}\right)\left(1 + \frac{n_o}{H}\right)^2$
Cheslak et al (1969)	$\frac{\dot{M}}{\rho_L g H^3} = \left(\frac{\pi}{2K1^2}\right)\left(\frac{n_o}{H}\right)\left(1 + \frac{n_o}{H}\right)^2$
Shrivastava et al (1976)	$\frac{n_o}{\left(H + n_o\right)} = 37.5\left(\frac{\dot{M}}{\rho_L g\left(H + n_o\right)^3}\right)$
Baker (1977)	$\frac{\dot{M}}{\rho_L g H^3} = \left(\frac{\pi}{115}\right)\left(\frac{n_o}{H}\right)\left(1 + \frac{n_o}{H}\right)^2\left(1 + \frac{116.5\sigma_L}{\rho_L g H^2}\right)$
Bin (1985)	$\frac{\dot{M}}{\rho_L g H^3} = \frac{\pi}{125.7}\left(\frac{n_o}{H}\right)\left(1 + \frac{n_o}{H}\right)^2 \quad \text{for } \frac{H}{d_o} > 8$

investigators. Strictly, the equations taking into account surface tension e.g. those by Wakelin and Banks and Chandrasekhara are the most precise. The others, however, are good approximations over the experimental conditions studied. Theoretically, Shrivastava et al's use of $H + n_o$ rather than H is correct, though for large nozzle to liquid heights $H >> n_o$. Bin's equation is of note because it was deduced after plotting all the available gas jet/liquid and liquid jet/liquid data published in the literature.

Flinn and coworkers (1967) have produced an empirical equation for an actual LD converter:

$$n_o \text{ (inches)} = 1.5 \left(\frac{P_d \, D_t}{\sqrt{H}} \right) + 1.5 \qquad (2.1.12)$$

JET FORCE NUMBER

where P_d = Nozzle pressure; psia

D_t = Nozzle throat diameter; inches

H = Nozzle height above bath; inches

Lohe (1966) has produced the equation

$$n_o = \frac{\rho_g}{\rho_L} \cdot \frac{U^2 \left(H + n_o \right)}{2g} \qquad (2.1.13)$$

to predict cavity depth.

He also gives for the trough diameter:

$$2R_o = (1/C) \cdot d_o(1 + 0.285\ H/d_o) \qquad (2.1.14)$$

where C is an empirical constant that he proves to be 1.

Since the shape of the cavity approaches that of a parabola both Cheslak et al (1969) and Rosler and Stewart (1968) derive theoretical equations for the depression profile:

Cheslak et al;

$$\frac{2R_o}{n_o} = 2.8284\left[M_3/\pi - 1 + \left(2M_3/\pi + 1\right)^{1/2}\right]^{1/2} \qquad (2.1.15)$$

where $M_3 = \dot{M}/\rho_L\, g\, n_o{}^3$

Rosler and Stewart;

$$n = \frac{4}{R_o^6} \int_0^{R_o} H\left(R_o^2 - r\right)^2 r\, dr \qquad (2.1.16)$$

Both Ito et al (1981) and Bin (1985) derive equations that are essentially error function curves that describe the crater profile and fit their data:

Ito et al;

$$n/n_o = \exp\left[-\left(0.8326\left(r/R_o\right)\right)^2\right] \qquad (2.1.17)$$

Bin;

$$n/n_o = \exp\left[-\left(2\,K1\left(r/H\right)\right)^2\right] \qquad (2.1.18)$$

Fagela-Alabastro et al (1967) as well as Olmstead and Raynor (1984) have used analytical techniques to predict the increase in cavity depth with increasing gas velocity. Fagela-Alabastro's model also predicted the contour of the lip associated with the jet depression as well as the surface waves that emanate outwards from the cavity.

2.1.3.3 Critical Depth of Depression and the Onset of Splashing

Extensive research has been carried out in the field of predicting the onset of splashing for a given system and the effects of this unstable indention mode (Li, 1960; Chatterjee and Bradshaw, 1972). Under vigorous splashing such as in the LD steelmaking process, mass transfer through the steel droplets dispersed into the gas phase may contribute significantly to the overall rate of oxygen mass transfer. In connection with the smelter being commissioned in this School splashing is very undesirable.

A non-splash mode of operation is preferable because:

a) Splashed droplets cause both physical wear and chemical attack of the refractory walls of the vessel and jet nozzles.

b) Control of mass transfer during excessive splashing is very much impaired though Wakelin (1966) reports good mass transfer predictions under a mild splashing régime.

Chatterjee and Bradshaw (1972) have shown that once a system is in the splashing mode a maximum amount of splashing could be obtained at a given momentum flux or lance height. A further increase in momentum flux or decrease in lance height only decreased the amount of splashing.

Chatterjee and Bradshaw developed the following correlation for predicting the critical depth of depression, n_c, for the onset of splashing:

$$\left[\frac{g\,\mu_L^4}{\rho_L\,\sigma_L^3}\right] = 4.3 \times 10^{-22} \cdot \exp\left(4.34 \cdot \left(\frac{g\,\rho_L}{\sigma_L}\right)^{1/2} \cdot n_c\right) \qquad (2.1.19)$$

(M Number)

for $10^{-14} <$ M Number $< 10^3$

Hence for a given physical system splashing will start at a definite depth of depression. Mathieu (1960) and Wakelin (1966) do note however that the value for n_c will decrease at greater lance heights for a given momentum flux.

Banks and Chandrasekhara (1963) report values of n_c for air jets (both circular and plane) impinging on water in the range 0.82 - 1.59 cm for both stationary and flowing liquid phases. Schmitt and Wuth (1981) give experimental values of n_c for a copper melt/reducing gas jet system of 1.5 -

2.0 cm. Chatterjee and Bradshaw (1972) predicted values of n_c for steel and converter slag of 2 cm and 3 cm respectively. Their experimental n_c values for air jets on water varied from 1.26 - 1.4 cm. Jones (1986) also used the above equation to predict for a Cu/Zn/Pb matte an n_c value of 2 cm and for the resultant top-blown slag a figure of 3.2 cm is estimated.

Shrivastava et al (1976) have also produced a correlation for their data using different types of lances as well as including some of Chatterjee and Bradshaw's results. They predict splashing to occur at:

$$\left(\frac{\sigma_L}{\rho_L\, g\left(H+n_c\right)^2}\right) = 0.12\left(\frac{\dot{M}}{\rho_L\, g\left(H+n_c\right)^3}\right) \qquad (2.1.20)$$

2.1.4 Induced Liquid Circulation Patterns During Top-Blowing

2.1.4.1 Single Lance Fluid Flow Phenomena in Stationary Baths

When a gas jet impinges normally onto a liquid surface a fraction of its momentum (and hence its velocity) is transmitted across the interface due to shear stresses. For a solitary round jet the imparted surface flow is radial emanating from the centre of impact and extending outwards from the depression.

Ito (1981) has studied the imparted surface velocity of the liquid, U_S, when a gas jet impinges on the surface in the non-splash régime. By the use of small hydrogen bubbles emitting from a cathode and timed photographs he measured values of U_S. He also utilised an analytical static pressure distribution technique to obtain the following relationship between gas and liquid velocities (refer to Figure 2.1.4.1 for symbols):

$$\frac{U_s}{U_{g\infty}} = 1.170\left(\rho_o/\rho_L\right)^{2/3}\left(\nu_o/\nu_L\right)^{1/3} \qquad (2.1.21)$$

where $U_{g\infty}$ is the velocity of the air outside the boundary layer obtained from this equation:

$$P_o - P_s = \rho_o U_{g\infty}^2/2 \qquad (2.1.22)$$

FIGURE 2.1.4.1: COORDINATES FOR ITO'S SYSTEM

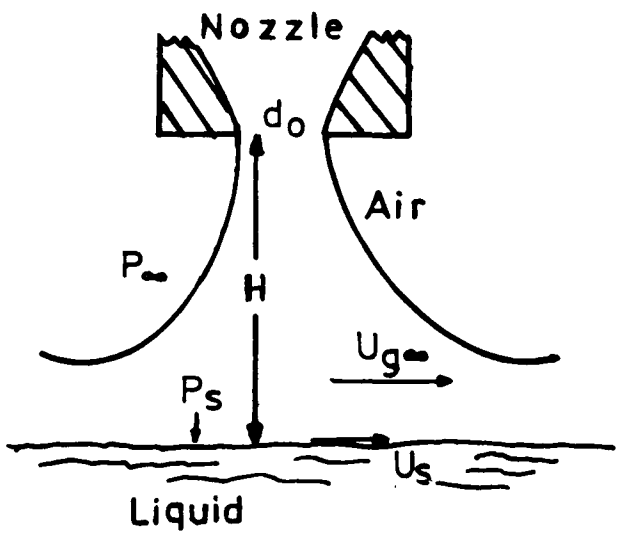

It should be pointed out that Ito's work dealt with laminar gas jets operating at H/d_o ratios of nearly 3. As such the analysis may not apply to the present situation.

Early work was carried out by Hasimoto (1958) and Holden and Hogg (1960) to qualitatively elucidate fluid flow patterns both in the liquid and gas phases especially in connection with steel making. Holden noted flow patterns in single and two-liquid top-blown model systems. He reported a common flow pattern in the bulk liquid phase that was virtually unaffected by the angle of the impinging jet and the lance height. The patterns discovered in the liquid phase are reproduced below.

The diagrams show that the liquid flowed radially outward across and close to the surface. The flow was deflected by the containing bath wall carrying the stream down the wall and back to the centre forming a recirculating toroidal vortex. The authors also report enhanced stirring within the liquid as a consequence of increasing the gas flowrate or decreasing the jet nozzle diameter. It was found that the intensity of circulation was reduced when larger baths were used. This was due to the

surface velocities decaying prior to deflection at the bath wall. It was also discovered that liquid movement in the zone below the central depression was more pronounced when shallow baths were used.

FIGURE 2.1.4.2: CIRCULATION PATTERNS OBSERVED IN A LIQUID IMPINGED UPON BY AN INCLINED JET

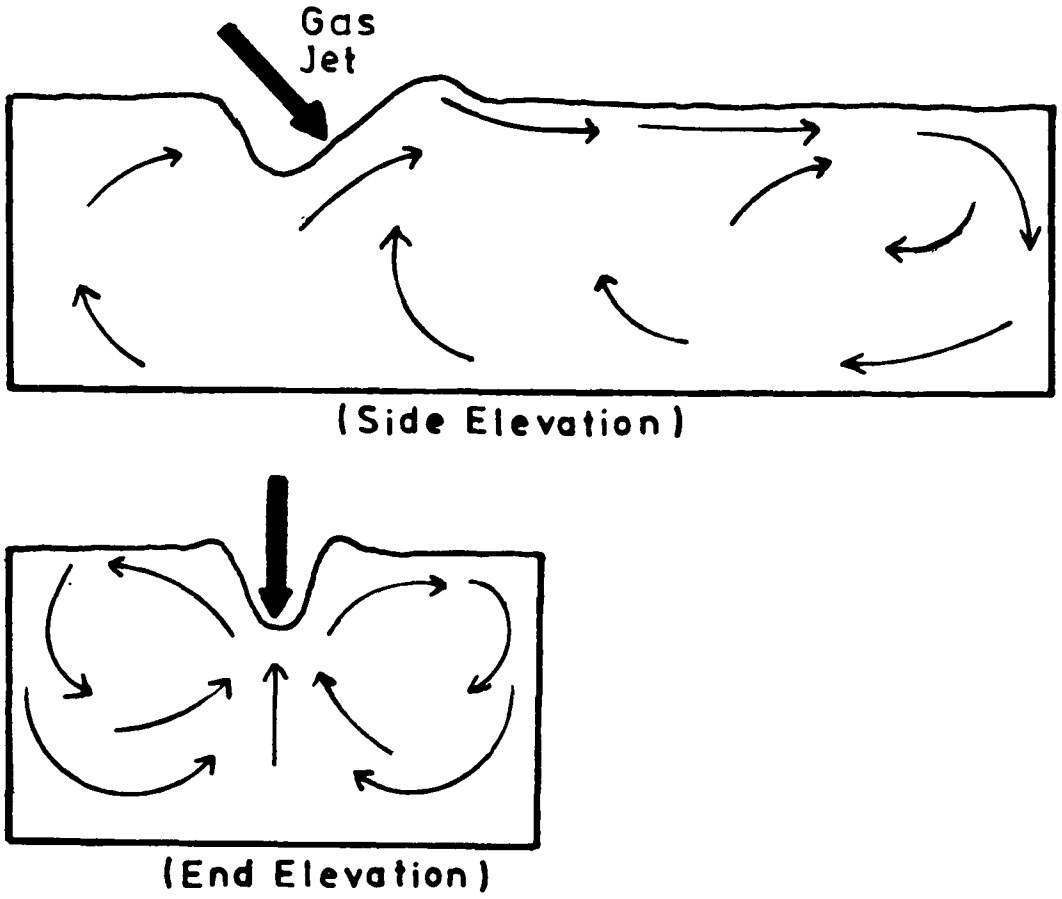

Mathieu (1960, 1962) has used suspended particles in a water bath to measure the mean period of rotation for the circulation pattern caused by a single air jet. This period was found to decrease for increasing values of the term $(U_o^2/2d_og)$. If this term was kept constant there was a minimum in the value of the rotation period as H/d_o increased. Such a minimum may partly explain the peaks in liquid phase mass transfer coefficients as H is increased reported by Wakelin (1966), Baker (1977) and Jones (1986).

Szekely and Asai (1974) have solved a mathematical model of a single lance stationary bath top-blown system. WIth it they were able to predict streamlines and velocity contours in a cylindrical bath agitated by a turbulent impinging jet. They noted that turbulent energy is only significant in the direct impingement area and not on the free liquid surface. Figure 2.1.4.3 shows two typical experimental flow patterns for the given sets of jetting parameters. Their experiments gave good quantitative agreement with the theory and help to support the use of a surface renewal type model to describe mass transfer. It is interesting to note that two stagnant areas are visible, one in the lower half of the bath directly under the jet and another forming an annulus bounded by the bottom and outside wall of the container. Referring to Figure 2.1.4.3 it can be seen that the circulation pattern formed by the more distant jet shows a much greater transference of kinetic energy to the liquid than that obtained when the jet was closer to the surface. Even at the lowest momentum fluxes and at the largest nozzle heights the mixing action of the jet on the water is sufficient to ensure that the contents of the bath are homogeneous.

2.1.4.2 Multiple Lance Fluid Flow Phenomena with Superimposed Channel Flow

The previous section dealt with stationary baths but much more relevant to this study is the practical case of a flowing liquid phase being top-blown by turbulent gas jets. There have been three studies associated with this important field. In a preliminary study Banks and Chandrasekhara (1963) used a 0.30 m wide by 0.46 m high by 5.49 m long horizontal channel with water pumped through it at rates of up to 1.48 m^3/hr. In their tests a plane jet orifice of length 0.30 m by 1.59 mm wide acted as a nozzle.

FIGURE 2.1.4.3 : FLOW PATTERNS IN A LIQUID CAUSED BY AN IMPINGING JET (After Szekely and Asai)

$\dot{M}$=0·1470N , H=17cm

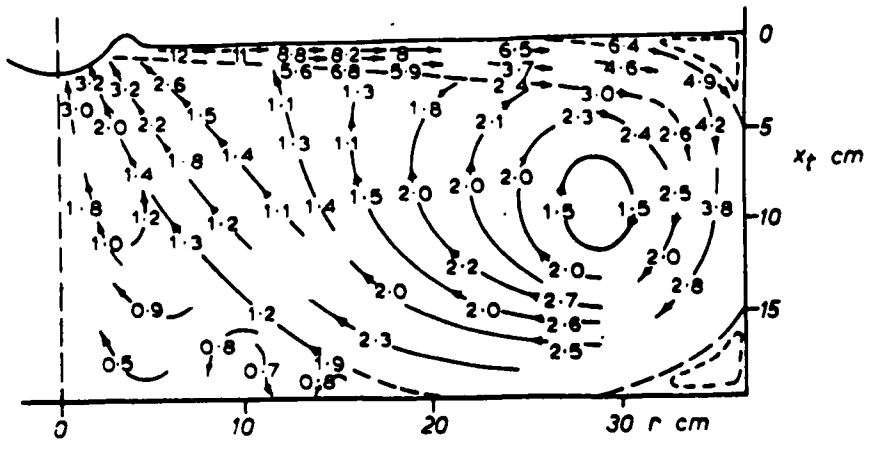

$\dot{M}$=0·0865N , H=8cm

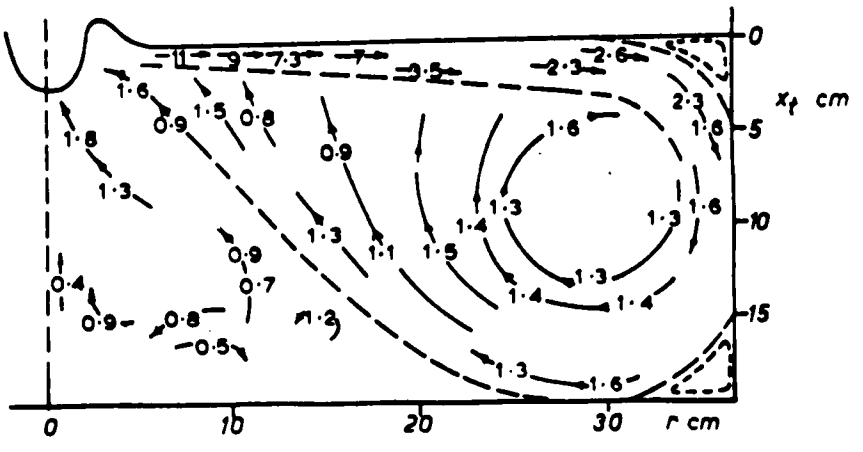

Numbers inside the diagrams refer to velocities in cm sec^{-1}

For a wide range of system variables comparative tests between a still liquid phase and a moving liquid phase were carried out. On a plot of n_0/H versus $M/\rho_L gH^2$ they found that the flowing liquid phase produced cavity depths (n_0) that were 30% lower than the corresponding quiescent liquid data. It was noted, however, that the cavity depth appears to be independent of water velocity and that with the water in motion the cavity becomes asymmetrical with the point of maximum depth displaced downstream.

Banks (1962) in a previous study used classical wave theory to predict the presence of gravity waves of length λ_1 and capillary waves of length λ_2 appearing respectively downstream and upstream of the centre plane of the impinging jet. The amplitude and wavelength of the capilliary waves were found to be smaller than those of the gravity waves. To verify this he used a 2.44 m long, 0.04 m wide channel with water circulating through it at depths of up to 0.51 m. A plane jet nozzle was constructed such that nozzle widths from zero to 3.18 mm could be employed; the slot length being 0.04 m. Water flowed through the channel at rates between 2.23 and 9.85 m^3/hour. Momentum fluxes of up to 0.5 N were used together with lance heights ranging from 0-0.22 m. The bath depth varied from 0.05-0.29 m. In his work Banks was able to predict a critical capilliary wave velocity below which a given channel velocity would not produce capilliary waves upstream. Banks also noted that for values of $(UH_2O)^2/gH < 0.1$ the results fell into the same range as the still water data.

The Australians, Conochie and Gray (1979), used a 10 cm wide by 100 cm long perspex channel to study mixing patterns visually using methylene blue dye and more accurately via an onstream spectro-photometer. A relatively shallow liquid depth of 3.1 cm was used and very slow water flowrates of around 0.06 m^3/hr (0.54 cm/s) were utilised. Up to

six circular lances were staggered along the length of the channel. The lance height was varied from 0-25 cm and momentum fluxes up to 0.21 N reported. The authors used Cu^{24} tracers in the water injected into the inlet stream to monitor residence time distributions.

Single jet mixing studies indicated that a primary mixing swirl similar to that obtained by Szekely and Asai (1974) rose upwards under the lance. As jet momentum was increased a secondary swirl in counter rotation to the first formed (see Figure 2.1.4.4). As jet momentum was further increased in size the primary swirl increased more but the secondary swirl showed little further increase. Fluid velocity was much greater in the primary swirl than the secondary swirl and the velocity in both swirls increased as jet momentum increased. In the shallow channel used the primary swirl became elongated and there was a steep velocity gradient from the top of the flow pattern to the bottom. It was thought that the velocity gradient at the edge of the primary swirl produced a shear force sufficient to set up a secondary swirl in counter rotation to the first. These two swirls appear both up and downstream of the impinging jet and they make up the mixing zone of the jet.

The authors showed that if two lances were placed at a spacing greater than twice the length of the mixing zones then there was no intermixing of adjacent zones. For this condition they concluded that the fluid flow in the channel could be described by a stirred-tanks-in-series model with intermixing of adjacent tanks. If, however, the interlance spacing decreases to less than twice the length of the mixing zones the extent of intermixing increases though complete mixing never occurs.

FIGURE 2.1.4.4: FLOW PATTERNS OBSERVED BY CONOCHIE AND GRAY (1979)

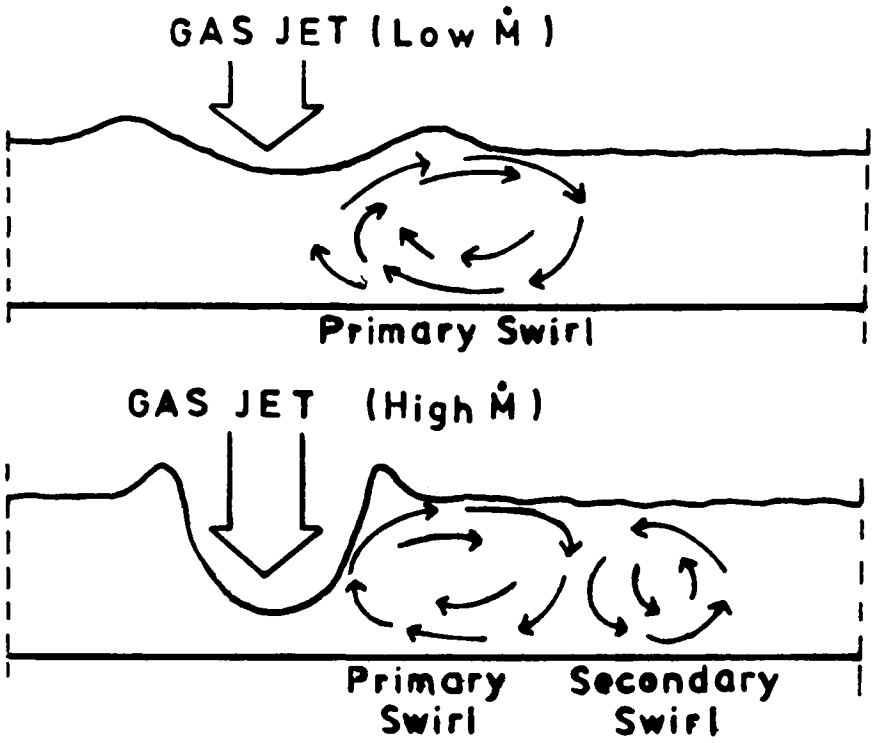

2.1.5 Multiple Jet Flow Phenomena

2.1.5.1 Interference Between Jets in a Multiple Jet Array

Tuve (1953) has analysed jet flow patterns from grilles, grids and perforated panels. His tests showed that the jet constant, K1, for a 20 cm nozzle was 6.2 but when the nozzle was covered with a perforated plate of 9.1% free area K1 decreased to 4.5. He stated that for multiple outlets of 3-10% free area K1 varies from 3.0 to 4.5 and between 4.5 to 6.0 for greater free areas. When the free area is 50-60% or above the behaviour is much like that of an open outlet of the same free area. Hence the presence of adjacent jets very close together decreases a given jet's velocity at a point x downstream compared to that of a similar free jet.

Martin (1977) in a comprehensive study of heat and mass transfer between impinging gas jets and solid surfaces developed numerous equations for single round impinging jets, arrays of round jets, single slot jets and arrays of slot jets. Quite low lance height, H, to nozzle diameter, d_o, ratios were used ranging up to 10. He studied the drying effect of moist solid surfaces impinged by multiple round jet arrays in both triangular and square pitch arrangements. Mass transfer Sherwood Numbers and heat transfer Nusselt Numbers were calculated for each system. It was found that at relatively high H/d_o ratios uniform transport phenomena occurred whereas at lower ratios peaks and troughs were observed. For arrays of nozzles he defines mean transfer coefficients per lance by averaging over those parts of the surface area attributed to one nozzle. Referring to Fig. 2.1.5.1 for a square pitched array of round nozzles he showed that each nozzle influences a portion of surface area equivalent to a square with edge length

FIGURE 2.1.5.1 : THE SPACIAL ARRANGEMENT OF ROUND NOZZLES IN REGULAR ARRAYS

a) Square-pitched Array

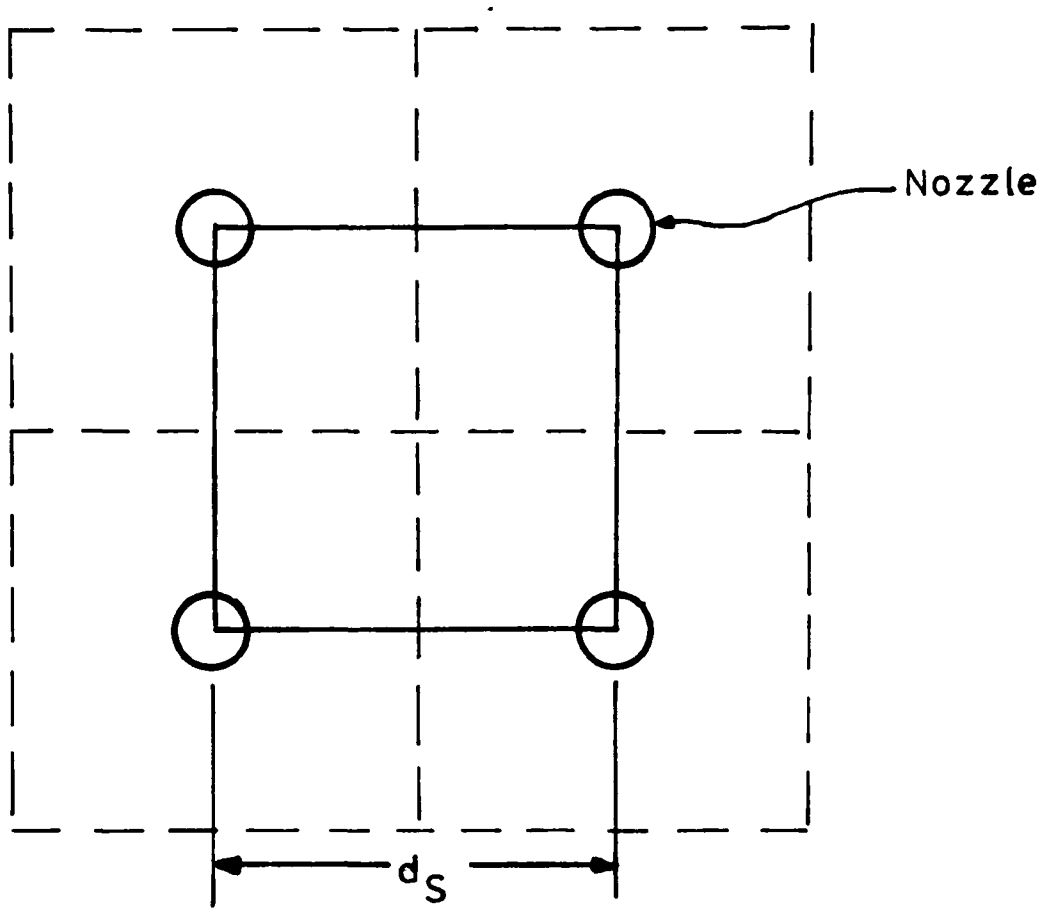

b) Triangular - pitched Array

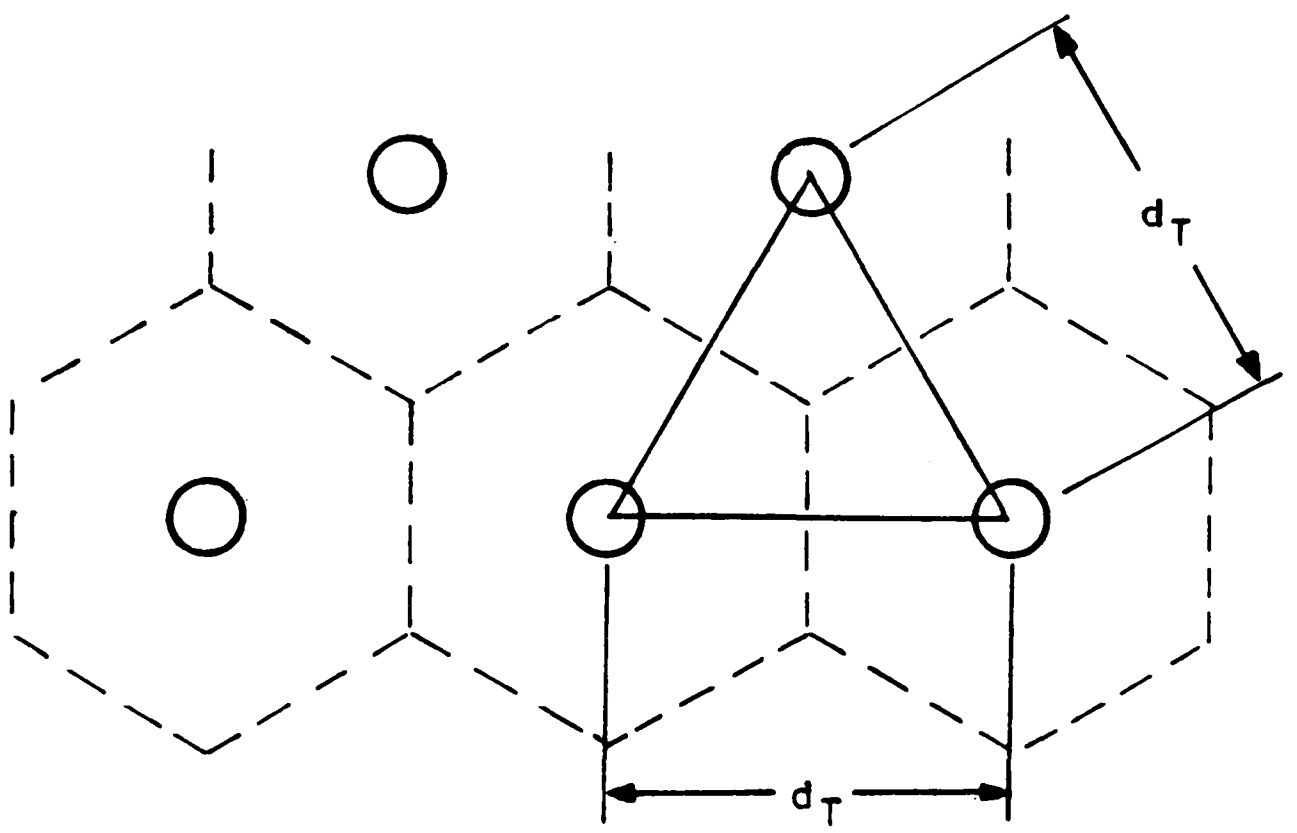

d_S. For a triangular pitch nozzle array each nozzle has a corresponding area equivalent to a hexagon with edge lengths equal to $d_T/2$. Martin also defines a relative nozzle area, f, as the ratio of the nozzle exit cross section to the area of the square or hexagon attached to it i.e.,

$$f = \frac{\pi/4\, d_o^2}{A_{square/hexagon}}$$

So for triangular pitch arrays:

$$f = \frac{\pi}{2\sqrt{3}} \left(\frac{d_o}{d_T}\right)^2 \qquad (2.1.23)$$

and for square pitch arrays:

$$f = \frac{\pi}{4} \left(\frac{d_o}{d_S}\right)^2 \qquad (2.1.24)$$

For an array of round nozzles Martin defines

$$r_{av} = d_o/(4f)^{1/2} \qquad (2.1.25)$$

where r_{av} is the average impact jet radius of a jet in the multiple lance array to be used in heat and mass transfer coefficients. d_o is the nozzle diameter.

Multiple air jets are frequently used in the paper industry to dry paper efficiently and uniformly. Daane and Han (1961) and Huang (1963) report interference effects when the impingement flow of one jet in an array is cut by the spent air flow from a neighbouring jet when both are active as jets. The impinging flow from the jet at the edge of the array suffers most as a result of the accumulation of spent air exhaust flow from all the other jets. Daane and Han define the amount of interference, I, for close-packed arrays as

$$I = \left(A_f\right)_{eff} \quad L/H \qquad (2.1.26)$$

where $(A_f)_{eff} = A_f \cdot C_d$

For values of effective free area, $(A_f)_{eff}$, less than about 0.005 together with values for H/d_o less than about 6 interference will be insignificant. However, as $(A_f)_{eff}$ or H/d_o is increased the jets come relatively closer together and the separate jets begin to overlap, and part of the potential effectiveness of each jet is lost, i.e. interference increases. With low amounts of interference it can be expected that the jets themselves and the important part of the flow immediately after impingement only occupies a small part of the volume under a typical impingement system. This leaves a large amount of space for the flow of spent air towards the spent edge of the system. Daane notes that in his experiments the holes were spaced in an equilateral triangular array to give the most coverage with the least interference.

In a recent article by Goldstein and Timmers (1982) a novel visualisation technique for measuring heat transfer from arrays of impinging jets was employed. A film of liquid crystals coated onto a mylar sheet was used to locate isotherms on a heated surface impinged by gas jets. These contours were used to determine areas of constant heat transfer. The authors used 1 cm diameter nozzles in triangular pitch arrays. H/d_o ratios of 2 and 6 were employed at a constant jet Re of 40,000 for a single jet as well as a 3 and a 7 jet array.

Figure 2.1.5.2 is taken from the authors' paper. Figure 2.1.5.2 (a) and (b) shows that for a single impinging jet a local minimum in Nusselt Number is observed near the centre of impingement (the stagnation point) for $H/d_o = 2$ whereas higher heat transfer coefficients occur at $H/d_o = 6$.

For the array of three colinear jets in Figure 2.1.5.2 (c) and (d) a local minimum is observed for the central jet but not for the outer jets (at $H/d_o = 2$). For the cases illustrated by Figure 2.1.5.2 (e) and (f) the outer jets in both the 7-jet arrays are moved outwards due to crossflow. Hence the maxima in the heat transfer coefficient for these jet arrays occurs away from the geometrical centres of the jet orifices. With these arrays higher heat transfer occurs with the smaller $H/d_o = 2$ spacing than with the larger H/d_o spacing. With multiple jets, flow interaction can cause the mixing-induced turbulence to penetrate further towards the centre of individual jets. This causes the local minimum at the stagnation point to be absent at small H/d_o ratios with the array of seven jets and to occur only for the centre jet with the three co-linear lances.

FIGURE 2,1,5,2 : LINES OF CONSTANT NUSSELT NUMBER FOR IMPINGING HEAT TRANSFER FROM ARRAYS OF JETS (After Goldstein and Timmers)

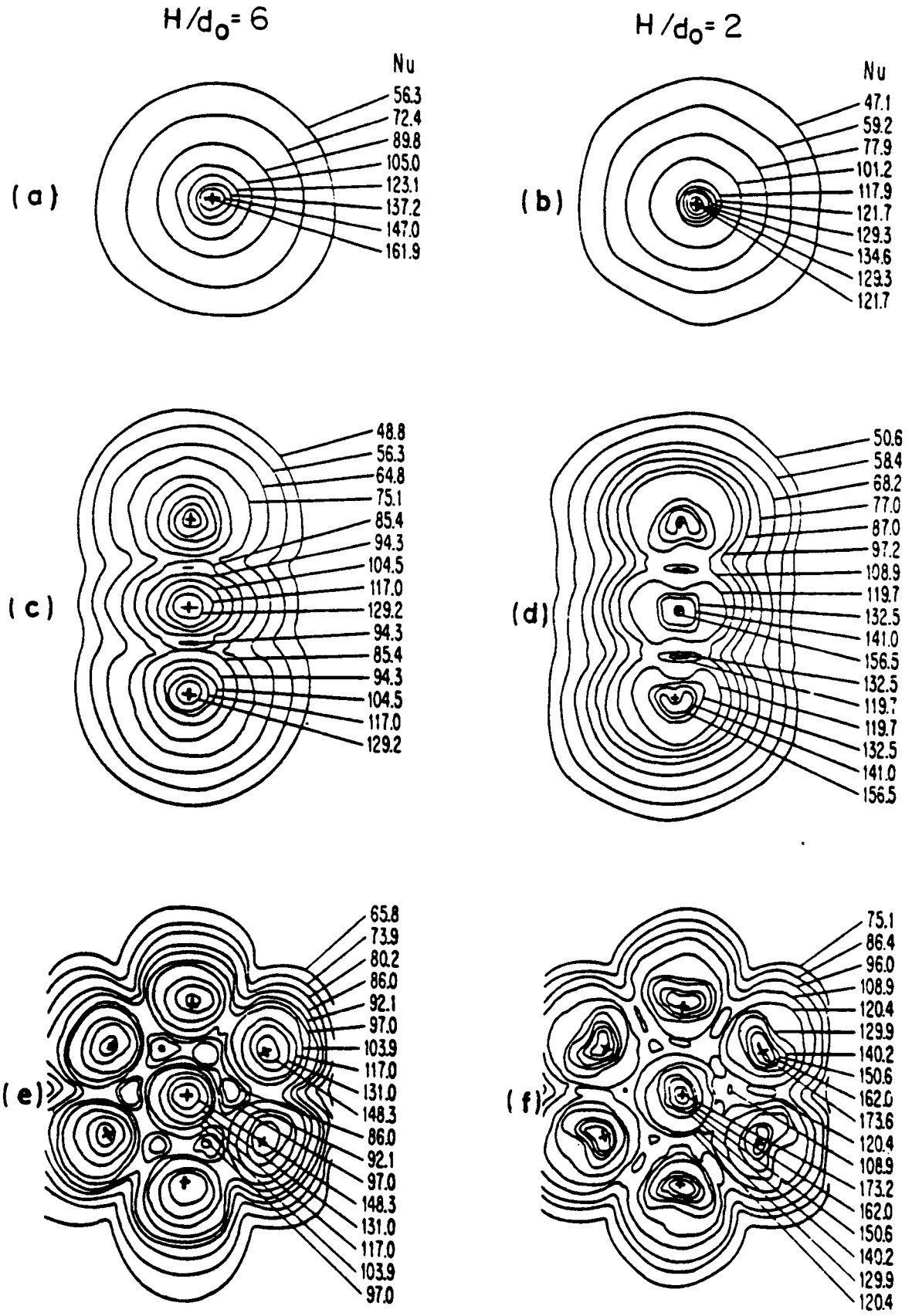

2.1.5.2 The Effect of Containing Vessel Walls on Jet Flow

Several experimental investigations attribute anomalies in experimental results to vessel wall effects. Banks and Chandrasekhara (1963) and Banks and Bhavami (1965) report a scatter in their plane jet results which they ascribe to the proximity of side walls and possible boundary layer formation together with other 3-dimensional effects. Molloy (1970) notes that in the splashing region side walls will reflect droplets back into the entrainment region of the jet. Tuve (1953) reports that when the axis of a jet is too close to a wall the spread of the jet in that direction is reduced.

Abramovich (1963) has shown that the drop in axial velocity of an axially symmetric jet flow in a deadend channel is greater than that for a plane jet flow. For the case of a jet close to a containing wall he states that:

i) a solid wall has little effect on the variation of the jet's thickness.

ii) the velocity along the axis of a jet, which is expanding along a wall in an accompanying flow, dies out significantly more quickly than in the analogous free jet.

Hasimoto (1958) has used a water/mercury model of a top-blown oxygen converter to simulate the flow patterns in the jetting medium. He showed that at low jet momenta (Figure 2.1.5.3) the main body of gases crept along the bath surface and up the walls before exiting the vessel. Some recirculation was apparent. At higher momentum fluxes most of the gas went straight out.

FIGURE 2.1.5.3: CIRCULATION IN A MODEL WITH WEAK BLOWING
(After Hasimoto, 1958)

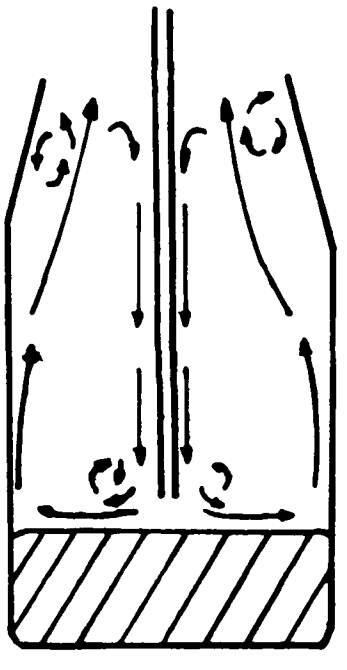

Bacon et al (1960) have studied jet flow patterns in 3-dimensional shapes like a cube, simulating flow patterns in a furnace. The gas flow was shown to circulate around the walls entraining back into the oncoming jet. They discovered that enclosed jets tend to behave initially like free jets but differ in that they do not entrain along the whole of their length. The zone of entrainment is finite dependent upon particular experimental conditions. Both Bacon et al and Barchilon and Curtet (1964) have studied the effect of an axisymmetric jet impinging on surrounding ducting. A typical flow pattern such as Figure 2.1.5.4 was discovered to form. A strong recirculation zone was visible at the wall, the size of this region decreasing with increasing jet velocity.

FIGURE 2.1.5.4: RECIRCULATION PATTERNS ASSOCIATED WITH A CONFINED AXISYMMETRIC JET

(After Barchilon and Curtet, 1964)

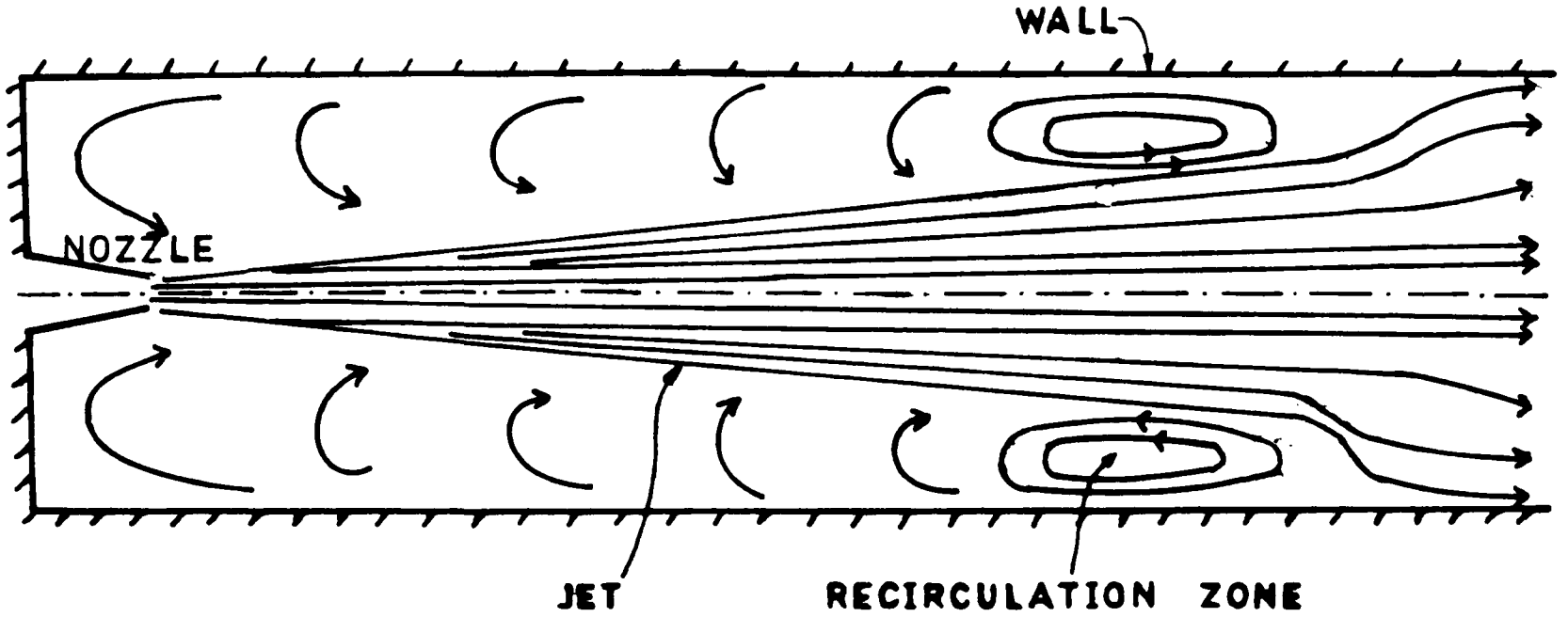

2.1.6 Interfacial Phenomena Associated with an Impinging Gas Jet

Since mass transfer from a gas jet to a molten metallic phase takes place across the surface or interface between the two, this region is very important. At high temperatures, metallurgical reactions tend to be transport controlled since the chemistry is usually very rapid. Although interfacial phenomena have no effect on the equilibria between metals, slags and gases they affect the rates of reactions across interfaces involving these phases. Richardson (1982) outlines three mechanisms that have an effect on mass transfer rates:

i) Surface Blocking

Non-reacting surface-active solutes tend to keep reactants which are less surface-active out of the interface and so retard reactions. They do this by raising the free energy of the reactants in the interface and thereby introduce an additional (chemical) resistance term in the rate equations. Surface-active solutes may either slow down or accelerate mass transfer rates across the interface because of their effects on surface tension.

ii) Damping of Surface Renewal

Surface-active solutes can also damp surface renewal. This effect is produced when circulating eddies from the bulk are exposed to the interface clearing surface-active solutes (of lower surface tension) to either side. The surface tension differences at the new surface are in opposition to the underlying surface renewal circulation patterns thus damping them. This phenomenon may lower mass transfer coefficients by a factor of up to 4 to 5 times that normally expected. Both oxygen and sulphur in liquid iron, for instance, slow down the

rate at which nitrogen can be removed from the melt.

iii) Interfacial Turbulence

Spontaneous interfacial motion occurs in reactions where inequalities of surface tension i.e. gradients, arise over the interface across which the reaction occurs. This effect is known as interfacial turbulence or the Marangoni effect and it is very important because it occurs in the vital interfacial region where reaction takes place. Here again, surface-active solutes act to raise and lower surface tension at different points in the interface due to solute concentration differences causing spontaneous eddies to form. This localised surface eddy movement enhances any convective flows already existing in the liquid phase and thus it increases mass transfer rates.

Both Barton and Brimacombe (1977) and Brimacombe and Weinburg (1972) report that during copper, iron and tin top-blowing studies using oxygen jets Marangoni effects enhance mass transfer by an order of magnitude. However, relatively gentle blowing conditions ($\dot{M} < 5 \times 10^{-4}$ N) were used in the studies. Even so, surface tension gradients were formed between the oxygen-rich central oxide patches (with low surface tensions) and the remainder of the interface. The authors note that this Marangoni effect could markedly accelerate mass transfer in systems already highly stirred by forced convection. This is because the velocities of spontaneous motions at the interface would be sufficiently high as to rival the motion imparted there by top-blowing. It is important to consider that this spontaneous interfacial movement stirs up the liquid region where the resistance to interphase mass transfer is greatest i.e. next to the surface. In addition, the generation of ripples and waves

increases the area of the interface.

Herbertson et al (1983) in a series of carefully controlled non-jetting, kinetic studies using gravimetric techniques found that in oxygen desorption experiments with molten silver, Marangoni effects were apparent. This tended to be more pronounced in the naturally unstable direction of mass transfer, e.g. for oxygen jets, desorption from melts is more unstable than absorption. No interfacial movement was discovered for oxygen absorption tests compared to oxygen desorption tests. Sano and Mori (1974) report similar experimental trends. Baker (1977) in a similar study to Herbertson et al produced completely opposite results but this was probably due to Baker top-blowing in the splashing régime producing uncontrolled mass transfer.

Both of the hydrodynamic effects described in (i) and (ii) above are most significant in weakly stirred systems. Richardson (1982) does acknowledge that to separate the effects caused by simple blocking of the interface with those caused by retardation of surface renewal may be rather difficult. Richardson also notes that effect (i) may be 10 times greater than (ii) and (iii) put together. Elliott (1985) states that the effects of surface and interfacial tension-driven flows at gas-liquid and liquid-liquid interfaces can cause erosion of a refractory container wall. In addition, the relatively high viscosity of many metallurgical slags may tend to suppress interfacial turbulence.

In terms of low temperature modelling of high temperature processes, simulation of interfacial phenomena can be very difficult especially if little information on enhancement or retardation of mass transfer at the interface

in the high temperature situation is available. Moreover, in low temperature analogues density, interfacial tension and adsorption effects are considerably less than the corresponding molten metallic phase that is being simulated. Because of the above reasons no attempt at such a simulation of interfacial effects has been made in this work though the problem is acknowledged here. With regard to the high-temperature poly-metallic smelter, interfacial effects should have a minimal influence on liquid phase mass transfer in the top-blow region during copper matte conversion. This would seem to be justified by Rottmann and Wuth's (1975) single lance copper matte conversion experiments under similar non-splashing ($\dot{M}$ < 0.17 N) jetting parameters to those considered in this work. They found that rates of oxygen mass transfer were close to the theoretical values calculated assuming a smooth surface for air jets and dilute air/oxygen jets. Significant deviations occurred as mole fraction of oxygen in the jets approached 100%, i.e. pure oxygen jets. They attribute this enhanced mass transfer to the fact that the surface of the reaction area is broken up by the SO_2 formed during the reaction, and part of the surface penetrates through the viscous sub-layer of the jet into the bulk jet stream, where it is in a favourable position for mass transfer.

As far as the polymetallic smelter is concerned the only concrete way of checking for interfacial phenomena is to analyse the amount of liquid phase oxygen mass transfer produced during a run. This value could then be compared with theoretical predictions derived from Jones' (1987) correlation (see Section 2.1.8) to reveal if any interfacial effects are present.

2.1.7 Impinging Gas Jet Transport Phenomena

2.1.7.1 Simultaneous Heat and Mass Transfer

When a gas jet strikes a liquid surface three transport mechanisms can occur. These are mass, heat and momentum transfer. In the case of an air jet impinging on water all three occur simultaneously. The transfer of momentum from the jet to the liquid induces a surface renewal circulation pattern in the liquid phase (see Section 2.1.4). This in turn dictates liquid phase mass transfer of the solute under study.

With air jets and water heat transfer may take place either from or to the liquid surface depending on the temperature and humidity of the impinging gas jets. This heat transfer process will involve both latent heat transfer due to vaporisation of water molecules if the jet is unsaturated with moisture (i.e. a mass transfer process is induced) and sensible heat transfer owing to the temperature difference between the air and the water.

If the impinging jet is unsaturated the vapour pressure of water at the bath surface will be higher than the partial pressure of moisture in the gas thus causing water molecules to evaporate from the surface and diffuse into the gas. The latent heat required for this evaporation is initially supplied by the sensible heat present in the surface water layer thus causing it to cool down. As soon as the temperature of this surface water region is reduced below the dry bulb temperature of the impinging gas, heat will transfer from the gas to the liquid, the rate of heat transfer increasing as the temperature gradient increases. Eventually the heat transfer rate from the gas jet to the liquid is equal to that necessary for the evaporation process. In practice this equilibrium is reached very quickly; the temperature the liquid stabilises at is called the "wet-bulb temperature".

All the results in this work have eliminated this problem of mass transfer through simultaneous heat transfer. In line with Lohe's (1966) and Jones' (1986) techniques the present study has involved the adjustment of the gas jet temperature such that the jet's wet-bulb temperature corresponds to the temperature of the water. Over a run the flowing water in the channel model changed little in temperature making temperature adjustment easy. If this adjustment of the gas jet temperature was not implemented then the possibility might arise that the surface temperature might be higher or lower than the bulk liquid temperature thus creating a temperature gradient. Since the interfacial liquid temperature is critical for determining mass transfer coefficients and because only bulk liquid oxygen concentrations can be measured it is imperative that both temperatures are the same. From published data (Handbook of Physics and Chemistry, 1971-72) it is possible to calculate the dry-bulb temperature required for the gas phase knowing the liquid phase temperature and the humidity of the impinging jet. Such a method was utilised in this work.

2.1.7.2 Development of a Theoretical Model for Multiple Gas Jet Liquid Phase Mass Transfer During Channel Flow Including Governing Equations

Nearly all of the previous work into liquid phase mass transfer during top-blowing has concentrated on single lances. The model outlined below is an extension of the single lance theory and it also incorporates a superimposed channel flow rather than the previously considered stationary bath models. Liquid phase mass transfer in a top-blown system may be satisfactorily described by a combination of Whitman's two-film theory (1923, 1924) with resistance to mass transfer limited to a single phase, and a

surface renewal mechanism proposed by Higbie (1935) and subsequently developed by Danckwerts (1955).

Davenport et al (1966) have used both surface renewal and mass transfer theories to develop a model applicable to a single top-blowing jet situation when the gas in the jet is soluble in the liquid phase. They showed that if a radial flow of fluid, close to the surface originating at the centre of the jet depression and deflected downwards by the containing walls is assumed then a mass transfer rate can be derived. Elements of fluid arriving at the surface under the jet depression travel across the liquid close to the interface, mass transfer taking place by diffusion through the thin liquid film in contact with the gas phase. The authors derived theoretical expressions for the mean liquid phase mass transfer coefficients under two fixed conditions, namely:

i) $$k_L = \frac{4}{\sqrt{3\pi}} \left(\frac{U_r \cdot D}{r_b} \right)^{1/2} \qquad (2.1.27)$$

When the liquid surface velocity, U_r, is constant over the whole surface of radius, r_b, and

ii) $$k_L = 2\sqrt{\frac{2}{\pi}} \cdot \left\{ \left(U_r \cdot r \right) \cdot D \right\}^{1/2} \cdot \frac{1}{r_b} \qquad (2.1.28)$$

when the surface velocity is inversely proportional to the radial distance, r, so that the term in parenthesis, $(U_r.r)$, is constant.

A comparison of transfer coefficients calculated from surface velocity measurements with experimentally obtained coefficients from the authors' work indicated that the latter flow régime was in operation. The fact that $k_L \propto D^{1/2}$ is typical of surface renewal systems and it implies that $Sh \propto Sc^{1/2}$.

To determine mass transfer coefficients from experimental data the governing mass transfer equations must relate the interfacial concentration of the transferring species, C_L^i, to the concentration of the transferring species in the bulk liquid, C_L^b. To do this the following assumptions applying to surface renewal systems also adopted by Wakelin (1966), Davenport et al (1966) and Jones (1986) are incorporated into the present model:

1. Equilibrium at the surface is attained immediately.
2. The depth of fluid elements travelling across the surface is infinite which is reasonable if the time of exposure of elements is sufficiently short for penetration to be confined to the surface.
3. Once the fluid elements arrive at the surface in the region of the central depression no further turbulent interaction with the bulk liquid occurs until the element reaches the bath wall, where it once again becomes mixed with the bulk.

The mass transfer model used in this work also includes a moving liquid phase and is thus an extension of the "stationary bath" model reported by a variety of authors e.g. Wakelin, Jones etc. The model is based on Whitman's two-film theory which assumes that resistance to mass transfer lies exclusively in two thin films either side of the interface, one in the gas phase and one in the liquid phase (see Figure 2.1.7.1).

FIGURE 2.1.7.1: Whitman's Two Film Model

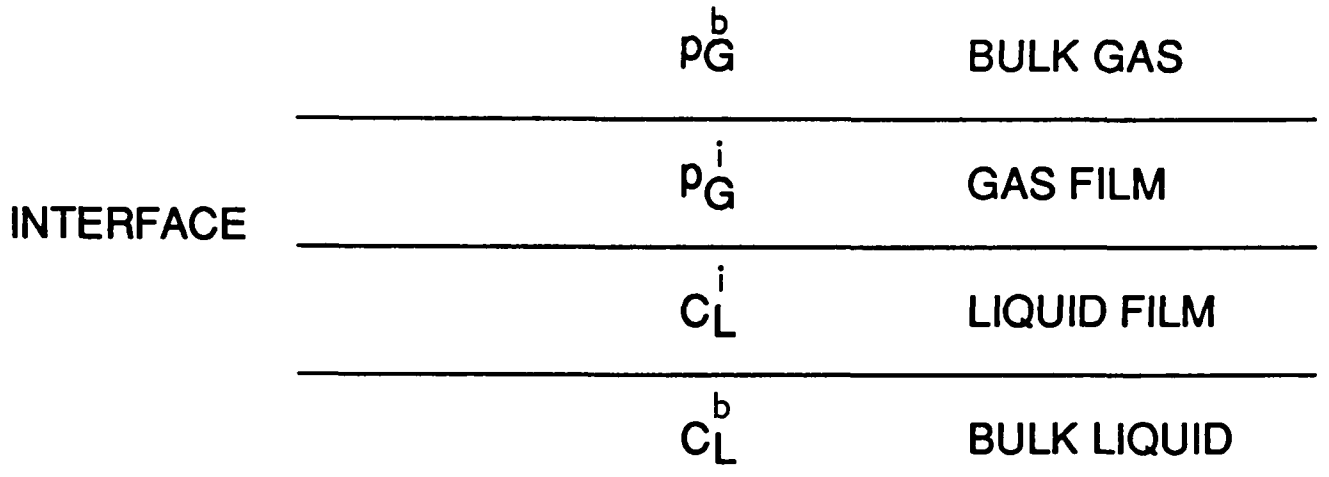

Mass transfer may be described (for gas absorption) by:

$$\bar{n} = \bar{k}_L A \left(C_L^i - C_L^b \right) \qquad (2.1.29)$$

where $\bar{n}$ = rate of oxygen mass transfer over area A, kg/s

$\bar{k}_L$ = mean liquid phase mass transfer coefficient for area A, m/s

A = interfacial area over which the mass transfer occurs (in this study it is the top-blow region), m^2

C_L^i = liquid phase interfacial oxygen concentration, kg/m^3

C_L^b = bulk liquid phase oxygen concentration, kg/m^3

It is the oxygen concentration differential, $(C_L^i - C_L^b)$, that is the driving force for mass transfer. For the water model, the equilibrium concentration of oxygen in water at the interface is related to the partial pressure of oxygen in the gas phase by Henry's Law:

$$C_L^i = p_L^i/H \tag{2.1.30}$$

where H is Henry's constant.

During the diffusive absorption of a soluble gas into a flowing liquid phase being top-blown by one or more gas jets the following equations are applicable (refer to Figure 2.1.7.2 for definition of symbols):

$$\dot{n} = k_L\left(C_L^i - C_L^b\right) dA \tag{2.1.31}$$

and

$$\dot{n} = Q_L . dC_L^b \tag{2.1.32}$$

Equation 2.1.31 gives the rate of mass transfer between the bulk liquid and the surface over incremental area dA.

Equation 2.1.32 gives the bulk liquid mass transfer change in the moving increment as it passes under the area dA.

where k_L = Liquid phase mass transfer coefficient (m/s)

$\dot{n}$ = Solute mass transfer rate (kg/s)

Q_L = Volumetric water flowrate through the top-blow region (m^3/s)

and A = top-blow area (m^2).

Equating equations 2.1.31 and 2.1.32 and integrating gives:

$$k_L\left(C_L^i - C_L^b\right) dA = Q_L d\, C_L^b$$

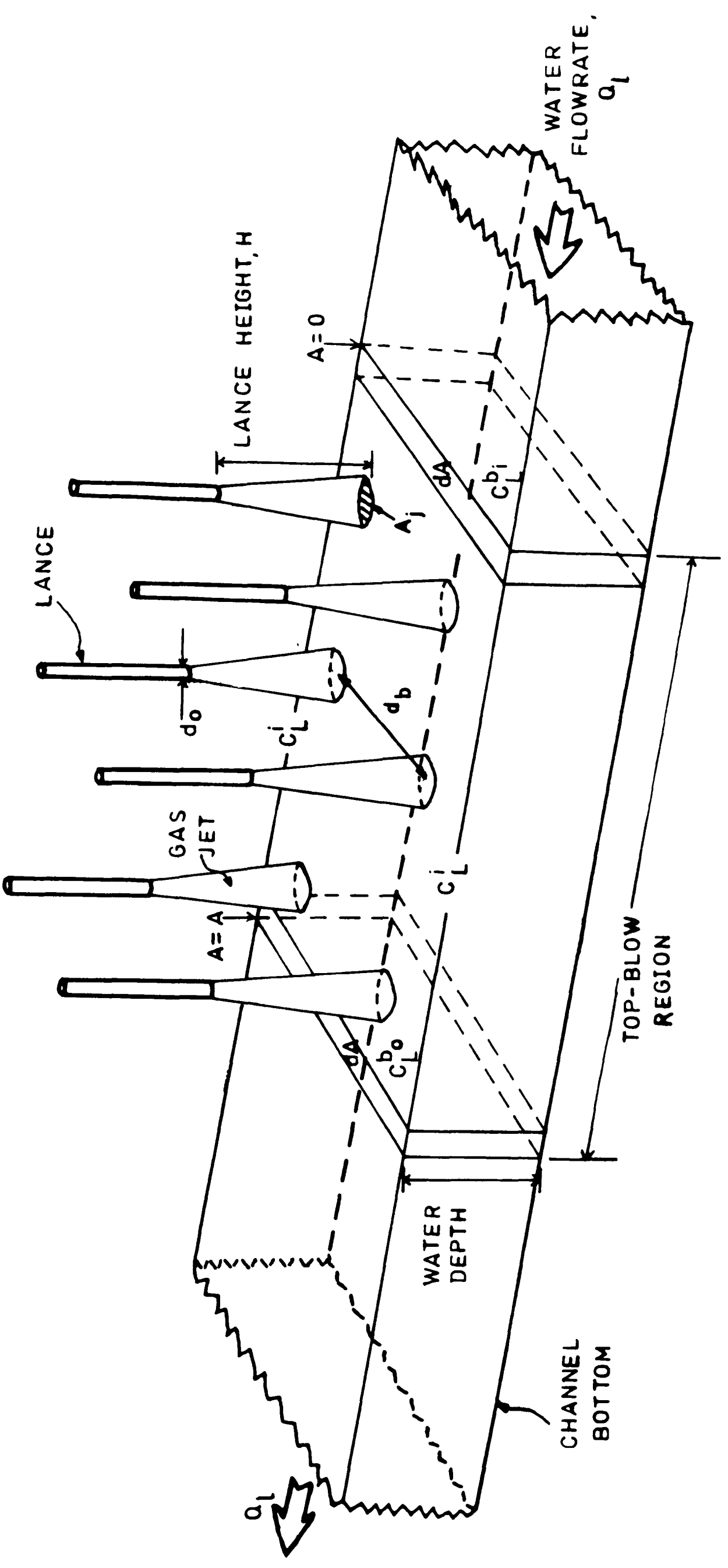

FIGURE 2.1.7.2 : LIQUID PHASE MASS TRANSFER MODEL

$$\int_0^A k_L \, dA = \int_{C_L^{b_i}}^{C_L^{b_0}} \frac{Q_L \, d\, C_L^b}{C_L^i - C_L^b}$$

where C_L^i is constant

hence

$$-\frac{k_L A}{Q_L} = \left[\ln\left(C_L^i - C_L^b \right) \right]_{C_L^{b_i}}^{C_L^{b_0}}$$

and

$$k_L A = Q_L \ln \left(\frac{C_L^i - C_L^{b\,i}}{C_L^i - C_L^{b\,0}} \right) \qquad (2.1.33)$$

$k_L A$ provides an estimate of overall liquid phase volumetric mass transfer in the top-blow region.

The experiments considered in this work utilise liquid phase desorption of oxygen from water as a mass transfer analogue of the smelter situation where oxygen is absorbed into the flowing matte phase. For both situations

mass transfer of oxygen from one phase to the other is liquid phase diffusion controlled, i.e. nearly all the resistance to mass transfer lies in the interfacial liquid film. The majority of experiments in this work involve superoxygenating a flowing water phase (relative to the normal 10 ppm oxygen inherent in water) and then desorbing the oxygen from the liquid phase via top-blown air jets. A typical experimental run, AOD.1b, is illustrated by Figure 2.1.7.3.

For each experimental run channel flowrate and jetting parameters are set and readings for $C_L^b i$ and $C_L^b 0$ are taken. These, together with a water temperature reading, which gives a value for C_L^i, provide enough information to calculate $k_L A$ for the system at any time during the desorption process, using Eq. 2.1.33. As the water flows in the channel and before the jets are turned on there is a certain amount of natural desorption from the superoxygenated water to atmosphere (as it passes through the top-blow region) equal to $C_L^b i - C_L^b 0$. Once the jets are switched on the downstream bulk liquid phase oxygen reading takes a few minutes to reach steady state. The quantity of desorption produced represents a combination of natural desorption and the forced desorption associated with the top-blown jets and the induced surface renewal they create in the liquid phase. The mass transfer due to the jets alone is thus the difference between the mass transfer at T = steady state and that when the jets are just switched on (T = 0). Hence equation 2.1.33 can be used twice for each component to give:

$$\left(k_L A\right)_{JETS} = \left(k_L A\right)_{T = St.\ St.} - \left(k_L A\right)_{T = 0}$$

which after rearranging gives

FIGURE 2.1.7.3 : TYPICAL EXPERIMENTAL TOP-BLOW RUN GRAPHICAL PLOT, RUN No. AOD.1b

($\dot{M}$=0·15 N, d_o=2·26mm, X=35, H=20cm, Q_L=1·0m^3/hr, Q_g=1320l/min, d_b=74.2mm, Close-Packing)

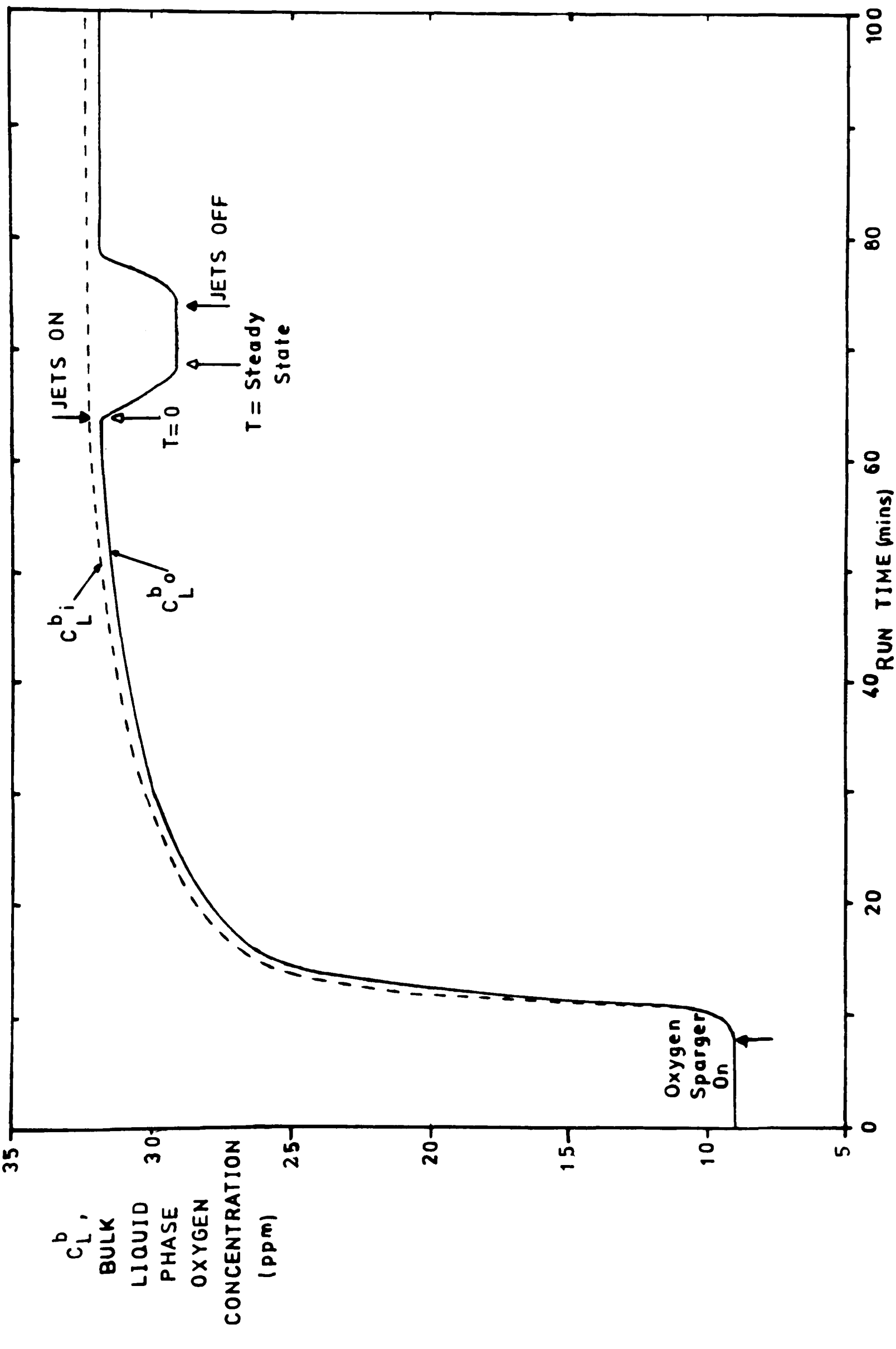

$$\left(k_L A\right)_{Jets} = Q_L \ln \left\{ \left(\frac{C_L^i - C_L^b i}{C_L^i - C_L^b 0} \right)_{T = \text{steady state}} \Big/ \left(\frac{C_L^i - C_L^b i}{C_L^i - C_L^b 0} \right)_{T=0} \right\} \qquad (2.1.34)$$

Jones (1986) defines for his multiple lance runs the following relationship:

$$\left(k_L A\right)_{Jets} = X.k_{Lj} \,.\, A_b \qquad (2.1.35)$$

where, k_{Lj} is the mass transfer coefficient per lance in a multiple lance array,

X is the number of lances,

and A_b is the area associated with a circle of diameter d_b where d_b is the interlance spacing. Note that A_b is equal to A_j, the jet impact area, for close-packed arrays.

In a similar manner the mass rate of mass transfer over the top-blow region during desorption, $\dot{n}$, can be estimated by subtracting the natural desorption component from the steady state component obtained from Equation 2.1.32:

$$\left(\dot{n}\right)_{Jets} = Q_L \left\{ \left(\Delta C_i - \Delta C_o\right) T = \text{steady state} - \left(\Delta C_i - \Delta C_o\right) T = 0 \right\}$$

where $\Delta C_i = C_L^b i - C_L^i$

and $\Delta C_o = C_L^b o - C_L^i$

or

$$(\dot{n})_{Jets} = Q_L\left\{\left(C_L^b i - C_L^b 0\right)T = \underset{\text{state}}{\text{steady}} - \left(C_L^b i - C_L^b 0\right)T = 0\right\} \quad (2.1.36)$$

All liquid phase equilibrium and physical data for the oxygen/water system used throughout this study are included in Appendix 1 together with experimental results in Appendix 2.

2.1.8 Similarity Criteria for High and Low Temperature Top-Blowing Systems: DImensionless Correlations

Due to the difficulties involved with producing good top-blowing mass transfer data in small scale high temperature experimental systems it is desirable to produce a suitable dimensionless correlation. Dimensionless correlations are empirical plots that bring together physical variables for dynamically similar high and low temperature systems in the form of dimensionless groups. The advantages of this technique are that it is independent of any system of units and it gives a useful first order approximation to what will happen in a complicated high temperature heat and mass transport system.

Jones (1986, 1987) has successfully used this dimensional analysis technique to correlate his own low temperature data, low temperature data from Chatterjee and Bradshaw (1972) and high temperature data from Chatterjee et al (1972), Rottmann and Wuth (1975) and Baker (1977). His correlation is illustrated in Figure 2.1.8.1 together with scatter limits. His approach reconciles the fact that though there is a large temperature difference between room temperature and smelting temperatures the fundamental transfer mechanisms are the same. It must be emphasized that all the data used in developing the correlation comes from stationary bath experiments with the jetting parameters lying in the non-splashing mode. Each dimensionless group used in the correlation is defined in the nomenclature.

The SHERWOOD NUMBER, Sh, represents mass transfer in the liquid phase and incorporates the mass transfer coefficient.

The SCHMIDT NUMBER, Sc, represents the physical properties of the system.

FIGURE 2.1.8.1 : JONES' LIQUID PHASE MASS TRANSFER CORRELATION (1987)

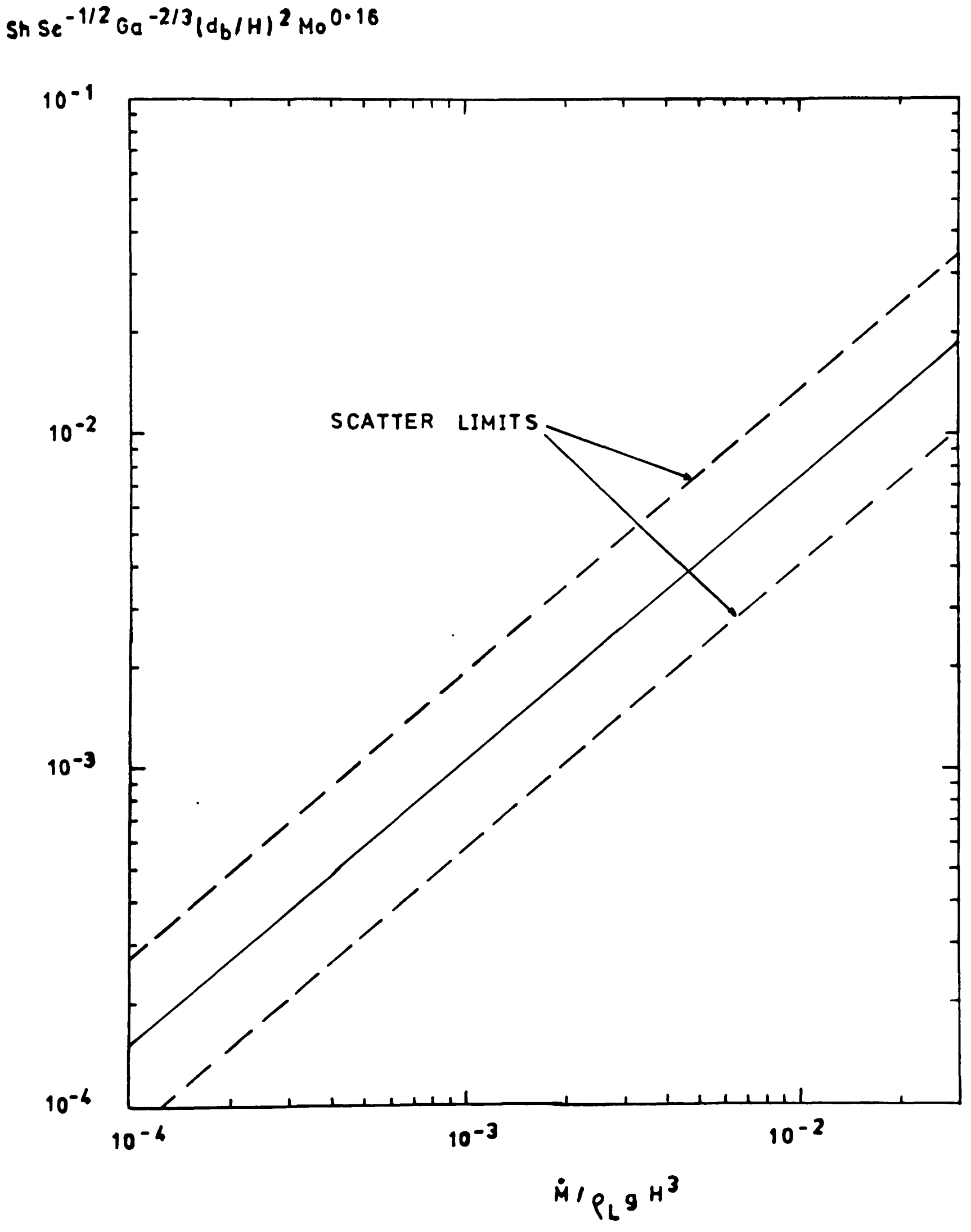

The GALILEO NUMBER, Ga, represents conditions of fluid flow in the liquid phase and incorporates the effects of inertial, gravitational and viscous forces acting in the liquid.

The MORTON NUMBER, Mo, represents the effect of surface tension in the liquid phase.

Lohe (1966) also attempted a similar dimensionless correlation to Jones though he only used his own data and it is thus not as comprehensive as Jones' work.

2.2 CONDENSATION AND FOG FORMATION THEORY

2.2.1 Condensation Under Normal Atmospheric Pressure

2.2.1.1 Pure Saturated Vapours

When a pure saturated vapour is brought into contact with a cold surface that has a temperature below the vapour's saturation temperature a film (or in certain cases, droplets) of condensate is (are) produced. Nusselt in 1916 was the first to develop mathematical expressions in the form of heat and mass balances to derive the following theoretical equation. It yields a value for the heat transfer coefficient of a pure vapour condensing as a film on a horizontal tube:

$$h_{Nu} = 0.725 \left[\frac{K^3 \rho_L^2 \lambda_g}{D \Delta t \mu_L} \right]^{1/4} \qquad (2.2.1)$$

where

$$q_c = h_{Nu} A \left(t_v - t_w \right) \qquad (2.2.2)$$

Since Nusselt assumed that the rate controlling step during condensation is heat conduction through the condensate then the interfacial vapour/liquid temperature is inferred to be equal to that of the bulk vapour. Nusselt also confined his analysis to a pure, quiescent, saturated vapour condensing on an isothermal surface. Hence, his equation is restricted to a limited number of applications where the above conditions are satisfied.

Various authors in this field (Minkowycz, 1966; Denny et al, 1971) do use Nusselt's theoretical heat transfer rates as a comparison against their experimental or calculated heat transfer rates for non-ideal conditions.

2.2.1.2 Vapour/Inert Gas Mixtures

Industrially, the most common condensable mixture tends to be a vapour/inert gas mixture, the inert gas usually being air. The presence of even small amounts of noncondensing inert gas with a condensing vapour will seriously reduce the rate of condensation. This is because the condensate surface is blanketed by a vapour/gas mixture in which the concentration of vapour is lower than that in the main body of the mixture. There have been numerous studies in this field, the pioneering work being that by Colburn and Hougen (1934). They considered the case of a saturated vapour/inert gas mixture condensing and duly derived a trial-and-error technique to determine condensing surface area requirements.

The authors showed that heat flows from the vapour in the mixture to the cold surface during condensation by two parallel routes. First, because of the temperature gradient across the gas film sensible heat is transferred to the condensate surface by conduction-convection processes, and secondly, since the concentration (partial pressure) of the vapour in the main stream is greater than that in the gas film at the condensate surface, vapour molecules diffuse to the surface releasing their latent heat. The actual rate of condensation is then determined by a combination of these two effects. When the amount of noncondensing gas is small the sensible heat effect is negligible since nearly all the heat carried from the gas phase to the

condensate is by the latent heat of condensation. On the other hand, when the mixture is largely depleted of condensable vapour the sensible heat component will be a significant part of the total. Hence, the rate of condensation is diffusion controlled due to the presence of the inert gas.

Figure 2.2.1.1 illustrates schematically the overall situation being considered. Colburn and Hougen's method required the rigorous solution of equation 2.2.3 which quantitatively equates the heat flow to the condensate surface (from the condensing vapour) to the heat flux carried away from the surface (by the cooling medium) at any point in a condenser:

$$q_S + q_L = q_C = U \cdot \Delta t_{ov}$$

$$h_g\left(t_v - t_c\right) + k_g \lambda \left(p_v - p_c\right) = h_{comb}\left(t_c - t_{cm}\right) \qquad (2.2.3)$$

where

$$A = \int_0^{q_T} \frac{dq}{U\Delta t_{ov}}$$

This solution requires the choice of several vapour/gas mixture conditions (t_v, p_v) within the condenser. At each point corresponding values of interfacial vapour temperature and pressure are deduced by a trial-and-error solution of both sides of equation 2.2.3; all other variables being estimated. At each point both the heat flux, U Δt_{ov}, and the rates of

FIGURE 2.2.1.1: SCHEMATIC DIAGRAM OF TYPICAL PROFILES OF PARTIAL VAPOUR PRESSURE AND TEMPERATURE NEAR A CONDENSER WALL WHEN CONDENSING A VAPOUR/GAS MIXTURE

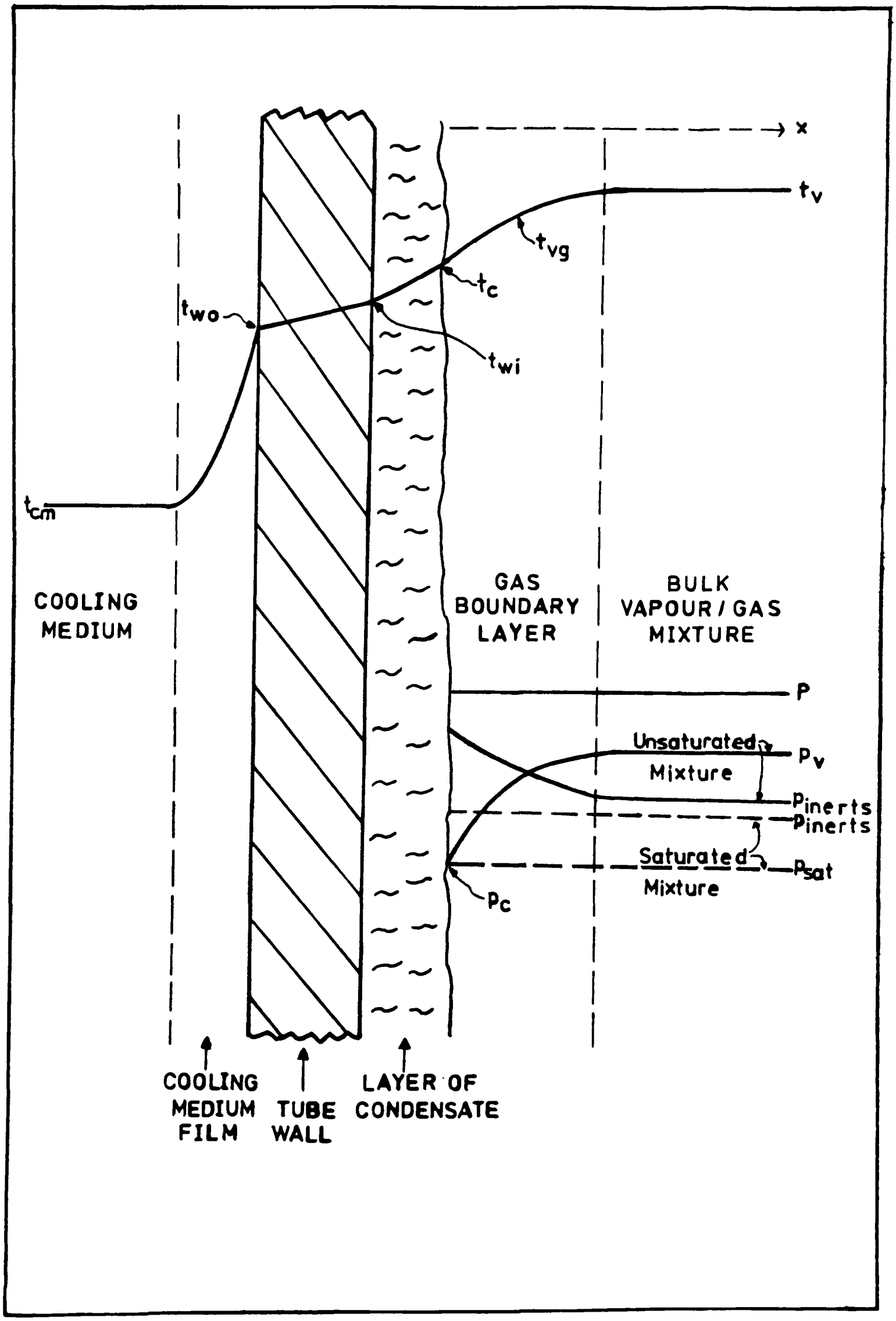

heat transferred can be determined from the above solution. When all the values of $1/U\Delta t_{ov}$ are plotted against the values for q, the heat transferred, the area under the curve (by any numerical technique) yields an estimate for the condenser area.

For the case where the vapour/gas mixture entering a condenser is unsaturated Bras (1953a, 1953b) has extended Colburn and Hougen's technique. He used a direct graphical solution on a pressure/temperature diagram as shown by Figure 2.2.1.2. The diagram depicts both the driving forces for sensible heat and mass transfer, namely, (t_v INLET - t_c) and (p_v INLET - p_c) respectively. Bras theoretically proved that the line between the inlet vapour/gas condition and the condensate interfacial condition is not a straight line, rather, it is a curve. This operating line has a slope given by equation 2.2.4:

$$\frac{dp_v}{dt_v} = \left(\frac{P - p_v}{p_{BM}}\right)\left(\frac{Pr}{Sc}\right)^{2/3}\frac{\left(p_v - p_c\right)}{\left(t_v - t_c\right)} \qquad (2.2.4)$$

Hence if the condenser inlet condition, 1, is known a corresponding condensate interfacial condition, 1', can be obtained from equation 2.2.3. A tie-line between the two points will have a slope dp_v/dt_v and will represent with little error the change in the vapour/gas condition for a small section of the condenser at the inlet. Point 2 is then chosen arbitrarily depending on how accurate one wishes to be. Point 2 will have an equilibrium condition of 2' which will be sufficiently different from 1' to warrant recalculation of the slope of the operating line and the driving force (t_v - t_c). The process is repeated through points 3, 4 and so on until the gas outlet condition, (t_v,

FIGURE 2.2.1.2 : DRIVING FORCES (a) AND STEPWISE CALCULATION PROCEDURE (b) FOR A CONDENSER

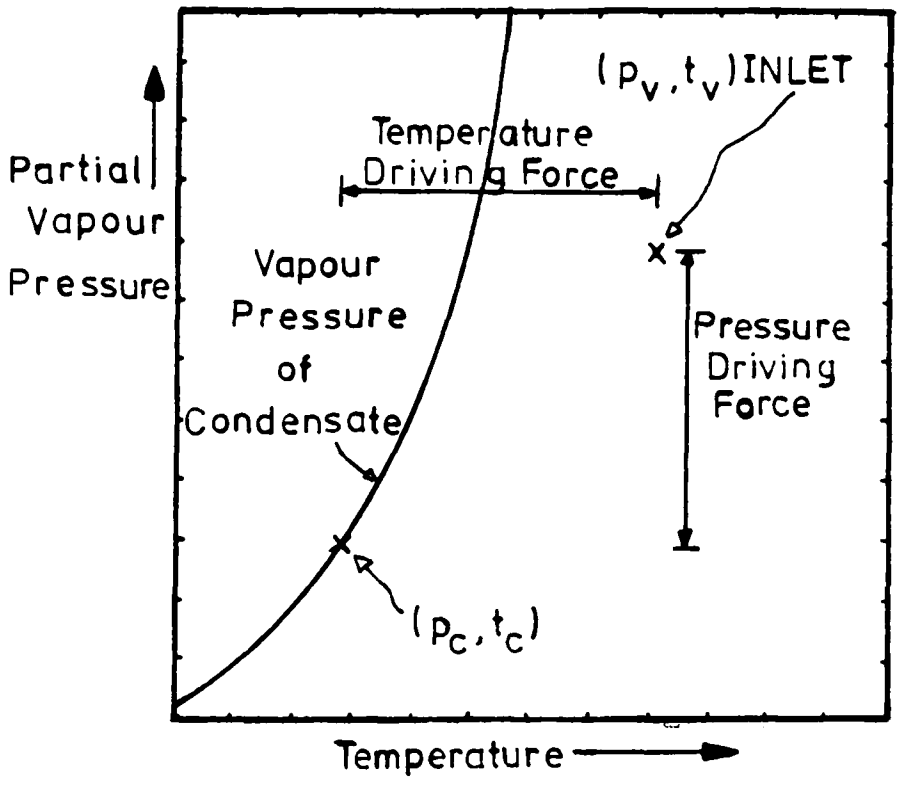

(a)

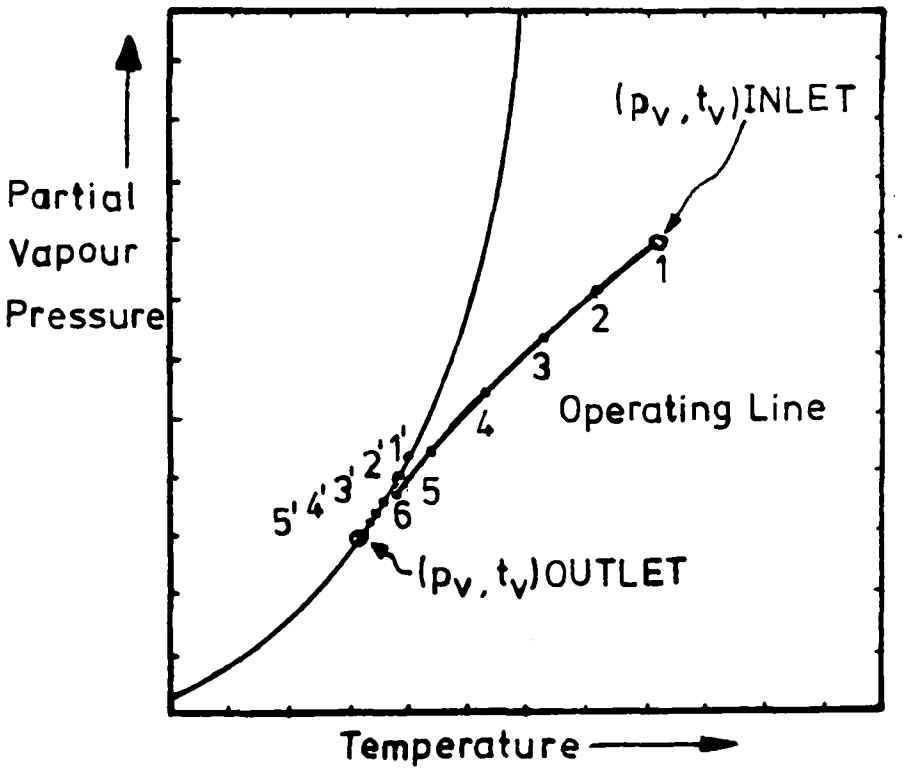

(b)

p_v) OUTLET, is reached. Meanwhile, at each point values for U Δt_{ov} and q will have been obtained so that a similar graphical technique to that proposed by Colburn and Hougen will produce a value for condenser area, A.

Since the early work by Colburn and Hougen and later extensions by Bras there have been numerous experimental investigations into the condensation of vapour/inert gas mixtures such as Cairns (1953), Levine et al (1960) and Schrodt et al (1965). Various workers have utilised simplifying assumptions to solve the Colburn and Hougen/Bras equations such as Bras (1956; 1954) and Cairns (1954). Several authors have attempted computer solutions of the transport equations to provide quick and accurate estimates of the required condenser size such as Franks (1960) and Denny et al (1971). Both Denny et al (1971) and Emerson (1974) note that the retardation of heat transfer due to the presence of noncondensables is most marked for low vapour velocities and large inert gas concentrations.

In an article by Mori et al (1977), the coworkers show that when the molecular weight of the vapour is very much greater than the noncondensable gas (or vice versa) a state of separation between the two constituents will occur. The larger the difference between the two the greater will be the resulting heat transfer fluxes. Balekjian and Katz (1958) have reported the actual thickness of the interfacial condensate film to be of the order of a molecular mean free path.

Recently, several Russians (Ivanov, 1962; Amelin, 1967 and Lekae et al, 1981) have studied this vapour/gas condensation phenomenon deriving new theoretical analyses which fit their experimental data. The work reported by Lekae et al on sulphur/inert gas condensation is noteworthy because of the high molecular weight of the condensing sulphur molecules

which make it comparable to high molecular weight condensable metallic vapour/inert gas mixtures.

2.2.1.2.1 High Vapour Concentrations

An early experimental investigation by Othmer (1929) reported that when only 0.5% air was present in a mixture with steam the heat transfer coefficient was half that for pure steam. Meisenburg et al (1935) correlated their data for steam/air condensable mixtures containing 0.10 to 4.00% air by a modified Nusselt equation.

$$h_{Nu} = 0.670\left[\frac{k^3 \rho_L^2 \lambda g}{D \Delta t \mu_L}\right]^{0.25} \left(\frac{1}{C}\right)^{0.11} \qquad (2.2.5)$$

where C is the concentration of air in the mixture (mass fraction).

It must be pointed out that the rigorous Bras method will take account of high vapour concentrations as observed by Mizushima et al (1959). These authors do, however, approach the high vapour concentration problem from a different angle by using an enthalpy/temperature diagram for the process. This technique was simplified further by Sadamoto (1964) and compared with the Colburn and Hougen/Bras method.

The Australians, Cairns and Roper (1955, 1954) considered simultaneous heat and mass transfer during the operation of an adiabatic wetted-wall column. They demonstrated that at high vapour concentrations the normal Chilton-Colburn j-factor equations beak down. Instead, by an

empirical correlation of high humidity data they deduced a new j-factor for mass transfer.

$$j_D = \left(\frac{k_g p_{BM} M}{G}\right) Sc^{2/3} \left(\frac{p_{BM}}{P}\right)^{-0.17} \qquad (2.2.6)$$

together with new j-factors for heat transfer for the instances of co-current and countercurrent contact between humid air and a falling water film:

$$j_H = \left(\frac{h_g}{C_p G}\right) Pr^{2/3} \left(\frac{p_{BM}}{P}\right)^{-0.22} \Big/ \left(1 + \frac{a}{2}\right) \qquad (2.2.7)$$

(CO-CURRENT CONTACT)

and

$$j_H = \left(\frac{h_g}{C_p G}\right) Pr^{2/3} \left(\frac{p_{BM}}{P}\right)^{-0.27} \qquad (2.2.8)$$

(COUNTERCURRENT CONTACT)

Sparrow, Minkowycz and Saddy (1967) have predicted a quick build-up of noncondensing gas at the interface during high rates of vapour condensation. The interfacial mass fraction of the noncondensable may exceed the free stream value by a factor of 10 to 20.

2.2.1.2.2 Metallic Vapours and the Effect of Interfacial Thermal Resistance

Several investigators have studied the condensation of metallic vapours under atmospheric pressure notably Misra and Bonilla (1956), Sukhatma and Rohsenow (1966), Turner (1971), Huang (1971) and Turner et al (1973). All report large reductions in heat transfer during condensation when small amounts of noncondensable gas infiltrate the condensing vapours. Turner et al, however, do state that the problem can be alleviated if high vapour velocities past the condensation surface are utilised. Turner (1971) also indicates that for condensation of liquid metals the temperature drop across the condensed liquid film is very small due to the high thermal conductivity of metals. Low Prandtl Number liquids like molten metals have been shown to have heat transfer rates 5-15% of that predicted by Nusselt's classical theory (Misra and Bonilla, 1956). Huang (1971) reports that the presence of a noncondensable gas is less important in steam or organic vapours than in heavier metal vapours.

A solution for the problem of low observed heat transfer rates during the condensation of metallic vapours has been suggested by several investigators (Schrage, 1953; Sukhatma and Rohsenow, 1966). They attribute the reduction partly to an interfacial resistance resulting from the fact that the net condensation of vapour at the interface is actually between the simultaneous processes of evaporation and condensation. The kinetic theory of gases indicates that an imbalance between these two processes will exist such that they will be accompanied by a temperature jump at the interface, whence the additional thermal resistance. So, in effect these models state that the saturation temperature of the vapour adjacent to the surface of the condensate is different from the temperature of the liquid at the

surface (the conventional assumption for condensation). Schrage's (1953) equation which Sukhatme and Rohsenow (1966) modify slightly is:

$$\frac{W}{A} = \left(\frac{\alpha}{2-\alpha}\right)\left(\frac{2}{\pi R_v^3}\right)^{1/2}\left(\frac{\lambda p_{sat}}{t_{sat}^{5/2}}\right)\left(t_{sat} - t_c\right) \qquad (2.2.9)$$

where W/A is the interfacial mass flux equal to $(q/A\lambda)$.

α is the condensation coefficient which is less than or equal to unity. For metals, values of α of up to 1 have been reported especially at low pressures (Sukhatme and Rohsenow, 1966), dependent on the purity of the condensate and the presence of oxide films.

Sukhatme and Rohsenow estimated values for the interfacial temperature drop, $(t_{sat} - t_c)$ for water, mercury and sodium at vapour pressures of 760 mm, 100 mm and 10 mm based on a temperature drop across the condensate film of 2.78°C. Their results are reproduced below:

TABLE 2.2.1.1: Temperature Drop at a Liquid/Vapour Interface for $(t_c - t_w) = 2.78^oC$

Vapour	Assumed Value of α	$(t_{sat} - t_c)$, °C, with pressure of		
		760 mm	100 mm	10 mm
Water	1.0 0.04	0.0017 0.0556	0.0056 0.3892	0.0556 2.6688
Mercury	1.0 0.1	0.1668 3.2804	0.8896 16.4576	5.5600 N/A
Sodium	1.0	0.3336	1.5568	10.0080

Table 2.2.1.1 indicates that for any fluid under conditions of a low enough pressure and/or a low value of α, the interfacial resistance can become significant. Other parameters being equal, the drop $(t_{sat} - t_c)$ for a metallic vapour is much higher than that for a commonly used fluid like water. This is primarily due to the fact that

i) for the same pressure, the liquid metal has a much higher saturation temperature

and ii) the liquid metal has a higher thermal conductivity.

It must be remembered that the effect of interfacial thermal resistance on metallic vapour condensation is contributory to the reduction of heat transfer in parallel with that associated with the presence of inert gases in the condensing mixture.

2.2.1.3 Multiple Vapour/Inert Gas Mixtures

The problem of trying to simultaneously condense several vapours in the presence of noncondensables is even more complex than the single vapour case. It is a common problem in the petroleum industry and the first attempt at a quantitative analysis was by Kirkbride in 1933. He considered the condensation of benzene and steam in the presence of nitrogen experimentally and showed that the condensate was not in equilibrium with the main stream of vapour. In 1937, Colburn and Drew considered the problem of mixed vapour condensation taking into account the additional transfer of heat by the unidirectional diffusion of vapour through the gas film (not considered by Colburn and Hougen (1934) - important when vapours are highly superheated). The authors derived the following equation to quantify the rate of change of partial pressure of the vapour with temperature

during condensation (effectively an operating line similar to that derived by Bras - see equation 2.2.4).

$$\frac{dp_v}{dt_v} = \left(\frac{p_v - p_c}{t_v - t_c}\right)\left(\frac{P - p_v}{P_{BM}}\right)\left(\frac{e^a - 1}{a}\right)\left(\frac{Pr}{Sc}\right)^{2/3} \qquad (2.2.10)$$

$$\text{where} \quad a = \left(\frac{Pr}{Sc}\right)^{2/3} \cdot \ln\left(\frac{P - p_c}{P - p_v}\right)$$

The term $(e^a-1)/a$ corrects for the amount of heat conducted to the interface by the diffusion of the vapour. The term is significant at high rates of condensation, that is, when the relative amount of inert gas present is low.

It was not until 1963 that multiple vapour/inert gas condensation was again addressed, this time by Porter and Jeffreys. They considered an ethanol-steam/air (or nitrogen) condensable mixture both theoretically and experimentally. A mathematical and graphical method for predicting the temperature and composition of the condensate at different points on the condensation surface was proposed. Another mathematical model to reconcile this problem was offered by Schrodt and Gerhardt (1965) and Schrodt (1973) to overcome the shortcomings of Porter and Jeffreys' work. They showed that the rate of condensation and the composition of the condensate in a multivapour/inert gas condensation process are functions of the main stream composition, mass transfer coefficients and interfacial temperature. To verify their theory they considered the methanol-water/air and the toluene-ethanol/air systems.

In 1971, Krishna and Panchall studied the methanol-water/air system and formulated a matrix analysis of the interfacial mass transfer rate relations. A film model for multicomponent mass transfer was used to calculate the mass transfer coefficients in the ternary vapour phase. With the aid of a computational example they demonstrated that diffusional interactions can significantly affect condensation rates. Bandrowski and Kubaczka (1981) claimed that their latest model based on an on-going research programme in Poland has solved the problem of multivapour/inert gas condensation. By applying a statistical analysis to all published data in this field they attempt to substantiate this claim. They do point out, however, that their model (as indeed for all the aforementioned models) is only one-dimensional in so far as they neglect the potential complications of vapour forming as fog in the gas phase. Kotake (1985) has analytically studied this same multivapour problem. He set up and solved the governing equations of mass transfer and phase equilibrium of the multicomponent species at the liquid/vapour interface using the perturbation method taking into consideration a small amount of noncondensable gas present in the mixture. He does report that for small temperature differences across the condensate layer, the condensation rate decreases proportionally to the mole fraction of noncondensable gas accumulated at the interface. Emerson (1974) has made a summary of some of the foregoing theories.

2.2.1.4 The Imperial Smelting Furnace Zinc Condenser

An Imperial Smelting Furnace (ISF) treats 40% zinc/20% lead oxide sinter ore feeds in a shaft type furnace to produce lead and zinc simultaneously (Gammon, 1989; Warner, 1970). Hot coke and air produce the gaseous reductant, carbon monoxide, by the following reaction:

$$C\ (s) + CO_2\ (g) = 2CO\ (g)$$

that then reacts to give elemental lead and zinc:

$$ZnO\ (s) + CO\ (g) = Zn\ (g) + CO_2\ (g)$$

$$PbO\ (s) + CO\ (g) = Pb\ (l) + CO_2\ (g)$$

Lead bullion is tapped at the bottom of the smelter together with an iron rich slag. From the top of the furnace gases are volatilised off leaving the shaft at about 1000°C. They contain 7% zinc, 12% CO_2, 20% CO and 61% inerts (mostly nitrogen) together with numerous particulates.

The key to the blast furnace lies with the lead splash 'condensers' either side of the shaft where the zinc vapour is contacted with molten lead droplets splashed up by mechanical rotors. The name 'condenser' is misleading as the principal recovery mechanism is one of absorption. It consists of rectangular brickwork containing a pool of lead 40 cm deep, divided by baffles into four sections each of which contains two rotors (suspended from the roof). It is the lead droplets (< 2 mm diameter) thrown up by the rotors that shock-chill the zinc vapour during absorption preventing any zinc reoxidation. Each of the four sections has lead bullion at different

temperatures and it can be viewed as a four stage condenser unit with lead bullion (containing 2.5% zinc) temperatures of around 610^{o}C, 520^{o}C, 460^{o}C and 450^{o}C respectively. Each stage has a typical transfer efficiency of between 70-80%. During operation of an ISF condenser, between 5-15% of the zinc entering is not collected. It passes through as a combination of equilibrium vapour and zinc fog losses together with reversion losses. These losses appear as a blue oxide fume that is scrubbed from the gas phase and recirculated to the front-end of the furnace. For every tonne of zinc produced 400 tonnes of lead bullion needs to be recirculated. Figure 2.2.1.3 is a schematic diagram of the ISF condenser and plate 2.1 is a photograph of a typical dust sample from the zinc condenser off-gas.

FIGURE 2.2.1.3 PROCESS FLOWSHEET OF THE IMPERIAL SMELTING LEAD/ZINC FURNACE

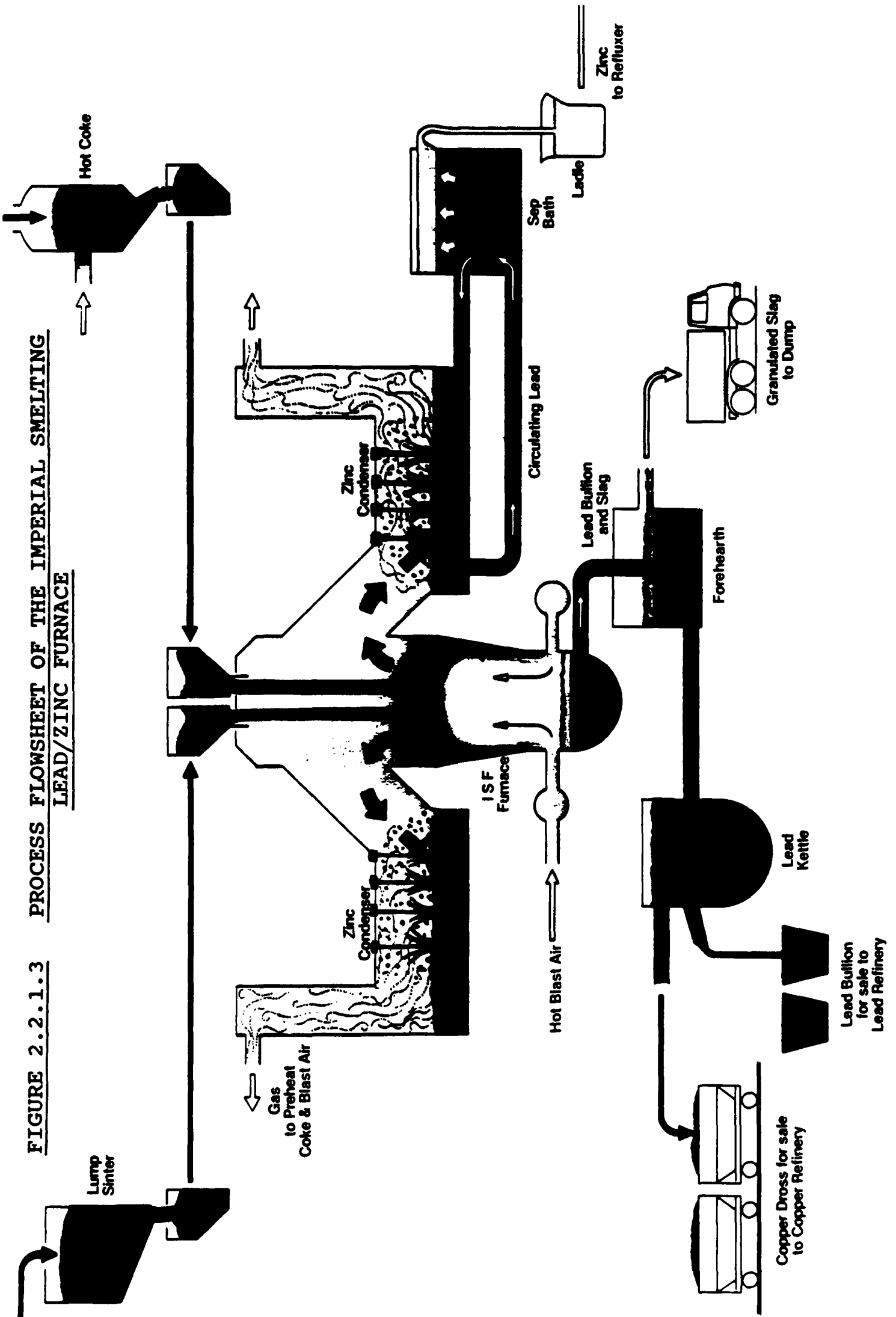

PLATE 2.1

TYPICAL IMPERIAL SMELTING

FURNACE "BLUE DUST"

2.2.2 Condensation Under Vacuum

The use of a vacuum during vapour condensation has distinct advantages in both the condensation of low temperature and high temperature vapours. The condensation of steam under vacuum is common practice in electricity generation in power stations because of thermodynamic advantages. From a metallurgical viewpoint vacuum distillation and condensation plays an important role in the production and/or refining of several metals. The advantages inherent in reduced pressure evaporation over atmospheric evaporation are:

a) the net rate of evaporation is increased as the pressure of inert gas in the system is decreased. In effect distillation of metals from a melt can be effected at a lower temperature than at atmospheric pressure,

b) much better separation of volatile components as the operating pressure is lowered,

c) any contamination by oxidation and unwanted side reactions can be almost avoided,

and d) reduction processes involving a volatile phase may be more efficient or may be operated at lower temperatures if the volatile product is continuously removed (Martin, 1950; Kroll, 1951; Davey, 1962; Warner, 1968; Winkler and Bakish, 1971).

If both the residual gas pressure is considerably reduced and the distance between evaporating and condensing surfaces decreased, so that relatively few interatomic collisions occur in the interspace, a concentration gradient cannot arise, and the rate of distillation is increased considerably. This condition can only be attained in practice in a high vacuum and the

process is known as "molecular distillation". Molecular distillation could be expected to occur if the distillation path, i.e. the distance from evaporating surface to condensing surface, is a fraction of 1 cm. The evaporation of a metal under vacuum is essentially a surface phenomenon due to the metal's high density such that hydrostatic pressures are rarely sufficient for bubble formation. Hence molten metals do not "boil" under vacuum unless very high heat fluxes are applied.

2.2.2.1 Low Temperature Vapour/Inert Gas Studies

Sparrow et al (1967) in their analytical study of vapour/inert gas condensation have noted that the presence of the noncondensable has a greater effect when the condensation takes place at sub-atmospheric pressures. It is made worse if there are high levels of the noncondensable in the mixture. The authors attributed decreases in heat transfer rate to the build-up of noncondensable gas at the interface. This build-up lowers the corresponding partial pressure of the vapour, which, in turn, lowers the interface temperature at which the condensation occurs (assuming the interface is in a saturation state). Hence the thermal driving force, $(t_c - t_w)$, drops and by implication the heat transfer rate.

Shumskii (1962a, b) in Russia has worked on vapour condensation under vacuum especially desublimation of steam to the solid state. He reports that with only 1% air present in a vapour/air mixture condensing to the liquid phase under vacuum it reduces the heat transfer coefficient by 60%. Intrigingly, he asserts (with experimental justification) that the rate of vapour condensation from a vapour/gas mixture below its triple point increases with an increase in the content of air (or other gases) in the gas

phase. He adds that in condensation of vapours to the solid state (as opposed to the liquid phase) there is formed no layer which is saturated with the noncondensing gas. He proposes that the molecules of noncondensing gas arriving at the condensate interface are reflected from the surface like elastic spheres due to their motion. This theory is inadequate, however, as he himself points out since experimentally the rate of desublimation of steam for a given partial pressure in a mixture is higher that that for the pure vapour at the same pressure. To cope with this he suggests that for a given vapour/gas mixture the gas molecules behave like carriers of the vapour molecules, transporting them from the bulk to the interface. He calls these carrier molecules "complex molecules". In an effort to prove his theory he condensed pure steam under vacuum, then a mixture of steam and air under vacuum. The latter produced twice as much condensate, everything else being equal. The author then added that if the condensation is carried out in a heterogeneous electric field (i.e. an ionic condenser) such that the complex molecules become charged then the amount of condensate is eight times that for the pure vapour. Shumskii also gives an equation that provides an estimate for the rate of vapour condensation to the solid state in the presence of noncondensing gases. It must be pointed out that no consideration of potential fog formation was taken into account by Shumskii and his condensation surface temperatures ranged down to - 30^{o}C.

Axe (1972) in America has tackled this same problem of condensation to the solid state. He concludes that both the condensate layer and the noncondensable gas serve as barriers to the transfer of mass and heat, the inert gas being the more significant of the two. Moreover, the rate of heat and mass transfer is dependent upon the amount of noncondensable gas in the diffusion region near the condensing surface rather than the total amount

of gas in the system.

2.2.2.2 High Temperature Metallic Vapour/Inert Gas Studies

2.2.2.2.1 Laboratory and Nuclear Distillation

Besides the metallurgical industry where vacuum distillation and condensation is utilised there has been a sizeable body of research into metallic vapour condensation in connection with nuclear reactors (alkali metals being used as coolant media) (Burnet and Buchanan, 1971). Huang et al (1972) have considered metallic vapour condensation at low pressures and they state that the resistance to heat transfer increases with decreasing vapour pressure. In a room temperature system, for instance, or for non-metallic fluids, this resistance becomes negligible and Nusselt's theory (1916) is a good approximation.

Both Misra and Bonilla (1956) and Turner et al (1973) have studied mercury and sodium vapour condensation under vacuum. Although Misra and Bonilla say that they eliminated all inert gas from their equipment their heat transfer coefficients were significantly lower than predicted. Sukhatme and Rohsenow (1966) have suggested that this was due to the presence of a low level of noncondensables as well as the problem of interfacial thermal resistance (see Section 2.2.1.2.2).

2.2.2.2.2 Industrial Vacuum Dezincing Processes

Over the last fifty years several vacuum dezincing (VDZ) processes have been developed and implemented to either improve lead bullion quality or to produce a separate zinc product.

THE PORT PIRIE VDZ UNIT

The Broken Hill Associated Smelters in Port Pirie, South Australia produce lead bullion from ore feed transported from the Broken Hill Pty. Mines, New South Wales. A semi-continuous VDZ unit was developed and commissioned in the 1950s (Davey and Williams, 1956; Davey, 1962; Dawson, 1989).

The VDZ processing flowsheet and the unit itself are illustrated in Figure 2.2.2.1. The lead bullion prior to VDZ is first heated up to 600^{o}C :it contains about 0.6% Zn. The unit treats between 20-36 tph bullion recovering 90-95% of the dissolved zinc to leave a product with 0.05% Zn at 500^{o}C. To achieve high zinc recoveries with large lead throughputs, the vacuum vessel requires a rapid exposure of a large surface area of lead. As the vessel is relatively small (2.2 m diameter) this is achieved by allowing the lead to spill over a circumferential weir at the top of the vessel so that it is spread in a very thin layer (about 3 mm thick) over a slightly conical spreading surface. The vacuum imposed within the unit is about 20-50 μm and the pumpdown time is 20 minutes.

A conical water-cooled condenser sealed to the top of the chamber with a rubber ring collects solid zinc crystals in the form of acicular dendrites (see Plate 2.2). The typical gap between the evaporation and condensation surface is about 400 mm. The surface temperature of the condenser is maintained at about 30-40^{o}C and the fins on the surface aid in stripping and also increase the condenser's surface area. After 8 hours of operation a 2-3 tonne zinc deposit is formed typically between 50 to 70 mm thick. At this point the vacuum is switched off for a few minutes while the condenser is changed for a new one.

FIGURE 2.2.2.1 PROCESS FLOWSHEET OF THE PORT PIRIE VDZ OPERATION AND EQUIPMENT DESIGN

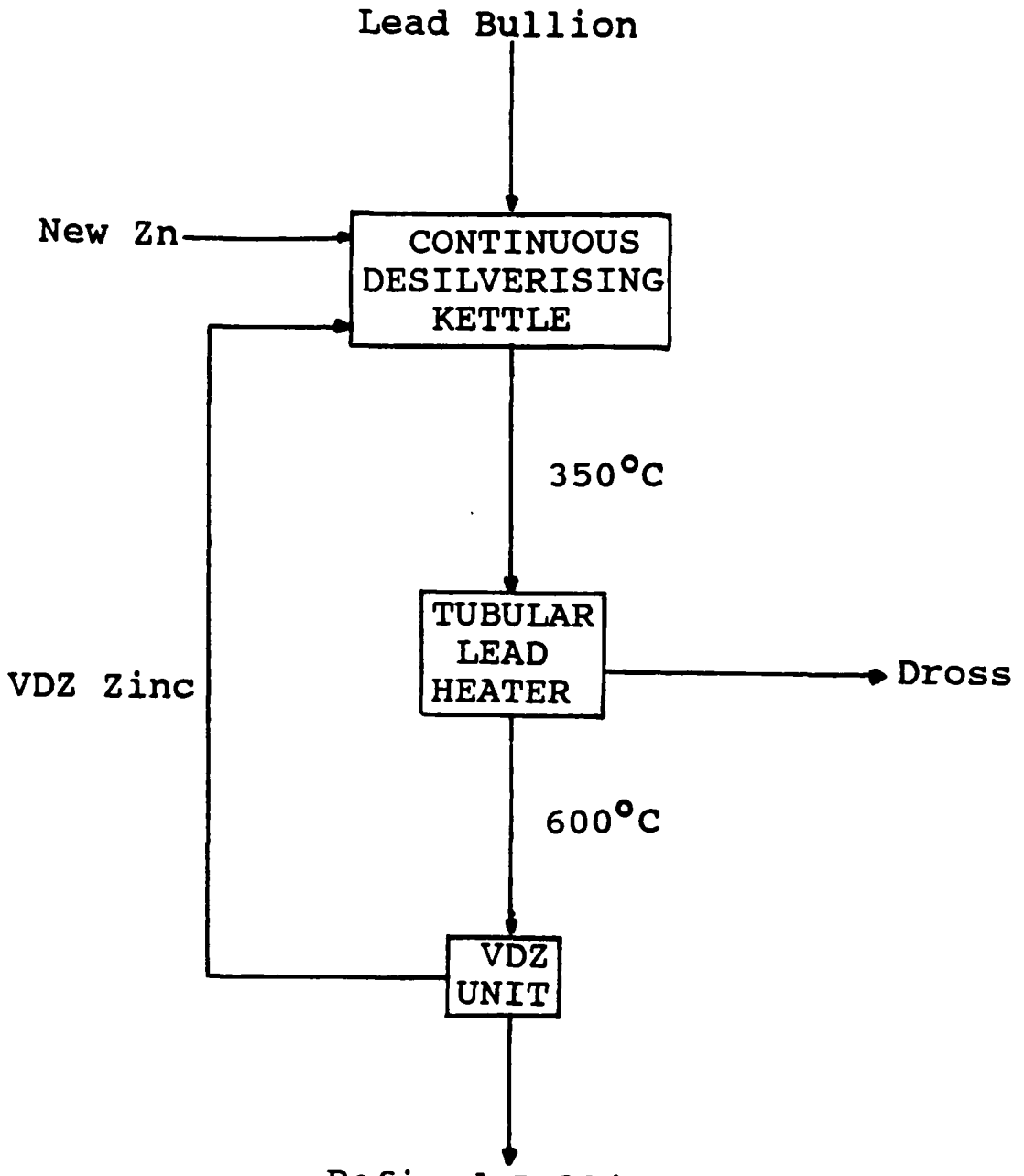

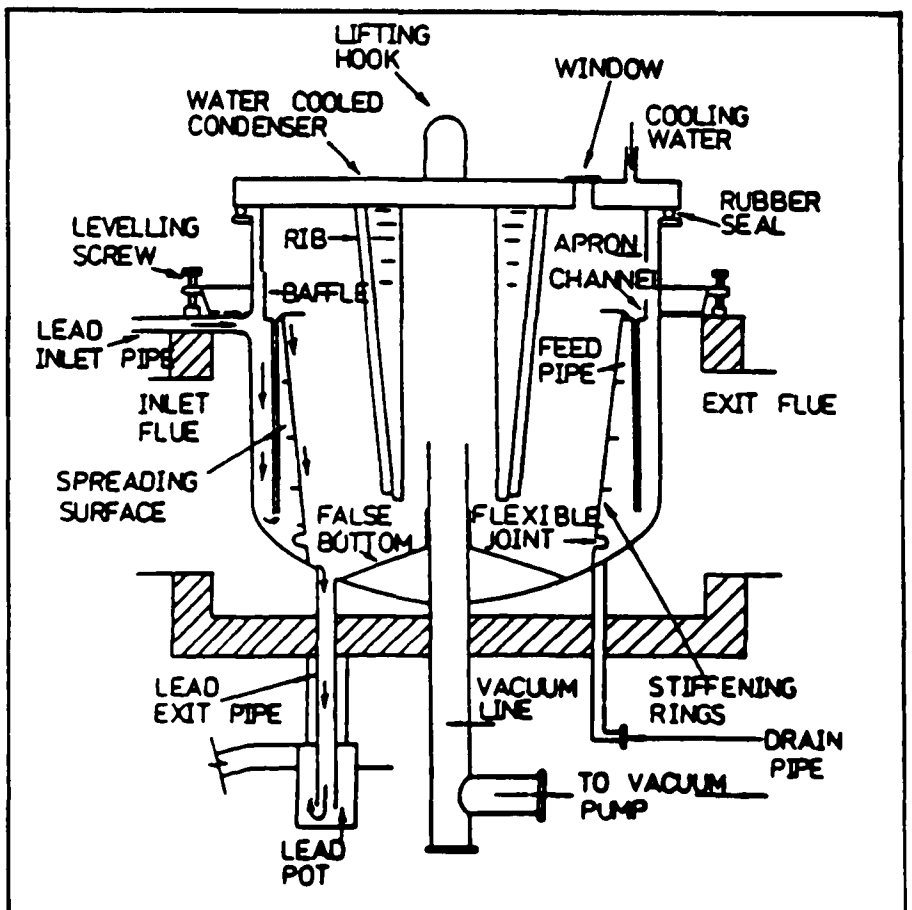

Diagrammatic sketch showing the main features of the continuous vacuum dezincing unit developed at Port Pirie

PLATE 2.2

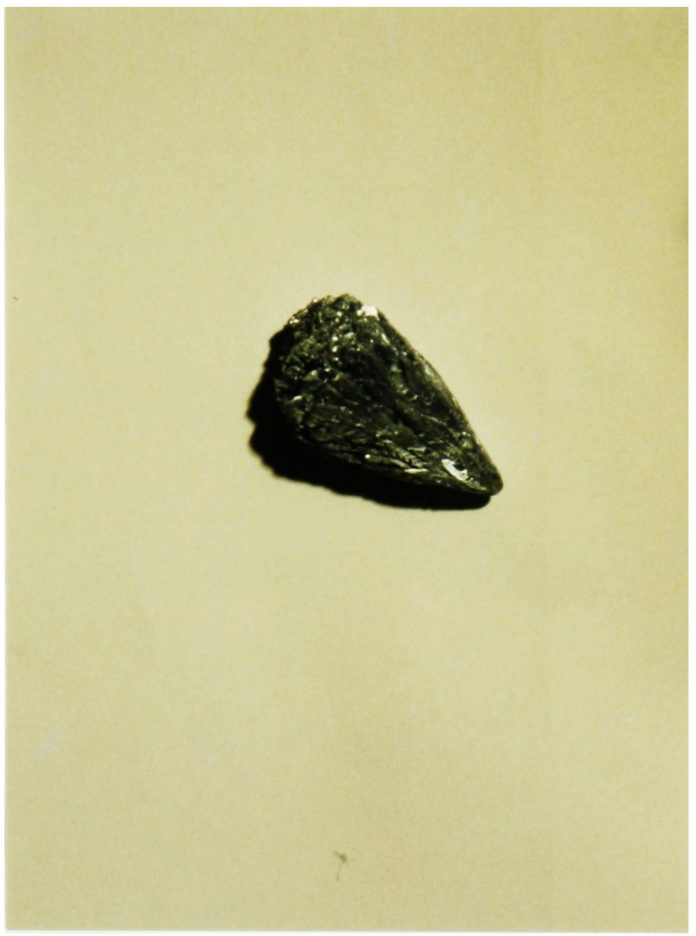

TYPICAL PORT PIRIE VDZ

ZINC DEPOSIT

THE IMPERIAL SMELTING FURNACE CONTINUOUS VDZ UNIT

A considerable body of work (Anon, 1967; Warner, 1968; Herbertson and Warner, 1973) on an operating VDZ unit for use on the Imperial Smelting Furnace has been published. A unit was commissioned at Swansea, S. Wales in 1967 and it ran until 1971 when it was closed. The process flowsheet and the VDZ unit are illustrated in Figure 2.2.2.2. The unit was able to treat 1400 tph lead bullion containing 2.5% zinc at a temperature of 550^{o}C recovering zinc with a purity of 99.9 + %.

Although similar in design to the Port Pirie VDZ unit, a greater throughput was achieved by passing the lead bullion from the top to the bottom of the vessel in a cascade by means of a continuous tray spiral launder. The turbulent flow down the spiral launder created sufficient free surface for zinc evaporation. For this unit the condensation of liquid zinc was effected on a central cylindrical condenser, the surface of which was maintained at the zinc melting point (420^{o}C) by the establishment of a solid zinc layer on the water-cooled core. Indicated vacuums of the order of 100 μm were maintained in the vacuum offtake. The unit produced 3-4 tph zinc and it was a truly continuous dezincing operation.

THE BRITANNIA VDZ PROCESS

Britannia Refined Metals at Northfleet in Kent have developed a batch vacuum dezincing process that is integrated into their lead bullion processing operations (Barrett and Knight, 1985). Figure 2.2.2.3 depicts both the desilverising/dezincing flowsheet for the refinery and a diagram of the actual VDZ unit. The vessel is used ostensibly to recover and recirculate zinc back to the lead bullion upstream unit operation where silver is precipitated out of solution (the Parkes Process).

FIGURE 2.2.2.2 PROCESS FLOWSHEET OF THE IMPERIAL SMELTING FURNACE VDZ OPERATION AND EQUIPMENT DESIGN

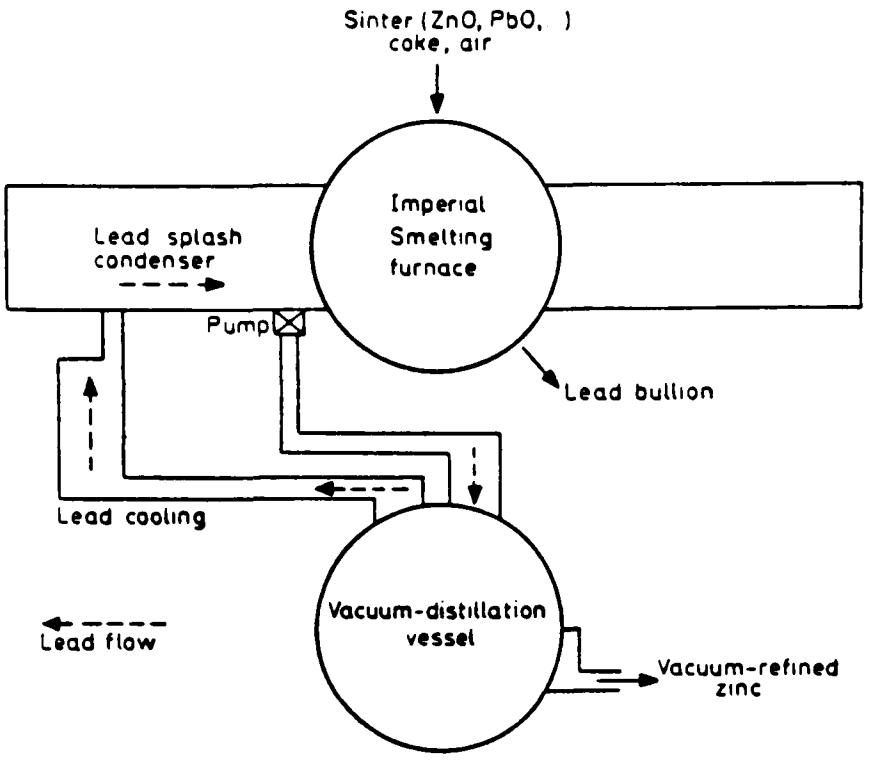

Layout of Imperial Smelting furnace and vacuum-dezincing process

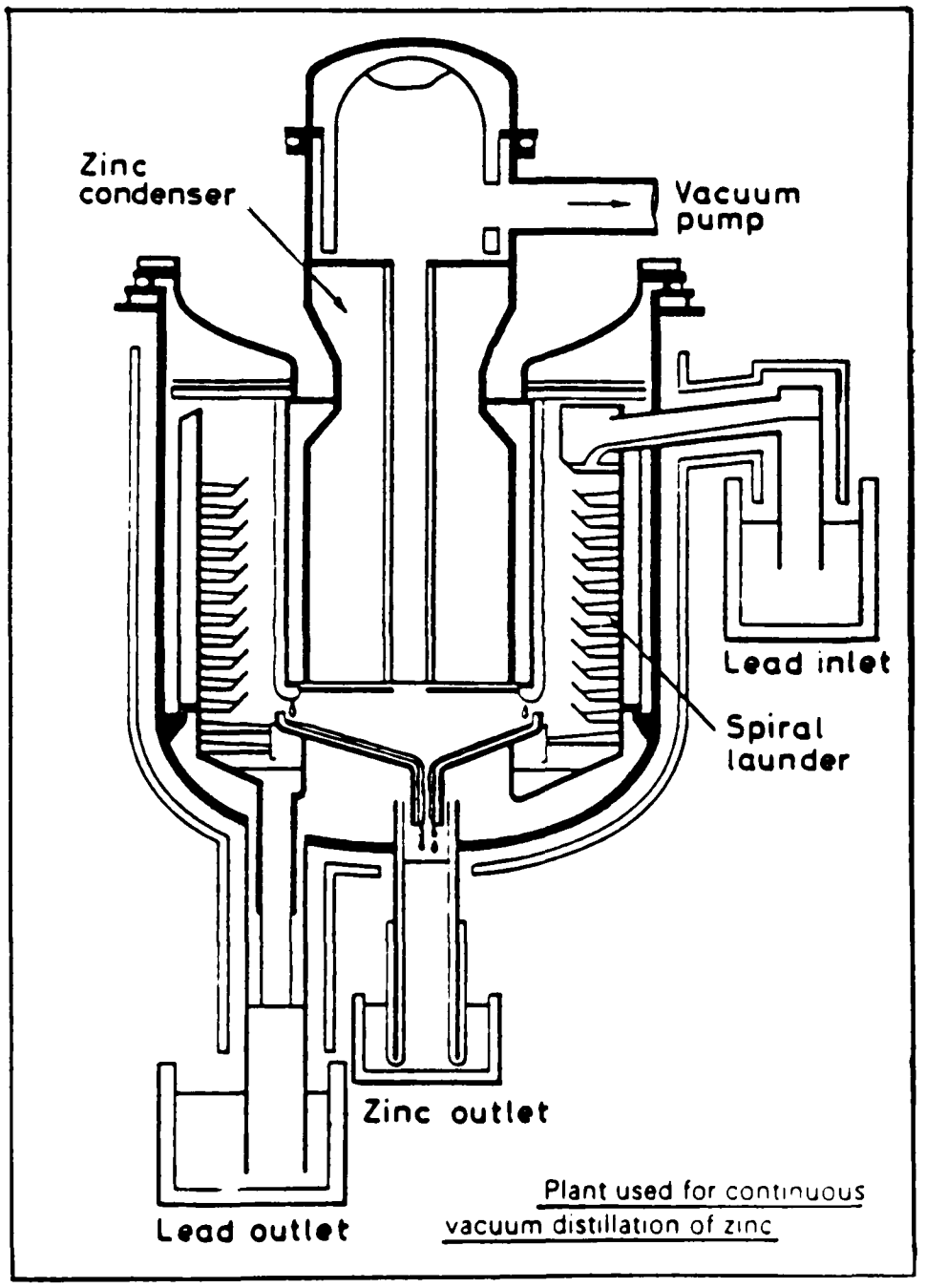

Plant used for continuous vacuum distillation of zinc

FIGURE 2.2.2.3 PROCESS FLOWSHEET OF THE BRITANNIA VDZ OPERATION AND EQUIPMENT DESIGN

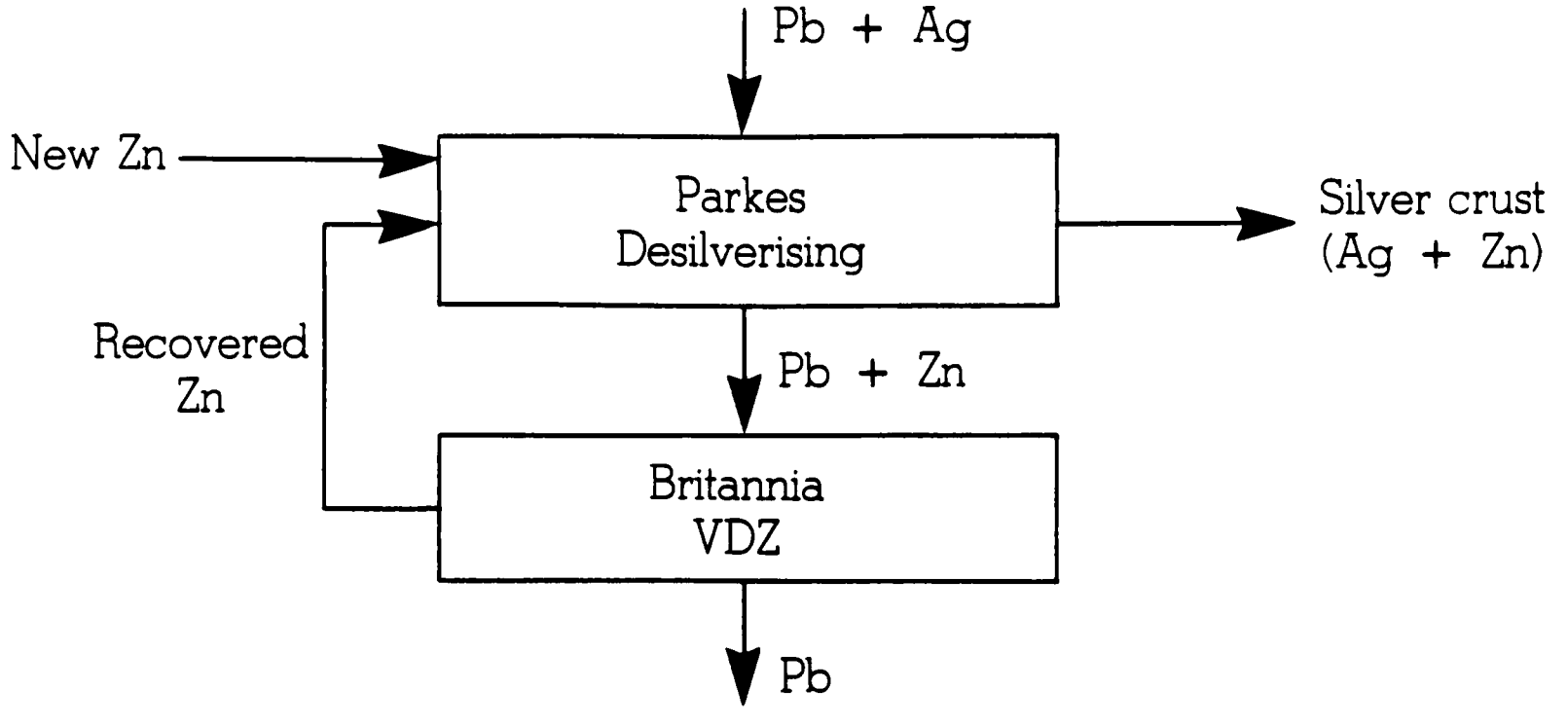

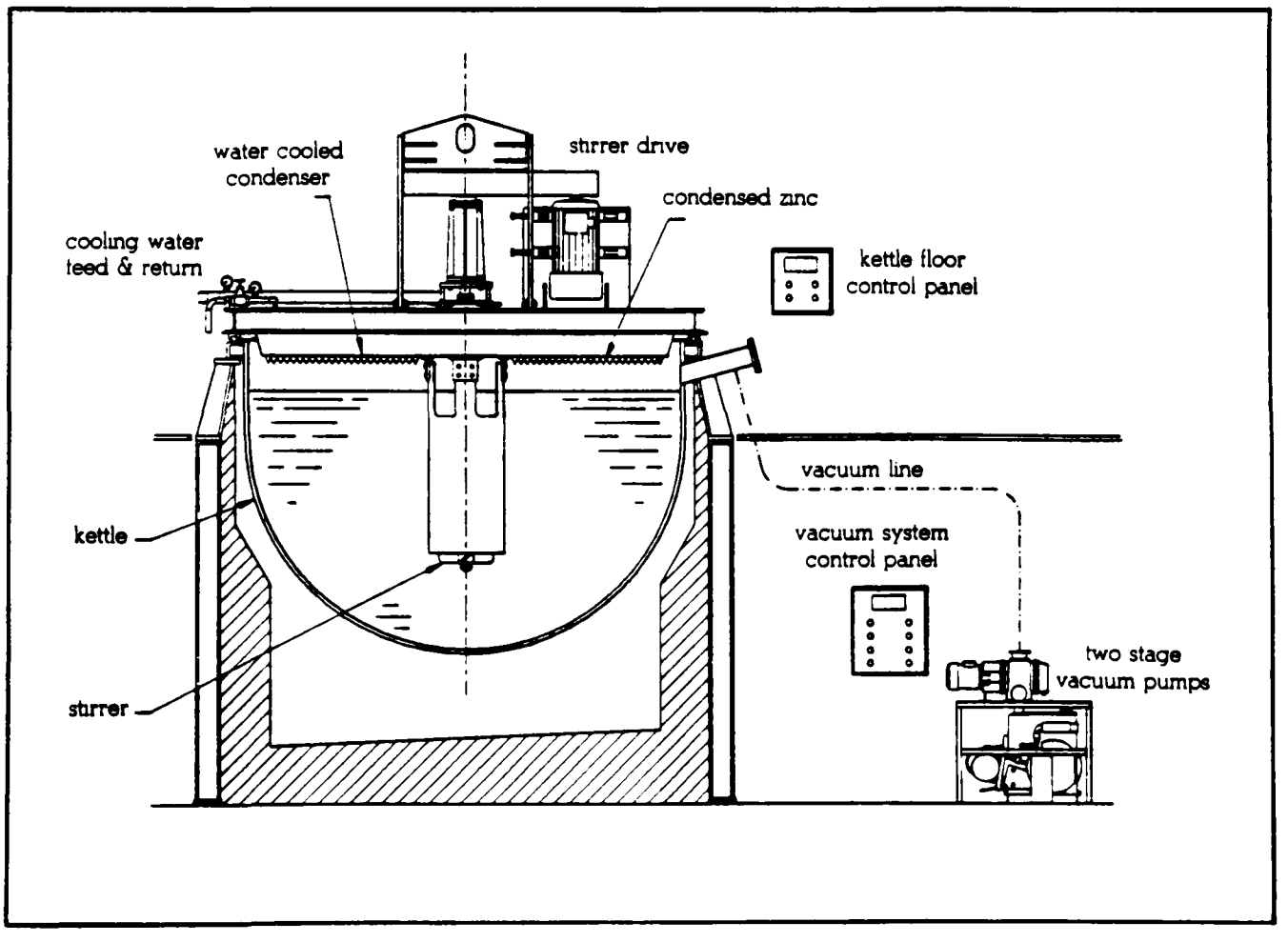

The VDZ unit consists of a steel bell-shaped kettle of between 60 to 300 tonne capacity that is charged with lead bullion containing 0.6% Zn at 590-600^{o}C. A water-cooled condenser assembly with a rubber 'O' seal which rests on the rim of the kettle is winched into position. The condenser assembly includes a mechanical stirrer unit to provide greater surface area in the bullion and to promote surface renewal once the unit is evacuated. A residual vacuum of 10-100 µm is typical of the unit and a solid zinc deposit containing a few percent lead grows on the cold condenser surface (kept at 30-40^{o}C) over a run of several hours duration.

Once the rate of zinc depletion from the bullion falls to a nominal amount and over 90% of the zinc is recovered from the bullion the vacuum seal is broken and the condenser lid removed to strip the deposit off manually. Plate 2.3 shows a sample of zinc deposit taken from a Britannia VDZ unit. The morphology of the zinc is nodular and the characteristic white oxide crust shown develops on exposure to air. During normal operation a nominal amount of vapour carry-over towards the vacuum pumps and subsequent fume formation is experienced.

THE LIFT-SPRAY VACUUM REFINING APPARATUS

A body of research in Canada by Harris (1988, 1989) on a process similar to the RH vessel in the Warner Smelter is currently being carried out (Figure 2.2.2.4). The process has been proposed as a production route for various metals including zinc, lead, copper, tin and aluminium. Although still on a laboratory scale, good separation of several metals from a melt has been reported. A satisfactory means of selectively condensing the resulting metallic vapours has not as yet been devised for the process. As much as 3-5% of the vapours produced in the unit have been reporting back to the

PLATE 2.3

TYPICAL BRITANNIA VDZ

ZINC DEPOSIT

vacuum pumps.

FIGURE 2.2.2.4 SCHEMATIC DIAGRAM OF A LIFT-SPRAY VACUUM REFINING APPARATUS

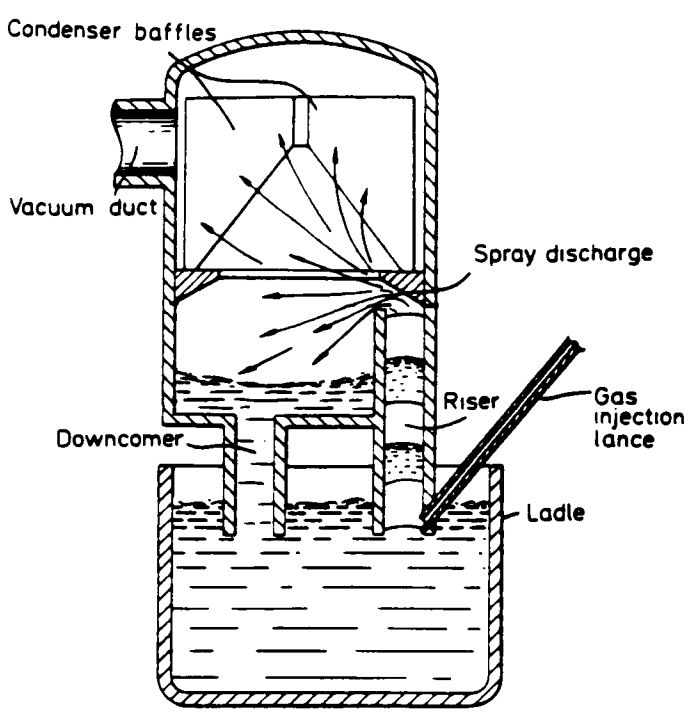

2.2.3 Fogging in a Vapour/Gas Mixture

2.2.3.1 Introduction and Definitions

The condensation of a vapour as droplets in the gas phase rather than on a surface is known as fog or mist formation. This pernicious problem has always plagued the metallurgical industry during the condensation of metallic vapour and it necessitates the introduction of spray towers, filters or particulate entrainment systems downstream of the condensation stage to trap the dispersoids. Fogging is not restricted to the metallurgical and chemical industries, metereorologists have been trying to predict atmospheric fog formation for many years (Amelin, 1967). Fogging is not often reported as a problem in industrial condensers, because it is seldom looked for. Its presence becomes known only when yield losses or pollution or corrosion problems become apparent.

The possibility of metallic fog formation during condensation processes has been suggested by Kroll (1951) for aluminium, magnesium, zinc, lead and tin vapours. The problem has been referred to for zinc, lead and lead sulphide vapours by Morgan (1957), Davey (1962, 1953), Alcock and Howitt (1987), Harris and Allaire (1989) and addressed by Warner (1970) following work at Avonmouth zinc smelter (Gammon, 1970). Indeed, there are many metallurgical operations, where the mechanism of fog formation is most probably a contributing factor towards reported low metal recoveries though it is often not suspected or simply ignored until losses become too high. Moreover the mechanism proposed by Turkdogan (1964) to explain the enhanced vaporisation of steel and subsequent red oxide fume formation is also a fogging phenomenon.

Fog and mist formation is also the bane of many processing operations in the chemical industries. Silver in 1947 reported the presence of tar fogs during the purification of coal gases. Shortly afterwards, Mickley (1949) studied ways of restricting steam fogs that tended to form in his air conditioning equipment. Johnstone et al (1950) used a qualitative experimental approach to predict fog formation in sulphur/nitrogen, steam/nitrogen and n-butyl alcohol/nitrogen vapour/gas mixtures. Hampson and Furman (1953) estimated amounts of fog formation during the condensation of steam, in the presence of CO_2, on a horizontal tube. During the condensation of steam and benzene Sikchi (1956) discovered fog formation to be a problem. Schuler and Abell (1956) considered fog formation as a possible cause for low recoveries in the titanium tetrachloride/nitrogen system. Kusak in 1958 discovered fog formation during the condensation of heavy organic vapour/inert gas mixtures whereas Olander (1961) noted its presence in direct contact condensers. Lewin and Dalin (1965) refer to the possibility of sulphur fogs in their article on laboratory instruments for condensing and absorbing vapours. Hayashi et al (1976) have artificially induced mist formation in a natural convective field during the sublimation of naphthalene. Paskall (1981) has tackled the problem of sulphur fog and mist formation in Claus process condensers where it contributes to low sulphur recoveries and catalyst deactivaton downstream of the condensers. The frequent problem of sulphuric acid mists has prompted Lo Pinto (1982) to offer helpful suggestions on how to solve them. Schotte (1989) with a pair of articles has recently studied HCl and HF fog formation by adiabatic expansion in mixtures with air.

It is difficult to classify disperse liquid or solid particulate systems in gases on the basis of their nature, origin and particle size. There is usually

an overlap between definitions and between popular and scientific descriptions. Figure 2.2.3.1 characterises the various terms used in this field (Green and Lane, 1964; Steinmeyer, 1972; Lo Pinto, 1982; Perry and Green, 1984).

Fog

Industrially, a fog is a suspension of fine, spherical droplets ranging from < 1 μm up to about 10 μm in diameter. Such droplets are sufficiently small that they behave as a gas and are not captured by impingement devices. In terms of opacity, fogs are optically more dense than mists reducing the visual range appreciably. 'Haze' and 'smog' occur in the atmosphere when fogs form on atmospheric pollutants and dust particles.

Mist

Globules which may be formed by the growth of fog particles, or spray that is created by the entrainment of liquid into a gas stream from the tube wall of an industrial condenser because of excessive gas speeds, are classed as mists. Mists may range in size from 10 μm to a few millimetres in diameter. Mist particles tend to be spherical, larger than fog and of a low number density.

Smoke

Smokes consist of a wide variety of gaseous dispersed systems consisting of irregularly shaped particles of low vapour pressure which settle slowly. Their mode of formation is quite characteristic and they are usually associated with combustion and destructive distillation products. Smokes are also produced by volatilisation and condensation, chemical and photo-

FIGURE 2.2.3.1 : CHARACTERISTICS OF SELECTED PARTICLES AND PARTICLE DISPERSOIDS

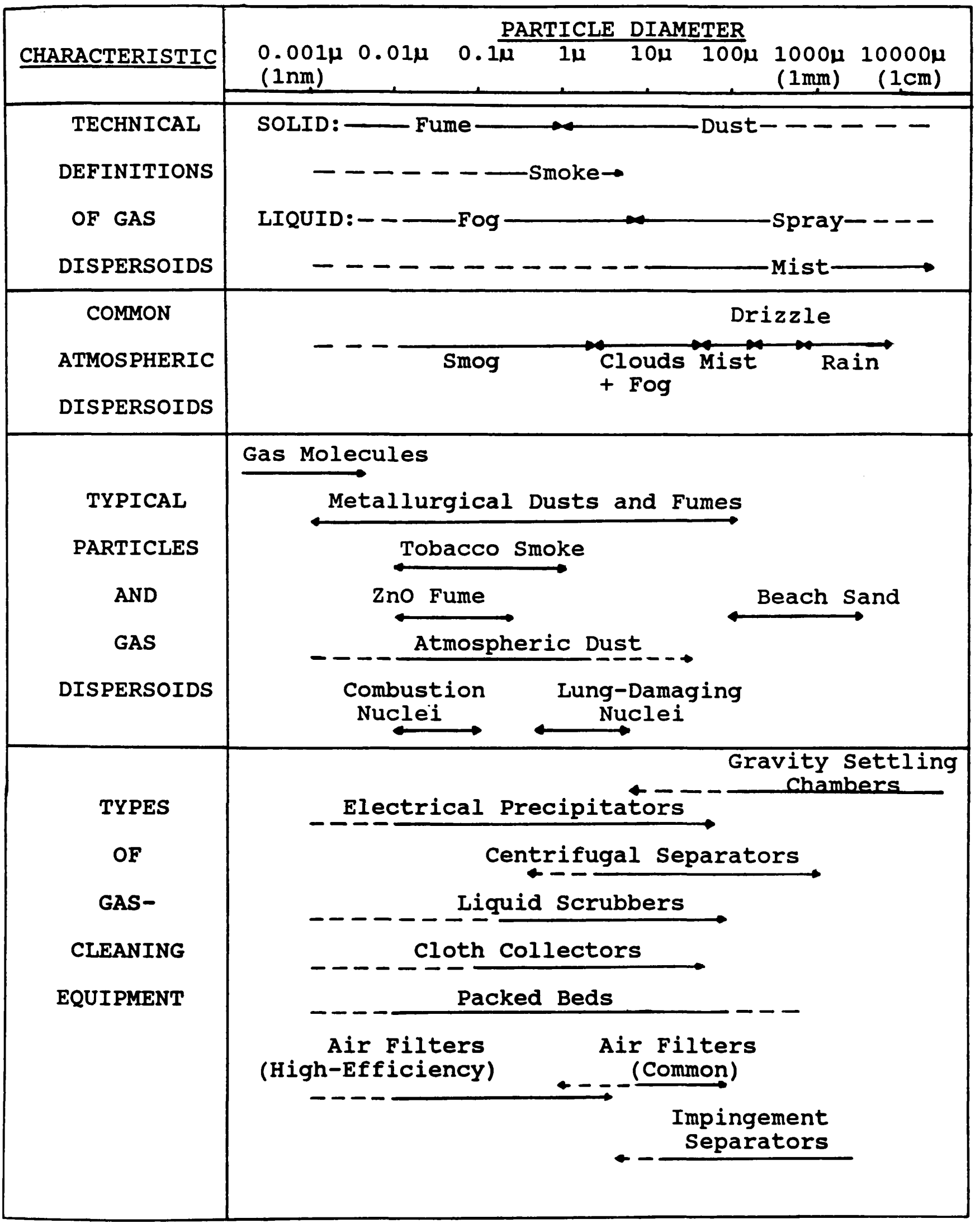

chemical reaction and electrical and mechanical pulverisation.

Fume

A fume occurs when a smoke is formed simultaneously with the production of a gas or vapour e.g. in smelting where metallic oxide smokes are generated simultaneously with SO_2. Fumes are usually < 1 μm in diameter. Sometimes the term is used merely to indicate the cloud of particles formed over a substance by vapour phase or other reaction.

Dusts

These are solid particles dispersed in a gaseous medium as the result of mechanical disintegration of matter. They usually are irregular and have a large size distribution being in the form of single units and aggregates but with low number density.

Aerosols

Here, the generic term is used i.e. aerial suspensions of limited size distribution and small particle sizes. They are stable and are thus not given to sedimentation. Certain dusts, fogs, mists and smokes can come within this definition. Any peculiar properties of aerosols can be traced back to the high specific surface and correspondingly high surface activity of a system of finely dispersed particles.

Particles that are > 100 μm are readily collected by simple inertial or gravitational methods. The most difficult collection problems are associated with particles in the range of about 0.1 - 2.0 μm in which forces for deposition by inertia are small. For collection of particles under 0.1 μm diffusional

deposition becomes increasingly important as the particle size decreases. There are essentially three indices for describing a fog population:

i) Dispersity = the drop size distribution. A monodisperse fog consists of droplets of equal radius. A polydisperse fog has a drop size distribution that can be described approximately by the mean drop radius (arithmetic mean, root-mean-square, root-mean-cube etc).

ii) Number Density, N = the number of droplets per unit gas volume and expressed in cm^{-3} or m^{-3} at normal temperature and pressure.

iii) The Mass Concentration of Fog, G = the droplet mass in unit gas volume, g/cm^3 at normal temperature and pressure.

The three indices change continuously as the droplets coagulate, evaporate, or grow by vapour condensation on their surface. The properties of the fog are therefore also variable. The number density and the droplet size range will be between very wide limits dependent on the condition of fog formation and the variation of different parameters with time. The smallest droplets are aggregates of a few molecules whereas the largest mist droplets may have radii of a few millimetres; the number density may vary from 0 to 10^{12} droplets per 1 cm^3 of gas.

The number density at which the optical effect of the fog (i.e. the reduction in gas transparency) becomes visible to the naked eye depends on fog dispersity and on a variety of other factors like the thickness of the intervening gas layer, the position of the light source etc. For example, in atmospheric air, a slight fog is observed when N = 50 - 100/cm^3; a heavy fog with a visibility of less than 200 m has N = 500 - 600/cm^3. The mean drop size of atmospheric fog is 7 -15 μm, N always being variable with time.

At high supersaturations (where nucleation is offset by coalescence) the number density increases insignificantly. Once fog forms, the super-saturation decreases because of vapour condensation on fog particles which have a very large overall surface. The supersaturation falls off until an equilibrium is attained with S close to unity. The time to equilibrium depends on the nature of the condensation centres, their number density, the total vapour pressure and the maximum supersaturation.

Fog particles will grow because of excess saturation in a vapour/gas mixture. Sometimes this means that the gas phase is supersaturated (i.e. it is below the vapour's dewpoint). At other times fog can grow by dissolving in foreign nuclei at partial pressures below saturation. Either way, fogging results from an increase in the relative saturation, provided sufficient nuclei are present.

Two different modes of fog formation can occur, namely homogeneous and heterogeneous vapour condensation:

a) Homogeneous Fog Formation

This consists of 3 distinct stages:

i) the formation of supersaturated vapour.

ii) the spontaneous nucleation of vapour embryos.

iii) the condensation of vapour onto the embryonic surfaces and the growth of the embryos to the size of fog droplets.

b) Heterogeneous Fog Formation

This can be divided into two stages:

i) the formation of supersaturated vapour

ii) the condensation of vapour onto residual nuclei or gaseous ions present in the gas phase. These particles grow to the size of fog droplets.

In a 'partial' condenser, i.e. one that treats vapour/gas mixtures, fog will form dependent upon the relative rates of decrease of temperature and concentration (partial pressure). Theoretically, fog can only form once the mixture becomes supersaturated. Supersaturation occurs whenever the heat transfer rate from the vapour/gas mixture to the condensation surface is too high relative to the mass transfer rate. One of the contributing factors towards this will be a high Sc/Pr ratio greater than unity. The degree of supersaturation is measured by the ratio of the actual vapour pressure of the condensable vapour in the mixture to the saturation (or equilibrium) vapour pressure at the same temperature:

$$S = \left[\frac{p_v}{p_{sat}} \right]_{t_v} \qquad (2.2.11)$$

Referring to Figure 2.2.3.2; point X represents a vapour with a value of $S > 1$ (i.e. supersaturation); point Y has a value of $S = 1$ (i.e. saturation) and point Z has a value of $S < 1$ (i.e. unsaturation).

There are essentially six different means of achieving supersaturation and subsequent formation of fog (Amelin, 1967):

i) Fog formation by eddy and molecular diffusion and thermal conduction i.e. forced convective cooling, the typical industrial condenser situation (see for instance Gardner, 1957).

ii) Fog formation by radiative cooling i.e. of very high temperature condensable mixtures ($t_{vi} > 2000$ K) (Chan et al, 1980). Radio-active fall-out associated with nuclear explosions is a form of this type of fog. This form of fogging is enhanced for polyatomic

FIGURE 2.2.3.2 : DEFINITION OF SUPERSATURATION ON A PRESSURE - TEMPERATURE DIAGRAM

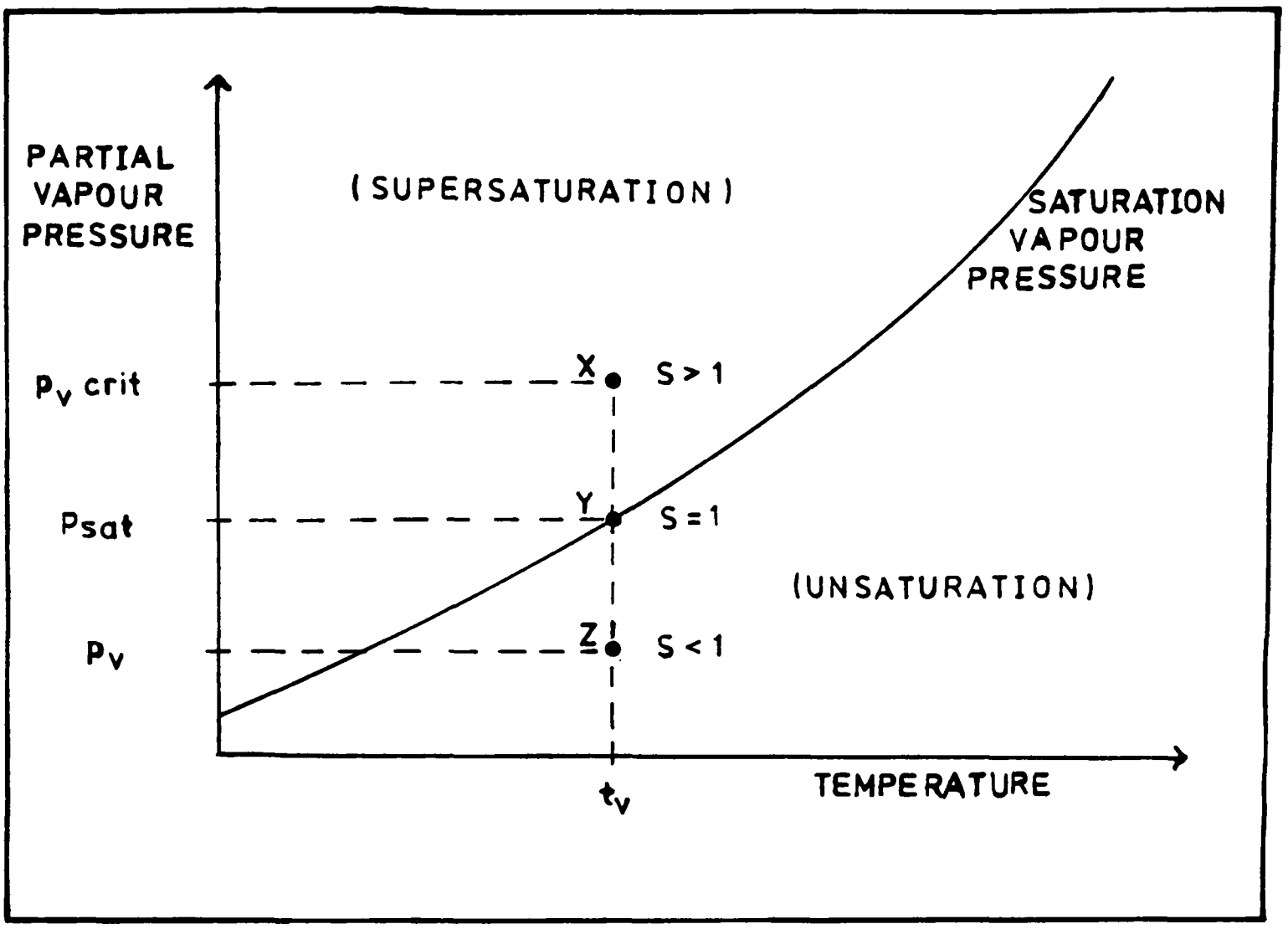

vapours and gases e.g. SO_3, H_2O, NH_3, that exhibit more pronounced radiation heat transfer components.

iii) Fog formation as a result of chemical reactions by vapours in a condensable mixture resulting in a product of lower vapour pressure than the reactants, e.g. in industrial sulphuric acid production (Lo Pinto, 1982).

iv) Fog formation in an adiabatically expanding vapour/gas mixture e.g. in the Wilson Cloud Chamber.

v) Fog formation due to the turbulent mixing of saturated vapour/gas streams at different temperatures e.g. in large scale atmospheric fog formation and also in mist formation associated with turbulent jets (see Levine and Friedlander, 1960). It is commonly seen in the plume from a stack or the exhaust from breathing on a cold day.

vi) Fog formation by molecular diffusion and thermal conduction e.g. radiative fogs that form at the end of a cloudless night in regions of stagnant air (in troughs or in forest clearings).

Clearly, of the six types of fog formation only types (i) to (iii) are of relevance to the present study. Hence these three are considered in detail, notably type (i) on which most research has been carried out. Type (i) is discussed in more depth in Section 2.2.3.9 of this thesis.

ii) Radiative Fog Formation

Amelin (1967) has observed that for certain gases and vapours with a sufficiently high temperature and molecular structure there will be an important radiant component of heat transfer to a cooling surface. With certain metallic vapours because of the high temperatures involved there is

a substantial radiative cooling effect especially at high vapour pressures during their condensation. This will cause a considerable rise in super-saturation.

iii) Fog Formation as a Result of Chemical Reaction

This problem is very common in the sulphuric acid industry when SO_3 reacts with H_2O to form H_2SO_4 (Amelin, 1967). Since the product vapour has a lower saturation vapour pressure than the reactants it will be instantly supersaturated as it forms and it will condense out as fog particles. In the metallurgical industry such problems are commonplace. Turkdogan et al (1976) report numerous intermediate condensates existing in most metallurgical reactions and indeed some may be necessary in aiding reactions to completion. By and large most are undesirable. Zinc for instance, in the vapour phase will react instantly with oxygen atoms to form zinc oxide especially if zinc is already in the form of a fog or mist (Warner, 1970). This zinc oxide as it cools forms a dust known as fume that has to be collected and recirculated to the feed end of the smelter. In connection with the Warner smelter being developed in this school, it is known thermodynamically that in the RH vessel numerous side reactions will occur whereby zinc vapour is converted to ZnS as well as ZnO plus lead sulphides and oxides will exist as fog nuclei in the gas phase. Clearly, these sorts of inter-vapour reactions will yield condensation nuclei prior to the bulk zinc condensation further downstream.

2.2.3.2 Detrimental Effects of Fog and Mist Formation

Industrially, fog and mist formation volunteers itself as a problem

primarily when product yield falls dramatically (sometimes sporadically) thus constituting a loss of a valuable material. If the fog is an aerosol having a corrosive or reactive condensate it may eventually settle and create corrosion problems downstream. Moreover, industrial fogs often contain components which are detrimental to vegetation and to the health of the population in surrounding regions.

In special cases, further cooling of liquid droplets will turn them to solid particles, and, if the material is liable to react with the atmosphere, it will be in a particularly active state. In this case special equipment will be needed to recover the particles in massive form followed by provision for remelting.

2.2.3.3 Formation and Growth of Liquid Droplets in a Vapour/Gas Mixture

In a gas volume vapour can condense on the surface of condensation nuclei, present in the form of suspended impurities or gas ions or on the surface of embryos (molecular aggregates which arise spontaneously as a result of statistical fluctuations in the gas medium). Above the convex surface of small liquid droplets (and of condensation nuclei in general), the saturated vapour pressure is higher than above a plane surface. It increases as the radius of curvature is increased. Hence, a certain degree of supersaturation is necessary before embryos grow perceptibly.

When equilibrium is established between a droplet and its surrounding medium its vapour pressure p_r becomes equal to p_v, the medium vapour pressure and then

$$\left|\frac{p_r}{p_{sat}}\right|_{t_v} = \left|\frac{p_v}{p_{sat}}\right|_{t_v} = S \qquad (2.2.12)$$

The relationship of the saturated vapour pressure above the droplet and of the vapour supersaturation to the droplet radius is expressed by Kelvin's equation:

$$\text{Ln}\, S_r = \text{Ln}\, \frac{p_r}{p_{sat}}_{t_v} = \frac{2\sigma_r M_v}{R t_v \rho_L r} \qquad (2.2.13)$$

where S_r = the supersaturation corresponding to the equilibrium saturated vapour pressure above the droplet

p_r = the saturated vapour pressure above the droplet (mm Hg)

p_{sat} = the saturated vapour pressure above a plane surface (mm Hg)

σ_r = the surface tension of the droplet (dyne/cm)

M_v = the molecular weight of the liquid or vapour (g)

t_v = the vapour temperature (K)

ρ_L = the density of the liquid (g/cm^3) - strictly $\rho_{gas} - \rho_L$

R = the universal gas constant (8.315×10^7 erg/^oC.mole)

r = the radius of the droplet (cm)

If the supersaturation of the bulk gas, S, is > S_r then vapour will condense on the surface of the droplet and the droplet radius will increase. Conversely, the drop will evaporate if S in the gas phase is less than S_r. If S = S_r then the processes of droplet growth and evaporation are equiprobable i.e., given a sufficiently large population of droplets in the gas phase, half will grow by condensation and the other half will shrink by evaporation. The saturation vapour pressure above each droplet and therefore S_r is metastable. σ_r is not equal to plane surface tension, σ_L. It is slightly lower:

$$\sigma_r = \frac{\sigma_L}{1 + 2\left(\delta/r\right)} \qquad (2.2.14)$$

where δ is a constant (see Amelin, 1967).

If the droplets are electrically charged, the saturation vapour pressure above the droplets and the corresponding supersaturation are less than the respective quantities for electrically neutral droplets of the same radius:

$$\ln S = \frac{M_v}{R t_v \rho_L}\left(\frac{2\sigma_r}{r} - \frac{e^2}{8\pi r^4}\right) \qquad (2.2.15)$$

where e = electric charge in E.S.U.

For small droplets ($< 10^{-7}$ cm) the effect of this charge is significant. Uncharged droplets therefore cannot exist in an unsaturated gas mixture, whilst charged droplets may be present in saturated and even unsaturated mixtures. If ions are present in the gas phase, minute droplets of liquid do not vaporise even if the vapour pressure is below saturation. These droplets cannot grow to a substantial size. For most liquids negative and positive ions have a different effect on critical supersaturation e.g. in air/water vapour mixtures negative ions act as condensation nuclei at S = 4.2 for a given temperature whereas with positive ions S = 6.0. For many other vapours in air, condensation on positively charged nuclei occurs earlier than on negatively charged ones; for others it is simultaneous.

Supersaturation is lower if the vapour reacts with the droplet (e.g. condensation of water vapour on droplets of sulphuric acid solution in water) or is soluble in the liquid. Vapour supersaturation is higher if the droplet

surface is not wetted by the condensing liquid. When vapour condenses on solid condensation nuclei, the mechanism of fog formation is the same as with liquid droplets, but the supersaturation corresponding to the saturation vapour pressure may differ for solid nuclei and droplets depending on the composition of the particles and their shapes. For example, if the condensation nuclei are made of chemically active substances (in relation to the condensing vapour) the conditions of equilibrium are substantially altered. If the condensation nuclei are porous condensation is influenced by capilliary forces. Droplet formation on solid particles is the result of the gradual accumulation of the condensing liquid. Regardless of the nucleus shape, the particle is gradually enveloped in a liquid film thus turning it into a droplet of approximately spherical dimensions.

The growth of nuclei and of embryos by vapour condensation on their surfaces is the principal process which governs the dispersity, or the drop size distribution, of the fog. Rate of vapour condensation on the surface of droplets is increased by Stefan Flow which is a dynamic flow caused by the vapour pressure gradient between the gas phase and the growing droplet. Fog droplets in a turbulent stream are entrained by the eddy pulsations and describe complex trajectories in the gas. The droplets, however, are not fully entrained by the pulsations and they additionally grow due to the intake of vapour transported by convective diffusion. The mass diffusion coefficient is therefore higher than in a still medium. The smaller the droplets are, the more readily they are entrained by eddy pulsations and the contribution from convective diffusion decreases. For droplets with radii less than 1 μm the effect of diffusion in a turbulent stream can be completely ignored.

Temperature of a Droplet in Supersaturated Vapour

When vapour condenses on the surface of a droplet, the latent heat of condensation is released and the temperature of the droplet becomes higher than the temperature of the gas. The temperature difference results in a transfer of heat from the droplet to the gas. This hinders the particle in the competition with the condensing surface (e.g. tube wall) for condensation of vapour, as the particle must dissipate the heat of condensation back to the gas. This forces the particle to run hotter than the gas and reduces the supersaturation that the particle sees. Calculations show that the temperature difference between a droplet and the gas phase increases with increasing droplet diameter to a certain maximum value and then subsides.

Stabilisation of Mists by Insoluble Monolayers

The lifetime of droplets coated by insoluble monolayers can be increased by factors up to several hundred, depending on ambient conditions, due to the retardation of molecular evaporation from the surface of the droplet.

2.2.3.4 Homogeneous Fog Formation

2.2.3.4.1 Kinetics of Homogeneous Fog Nucleation

Rate of fog nucleation comes under kinetics of phase change and in principle it is similar to other physiochemical processes like crystallisation in liquids. A concise history of the development of nucleation theory is summarised by Zettlemoyer (1969) together with the latest thinking. There have been two separate approaches to nucleation theory:

i) The 'Classical' (Kinetic-Thermodynamic) Model

This model embraces the work of Gibbs, Thomson (Lord Kelvin), Volmer and Weber, Zeldovitch, Becker and Doering, Frenkel and Lothe and Pound. Theories associated with this model are presented throughout this work. In its present form the kinetic model is less exact than the statistical-mechanical model since it is necessary to make assumptions regarding the rates of evaporation or condensation of the differently sized embryos; it is superior however in that it is applicable to systems removed from the stationary state.

ii) The Statistical-Mechanical Model

The model was instigated by Mayer's initial theories into this modern approach to nucleation. It has clarified ideas about phase change and it also focuses attention on the partition functions of embryos and how the concentrations of embryos are distributed with size.

It is the incessant statistical fluctuations in a vapour/gas mixture that leads to the formation and rapid dissipation of multi-molecular aggregates. These aggregates have different sizes and their relative content in the gas mixture decreases as the number of constituent molecules is increased. Some of the molecules grow to the critical size and the associated saturation vapour pressure becomes equal to the vapour pressure in the gaseous medium as expressed by eq. 2.2.13. The molecular aggregates thus develop into embryos. Once a single vapour molecule has condensed on the surface of the embryo the latter becomes a droplet whose radius grows by condensation at an accelerated rate (for constant supersaturation). If a single vapour molecule escapes from the surface of the embryo it reverts to a simple multimolecular aggregate of subcritical size which inevitably vaporises. Since embryo formation and dissipation are equiprobable, only

half of the embryos grow into droplets. As vapour saturation increases, the embryo radius decreases and the number of embryos rises, i.e. the rate of embryo formation becomes higher.

The work expended in the formation of a single embryo is the sum of the work done by the transition of particles from gas to liquid phase (in the case of supersaturated vapour this work is negative) and the work associated with the formation of a new embryonic surface. For embryos in unstable equilibrium with the supersaturated vapour; the total work according to Gibbs is given by

$$W = \frac{4 \pi r^2 \sigma_r}{3} \qquad (2.2.16)$$

If this equation is considered in conjunction with the Kelvin equation (2.2.13), then it is clear that the higher the degree of supersaturation is then the smaller the number of molecules necessary to form a cluster of critical size will be. The nucleation barrier will also decrease.

From the theory of fluctuations, the probability of formation of an embryo of a new phase in unit volume and unit time is:

$$I = K \exp^{-A} = K \exp^{-\left(W/k\, t_v\right)} \qquad (2.2.17)$$

where I is the rate of nucleation/cm^3.sec

where k is the Boltzmann constant

and K is the nucleation constant.

Both Becker and Doering and Frenkel specify complicated equations of this form. The Frenkel equation is in better agreement with experimental data and Amelin (1967) therefore recommends it for practical problems. The equation is:

$$I = 10^{26} \frac{\alpha}{S \rho_L} \left(\frac{p_v}{t_v}\right)^2 \left(M_v \sigma_r\right)^{1/2} \exp -\left[\frac{17.6}{\ln^2 S} \left(\frac{M_v}{\rho_L}\right)^2 \left(\frac{\sigma_r}{t_v}\right)^3\right] \quad (2.2.18)$$

where α is the accommodation coefficient

and p_v is in mm Hg; all other units are in the c.g.s. system.

The reduction of vapour concentration due to the formation of embryos is vanishingly small since the radii of the embryos are small ($\approx 10^{-7}$ cm).

2.2.3.4.2 Critical Vapour Supersaturation Criterion For Homogeneous Nucleation

Fortunately, supersaturation on its own (i.e. S just greater than 1) is not a sufficient criterion for fog formation. If it were, many, and perhaps most, of the process industry's partial condensers would be plagued by fog. Before fog can become visible by a light-scattering test, the mixture must reach a certain level of supersaturation. This level of visible fog formation is called the critical supersaturation ratio, S_{crit}. S_{crit} for homogeneous condensation of a vapour is defined as the supersaturation when embryos capable of further growth form at a rate of $I = 1$ cm^{-3} sec^{-1} (Bras, 1955; Amelin, 1967).

This definition is arbitrary since embryos will form even if $I < 1$ but the corresponding rates are too small to be seriously considered. Indeed, since vapour supersaturation appears as a power exponent, the rate of nucleation will therefore increase very steeply with supersaturation.

For example, with water vapour having values of S equal to 3, 4 and 5 the time required for the formation of 1 nucleus ml^{-1} $second^{-1}$ amounts to an average of about 100,000 years, 10 seconds and 10^{-8} second respectively. Table 2.2.3.1 gives typical S_{crit} values for particular vapours at certain temperatures.

TABLE 2.2.3.1: Typical Values of S_{crit} for Vapours. (Amelin,1967)

Vapour	t_v (K)	S_{crit}
Methyl Alcohol	270.0	3.21 ± 0.10
Ethyl Alcohol	273.2	2.30 ± 0.05
n-Propyl Alcohol	270.4	3.05 ± 0.05
Nitromethane	252.2	6.05 ± 0.75
Water	263.7	4.85 ± 0.08

For critical supersaturation in an ion-free gas, Frenkel's equation (2.2.18) can be solved for $I = 1/cm^3.sec$ to give an estimate of S_{crit} at t_v. Amelin has solved the Frenkel equation for water vapour at 273 K to produce this simplified version of the equation:

$$S_{crit} = \exp\left[0.56 \frac{M_v}{\rho_L}\left(\frac{\sigma_L}{t_v}\right)^{3/2}\right] \qquad (2.2.19)$$

where ρ_L = the liquid density (g/cm^3)

t_v = the vapour/gas temperature (K)

M_v = the molecular weight of the vapour (g)

σ_L = the surface tension of the liquid (dyne/cm).

This equation has been reproduced by Steinmeyer (1972), Lo Pinto (1982) and Perry (1984) and recommended for approximate use. Due to the simplifications inherent in the above equation's derivation the more complicated equation (2.2.18) is recommended as a means of accurately estimating S_{crit}. Eq. 2.2.18 can be solved by trial-and-error solution.

S_{crit} is a function of temperature and it will decrease as temperature increases - both σ_L/t_v and ρ_L decrease. This S_{crit} is still approximate since the vapour supersaturation at the instant of appearance of visible fog does not precisely correspond to the onset of vapour condensation on nuclei or embryos: it actually represents the time when the scattering of light by the formation of droplets has become strong enough to be detected visually. It will depend on the number density of droplets, their sizes and other fluctuations in the mixture. This time lag has been discussed by Dunning in Zettlemoyer's book (1969) whereas Amelin (1967) refers to a 'relaxation time', T_{re}. This is the time in which the number density N, attains a constant value and can be expressed by the equation:

$$T_{re} \approx 10^5 \, I^{-1/2} \text{ (c.g.s. units)} \qquad (2.2.20)$$

Accommodation Coefficients

At a liquid surface the number of vapour molecules impinging per unit surface area, W_c, is given by the Langmuir Equation:

$$W_c = \alpha\left(p_v - p_{sat}\right)\left(2\pi m k t_v\right)^{-1/2} \qquad (2.2.21)$$

where, α is the accommodation coefficient (for condensation); it expresses the fraction of impinging vapour molecules that 'stick' to the liquid surface,

k is the Boltzmann Constant,

and m is the mass of a vapour molecule.

The accommodation coefficient can vary dramatically between wide limits depending on the particular liquid and the physical conditions in the system. Surface impurities in the liquid are one of the factors which lower the experimental value of α. With clean liquid surfaces α approaches unity. In homogeneous vapour condensation the surface of the spontaneously forming embryos is impurity free and the kinetic factor, K, should be calculated using numerical data for very clean liquids. For some highly polar liquids, e.g. H_2O, C_2H_5OH, glycerine, the experimental values of α are lower than those for non-polar liquids. Amelin quotes a figure for glycerine of $\alpha = 0.05$ compared to mercury's value of 0.92 - 1.00.

2.2.3.5 Heterogeneous Fog Formation

Ion-free, clean gas phases are only produced by artificial means after several filtering and cleaning processes. In nature and in industry, process

gas streams invariably contain ions and minute liquid and solid particles in suspension; these are the condensation nuclei and it is on their surface that vapour first condenses to form fog droplets. Free organic radicals and single molecules may occasionally act as condensation nuclei. Condensation nuclei also result from the mechanical break-up of solids and pulverisation of liquids.

Foreign nuclei necessary for heterogeneous fog formation can come from various sources (Green and Lane, 1964; Amelin, 1967; Steinmeyer, 1972).

1) Solids External to the Process

   The obvious source is dust particles in process air streams. Air typically contains 1000 particles/ml in the 0.1 to 1 micron range suitable for condensation nuclei. When dust particles are completely wettable by the condensing liquid they will act like liquid droplets of the same radius.

2) Ions in Air or the Vapour/Gas Stream

   Gas streams with large multiply charged ions are the most susceptible to fog condensation. Typical ordinary air contains up to 60,000 ions per cm^3 compared to a few thousand in clean air. Ions will generally decrease S_{crit} values by 10 to 20%.

3) Entrained Liquid

   Production of small droplets is inherent in evaporation and bubbling processes. Typical number densities in the 0.1 to 1 micron range within evaporators will be about $100/cm^3$.

4) Upstream Reactions

   Probably the easiest way of ensuring an adequate nuclei count for a fog problem is to have an upstream reaction between two

vapours that yields a liquid or solid of much lower vapour pressure.

5) Solids Produced by Upstream Combustion and Corrosion Products

During combustion, poor mixing of partially burned gases produces enormous amounts of foreign nuclei for downstream equipment. Moreover, any corrosion or erosion products from the process lines if sufficiently small enough will act as nuclei sites.

The level of foreign condensation nuclei necessary to promote complete heterogeneous fog formation at $S_{crit} = 1$ will vary from system to system. Steinmeyer estimates that for $N = 1 \times 10^6$ to $1 \times 10^7/cm^3$ in his cited examples such a threshold is reached. Beyond this threshold nuclei concentration has no further effect on the quantities of fog produced. He also estimates that for vacuum condensation operations calculated equilibrium fog droplet diameters can be expected to be smaller than those estimated for atmospheric condensation processes (4 μm as opposed to 15 - 20 μm).

The fog potential of any particular industrial process thus depends not only on the number density of condensation nuclei in the initial gases, but also on the probable change in their number density during the processing of the gas; the conditions of fog formation (and the weight concentration of fog) may change considerably depending on the size and the number density of the condensation nuceli.

Green and Lane (1964) note that in order for a particle to act as an efficient condensation nuclei it must not only be sufficiently large, but must also have a small contact angle for the liquid. The effects of surface

structure are also important. Pits or steps on an otherwise perfect surface, if of suitable size, would be expected to lower the nucleation threshold. When the foreign solid particles are isomorphous with the condensed solid phase then these particles will induce solid condensation on their surface rather than liquid drops. Moreover, many of the really good nucleators are slightly vaprophobic.

If the foreign nuclei contain a substance which is soluble in the condensed liquid the vapour pressure of the latter is decreased and the supersaturation necessary for rapid condensation is reduced. Critical supersaturations are lower in the presence of ions, especially negative ions, because each droplet as a charged conductor carries a charge distributed uniformly over its surface. The charge tends to separate the molecules of the droplet, to enlarge the surface and to lower the vapour pressure, while the surface tension tries to exert the opposite effect.

If the gas temperature falls below the crystallisation point of the liquid, the droplets solidify and the fog turns into dust. Minute droplets, however, can withstand supercooling and the freezing point temperature of small droplets is therefore substantially lower than the tabulated figures for the same liquids in bulk. Water droplets can be cooled to - 40^{o}C. There are indications that in some cases the molecules pass directly from gas to the solid state, without the intermediate stage of a liquid phase.

There has been little published work in the field of heterogeneous nucleation of metalliferous vapours. Buckle and Pouring (1965) have nucleated water vapour on inorganic smokes (of 0.01 - 1.0 μm diameter) in an expanded flow of moisture-laden air. They discovered that the seeding effect was observable at concentrations of 10^{8} smoke particles/cm^{3} and

above. This in turn suggested that the concentration of homogeneous nuclei was very high too. Their results indicated a quick build-up of homogeneous nuclei (> $10^8/cm^3$) prior to the more gradual heterogeneous process. They pointed out that at high supply humidities the presence of seeded condensate interfered with the homogeneous nucleation. They also point out that preferential heterogeneous nucleation should occur for a seed material of similar morphology to the condensing vapour. Buckle (1989a) has also carried out calculations to verify that the onset of the heterogeneous seeding effect depends on both the concentration and size of the foreign nuclei in the gas flow.

Nicolaon et al (1971) used a nuclei-laden laminar gas stream (NaCl in helium) flowing up a vertical tube down which a heated film of dibutyl phthalate streamed. Fog nuclei were formed and an aerosol was produced. From their results they state that this mode of heterogeneous fog formation is primarily an equilibrium process, i.e., diffusion of vapour to the nucleus and the rate of heat transfer associated with condensation of the nucleus do not control the condensation process. Moreover, the mechanism of aerosol formation near the wall is similar to that in the central portion of the tube and in the time scale they were working with (up to 4 seconds) equilibrium was achieved rapidly once the nucleation process was triggered.

2.2.3.6 Coalescence of Fog Droplets

The property of continuous and spontaneous coagulation is one of the most striking characteristics of aerosols. The particles, of whatever substance they are composed, coalesce or stick together if they come into

contact, and the process goes on continuously so that the aerosol becomes coarser and finally flocculates out. It is most evident with oxide smokes.

The rate at which particles disappear by coagulation depends only on the square of the number density of particles present and the coalescence constant, K_C, so that

$$-\frac{dN}{dt} = K_C N^2 \qquad (2.2.22)$$

Thus, in any given smoke, coagulation is very rapid in the early stages when the number concentration is high and later it falls off rapidly.

Several factors affect coagulation rate by diffusion in aerosols (Green and Lane, 1964). They can be broadly divided into two groups:

i) those factors which affect the probability of collision between the aerosol particles, e.g. the size, size distribution and electrical charge distribution of the particles and the temperature and pressure of the gas.

ii) those factors which determine whether the diffusing particles stick together on colliding, e.g. shape and structure of the particles and the effect of vapours adsorbed onto the particles.

Mass Concentration and Particle Size

The coagulation constant, K_C, increases with decrease of mass concentration. This effect is explained by the fact that larger particles coagulate more slowly then smaller ones.

Polydispersity

The more closely an aerosol approaches to monodispersity the slower

it coagulates. This is in part due to the fact that the probability of collision between particles of unequal size must be greater than that between particles of equal size.

Differential Settling

In a polydisperse aerosol coagulation can also occur in another way. Under the influence of gravitational or centrifugal forces the large particles move faster than the smaller ones and the probability that they will collide with smaller ones is thereby increased. Coagulation due to differential settling rates, sometimes termed 'orthokinetic coagulation', is negligible in fine smokes with small particle size range, but it may become important in coarse aerosols when differences in settling rates of droplets are appreciable.

Temperature, Pressure and Viscosity of the Gaseous Medium

The coagulation constant, K_C, should be greater at higher temperatures for aerosols. The size of droplets produced can be much greater than normal the lower the viscosity of the carrier gas is, thus indicating increased coalescence. Coagulation rates increase markedly as the gas pressure falls.

Particle Shape

For aerosols composed of liquid droplets, new particles formed by collision must also be spherical, but for aerosols of solids, even if the original particles are assumed to be spherical, those formed by coagulation will be irregular. In the case of long chain-like structures, however, a considerable variation in the mobility, and consequently an increase in the coagulation rate, might be expected.

Effect of Foreign Vapours

If a thin layer of vapour or even of liquid is adsorbed onto aerosol

particles it may alter their surfaces in such a way that, on collision, the particles would not readily stick together. In some cases irregularly shaped particulates may, in the presence of a solvent vapour, tend to form spherical aggregates that will coagulate more readily.

Coagulation in Stirred Aerosols

A very simple way of increasing the coagulation rate of a particulate cloud is to make the air turbulent by mixing it with a fan or passing the aerosol through narrow, tortuous passages such as those of a packed bed. In the case of the fan, eddies and swirls are then formed and the velocity of the particles relative to each other becomes greater. The chances of collision of particles with one another must therefore be increased, and this implies an increased rate of coagulation.

Coagulation of Electrically Charged Particles

It can be shown that unipolar charging of aerosol particles (same polarities) will cause a marked reduction in the rate of coagulation and that bipolar charging (opposite polarities) should accelerate coagulation, but to a lesser extent.

Coagulation in an Acoustic Field

Small particles suspended in a gas can be readily aggregated by powerful sound waves (of both sonic and ultrasonic frequency), particularly if standing waves are set up in a resonant enclosure. Frequently, sonic agglomeration has been unsuccessful because of the high energy requirement. Most sonic generators have very poor energy-transformation efficiency.

Coagulation Scrubbing and Seeding

By introducing a controlled spray of cold liquid droplets into a relatively warmer vapour/gas stream, the reduction in vapour pressure at the surfaces

of the cold drops causes a hydrodynamic flow towards the drop known as Stefan flow. This enhances the movement of mist particles towards the drop. If the molecular weight of the diffusing vapour is different from the carrier gas, this density difference also produces a driving force, and the sum of these forces is known as diffusiophoresis (Perry, 1984). Thermal differences between the carrier gas and the cold scrubbing droplets can further enhance collection through thermophoresis. The introduction of particles 50 to 100 times larger in diameter than the aerosol can enhance coagulation but the addition of a broad range of particle sizes is not recommended (see Lo Pinto, 1982).

2.2.3.7 Fog Deposition and Settling

Suspended particles in a still atmosphere settle slowly under gravity and, in a closed vessel, eventually deposit themselves on the floor, although, if they are sufficently small, a proportion will be lost to the walls by diffusion. If the particles are subjected to inertial forces in a moving gas stream which is changing direction (turbulence), or to thermal or electrical forces, the picture becomes more complicated. In some cases these forces may be so strong that gravitational settling and diffusion may be neglected in comparison with them. For a concise exposition of droplet collection and deposition see Green and Lane (1964) or Perry (1984). Amelin (1967) reports that once fog forms near the surface of a condenser that is condensing a turbulent vapour/gas mixture the droplets are incapable of penetrating the turbulent core (Re > 10,000). They will settle on the pipe wall due to a combination of the diffusive current of vapour from the core to the condensate interface, thermophoresis and Stefan flow.

In laminar flow or when fog forms in the bulk and grows into a mist some of the droplets will experience Stokesian gravitational settling onto the condenser walls (Schuler and Abell, 1956; Toor, 1971a). Davey (1953) has considered this settling effect for the case of zinc (lead) condensation under vacuum and has remarked that it would have a significant effect in reducing fog losses for condensation flow up vertical condensation surfaces rather than flow along horizontal condensation surfaces.

In tests, Alexander and Coldren (1951) report that between 30 - 60% of water droplets (of average diameter 27 microns) in an aerosol will attach to duct walls (depending on the superimposed gas phase velocity). The main resistance to attachment lies in the gas film near the duct walls. Hutchinson et al (1971) have developed a stochastic attachment model for droplets in the 0.8 - 125 μm range in gas flows of $Re = 5 \times 10^3$ to 3×10^5. In the lower droplet size ranges low attachment to the wall was predicted and found to occur. Hence, it can be said that, dependent upon the condenser geometry a sizeable proportion of the fog formed in a condenser will be convected out whereas some mist attachment near the outlet can be expected. This mist attachment effect will help to reduce overall vapour losses.

2.2.3.8 Fog and Mist Preventative Measures Offered in the Published Literature

The following nine suggestions are a summary of numerous investigators' practical findings and are to be found in the published literature (Colburn and Edison, 1941; Bras, 1955; Minkowycz and Sparrow, 1966; Amelin, 1967; Steinmeyer, 1972; Lo Pinto, 1982):

1) Reduce the Temperature Differential Across the Gas Film in the Condenser, i.e. Increase t_c

This method decreases the driving force for heat transfer and for the same reason it is better to have countercurrent vapour/ coolant flow rather than co-current flow. As a consequence of this however, condenser surface area must be larger to compensate for the lost condensation capacity. Hence this modification may be expensive compared to other alternatives so a costing analysis is recommended.

2) Increase the Vapour/Gas Velocity

This will increase turbulence thus lowering the size of the gas film and increasing the heat and mass transfer coefficients.

3) Enter the Condensation Step with High Superheat

4) Use a Mist Eliminator

This is perhaps the easiest way to tackle a fog problem since it is always prudent to have a mist extractor downstream of a fogging condenser to eliminate particles in the > 5 μm size range. However, these units require large areas and they yield high pressure drops. Costs may soar if exotic materials of construction are specified. Perhaps a high velocity venturi may work just as well.

5) Filter the Feed Gases

All process gas streams will contain condensation nuclei and indeed filtration prior to condensation may prevent a potential fog problem. It is also beneficial to remove any substances that reduce the vapour pressure or the surface tension of the condensing vapours.

6) Seed the Gas Stream with Condensation Nuclei

This technique will produce droplets that can be captured by a conventional mist eliminator or settler. Though less conventional than the other suggestions it can be a cheap alternative. Testing is recommended to see if the scheme will work for the particular chemicals involved and the prevailing condensation conditions. It is best facilitated by using an atomiser spraying into the process stream prior to the inlet of the condenser. Seeding will almost invariably reduce the process stream's supersaturation. Lo Pinto (1982) outlines a typical problem of this nature.

7) Obtain Uniform Cooling

If several condensing surfaces are operated in parallel it is imperative to ensure that saturated or near saturated vapour/gas streams at different temperatures emanating from each unit are not mixed as the resultant mixture may be below the vapour's dewpoint.

8) Reheat the Gas Phase to Keep it Above Its Dewpoint

This method keeps the mixture in the unsaturated state and also evaporates fog and mist droplets. In the sulphur industry it is standard practice to reheat the vapour/gas mixture in between each condensation stage. Alternatively, the addition of inert gas to the middle of a condenser will produce the same nett result though vapour yield will fall due to the poorer condensation characteristics of the dilute mixture.

9) Other Considerations

Bras (1955) recommends the selection of the carrying inert gas such that the (Sc/Pr) ratio for the mixture is lower than unity. This

will result in a higher vapour diffusivity in the mixture. Dmytryseyn (1957) has pointed out that fog is most liable to form in process vapour/inert gas streams where the vapour has a high molecular weight and thus a low mass diffusivity. The presence of a higher molecular weight inert gas would increase the relative mass diffusivity of the vapour species. Bras (1955) has also developed a condenser with a conical shell and internal helically coiled cooler tubes showing a gradual decrease in coil diameter towards the bottom of the apparatus. It was claimed that this design eliminated a particularly nasty fog problem that had plagued a standard laboratory condenser.

2.2.3.9 Forced Convection Fog Formation Theories

A condensable vapour will form fog by eddy and molecular diffusion and thermal conduction. This is the most common industrial type of fog formation. It is not merely confined to condensers but also scrubbing towers, bubbling equipment and spray coolers. In a turbulent vapour/gas mixture moving along a cold surface, the vapour is transported by molecular diffusion across the boundary layer where it cools and condenses on the wall. The vapour/gas mixture is additionally cooled by molecular heat conduction. In the turbulent core of the stream, on the other hand, the concentration and temperature are equalised by turbulent mixing. The processes are thus governed by eddy, as well as molecular, diffusion and heat conduction.

Colburn and Edison (1941) have shown that there are three possible cooling paths a vapour/gas mixture can follow inside a condenser. Figure 2.2.3.3 illustrates the general principles involved. The temperature and partial vapour pressure differentials between points A and B in Figure 2.2.3.3(b) are the driving forces for the transfer of heat and mass from the vapour/gas mixture to the condenser wall. Point A represents the inlet conditions for the mixture whereas point B is typical of the interfacial vapour/gas conditions on the wall (and also possibly the outlet vapour/gas condition from the condenser if the outlet mixture is saturated). In Figure 2.2.3.3(a) the cooling curve or operating line represents the case where the heat transfer rate equals the mass transfer rate. In Figure 2.2.3.3(b) the heat transfer rate is greater than the mass transfer rate hence the curve bows to the left whereas in Figure 2.2.3.3(c) the mass transfer rate is greater than the heat transfer rate thus the operating line is concave. All the cross-hatched

FIGURE 2.2.3.3 : DIFFERENT TYPES OF VAPOUR/GAS COOLING CURVES

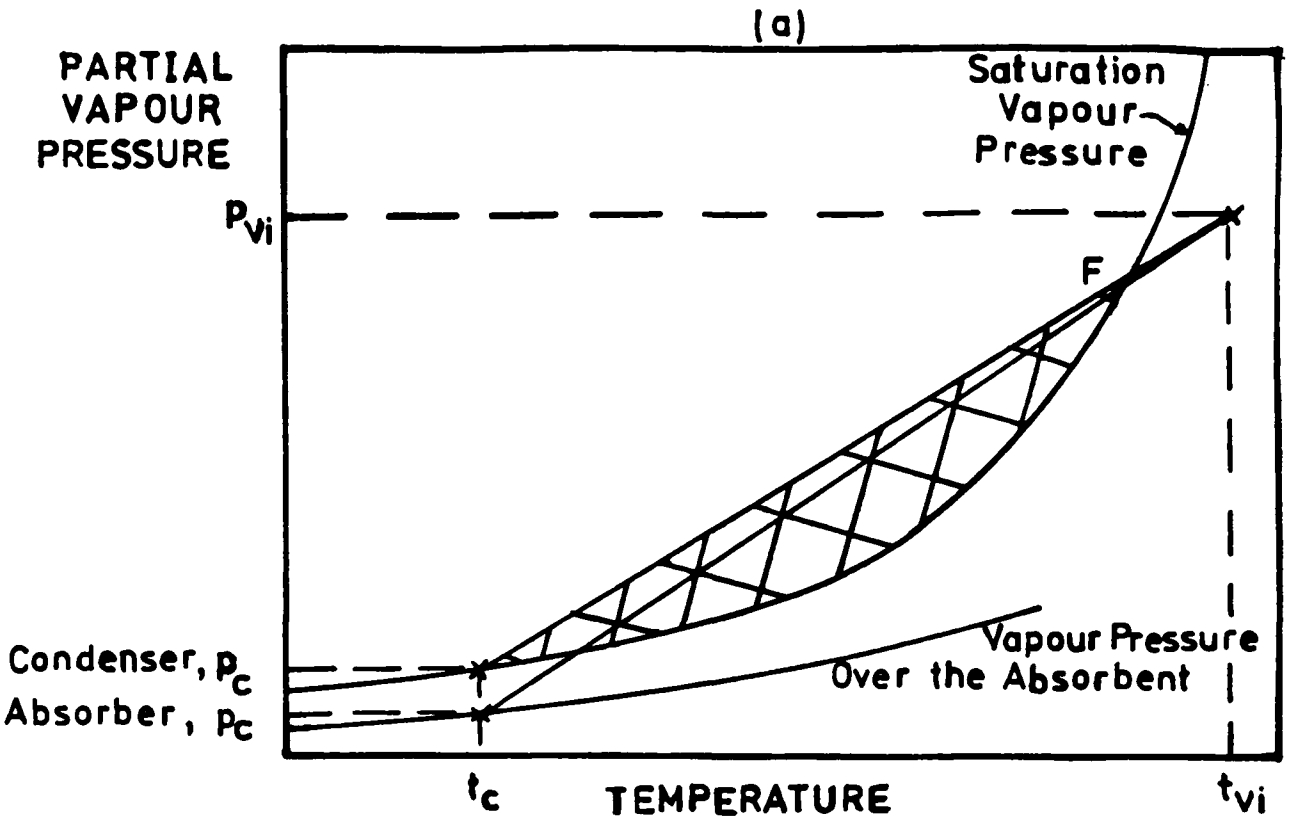

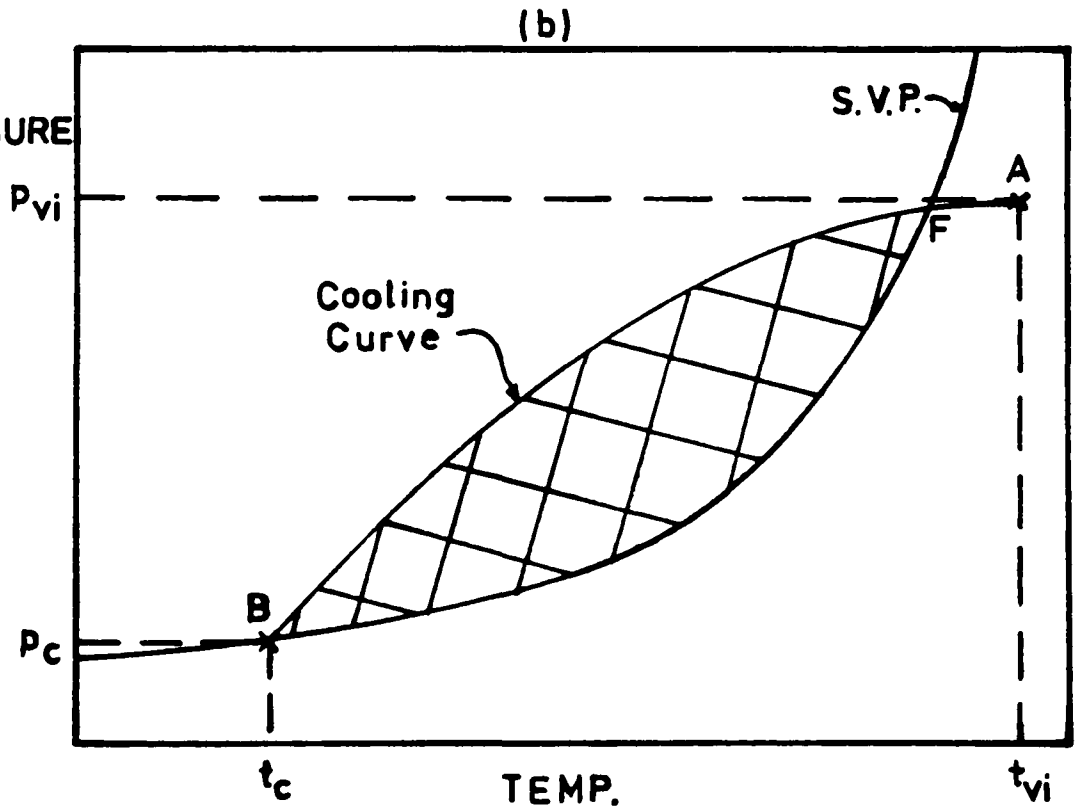

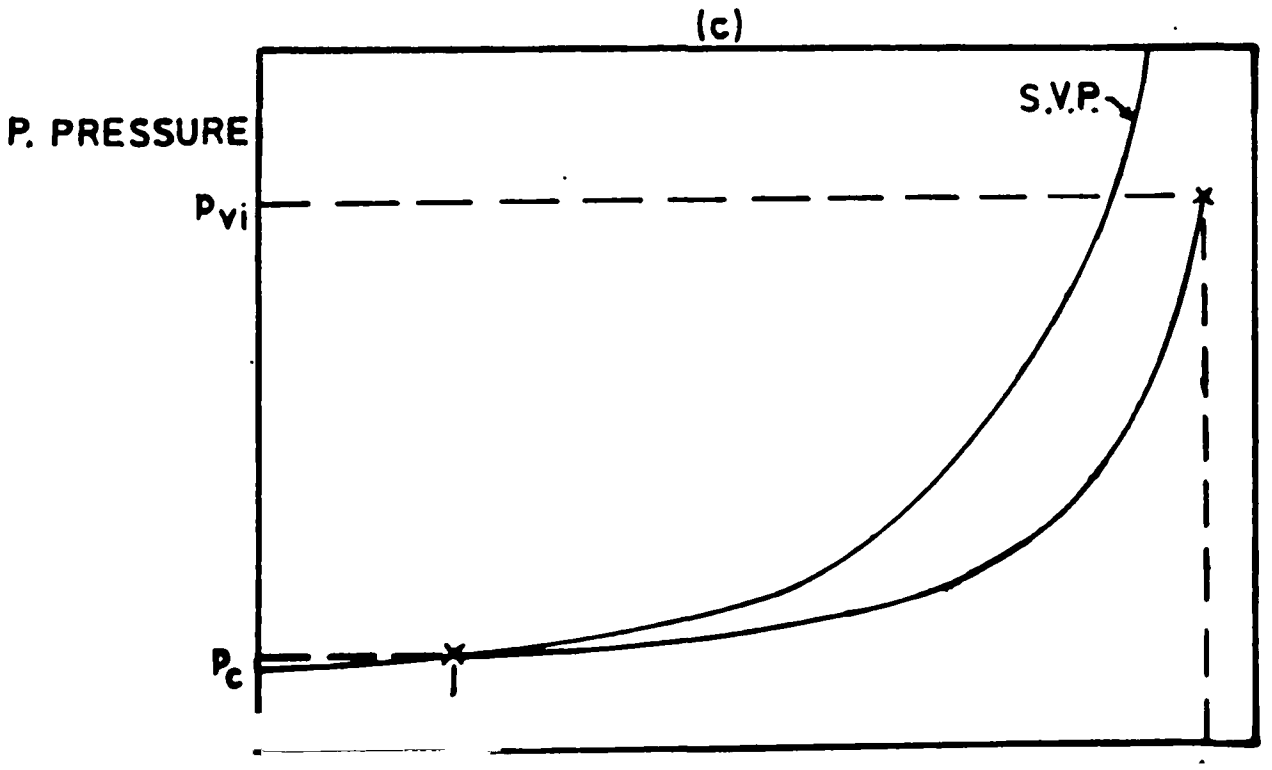

regions represent the parts of the cooling path where fog will potentially form given favourable nucleation kinetics. Figure 2.2.3.3(a) also illustrates the comparative difference between using a cooler absorber rather than a cold wall as the mode of condensation of vapour. The absorber uses a solvent as the cooling surface for collecting the vapour. As the solvent will have a solute vapour pressure that is lower than the saturation vapour pressure the point of incipient heterogeneous fog formation, F, will be lower than the comparable condenser situation.

The equation 2.2.10 derived by Colburn and Drew (1937) was modified slightly by both Bras (1955) and Gardner (1957). Gardner gives the following equation that traces the relationship between vapour pressure and temperature during the course of vapour condensation on a cold surface i.e. the cooling curve or operating line:

$$\frac{dp_v}{dt_v} = \left(\frac{1 - e^{-a}}{a}\right)\left(\frac{P - p_v}{p_{BM}}\right)\left(\frac{Sc}{Pr}\right)^{-2/3}\left(\frac{p_v - p_c}{t_v - t_c}\right) \qquad (2.2.23)$$

where $$a = \left(\frac{Pr}{Sc}\right)^{2/3}\left(\frac{M_v\, Cp_v}{M\, Cp}\right) \ln\left(\frac{P - p_c}{P - p_v}\right)$$

This equation must be solved by numerical integration so as to determine whether or not the cooling path of the vapour/gas mixture crosses the dewpoint curve at any point and hence if there is a possibility of fog formation.

Several authors (Johnstone et al, 1950; Bras, 1955; Amelin, 1967;

Rosner and Epstein, 1968) have theoretically shown that incipient homogeneous fog formation in dilute vapour/gas mixtures will always be a boundary layer phenomenon near the condenser's wall. This would seem to be borne out experimentally by Hampson and Furman (1953) who observed that in a horizontal condenser the first sign of fog was just below the pendant drops of condensate. Figure 2.2.3.4 illustrates the principle behind this point. The radial distance across a pipe within a condenser at which S_{max}, the maximum supersaturation occurs varies with distance along the pipe. Figure 2.2.3.4(a) illustrates this for a turbulent vapour/gas mixture moving along a cooled surface - the zone of maximum supersaturation shifts towards the turbulent core and $S < S_{max}$ is gradually established in the boundary layer. In laminar flow the processes which have been described for the boundary layer of turbulent flow extend over the entire pipe cross section (Figure 2.2.3.4(b)).

For the turbulent case, if $S_{max} > S_{crit}$ embryos will form in the boundary layer and fog droplets will first appear in the entrance section of the condenser. This fog formation will enhance the rates of mass and heat transfer in the boundary layer because the fine fog droplets are exceedingly good transferers of heat from the bulk vapour/gas stream to the interface. In effect, the temperature difference between the gas and the condensation surface is increased. Depending on the supersaturation in the turbulent core, the fog droplets formed in the boundary layer will, when they diffuse to the core, either evaporate suppressing further condensation or grow and intensify the rate of condensation.

Johnstone et al (1950) have rather elegantly shown that no fog can theoretically form in the boundary layer of a condenser within certain limiting restrictions given by this equation:

FIGURE 2.2.3.4 : SUPERSATURATION ACROSS A PIPE FOR a) TURBULENT AND b) LAMINAR FLOW (After Amelin)

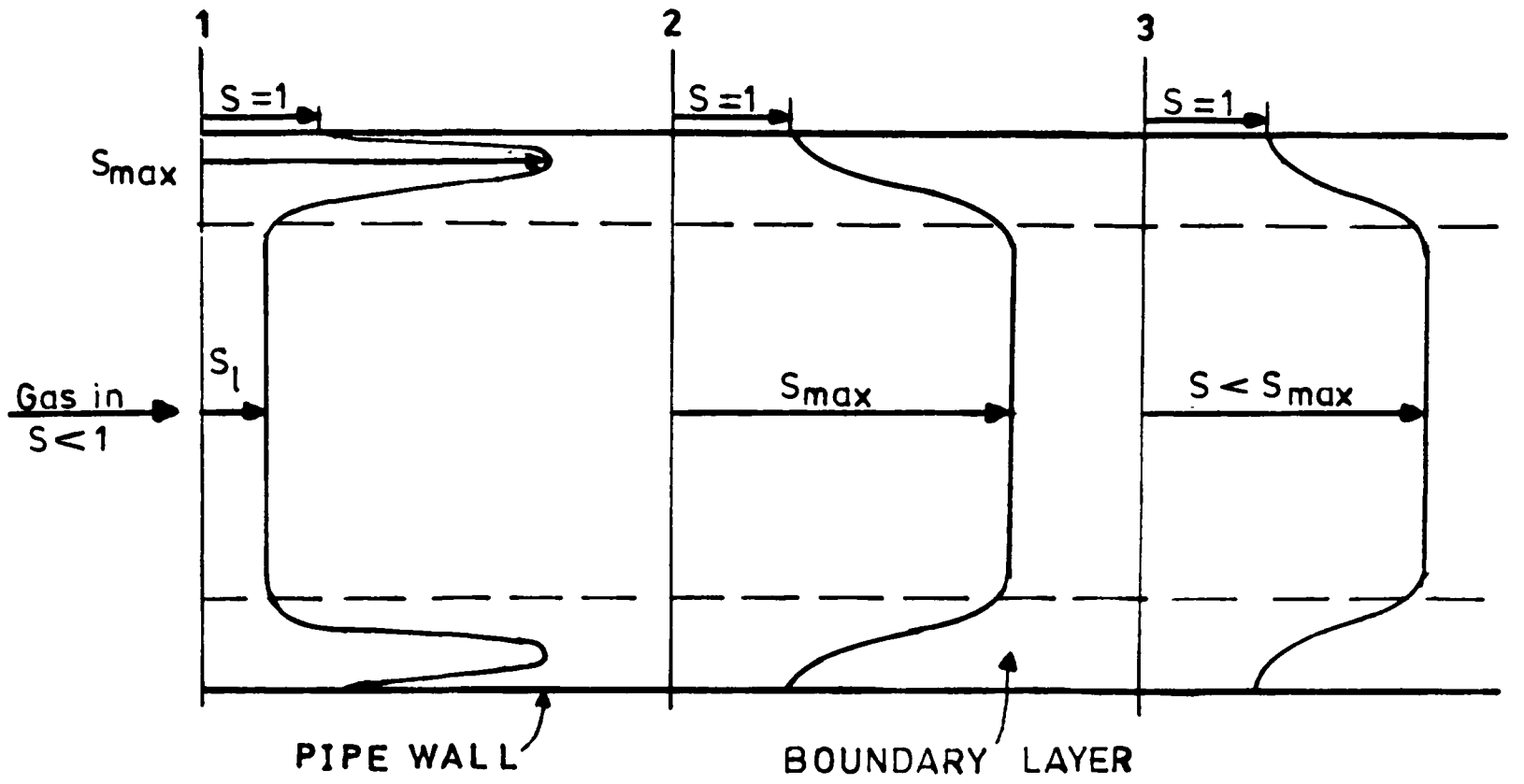

(a)

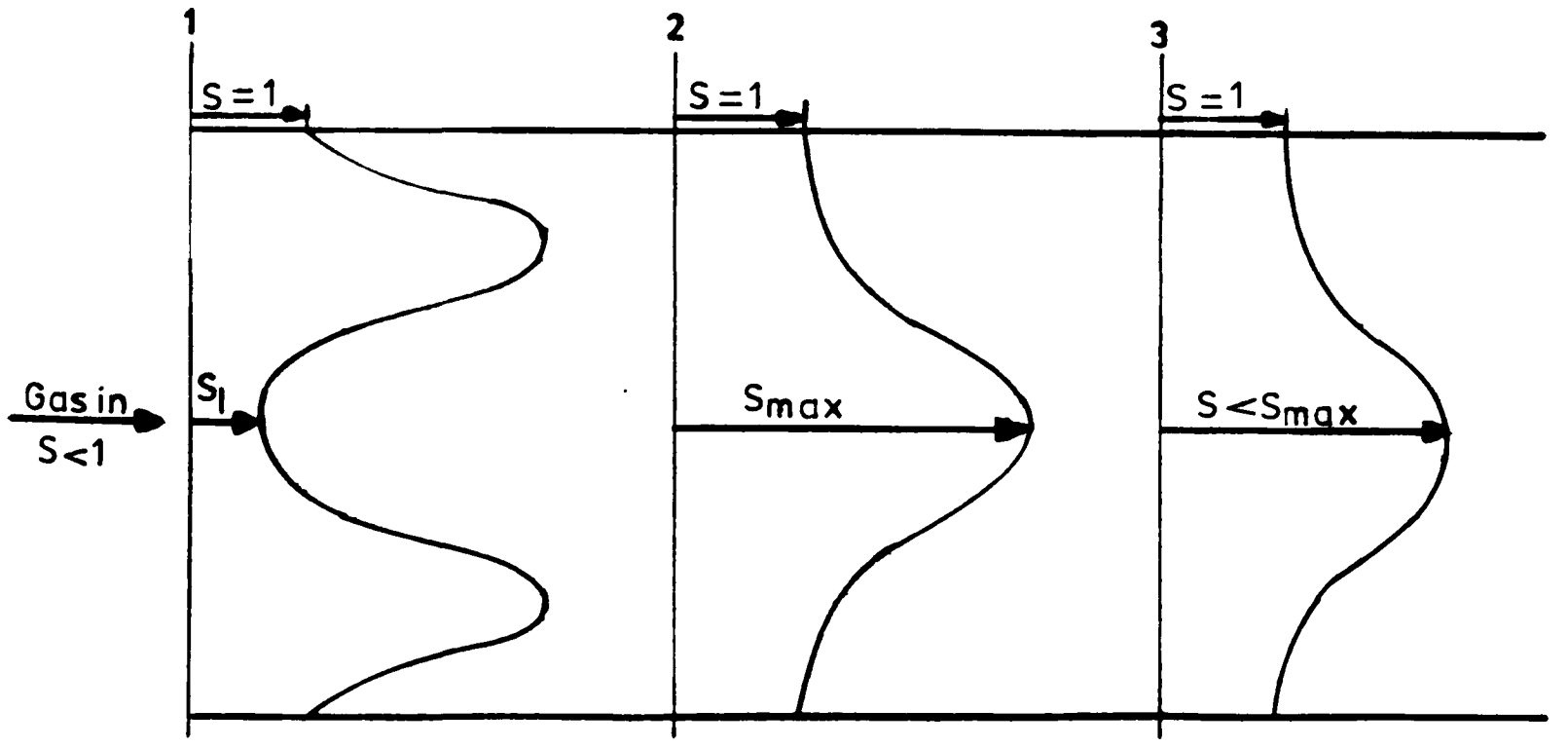

(b)

CROSS SECTIONS AT DIFFERENT POINTS ALONG THE PIPE

1= INLET SECTION

2= SECTION WITH $S=S_{max}$ AT MIDSTREAM

3= SECTION WITH $S<S_{max}$ AT MIDSTREAM

$$\left(\frac{p_v - p_c}{t_v - t_c}\right)_{crit} = \left(\frac{Pr}{Sc}\right)^{1/3} \left(\frac{a}{1 - e^{-a}}\right) \left(\frac{\lambda p_c}{R t_c^2}\right) \qquad (2.2.24)$$

The equation represents a straight line of slope $(p_v - p_c)/(t_v - t_c)$ which can be plotted on a pressure-temperature diagram. Figure 2.2.3.5 depicts several typical plots of the equation at different condensate interfacial temperatures, t_c, for any sulphur vapour/inert gas mixture. For example, assume a condensable mixture enters a condenser with inlet conditions pertaining to point A; then a condensate interface temperature of 220°C will produce fog whereas a t_c of 230°C will not produce fog. Hence, a fog can only form if a condensable vapour exists in a condition below the proposed t_c line. Johnstone et al proved the equation through qualitative observation of fog formation under controlled conditions for dilute steam/N_2, sulphur/N_2 and n-butyl alcohol/N_2 mixtures at atmospheric pressure.

Bras (1955) has proposed the following equation for determining the cooling curve in the boundary layer for a vapour/gas mixture:

$$\left(\frac{dp_v}{dt_v}\right)_g = \left(\frac{p_v - p_c}{t_v - t_c}\right) \left(\frac{P - p_c}{p_{BM}}\right) \left(\frac{Sc}{Pr}\right)^{1/3} \left(\frac{1 - e^{-a}}{a}\right) \qquad (2.2.25)$$

$$\text{where} \qquad a = \frac{M_v Cp_v}{M Cp} \left(\frac{Pr}{Sc}\right)^{2/3} \ln\left(\frac{P - p_c}{P - p_v}\right)$$

Here again, a numerical solution of this equation will provide information on whether the curve crosses the saturation vapour pressure line or not, i.e.

FIGURE 2.2.3.5 : LIMITS FOR FOG FORMATION OF SULPHUR VAPOUR (After Johnstone et al)

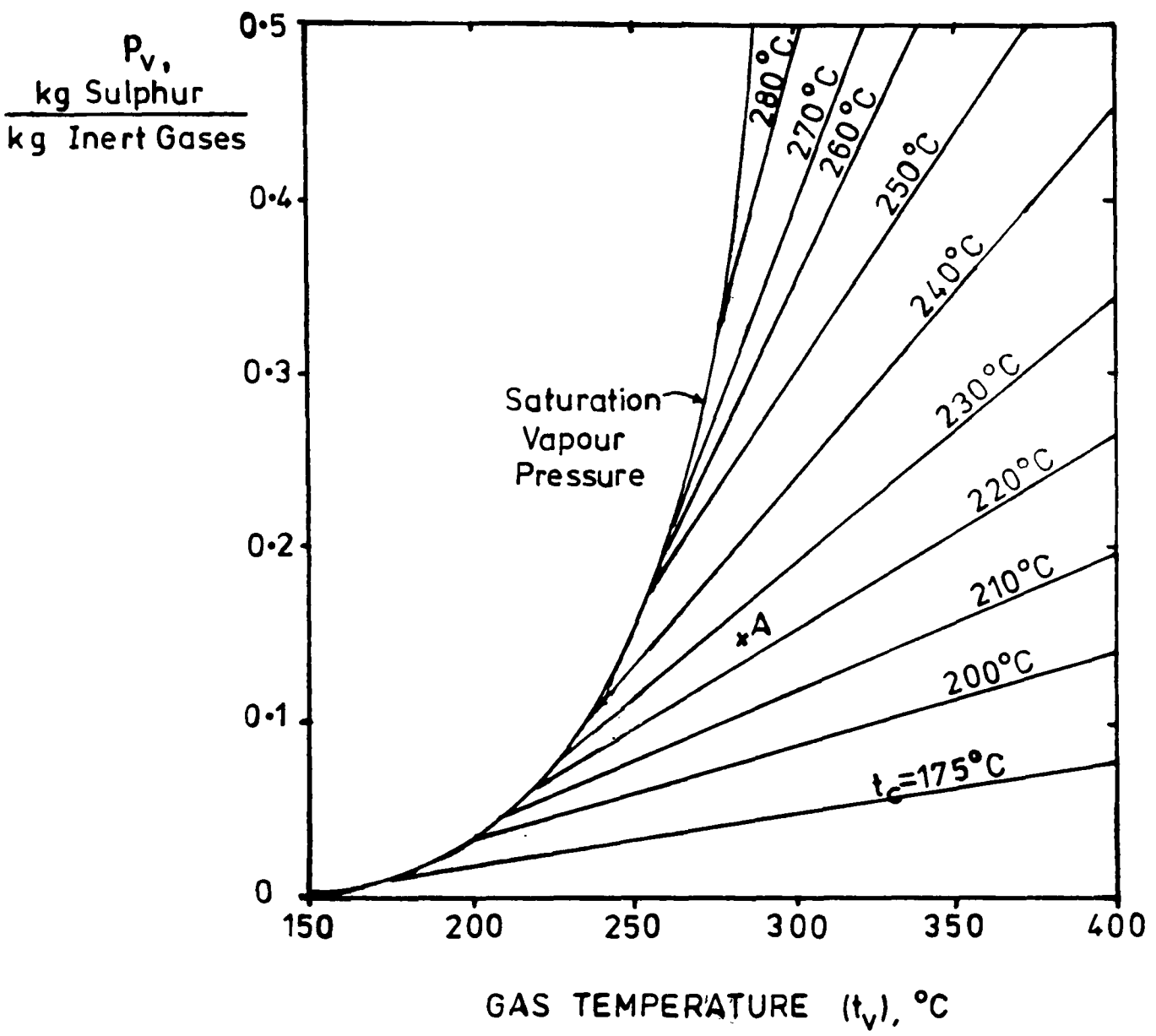

whether or not fog may form in the boundary layer.

Gardner (1957) has given an equation for determining the boundary layer cooling curve for any point within the condenser:

$$\left(\frac{t_{vg} - t_c}{t_v - t_c}\right) = 1 + \left(\frac{a}{1 - e^{-a}}\right)\left(\frac{Pr}{Sc}\right)^{1/3}\left(\frac{p_{vg} - p_c}{p_v - p_c}\right)\left\{1 + \left[\left(\frac{a}{1 - e^{-a}}\right)\left(\frac{Sc}{Pr}\right)^{1/3} - 1\right].\left(\frac{p_{vg} - p_c}{p_v - p_c}\right)\right\} \qquad (2.2.26)$$

where a is as defined in equation 2.2.25.

For the situations where inert gas concentration is relatively low and heat and mass transfer rates are high Bras (1953b) gives a variant of Colburn and Drew's (1937) equation for the bulk mixture:

$$\frac{dp_v}{dt_v} = \left(P - p_v\right)\left(\frac{p_v - p_c}{t_v - t_c}\right) \Bigg/ \left[p_{BM}\left(\frac{Sc}{Pr}\right)^{2/3} + \left(p_v - p_c\right)\left(\frac{M_v Cp_v}{MCp}\right)\right] \qquad (2.2.27)$$

In section 2.2.1.2.1 modified j-factors for high heat and mass transfer rates (equations 2.2.6, 2.2.7 and 2.2.8) as determined by Cairns and Roper (1955, 1954) were presented. If they are substituted into the derivation of the Gardner operating line (equation 2.2.23) rather than the conventional

Chilton-Colburn j-factors then the following equations result:

$$\frac{dp_v}{dt_v} = \left(\frac{1 - e^{-a}}{a}\right)\left(\frac{2}{2+a}\right)\left(\frac{Pr}{Sc}\right)^{2/3}\left(\frac{P - p_v}{p_{BM}}\right)\left(\frac{p_v - p_c}{t_v - t_c}\right)\left(\frac{p_{BM}}{P}\right)^{-0.05} \qquad (2.2.28)$$

for co-current condensers, and

$$\frac{dp_v}{dt_v} = \left(\frac{1 - e^{-a}}{a}\right)\left(\frac{Pr}{Sc}\right)^{2/3}\left(\frac{P - p_v}{p_{BM}}\right)\left(\frac{p_v - p_c}{t_v - t_c}\right)\left(\frac{p_{BM}}{P}\right)^{-0.10} \qquad (2.2.29)$$

for countercurrent condensers

where a is as defined in equation 2.2.25.

Other workers in this field (Schuler and Abell, 1956; Sikchi, 1956 and Coughanowr and Stensholt, 1964) have tried to predict actual amounts of fog formation. Here again, only local quantities of fog forming within a condenser were calculated. Thus, numerical or graphical integration techniques are required to estimate the maximum quantity of mist expected to leave the condenser. Moreover, certain simplifying assumptions are explicit in the equations presented by Coughanowr and Stensholt.

There has been a wide body of research in the related metallurgical field of the enhancement of diffusion-limited vaporisation rates by condensation within the thermal boundary layer (Turkdogan, 1964a,b; Hills and Szekely, 1969, 1964; Rosner, 1967). In essence, these authors were

studying the phenomenon of molten metals, on exposure to room temperature gases, producing rates of vaporisation considerably higher than those predicted for isothermal conditions using conventional mass transfer correlations. In effect, what was happening was that condensation in the boundary layer close to the evaporating surface was inducing fog nuclei to form. These nuclei provide a large surface area for further condensation thereby increasing the rate of evaporation by up to ten times greater than that normally expected.

From a different perspective Toor (1971a,b) has studied the same problem of fog formation in boundary value problems. With simplifying assumptions he uses the equations of energy and diffusion state to determine local rates of fog formation. He also postulates equations showing the discontinuous nature of the fog formed in the boundary layer. At the interface between clear and fog regions he shows that the fog vaporises discontinuously as there is continuous condensation in the fog region. He suggests that detached fogs will form within the boundary layer when the interfacial vapour condition is less than the saturated vapour pressure, i.e. there is an interfacial resistance. Quite separately, Hayashi, Takimoto and Kanbe (1976) and Buckle (1989) have reinforced the predictions of Toor's model in their experimental studies of induced fog condensation during the forced evaporation of vapours from sink liquids (the opposite transport flux to that considered in this work). The condensed metallic fog droplets produced by Buckle's experiments when collected as powders were shown to have much wider size distributions than powders produced by atomisation techniques.

Recently, Bettelheim et al (1980) have studied the rates of fog formation in flue-gas washing plants (cooler absorbers). Here again, dilute

vapour/gas mixtures were considered and predicted fog losses were of the order of 1-2%. They discovered that though fog condensation in the boundary layer has little effect on the overall rates of heat and mass transfer, neglecting its effect in their fog models underestimated the amount of fog formed by a factor of up to 3. Hence, most fog must have formed in the boundary layers. They also point out that the amount of fog formed increased when the coolant water temperature was decreased. Moreover, transition from fog condensation in the boundary layer alone to fog condensation in the bulk mixture was very rapid.

CHAPTER 3: TOP-BLOWING EXPERIMENTAL WORK

3.1 APPARATUS

3.1.1 Analogue Model of the Smelter Converting Hearth

A full-scale water model of the converting branch of the Warner smelter was used for all the experiments. A schematic diagram of the model with peripheral equipment is illustrated in Figure 3.1.1. Plate 3.1 shows the general layout of the model looking from above and up the channel.

The channel was constructed of mild steel plate with internal dimensions identical to that of the upper hearth of the smelter. It is rectangular, 3.96 m long by 0.35 m wide by 0.3 m deep. At the outlet end, the channel has a step of 7.6 cm depth to simulate a small forehearth in the real smelter. At this end of the channel there is an overflow weir with a 5 degree slope which simulates the crossover between the hearths in the actual smelter. The channel itself is raised at the feed end so that it has a 1^{o} slope to mimic that existing in the smelter.

It is important with this model to physically simulate the flow of fluids in the channel such that a direct analogue to the smelter is produced. In order to achieve this exactly similar tin-plated rectangular boxes were constructed to simulate the electrical heating anodes in the smelter. Water was fed to the channel through a 'snorkel leg' arrangement. This consisted of a 13 cm diameter pipe fitted with a retaining gauze at the outlet end and half-filled with pellets. This was developed to ensure a head of water in the pipe during operation so that water would enter the model uniformly. A polystyrene rectangular block was shaped and stuck to the pipe to mimic the

LEGEND TO FIGURE 3.1.1

A	Water Distributor
B	Water Rotameter
C	Oxygen Purge
D	Packed Column Absorber
E	Oxygen Sparger
F	Oxygen Cylinder
G	Compton Compressor
H	Cooling Coil
I	Gas Rotameter
J	Gas Thermometer
K	Gas Distributor
L	'Snorkel Leg'
M	Gas Manometers
N	'Anode'
O	Lance Holding Frame
P	Glass Lance
Q	Beckman Oxygen Monitor
R	Oxygen Probe
S	Channel Tank
T	Overflow Tank
U	Clear Plastic Cover
V	Liquid Thermometer
X	Valves
Ⓟ	Pressure Gauge

FIGURE 3.1.1 : SCHEMATIC LAYOUT OF THE TOP-BLOW MODEL OF THE CONVERTING BRANCH OF THE SMELTER

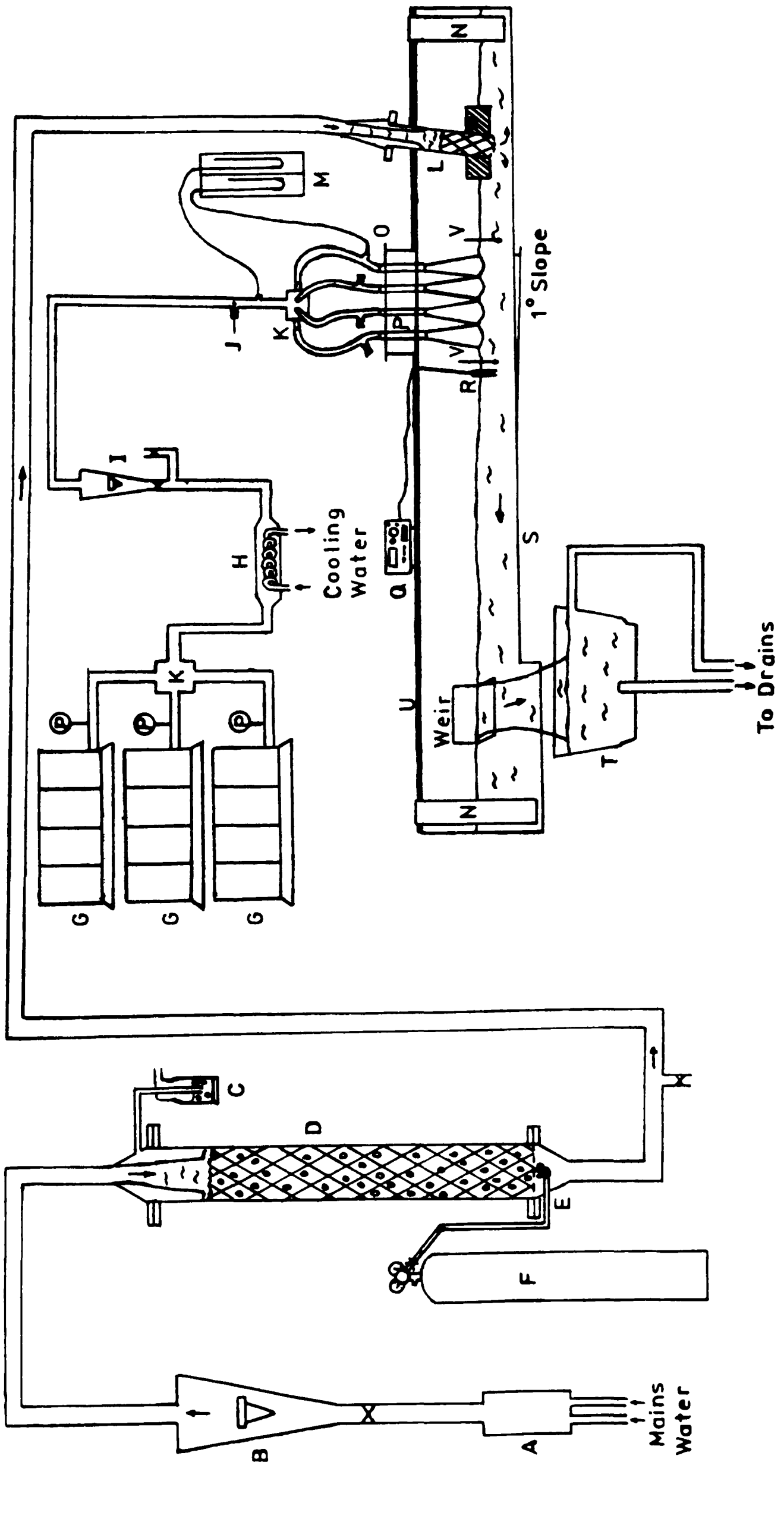

PLATE 3.1

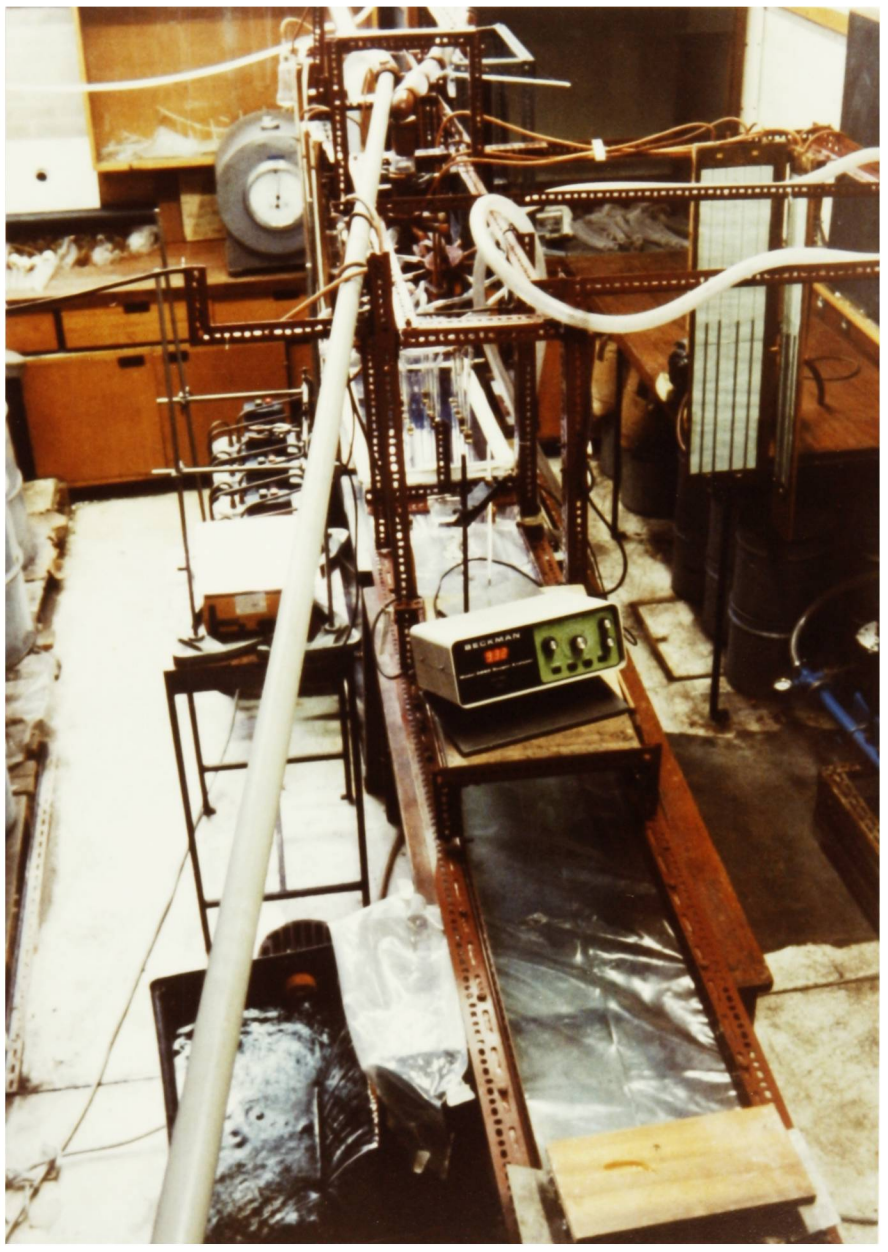

PHOTOGRAPH SHOWING GENERAL

LAYOUT OF THE TOP-BLOWING APPARATUS

refractory blocks around the actual RH snorkel leg in the smelter. The snorkel leg in the model was also tilted at an angle of 17^{o} to the normal to be in line with that in the high temperature rig. The whole of the top of the channel was sealed with clear plastic so that the off-gas from the impinging gas jets could only exit via the outlet weir. This ensures that gas phase flow patterns were comparable to that in the smelter. A perspex window was added to the side of the channel at the top-blow region to view the liquid phase flow patterns during top-blowing.

Water enters the channel from the mains after passing through a distributor, rotameter and absorption column. The column is a 15 cm diameter pipe with a retaining plate holding up a randomly packed bed of 1/2 inch PVC pall rings 80 cm high. The column was run liquid phase continuous due to the large volumetric flowrates of water fed through it. Oxygen was introduced into the column below the base plate through a sintered porous ceramic rod. A gas purge at the top via a Dreshell bottle permitted oxygen to exit the column. This method of superoxygenating the water relative to air before it is fed to the channel was used for the air jet oxygen desorption tests. A steady state bulk oxygen concentration in the feed water could be approached within about 30 minutes. The steady state level depended on the cylinder pressure used but was typically in the range 20 to 35 ppm (parts per million by mass). Normal water saturation concentrations are around 10 ppm. With the desorption runs using nitrogen gas jets the mains feed water was desorbed of its inherent oxygen content thus no superoxygenation was necessary.

It is important to note that the water system in the model is a once-through operation with no recycle. This ensures that the temperature of the water will vary little over a 10 minute top-blow run with the present

system. If a pump is used to recirculate the water in a closed system the water will steadily heat up thus making the calibration of the oxygen monitor and the recording of readings very difficult.

In the high temperature smelter the matte will circulate at a minimum flowrate of 90 litres/minute or a Re of 5248. To ensure dynamic similarity a comparable Reynolds number in the model is necessary. The 1^{o} slope of the model has a pronounced effect on the level of water at different points in the channel. For instance, a liquid depth of 10.5 cm at the snorkel end of the channel will rise to 16.0 cm at the weir. Over the top-blow region the level of the water rises from 12.4 to 13.6 cm. Taking an average value of 13.0 cm as the depth, an hydraulic mean diameter for the rectangular water profile in the channel of 0.293 m results. Assuming water to be at $10^{o}C$ then;

$$\rho_L = 999.7 \text{ kg/m}^3$$

$$\mu_L = 1.31 \times 10^{-3} \text{ Ns/m}^2$$

$$\text{Thus } 5248 = \frac{0.293 \times V_L \times 999.7}{1.31 \times 10^{-3}}$$

So $V_L = 2.35$ m/s or $Q_L = 3.68$ m^3/hr.

This flowrate of 3.7 m^3/hr was one of several flowrates used in the testwork to study the effect of a flowing liquid phase on oxygen mass transfer due to impinging gas jets. Higher flowrates were not used during the experiments as the O_2 concentration differentials across the top-blow region during a run became so small that the experimental error rose to unacceptably high

levels.

3.1.2 Gas Delivery to the Lances

Gas for the top-blowing lances was supplied either by compressors for the air jet desorption runs or by a set of cylinders for the nitrogen jet desorption runs. The compressors used for the tests were Compton 8D/416-6 reciprocating diaphragm type units. The compressors were completely free of oil thus eliminating the possibility of oil films adversely affecting mass transfer at the interface. They were also capable of producing a steady air flow without the need for additional smoothing. They also had filters on the inlet pipes thus eliminating any other foreign organic substances from entering the system.

As illustrated in Figure 3.1.1 air was supplied from the three Compton compressors to a distributor box and then a glass cooling coil where the temperature of the gas was adjusted. This facility was used to vary the inlet gas temperature to the lances such that it was at the dry bulb temperature of the water in the channel. After the cooling coil the gas flow was regulated by two valves; one to bleed to atmosphere and one to throttle the flow. The gas flow was then metered through a rotameter before entering the second distributor box. Prior to the distributor there was a thermometer in the line measuring the gas temperature as well as a second tapping to a mercury or water manometer (a pressure tapping). The distributor box was constructed such that all the outlet pipes were identical and equally positioned around the box. This was critical as it ensured equal gas distribution to each lance. Each lance was fed by an identical piece of tubing with identical pressure

tappings. During a run, several of the lance tappings were taken to manometers. These manometers provided a visual indication of identical blowing conditions for each lance.

3.1.3 Multiple Lance Assemblies

The four types of glass lance used in this study are illustrated in Figure 3.1.2, photographed in Plate 3.2. To cater for a possible large number of 2.26 mm lances in the top-blow region two different lance-holding steel plates were constructed. The triangular pitch plate is illustrated in Figure 3.1.3 and the square pitch plate in Figure 3.1.4. Also included in either figure is a depiction of the projected jet impact patterns in the channel for a specified lance height if a full array of lances is utilised.

The lance-holding plates in Figures 3.1.3 and 3.1.4 have an array of holes drilled in them 74.2 mm apart. The holes are 20 mm in diameter so as to hold corks with centrally bored holes through them of 7 mm diameter. This means that the lances could be pushed through the corks and then inserted into position on the plate. This method also allows for the option of variable lance height. A second steel plate identical to the first was screwed into position 10 cm directly above the lower plate by way of threaded rods. A second cork securely placed in the top plate and the lance inserted into it resulted in a securely held vertical lance. These double-plate lance-holding units were very flexible and provided scope for various permutations in interlance spacing during testwork.

For the 2.26 mm nozzles only close-packed arrays were considered as the 35 and 36 lance jet configurations stretched some 75 cm along the

FIGURE 3.1.2 : LANCES USED DURING THE TESTWORK

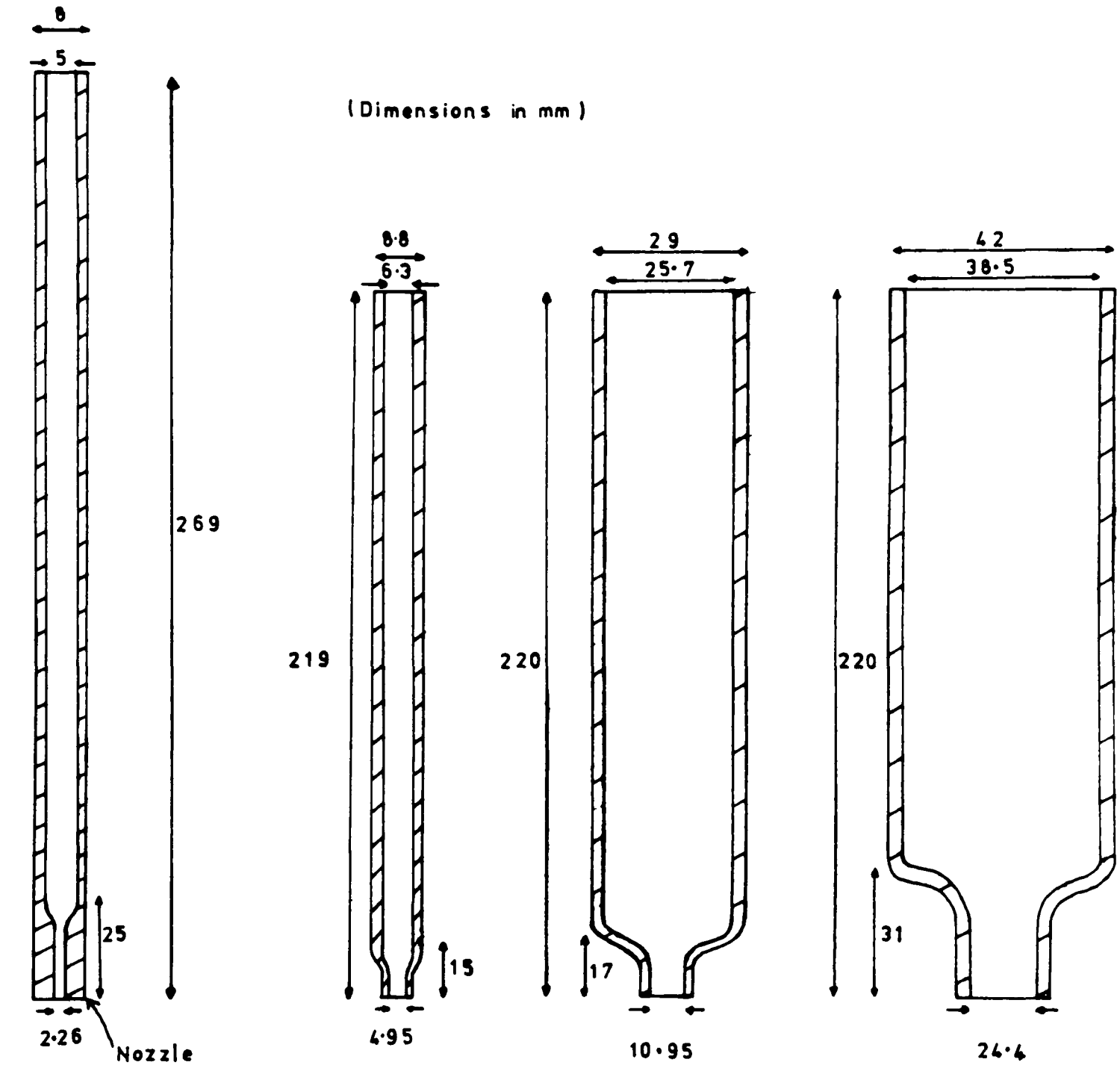

a) 2·26mm LANCE b) 4·95mm LANCE c) 10·95mm LANCE d) 24·4mm LANCE

PLATE 3.2

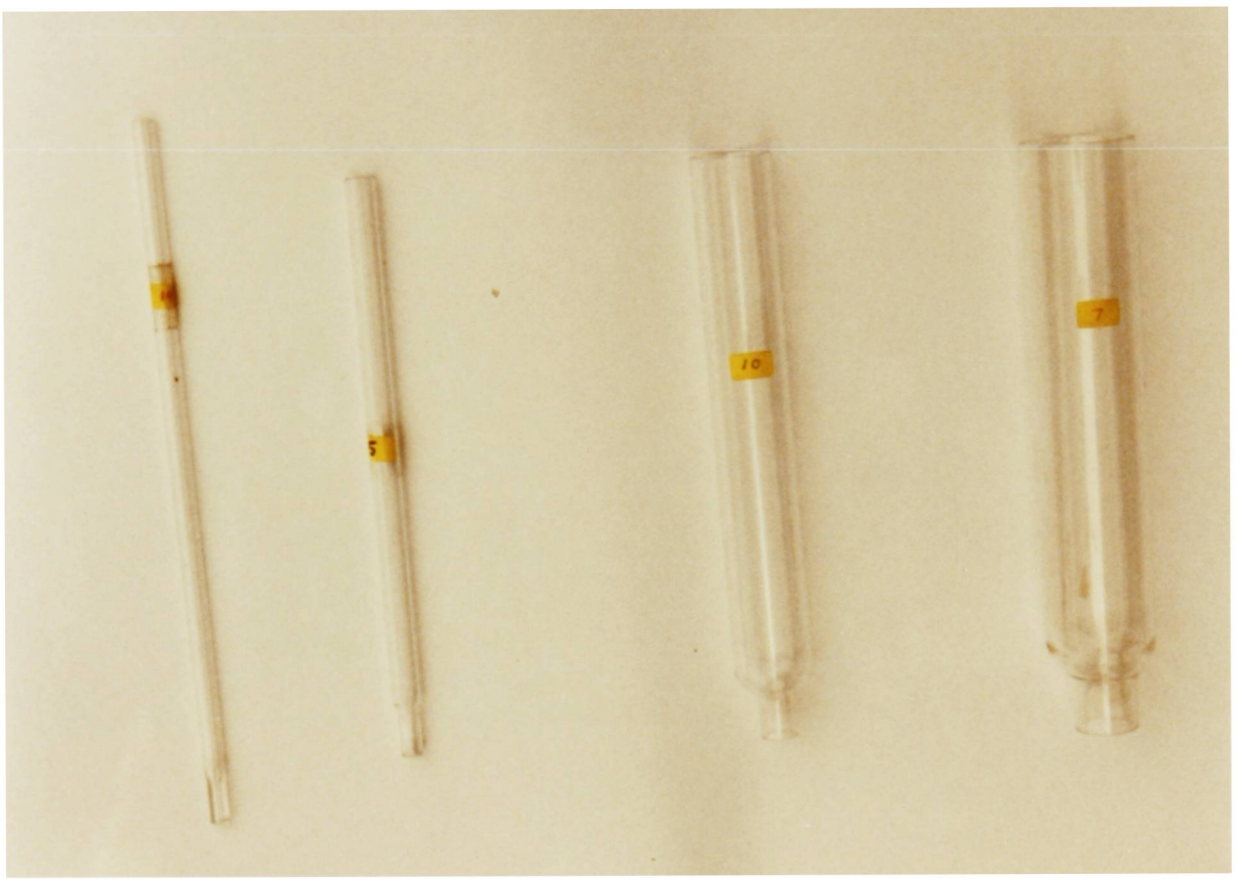

GLASS LANCES USED IN THE TESTWORK

FIGURE 3.1.3 TRIANGULAR PITCH LANCE-HOLDING PLATE,(a), AND CLOSE-PACKED PROJECTED JET IMPACT AREAS IN THE CHANNEL FOR 2.26mm NOZZLES,(b)

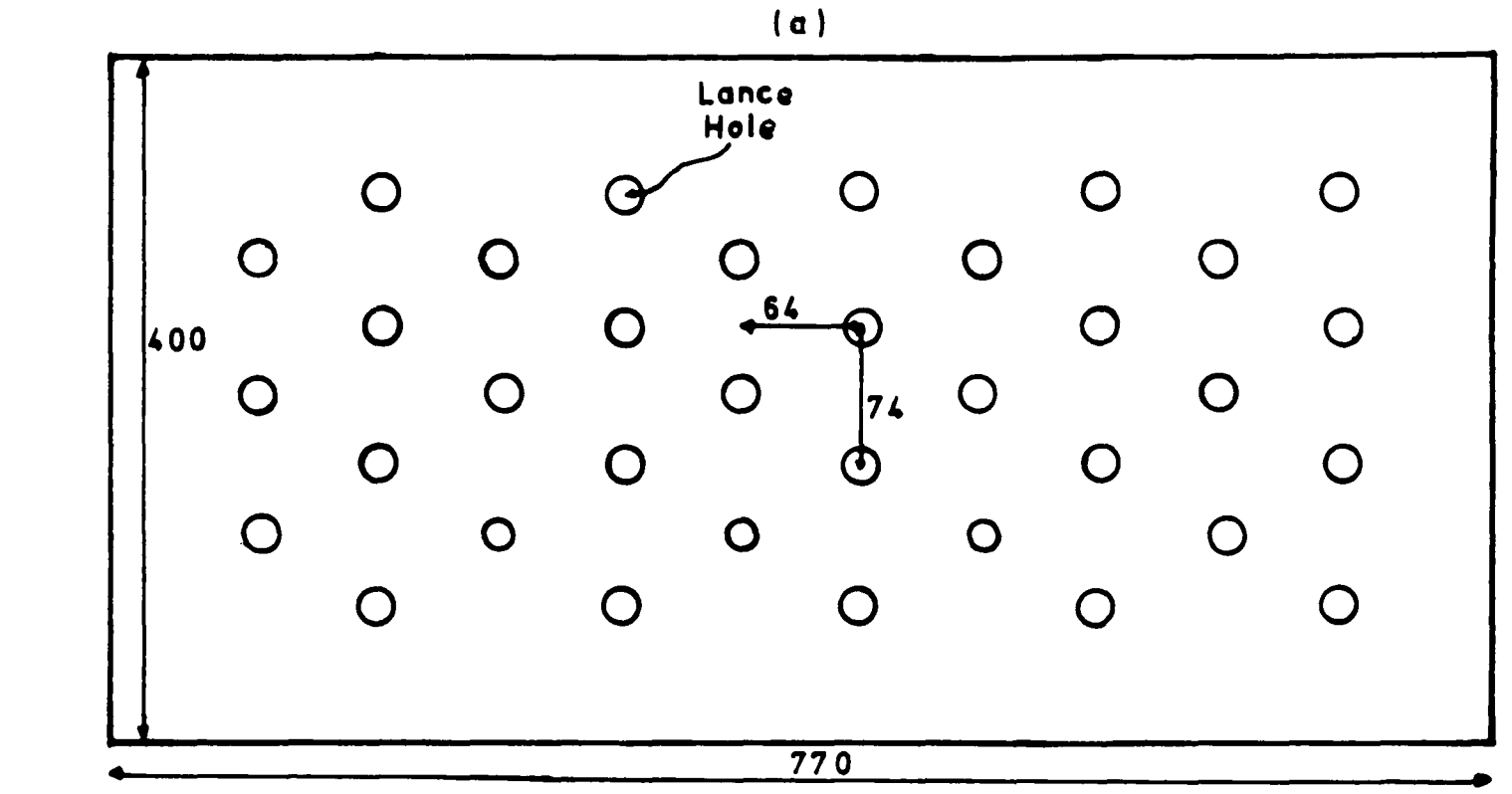

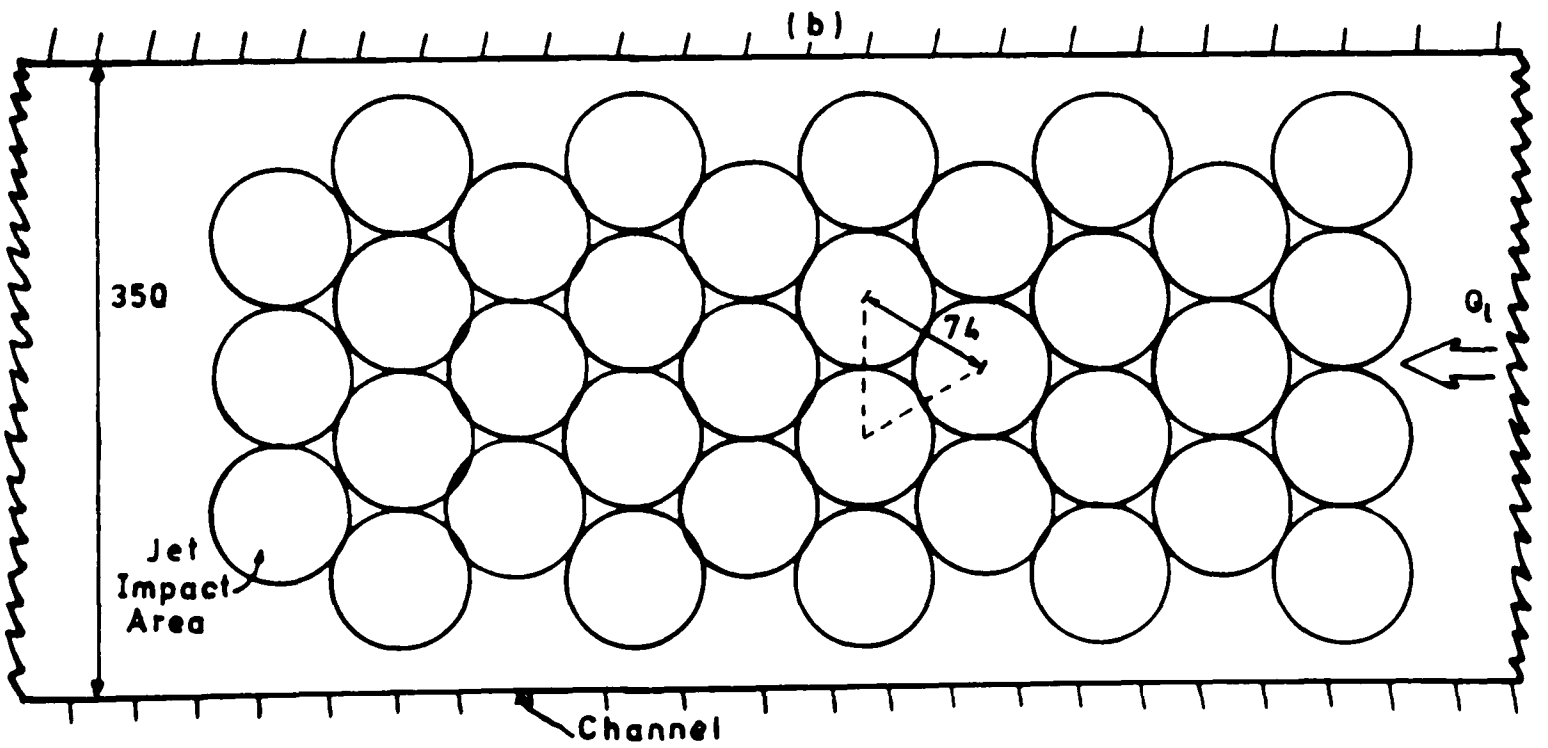

FIGURE 3.1.4 SQUARE PITCH LANCE-HOLDING PLATE,(a), AND CLOSE-PACKED PROJECTED JET IMPACT AREAS IN THE CHANNEL FOR 2.26mm NOZZLES AT H=20cm,(b)

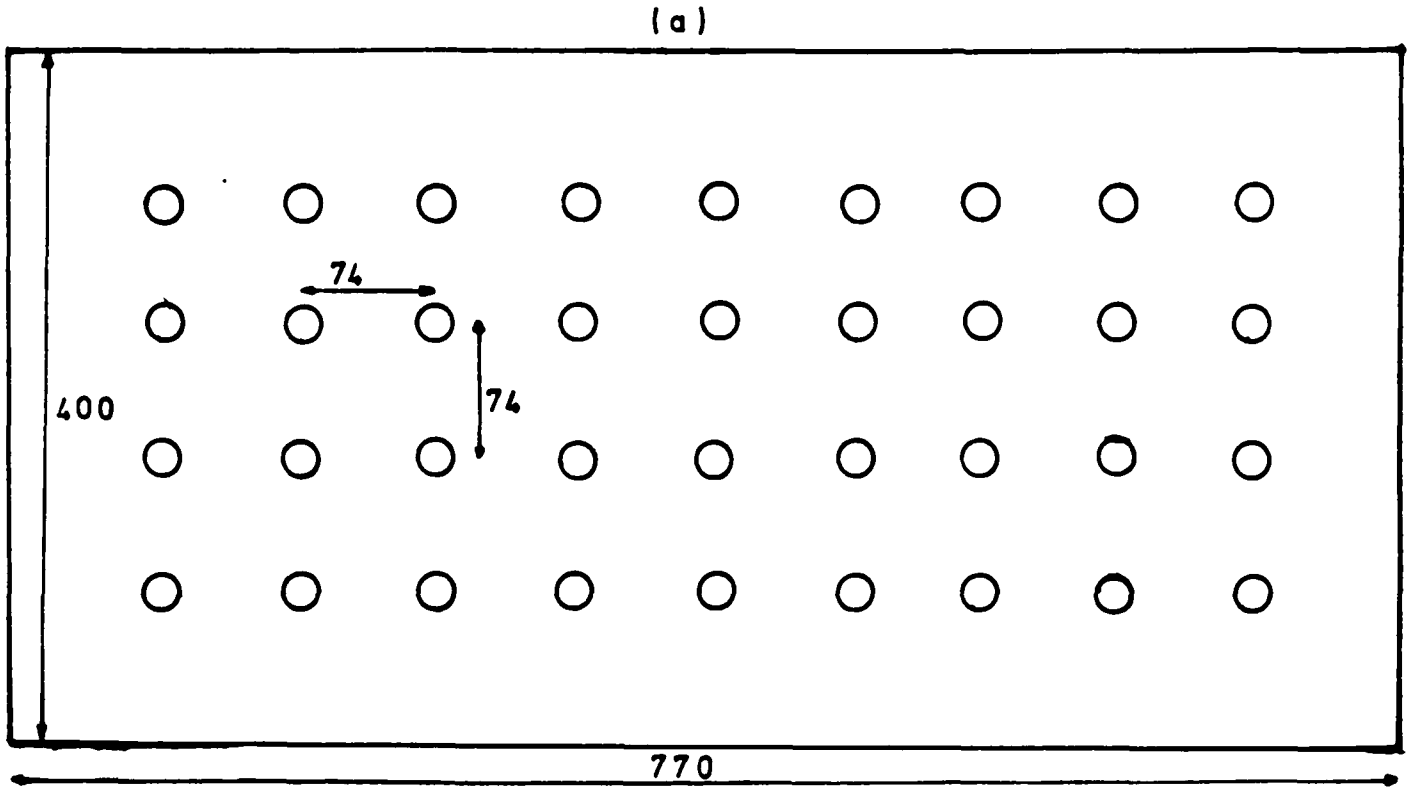

length of the channel. Due to practical restrictions the top-blow region in the pilot scale smelter is restricted to at most 1 m in length so that comparable 35 and 36 lance open-packed arrays of sufficiently large interlance spacing were not possible.

Six other multiple nozzle arrays were considered in the testwork, namely 16 x 4.95 mm, 7 x 10.95 mm and 4 x 24.4 mm nozzles (in open and close-packed formats). Figures 3.1.5 - 3.1.7 illustrate these multiple lance arrays in terms of the projected jet impact areas (for $\alpha = 21^{o}$) during channel flow.

3.1.4 Measuring Oxygen Concentration

A Beckman Model 0260 Oxygen Analyser (Plate 3.3) was used to measure both dissolved oxygen concentration in the liquid and gas phases. The instrument consists of a digital display that reads dissolved oxygen concentration to 0.01 ppm or 0.01% readability (for readings less than 20 ppm) together with an oxygen sensor on a flexible lead. For readings higher than 20 ppm it is accurate to 0.05 ppm. In operation the sensor is placed in the medium and oxygen from the medium diffuses through the sensor's membrane which separates the medium from the internal polarographic cell. Diffused oxygen is reduced electrochemically (consumed) in the cell, resulting in a current signal proportional to the oxygen partial pressure. The analyser has a temperature compensation control to allow for changes in medium temperature and for calibration.

In the case of water, variations in temperature will both affect oxygen partial pressure and solubility. Since the sensor only responds to partial pressure it is calibrated before each experimental run. This is done by

FIGURE 3.1.5 CLOSE AND OPEN-PACKED ARRAYS OF JET IMPACT AREAS IN THE CHANNEL FOR 4.95mm NOZZLES AT H=20cm

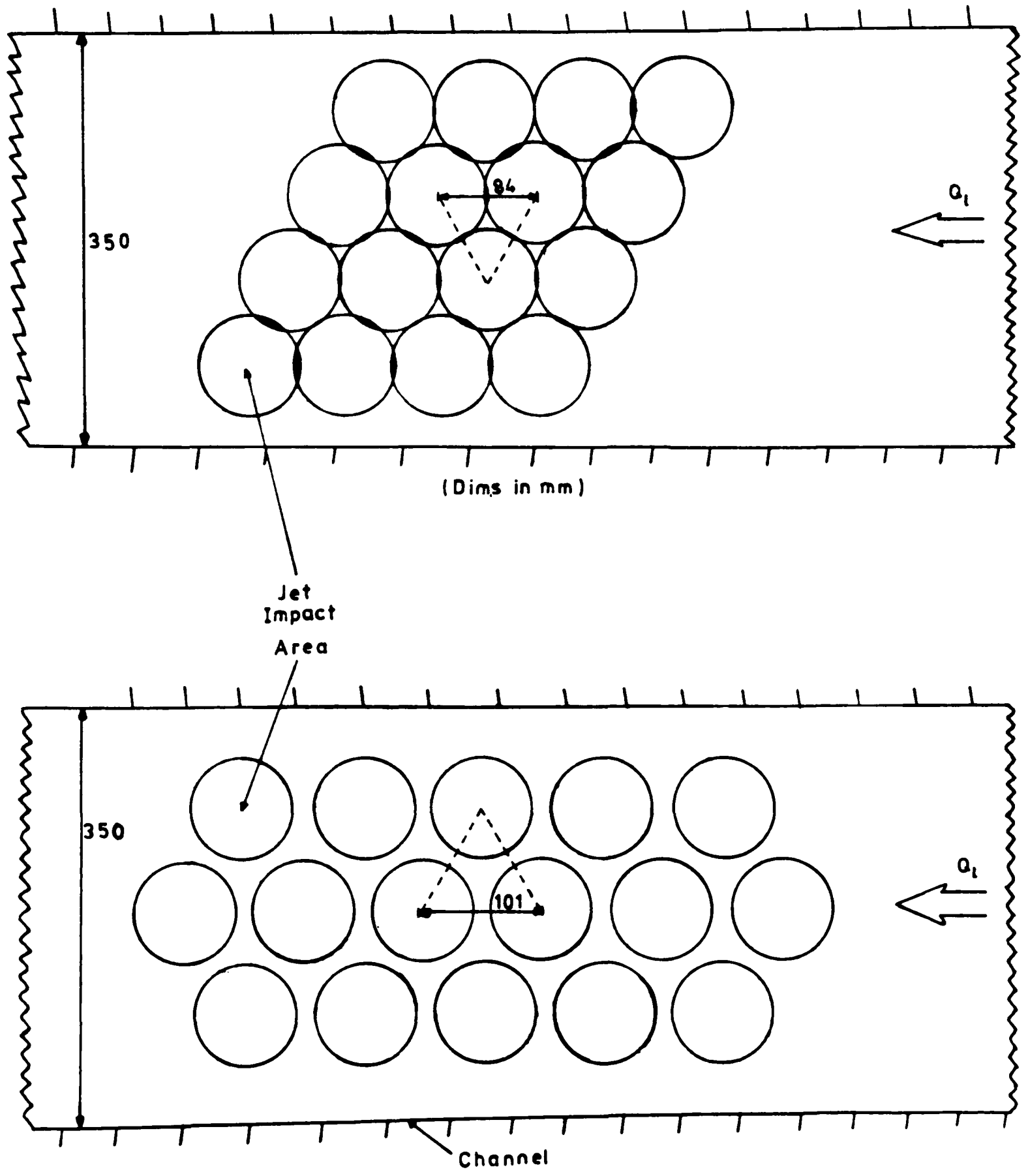

FIGURE 3.1.6 CLOSE AND OPEN-PACKED ARRAYS OF JET IMPACT AREAS IN THE CHANNEL FOR 10.95mm NOZZLES AT H=20cm

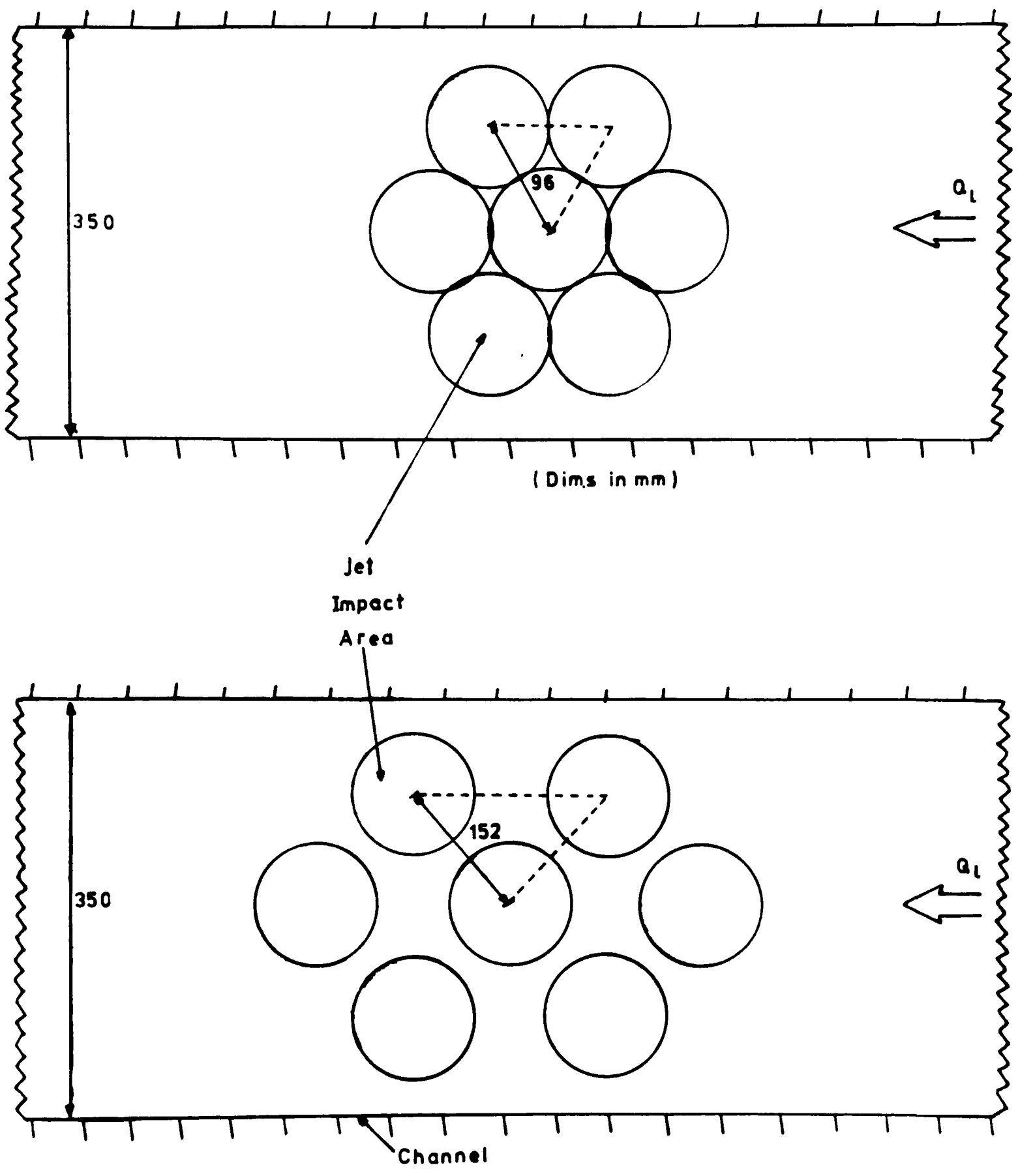

FIGURE 3.1.7 CLOSE AND OPEN-PACKED ARRAYS OF JET IMPACT AREAS IN THE CHANNEL FOR 24.40mm NOZZLES AT H=20cm

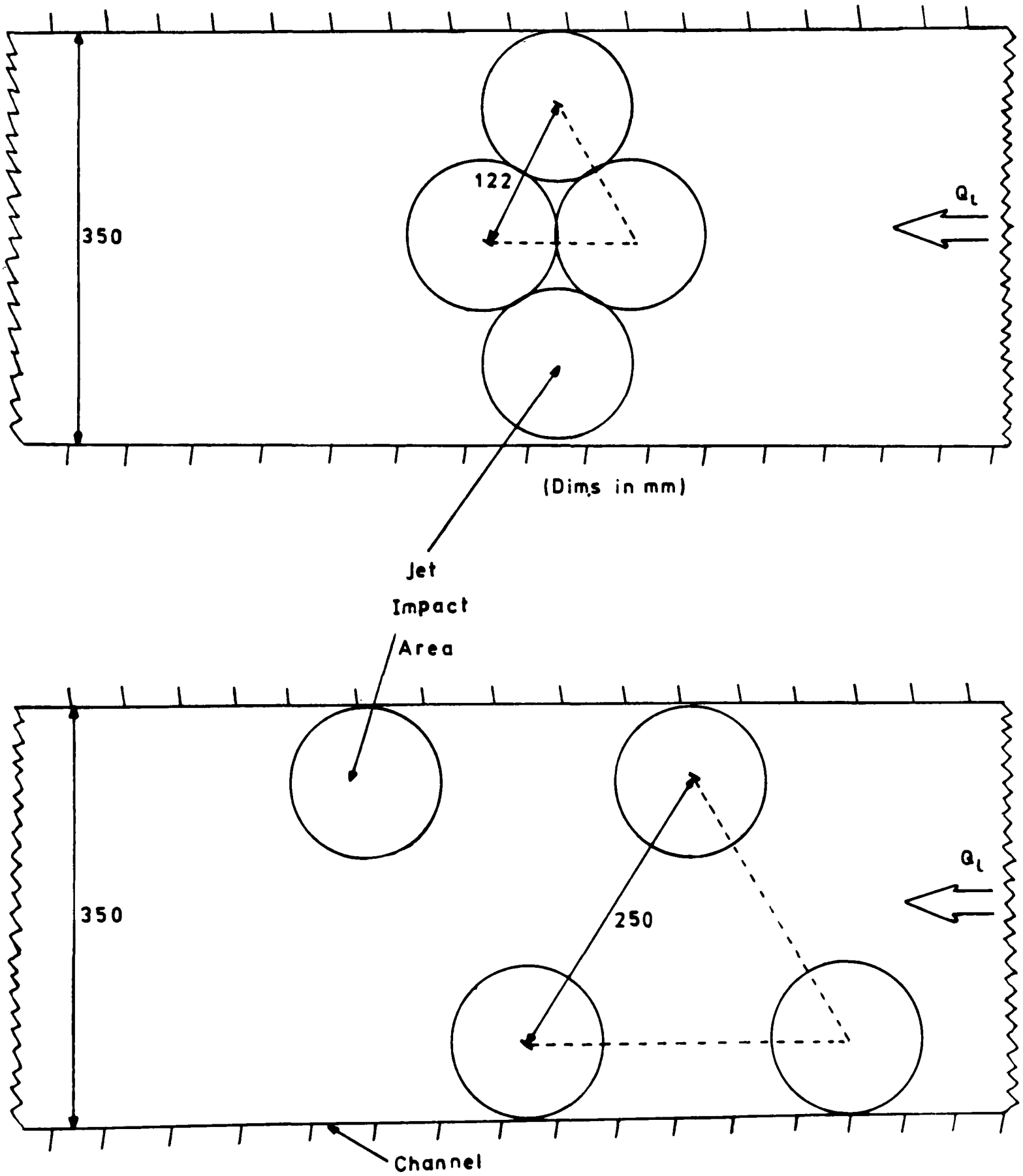

PLATE 3.3

BECKMAN OXYGEN ANALYSER AND

PROBE ASSEMBLY

taking a sample of water from the channel and bubbling air through it such that it is saturated. The manufacturers guarantee a less than 3% error in readings taken with a stationary probe in the medium. All experimental readings in this work utilised an auxilliary stirring accessory that allows the sensor to fit into it such that a small stirrer is directly below the membrane. This ensures a medium flowrate around the sensor of 3 m/s; enough to provide a maximum reading. A dexian support frame was constructed such that the sensor and stirrer could be lifted as a unit to take readings at any point across or along the channel. This meant that both upstream and downstream bulk liquid oxygen concentrations could be measured. For the runs where on-line readings were taken the probe was always 3.5 cm under the liquid surface. This was the lowest depth at which the stirring mechanism would work without the electrics being covered.

3.2 CALCULATION OF JETTING PARAMETERS

3.2.1 Comparison of Calculated and Measured Jet Momentum Fluxes and Mass Flowrates

In line with Jones (1986) and Wakelin (1966) the following assumptions governing sub-sonic flow through converging nozzles have been adopted for the purposes of calculating mass flow rates and momentum fluxes:

i) The flow through the nozzle is isentropic

ii) The gas expands adiabatically

iii) The pressure at the exit plane of the nozzle is atmospheric

iv) The velocity profile across the exit plane is uniform, which gives

$$\dot{m} = \rho_0 a_0 V_j \qquad (3.2.1)$$

These assumptions lead to the following expression for sub-sonic mass flow through a converging nozzle:

$$\dot{m} = a_0 \left[\frac{\left(\frac{2\gamma}{\gamma-1}\right) \cdot P_0 \cdot \rho_1 \cdot \left(\left(\frac{P_0}{P_1}\right)^{\left(\frac{2-\gamma}{\gamma}\right)} - \left(\frac{P_0}{P_1}\right)^{\frac{1}{\gamma}} \right)}{1 - \left(\left(\frac{P_0}{P_1}\right)^{1/\gamma} \cdot \frac{a_0}{a_1} \right)^2} \right]^{1/2} \qquad (3.2.2)$$

The upstream density, ρ_1, was calculated using the relation

$$\rho_1 = \left(\frac{P_1}{P_o}\right)^{\frac{1}{\gamma}} \cdot \frac{1}{\rho_o} \qquad (3.2.3)$$

where the upstream pressure, P_1, was measured by manometer.

The mass flowrate obtained from eq. 3.2.2 is the theoretical value that would be obtained for a perfect round nozzle with discharge coefficient, C_d, of unity. A value for C_d for a given nozzle can be obtained if the actual mass flowrate, over a range of operating conditions, is measured. For this analysis a Wright DM3F laboratory wet-type gas flowmeter was used to measure gas flowrate at atmospheric pressure: the actual mass flowrate being the product of the flowrate reading and ρ_o, the outlet density. The ratio of this actual mass flowrate to the theoretical mass flowrate gives a value for the discharge coefficient.

The value of C_d obtained using the above method was then incorporated into equation 3.2.2 and modified to include V_j such that the following expression for jet momentum flux is obtained:

$$\dot{M} = C_d\, a_o \left[\frac{\left(\frac{2\gamma}{\gamma-1}\right) \cdot P_o \cdot \left(\left(\frac{P_1}{P_o}\right)^{\left(\frac{\gamma-1}{\gamma}\right)} - 1 \right)}{1 - \left(\left(\frac{P_o}{P_1}\right)^{\frac{1}{\gamma}} \cdot \left(\frac{a_o}{a_1}\right) \right)^2} \right] \qquad (3.2.4)$$

$\dot{M}$ has units of force and for a given set of jetting parameters it can be compared with the actual force of the jet as measured on a Sartorius top-loading digital balance. A jet normally impinging on a flat surface will reverse on impact. The rebounding gas will be reentrained into the oncoming jet thus registering a higher momentum flux than is actually there.

Following the procedure of Wakelin (1966) a second plate with an 8.5 cm hole in the centre was supported by spacers and placed on the balance pan. The diameter of the hole was such that the jet passed between the two plates. The distance between the two was varied until an optimum of 0.5 cm was obtained. This was sufficient to contain the entire jet but small enough to prevent any entrainment of vertical velocity into the radial wall jet.

To compare the calculated and experimentally determined momentum fluxes over an extended range of nozzle Re, a series of calibration tests using a 2.26 mm glass nozzle blowing from a height of 0.20 m were carried out. Air was the jetting medium and a summary table of the results is presented below. The complete analysis is in Table A.1.2 of Appendix 1.

TABLE 3.2.1: Comparison of Calculated and Directly Measured Momentum Fluxes

Calculated Momentum Flux (N) (Eq. 3.2.4)	Measured Momentum Flux (N)	% Difference
0.0378	0.0373	1.1
0.0556	0.0564	1.4
0.0833	0.0829	0.1
0.1459	0.1511	3.9
0.2009	0.2157	6.9
0.2571	0.2726	5.7

Agreement between the two figures especially at the lower jet momentum fluxes is very good. All of the results reported in this experimental study have used jet momentum fluxes of around 0.15 N. A mean value for C_d, the discharge coefficient, for the 2.26 mm nozzle used was found to be 0.8317.

3.2.2 Variation in Radius and Area of the Jet Impact Region With Lance Height

Since a jet spreading angle of 21^o is assumed for the water model there is a relationship between the jet impact radius, r_j, and the lance height, H. This geometrical relationship is given by equation 3.2.5, the symbols defined by Figure 3.2.1.

$$r_j = d_o\left(1 + 0.1853\left(H/d_o\right)\right) \qquad (3.2.5)$$

FIGURE 3.2.1: DEFINITION OF r_j, A_j and H

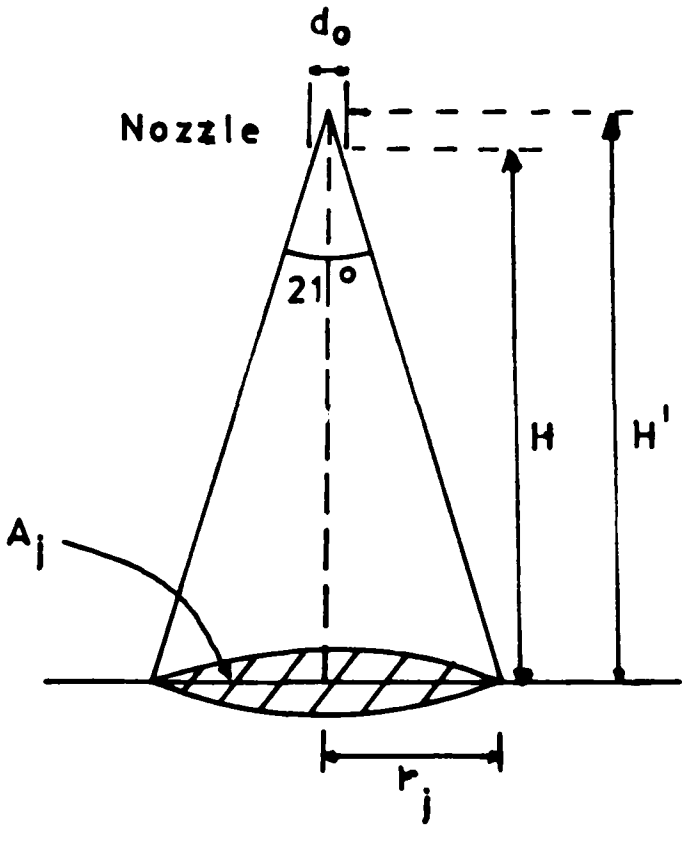

Note that the lance height is the distance from the nozzle tip to the impinging surface, i.e. an easily measured variable. Values for r_j and A_j for the lance heights and nozzle diameters utilised in this work are presented in Table 3.2.2 and Table 3.2.3.

TABLE 3.2.2: Variation of r_j and A_j at Different Lance Heights for a 2.26 mm Nozzle

Lance Height, H (m)	Projected Radius, r_j (m) x 10^2	Projected Area, A_j (m^2) x 10^3
0.200	3.932	4.857
0.175	3.469	3.780
0.150	3.006	2.839
0.125	2.543	2.030
0.100	2.079	1.358

TABLE 3.2.3: Variation of r_j and A_j for Different Nozzle Diameters at H = 0.2 m

Nozzle Diameter, d_o (m) x 10^3	Projected Radius, r_j (m) x 10^2	Projected Area, A_j (m^2) x 10^3
4.95	4.201	5.544
10.95	4.801	7.241
24.40	6.146	11.867

3.3 EXPERIMENTAL PROCEDURE

The procedure for a typical desorption run is best exemplified by Run No. AOD.1b the experimental plot of which is shown in Figure 3.3.1. Mains water was first turned on and allowed to fill the channel.A further half hour would elapse so that the water temperature in the channel stabilised. The Beckman oxygen probe was then calibrated with water from the channel and placed 10 cm downstream from the last row of top-blowing lances (the closest possible position). The oxygen cylinder feeding the sparger on the absorption column was turned on allowing oxygen absorption to commence. Meantime, the humidity of the air jets to be used in the run was determined by blowing one onto a wet and dry bulb sling psychrometer. This provides a value for the humidity of the jet and this coupled with the channel water temperature yields the optimum dry bulb temperature of the jetting medium for the run. This gas dry bulb temperature was produced by varying the water flowrate to the cooler on the gas line. The lances were then inserted into the holding frame at the correct lance height and array pattern.

As the oxygen concentration of the water was increasing a gravimetric flowrate of water exiting the weir-end of the channel was taken. When the bulk oxygen concentration of the feedwater was reaching a plateau the probe was switched to a point 10 cm upstream to determine the upstream reading for a period of time before being placed downstream again. Once the probe reading had stabilised again the compressor feeding the gas jets was switched on. Oxygen readings were then taken every half minute until a steady state level of desorption occurred. The period of time before steady state is reached varies dependent upon the channel flowrate, Q_l. For example, when Q_l = 1 m^3/hr it took 3-4 minutes to reach steady state

FIGURE 3.3.1 : TYPICAL EXPERIMENTAL TOP-BLOW RUN GRAPHICAL PLOT, RUN No. AOD.1b

($\dot{M}$=0·15 N, d_b=2·26mm, X=35, H = 20cm, Q_L= 1·0 m^3/hr, Q_g=1320 l/min, d_b= 74.2mm, Close-Packing)

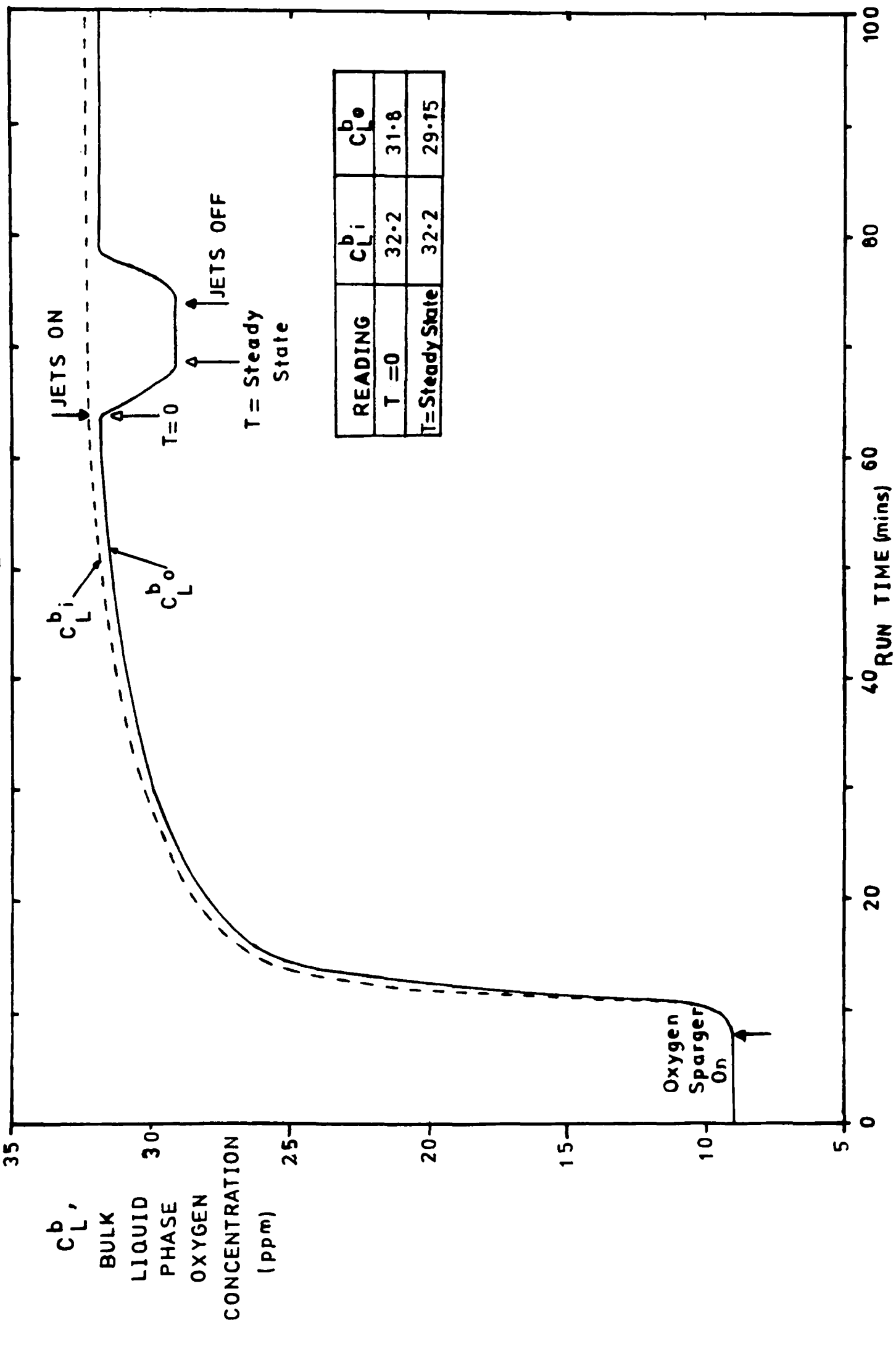

READING	$C_L^b{}_i$	$C_L^b{}_o$
T =0	32·2	31·8
T=Steady State	32·2	29·15

whereas at 3.7 m^3/hr a period of 1-1$^1/_2$ minutes was typical. Once steady state was reached the probe was again moved upstream (with the jets still on) to record upstream readings. The probe was then moved downstream again and once it had stabilised the jets were switched off. Further downstream readings were taken until the bulk oxygen concentration had reverted to what it was before the run.

After the run a second gravimetric water flowrate was measured; the average of this and the one beforehand being the value of Q_l for the run. During the run both upstream and downstream water temperature readings were taken and averaged to provide t_{av}, the average water temperature, for subsequent calculations. Both the gas-line temperature and channel gas phase temperature readings were also taken during the run. Several manometers were connected to selected lances during a run as a check to reveal any difference in the uniformity necessary for the multiple lance arrays. The gas-line rotameter was used to give an indication of compressor fluctuations as well as for metering the feed gas. Variations were minimal and easily rectified by way of the bleed valve.

3.4 TYPICAL TOP-BLOW RUN CALCULATION

As a direct comparison of these results for a moving liquid phase to those of Jones (1986, 1987) for stationary baths it was decided to plot them on Jones' correlation (Figure 2.1.8.1). This dimensionless correlation is a plot of $Sh.Sc^{-1/2}.Ga^{-2/3}\ (d_b/H)^2\ .\ Mo^{0.16}$ versus $\dot{M}/(\rho_L.g.H^3)$ calculated for single lances or per lance for multiple lance arrays. By inspection, it can be seen that the ordinate axis has k_{Lj}, the liquid phase mass transfer coefficient, incorporated in the Sherwood number. Hence, an ordinate value for a point is directly proportional to k_{Lj} and as such is a direct method of comparing liquid phase mass transfer for widely different top-blowing arrays.

Using Run No. AOD.1b as a typical run and referring to Figure 3.3.1, Figure 2.1.7.2, Table 3.2.2 and Appendix 1 the following calculation plots the result on Jones' correlation

Experimental Conditions

$\dot{M}$/lance	=	0.15 N
H	=	0.20 m
Q_l	=	2.8611×10^{-4} m^3/s
X	=	35[Close-Packing, Triangular Pitch, Figure 3.1.3]
Q_g	=	1320 L/min
d_b	=	7.42×10^{-2} m
d_o	=	2.26 mm
A_b	=	4.324×10^{-3} m^2

Experimental Results

$C^b_{Li}\ T=0$	=	32.2 ppm

$$C_{Lo}^{b}\ T=0 = 31.8 \text{ ppm}$$

$$C_{Li}^{b}\ T = \text{steady state} = 32.2 \text{ ppm}$$

$$C_{Lo}^{b}\ T = \text{steady state} = 29.15 \text{ ppm}$$

$$t_{av} = 19.0^{o}C$$

A) CALCULATING VARIABLES

i) Liquid Phase Mass Transfer Coefficient Per Lance, k_{Lj}

Using Jones' (1986) method and a combination of equations 2.1.34 and 2.1.35 the following equation results:

$$Xk_{Lj}A_b = Q_l \ln\left[\left(\frac{C_L^i - C_L^{b_i}}{C_L^i - C_L^{b_o}}\right)_{T=St.St} \Big/ \left(\frac{C_L^i - C_L^{b_i}}{C_L^i - C_L^{b_o}}\right)_{T=0}\right] \qquad (3.4.1)$$

Table A.1.1 provides a value for C_L^i for this run of 9.36 ppm. On substitution of data into eq. 3.4.1 one obtains a value for k_{Lj} of 2.38×10^{-4} m/s.

ii) Other Physical Variables

At $t_{av} = 19.0^{o}C$ the following variables have the values indicated (sources as shown):

ρ_L	=	998 . 405 kg/m^3	(Table A.1.3)
μ_L	=	1.025×10^{-3} Ns/m^2	(Figure A.1.3)
σ_L	=	7.290×10^{-2} N/m	(Figure A.1.2)

$D_{O_2\text{-}H_2O}$ = 1.95×10^{-9} m^2/s (Figure A.1.1)

B) DETERMINING CORRELATION ORDINATE AND ABSCISSA

The ordinate is $Sh.Sc^{-1/2}.Ga^{-2/3}.(d_b/H)^2.Mo^{0.16}$ where,

$$Sh = \frac{k_{Lj}\, d_b}{D_L} = \frac{2.38 \times 10^{-4} \cdot 7.42 \times 10^{-2}}{1.95 \times 10^{-9}} = 9\,056.2$$

$$Sc = \frac{\mu_L}{\rho_L . D_L} = \frac{1.025 \times 10^{-3}}{998.405 \times 1.95 \times 10^{-9}} = 526.5$$

$$Ga = \frac{d_b^3 . g . \rho_L^2}{\mu_L^2} = \frac{(0.074)^3 \cdot 9.81 \cdot (998.405)^2}{(1.025 \times 10^{-3})^2} = 3.772 \times 10^9$$

$$Mo = \frac{\sigma_L^3 \cdot \rho_L}{g \cdot \mu_L^4} = \frac{(7.290 \times 10^{-2})^3 \cdot 998.405}{9.81 \cdot (1.025 \times 10^{-3})^4} = 3.572 \times 10^{10}$$

Hence, $Sh.Sc^{-1/2}.Ga^{-2/3}.(d_b/H)^2.Mo^{0.16}$ = 1.094×10^{-3}

The abscissa or Momentum number is

$$\frac{\dot{M}}{\rho_L . g . H^3} = \frac{0.15}{998.405 \times 9.81 \times (0.2)^3} = 1.914 \times 10^{-3}$$

These coordinates are plotted on Jones' correlation in Figure 3.4.1. It shows that the experimental result lies just below the line representing the mean of Jones' data.

FIGURE 3.4.1 PLOT OF RUN AOD.1b ON JONES' CORRELATION

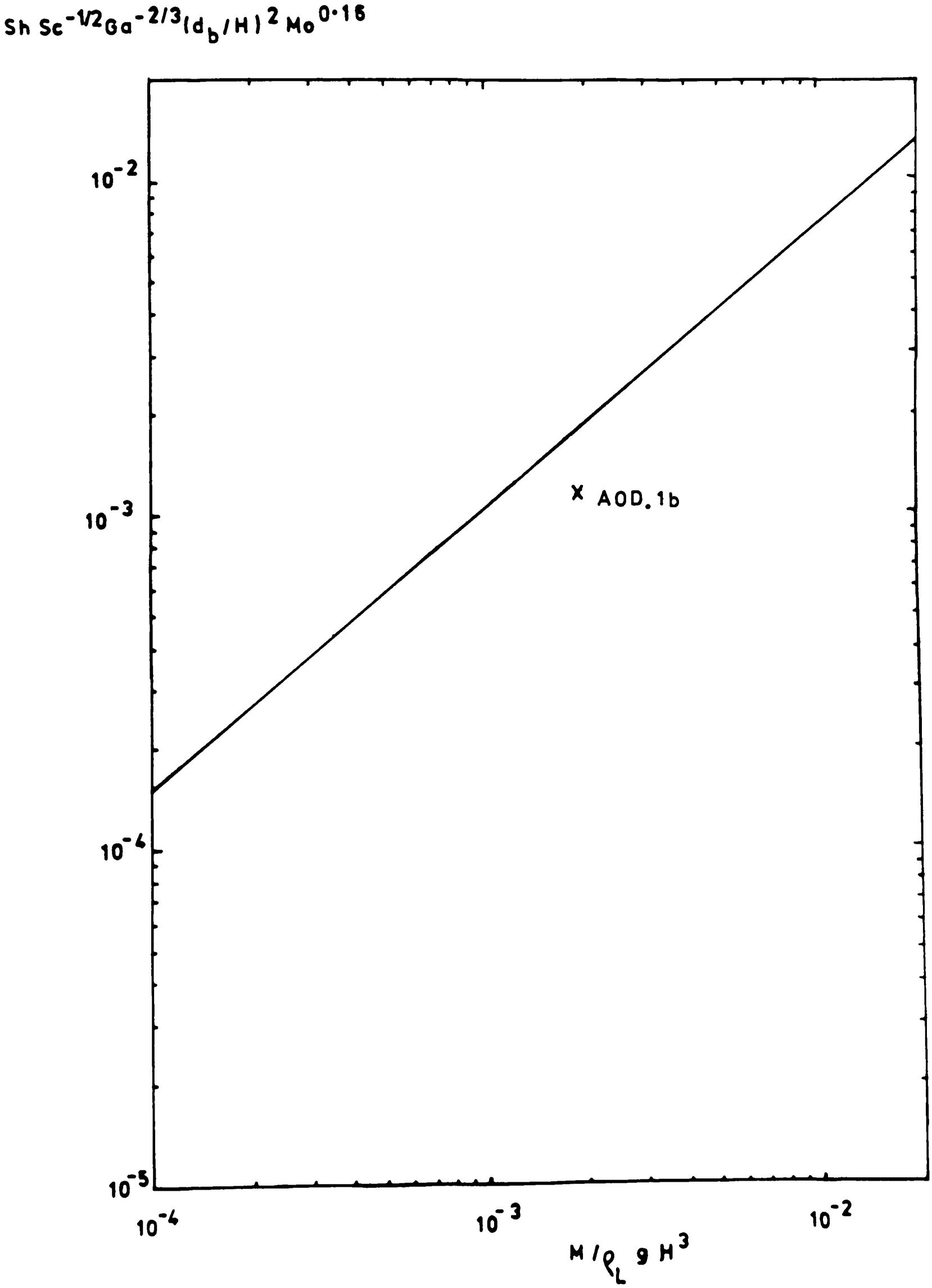

CHAPTER 4: TOP-BLOWING RESULTS

4.1 INTRODUCTION

There are effectively seven variables that can be manipulated during multiple lance top-blowing in channel flow:

i) Number of lances, X.

ii) Packing and pitch of the impinging jets.

iii) Momentum flux of the jets, $\dot{M}$.

iv) Lance nozzle diameter, d_o.

v) Lance height, H.

vi) Total gas flowrate, Q_g.

vii) Channel water flowrate, Q_l.

A rationale for the series of experiments was developed with the following objectives in mind:

a) Since no previous impinging jet mass transfer studies had utilised a flowing liquid phase, then Q_l was a major variable. Hence, its effect on mass transfer using the developed mass transfer model was to be assessed.

b) The gas flowrate was chosen to simulate that necessary for smelting requirements in the smelter pilot plant. It was kept constant at 1320 litres/min which corresponded to nearly all the compressors fully on. A constant Q_g also means that a direct comparison of results for widely differing lance configurations, nozzle sizes and lance heights could be forthcoming. For the 35

lance, 2.26 mm nozzle array a Q_g of 1320 litres/min produces a momentum flux per lance of 0.15 N.

c) $\dot{M}$/lance was kept at 0.15 N throughout most of the experimental runs because it corresponds to a non-splashing top-blowing jet/liquid interaction. As Jones' (1987) correlation was developed ostensibly from non-splashing jetting data it would therefore be the most appropriate momentum flux. Moreover it also corresponds to good surface renewal in the channel flow such that total mixing of the liquid phase is produced meaning the downstream oxygen concentration reading is representative of the bulk liquid phase.

d) Four nozzle diameters were chosen (2.26 mm, 4.95 mm, 10.95 mm and 24.4 mm) to assess the effect of d_o on liquid phase mass transfer for a constant Q_g.

e) The number of lances necessary for a given nozzle diameter was determined by the fixed Q_g and also by the requirement that each lance produced an $\dot{M}$ of 0.15 N or as close to it as the geometry of the gas delivery system allowed. For the 2.26 mm, 4.95 mm, 10.95 mm and 24.4 mm diameter nozzles this corresponds approximately to 35 (or 36), 16, 7 and 4 lances respectively.

f) Lance packing and interlance spacing, d_b, were other important variables in the analysis as it was thought that close-packed impact areas should result in lower liquid phase mass transfer. Hence for each nozzle array both open and close packing was considered. For the 2.26 mm nozzles the effect of triangular and square pitch packing of jets was also assessed. Open-packed and close-packed arrays were also chosen such that the jet impact areas traversed the channel width so that no asymmetrical oxygen

concentration gradients existed in the liquid phase. Good mixing in the liquid phase is essential in terms of representative bulk liquid phase oxygen readings.

g) For one series of experiments lance height was varied such that splashing was induced in the liquid phase for the lower lance heights. This served to illustrate the trends in liquid phase mass transfer for varying lance heights and to show the difference between splashing and non-splashing top-blowing conditions. By varying the lance height from 20 cm to 10 cm it offers jetting conditions ranging from surface dimpling to deep penetration of the liquid surface.

4.2 ACCURACY AND EXPERIMENTAL REPRODUCIBILITY

For all of the air jet oxygen desorption top-blowing experiments reported in this study two separate runs under the given top-blowing conditions were carried out to check for repeatability. Each run has been designated a or b so that for example there is an AOD.1a and AOD.1b. All of the top-blowing experimental data are tabulated in Appendix 2. A pair of readings for each experimental condition ensures a check on accuracy (and a mean value of k_L or $\dot{n}$ can be used) and the reproducibility of all the results can be seen to be quite high.

Some of the runs for the 35 lance, close-packed, 2.26 mm nozzle arrays with a channel flowrate of 3.7 m^3/hr (and lance height varying from 20 cm to 15 cm) are plotted on the Jones (1987) correlation in Figure 4.2.1. It is clear from the Figure that good reproducibility of experimental results is apparent. It is of note that the results for all of the air jet oxygen desorption experiments cover a range of bulk liquid phase oxygen concentrations ranging from 21 ppm to 33 ppm. This wide spread of C_L^b readings from the testwork helps to justify the use of equation 3.4.1. The addition of the bracketed 'S' after plotted points in Figure 4.2.1 denotes experimental conditions where liquid phase splashing was induced by the impinging gas jets.

FIGURE 4.2.1 TOP-BLOWING EXPERIMENTAL REPRODUCIBILITY

(Ql=3.7m3/hr, Qg=1320l/min, $\dot{M}$=0.15N, X=35, do=2.26mm, Open-Packing and Triangular Pitch)

$Sh\ Sc^{-1/2} Ga^{-2/3} (d_b/H)^2\ Mo^{0.16}$

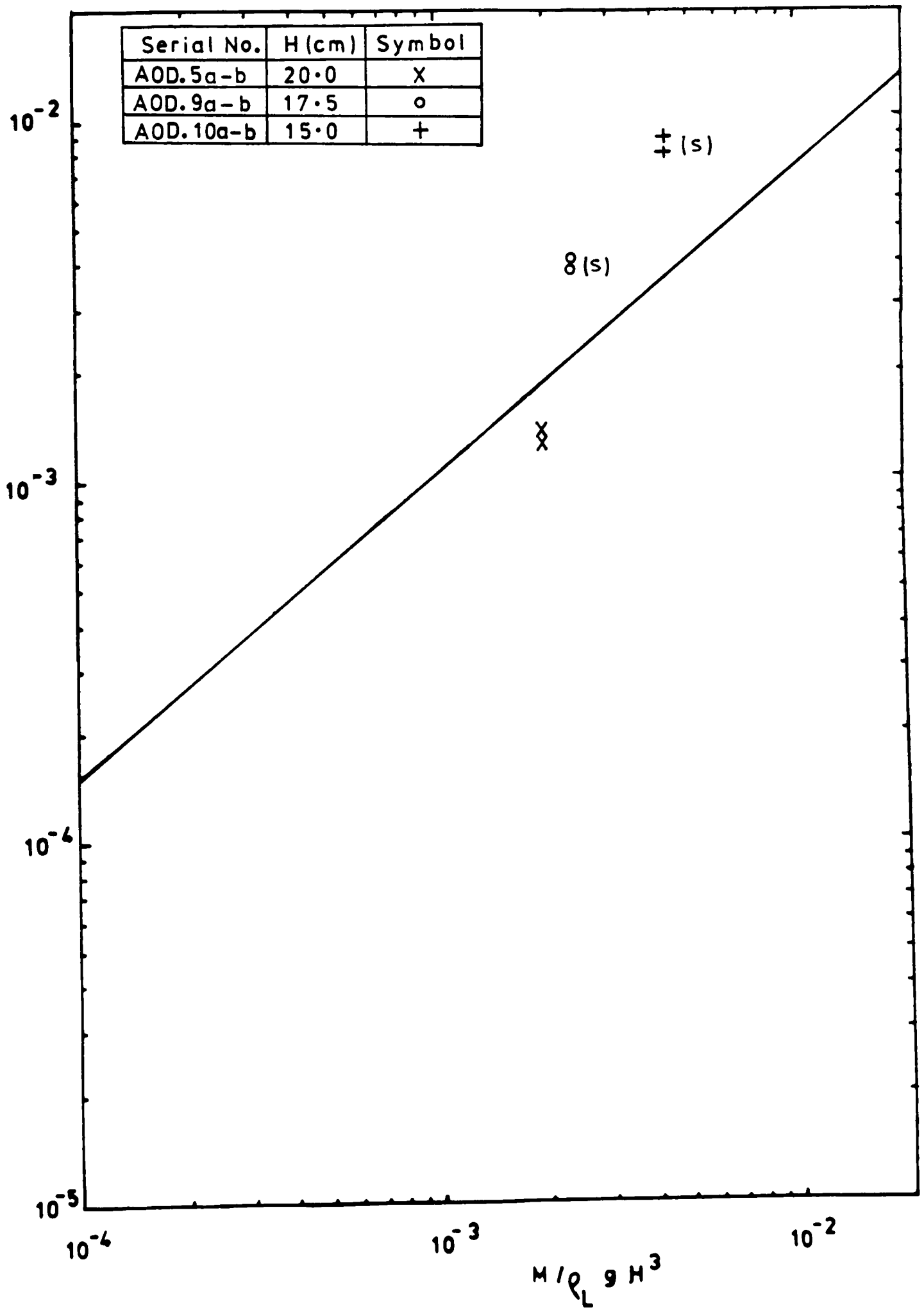

4.3 THE EFFECT OF CHANNEL FLOWRATE ON LIQUID PHASE MASS TRANSFER FOR CLOSE-PACKED TRIANGULAR AND SQUARE PITCH ARRAYS OF 2.26 mm NOZZLES

To assess the effect of channel flowrate, Q_l, on mass transfer and to check the mass transfer models, five channel flowrates (Q_l = 1.0, 1.7, 2.4, 3.0 and 3.7 m^3/hr) were considered for a typical close-packed 35 lance (2.26 mm nozzle) array with each lance blowing at 0.150 N and for a square pitch configuration of 36 nozzles of the same diameter (see Figures 3.1.3 and 3.1.4). For each array the same volumetric flowrate of gas was delivered (1320 litres/minute) though the greater number of lances in the square pitch array meant that each lance blew at 0.144 N. The relevant experiments have been designated AOD.1-8 in Appendix 2.

For comparison, two different means of presenting the results are given here. Figure 4.3.1 is a plot of data on a Jones correlation (each point is the mean of a pair of experimental results) and Figure 4.3.2 is a plot of the same data on an axis of $\dot{n}$ (the mass rate of mass transfer) versus channel flowrate. The $\dot{n}$ versus Q_l plot is a more direct comparison of mass transfer for the different configurations. The Jones correlation in Figure 4.3.1 shows a group of points just below the correlation line indicating a slight reduction in the predicted mass transfer for these close-packed arrays. Figure 4.3.2 indicates that $\dot{n}$ is apparently independent of channel flowrate above about 2.4 m^3/hr.

The lower rate of mass transfer (for channel flowrates less than 2.4 m^3/hr) may be due to back-mixing at the upstream edge of the top-blowing arrays where the oxygen probe was only 7.5 cm from the first jet impact areas. At Q_l = 1.0 m^3/hr the water velocity in the channel is 0.64 cm/s

FIGURE 4.3.1 THE EFFECT OF CHANNEL FLOWRATE ON LIQUID PHASE MASS TRANSFER PLOTTED ON A JONES CORRELATION

(Qg=1320l/min, X=35, H=0.2m, do=2.26mm, $\dot{M}$=0.15N, Close-Packing and Triangular Pitch)

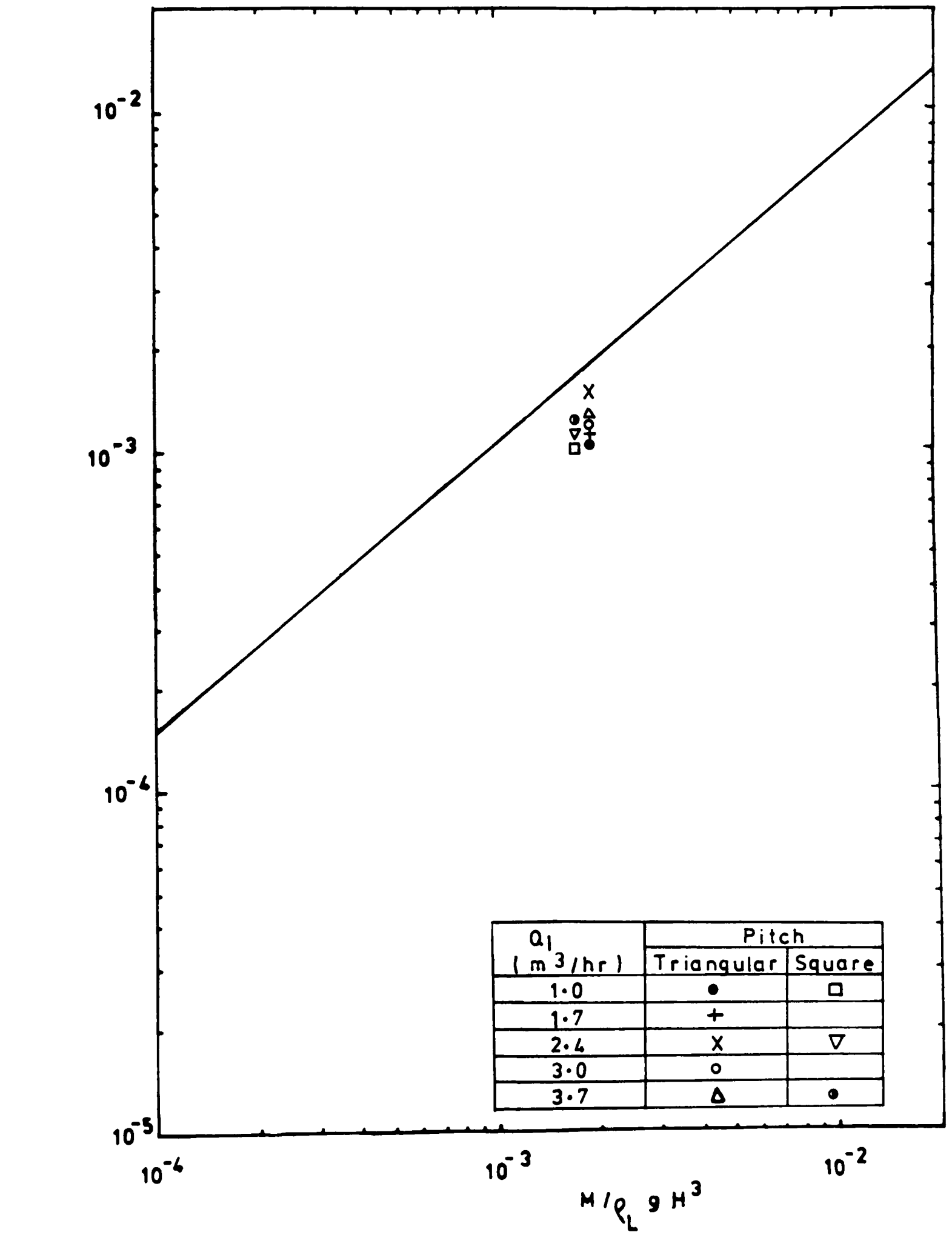

FIGURE 4.3.2 THE EFFECT OF CHANNEL FLOWRATE ON LIQUID PHASE MASS TRANSFER FOR CLOSE-PACKED 2.26mm ARRAYS

(Qg=13201/min, $\dot{M}$=0.15N, H=0.2m, X=35or36)

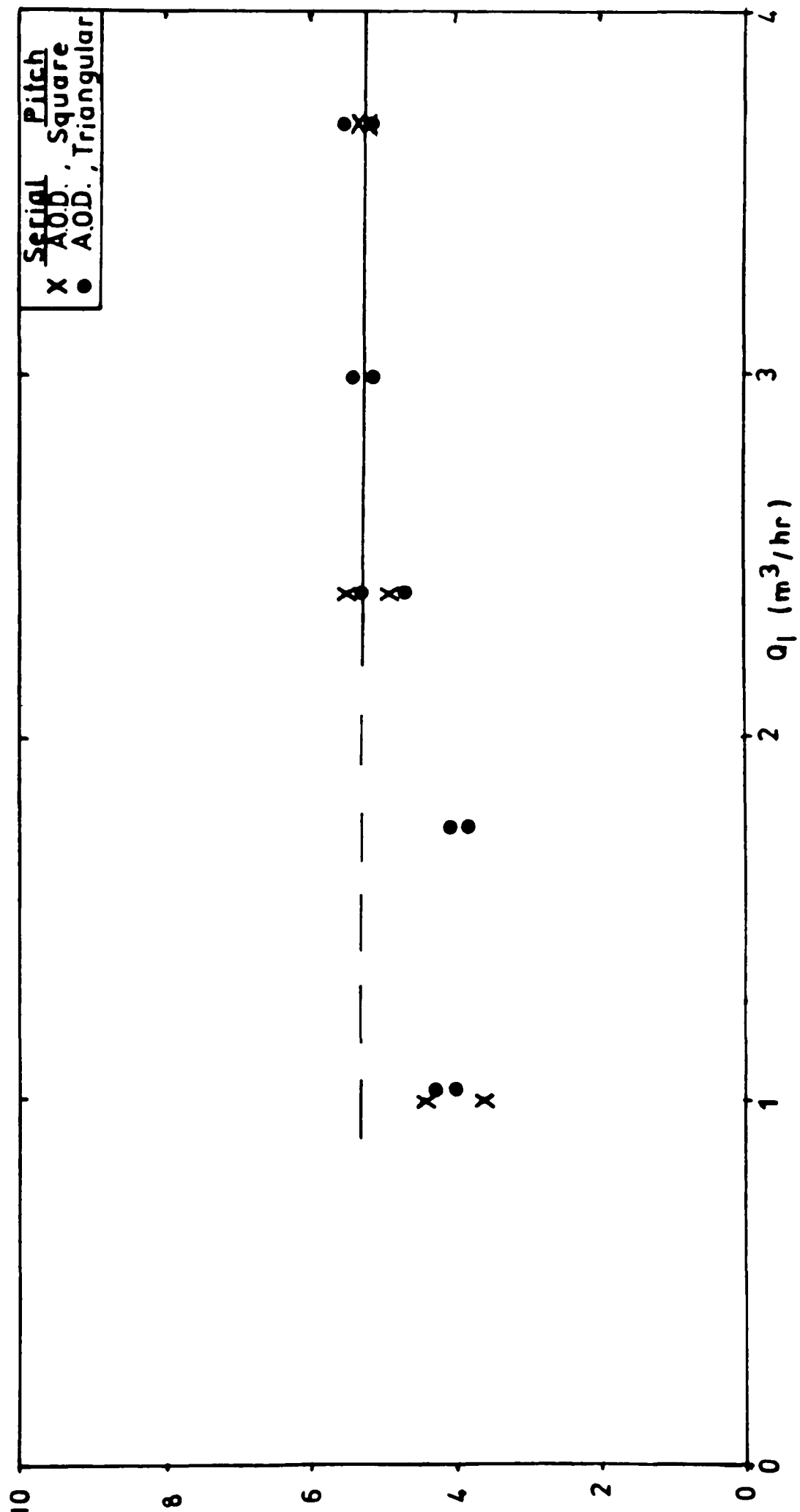

compared to 1.53 cm/s at Q_l = 2.4 m^3/hr and it is possible that the recirculation patterns caused by the first row of jets is causing back-diffusion up the channel against the gentle superimposed water flowrate. The upstream oxygen reading may thus be lower than it should be. At present it is difficult to prove this hypothesis as the only equation in the literature that estimates induced surface water velocities during top-blowing is eq. 2.1.2.1 by Ito et al (1981) which is only applicable to laminar jets and not the turbulent jets considered here. It can be seen however from Figure 2.1.4.3(a) taken from Wakelin's (1966) work that surface water flowrates due to recirculation patterns can be high quite a distance from the jet impact area under similar jetting conditions to this work. Unfortunately, Wakelin's top-blowing work used circular stationary baths such that clear-cut steady recirculation patterns were induced in the liquid phase. Under the channel flow conditions considered here such simple flow patterns are almost certainly not occurring. There is clearly a need for further investigation into liquid phase fluid flow phenomena in the channel for multiple lance top-blowing conditions.

Both figures also serve to show that, in terms of liquid phase mass transfer, there are no advantages to utilising a 36 lance square pitch array of nozzles over a 35 lance triangular pitch array of nozzles. The 35 lance array was opted for in subsequent experiments primarily because it took up slightly less top-blow area in the channel (one of the goals of this work is to minimise the top-blow area required in the smelter) and also because there was one lance less (the fewer lances present, the less complicated the gas feed lines). For a similar reason of space restriction triangular pitch packing within multiple lance arrays was also opted for in the larger nozzle configurations.

A supplementary test was also carried out at this stage to check for any possible "end effects" during multiple lance top-blowing. End effects are here classed as liquid phase oxygen desorption caused by the off-gas from the impinging jets as it passes over the water surface. For a series of tests a gas manifold was designed that delivered 1320 litres/minute air across the channel width and for a height of 5 cm above the water surface. The effective gas velocity out of the manifold was 1.42 m/s which according to Lohe's (1966) correlations corresponds to an off-gas surface velocity at a distance of four impact radii away from the centreline of the jet impact zone. For the case of 2.26 mm nozzles at a height of 20 cm top-blowing at 0.15 N this is equivalent to a distance of 7.5 cm from the jet impact zone.

During the tests the oxygen probe was used to take dissolved oxygen readings of the superoxygenated bulk liquid phase at different points down-stream from the manifold ranging from 10 to 50 cm. These readings could then be compared to oxygen readings taken when there was no gas passing over the surface, i.e. the "natural desorption" base case. For a range of water flowrates from 1.0 to 3.7 m^3/hr no end effects were detected during the testwork, i.e. just natural desorption was apparent. This would imply that during top-blowing in channel flow virtually all of the liquid phase oxygen mass transfer occurs at or close to the jet impact areas and the off-gas from the jets contributes little to liquid phase mass transfer.

4.4 THE EFFECT OF LANCE HEIGHT ON LIQUID PHASE MASS TRANSFER FOR CLOSE-PACKED ARRAYS OF 2.26 mm NOZZLES

In order to illustrate the effect of varying lance height on liquid phase mass transfer, all other top-blowing variables remaining constant, a series of experiments was carried out. The 35 lance, 2.26 mm nozzle, close-packed array was chosen and lance height was varied from 20 cm to 10 cm in 2.5 cm increments. Each jet in the array was blowing at 0.15 N. These experiments are characterised by serial Nos. AOD.5 and AOD. 9-12 and details may be found in Appendix 3. The change in lance height from 20 cm to 10 cm also serves to show the effect of varying the top-blowing jetting mode from conditions ranging from strong dimpling to near penetration (see Figure 2.1.3.1).

Figure 4.4.1 is a plot of the results on a Jones correlation whereas Figure 4.4.2 is a standard quantitative mass transfer plot. Splashing as predicted by the Chatterjee-Bradshaw correlation (eq. 2.1.19) occurs at H = 18 cm (the dashed lines) for the jetting conditions considered, and experimentally nominal splashing was observed at H = 17.5 cm but not at H = 20.0 cm. Splashing was most pronounced at H = 10.0 cm and H = 12.5 cm and still serious at H = 15.0 cm. It is clear from Figures 4.4.1 and 4.4.2 that a reduction in lance height such that the top-jetting causes excessive splashing results in a dramatic increase in liquid phase mass transfer. From H = 20.0 cm to H = 10.0 cm the quantity of liquid phase mass transfer increases six fold. Figure 4.4.1 also illustrates the applicability of Jones' correlation to the non-splashing top-blowing régime. The plotted results for H = 10.0 - 15.0 cm (the heavy splashing experiments) are well above the

FIGURE 4.4.1 THE EFFECT OF LANCE HEIGHT ON LIQUID PHASE MASS TRANSFER PLOTTED ON A JONES CORRELATION

(do=2.26mm,Ql=3.7m3/hr,Qg=13201/min,M=0.15N,X=35,Close-Packing and Triangular Pitch)

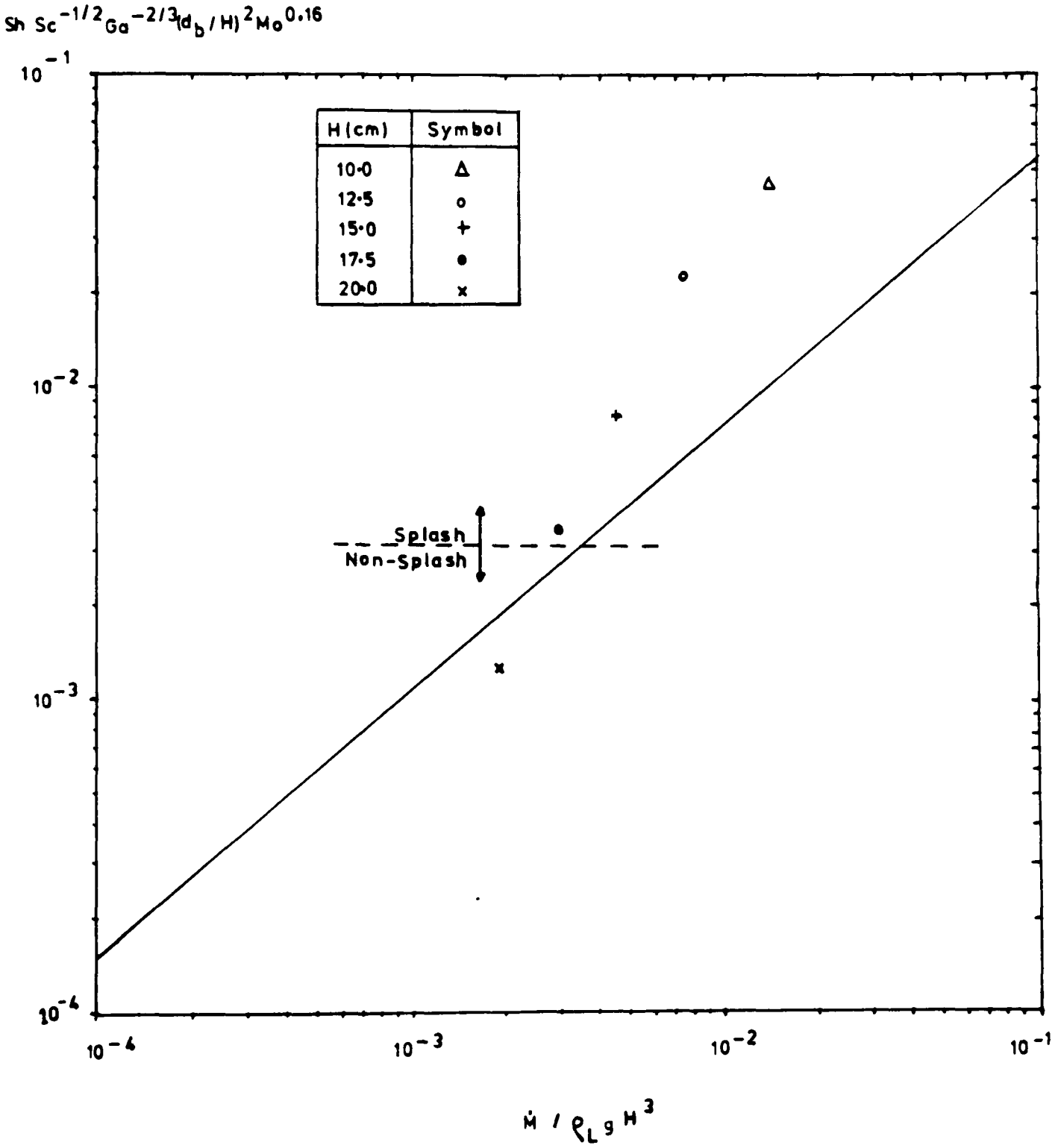

FIGURE 4.4.2 THE EFFECT OF LANCE HEIGHT ON LIQUID PHASE MASS TRANSFER

(do=2.26mm, Ql=3.7m3/hr, M=0.15N, Qg=1320l/min, X=35, Close-Packing and Triangular Pitch)

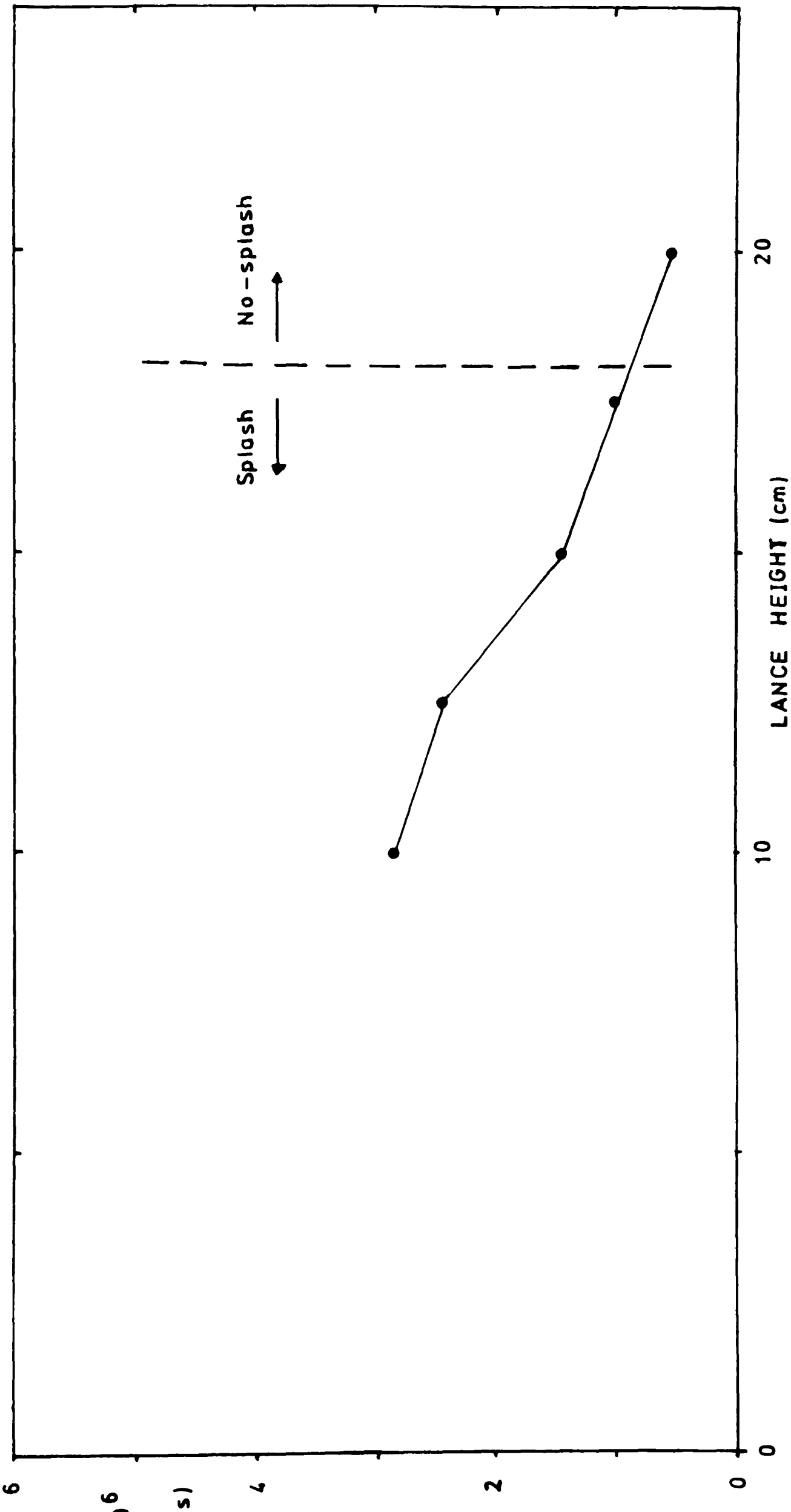

correlation line indicating large amounts of liquid phase mass transfer.

Plate 4.1 is a series of photographs (viewing left to right, top to bottom) of a 7 lance close-packed array of 2.26 mm nozzles at a height of 20 cm top-blowing onto a simulated slag layer. The material used for this was an ash residue derived from coal-burning power stations and called cenospheres. It consists of hollow spherical particles of mean particle size 150 μm and a bulk density half that of water when in a slurry form. It was used by Jones (1986) in his tests since unlike organic oils it provides no interfacial resistance or monomolecular films once blown from the impingement region.

In plate 4.1 the first photograph shows the lances blowing at 0.08 N. The other photographs are for jet momentum fluxes of 0.15 N, 0.24 N and 0.32 N per lance respectively. Clearly the lowest momentum of 0.08 N per lance was insufficient to clear the impingement surface of 'slag' though a jet force of 0.15 N was able to. Note the comparatively large wavelengths of the gravity waves downstream of the top-blowing region compared to the upstream capilliary waves, a fact reported by Banks (1962) in his work. The 0.32 N top-blowing array was in the extreme splashing régime as illustrated by the fourth photograph where large-scale surface break-up is evident. This plate visually indicates the distortion of neighbouring cavities in an array of close-packed nozzles. This is similar to the effect reported by Goldstein and Timmers (section 2.1.5.1) for their multiple lance configurations during heat transfer.

PLATE 4.1

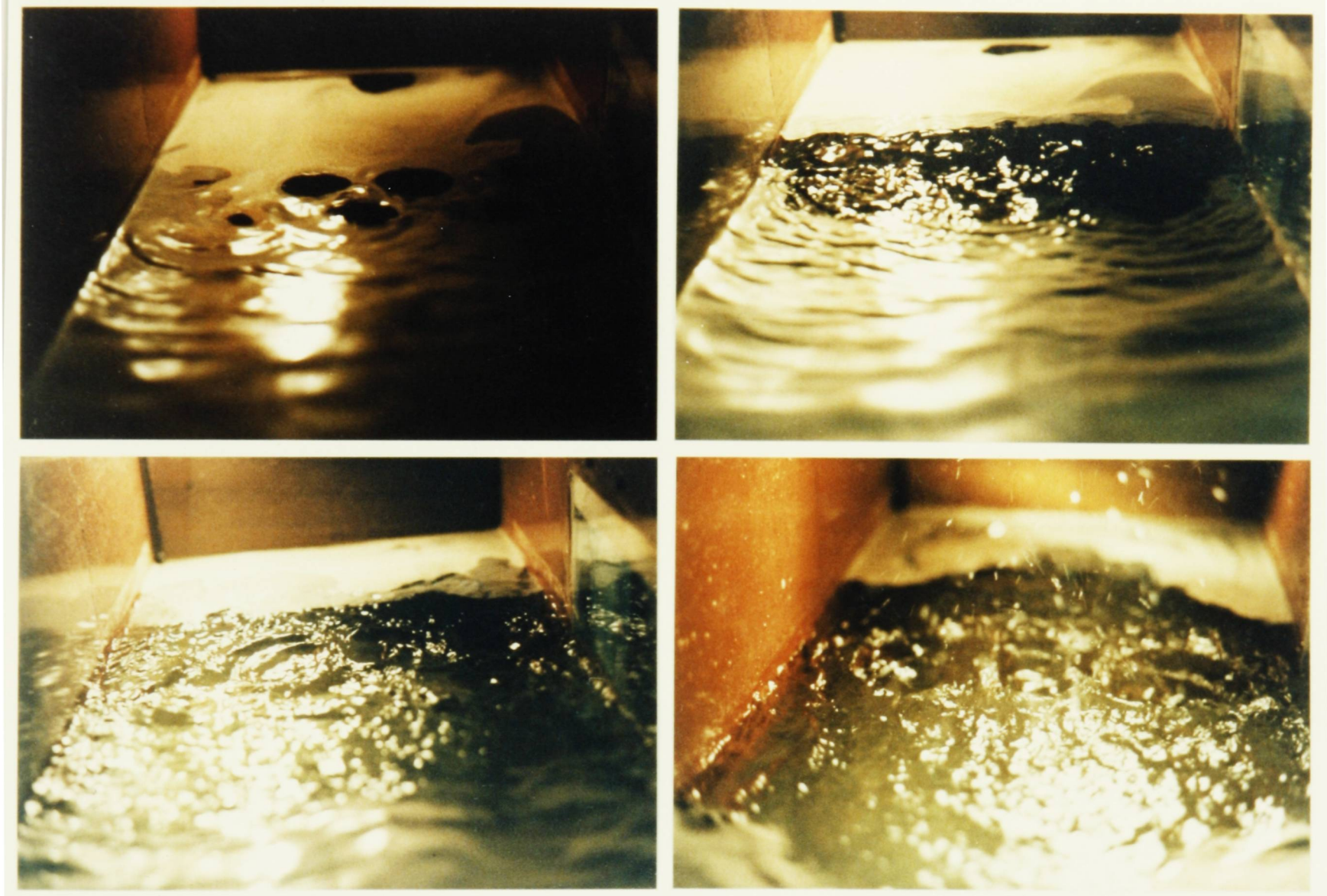

SERIES OF PHOTOGRAPHS OF A 7 LANCE CLOSE-PACKED ARRAY OF JET IMPACT CAVITIES INCLUDING A SIMULATED SLAG LAYER:

d_o= 2.26 mm, H = 20 cm: a) $\dot{M}$ = 0.08 N b) $\dot{M}$ = 0.15 N c) $\dot{M}$ = 0.24 N d) $\dot{M}$ = 0.32 N

4.5 THE EFFECT OF NOZZLE DIAMETER AND MULTIPLE LANCE PACKING ON LIQUID PHASE MASS TRANSFER

Four nozzle diameters were considered in the testwork; namely 2.26 mm, 4.95 mm, 10.95 mm and 24.40 mm. Open-packed and close-packed multiple lance arrays of these nozzles were devised (see Figures 3.1.3 - 3.1.7) to assess the effect of packing on liquid phase mass transfer. To deliver the same volumetric flowrate of gas at approximately 0.15 N per lance thirty five 2.26 mm nozzles, sixteen 4.95 mm nozzles, seven 10.95 mm nozzles and four 24.40 mm nozzles were required. The experimental details may be found in Appendix 3 for all the relevant runs, in this case Serial Nos. AOD.5, AOD.8 and AOD.13-18. For all of these experiments the channel flowrate was kept constant at 3.7 m^3/hr.

Figure 4.5.1 is a plot of the results on a Jones correlation whereas Figure 4.5.2 is a quantitative plot of liquid phase mass transfer. All runs were in the non-splashing régime. Figure 4.5.2 illustrates the advantages of using close-packed arrays over open-packed ones. For all nozzle diameters liquid phase mass transfer was less for close-packed arrays compared to their open-packed counterparts. In the case of the seven 10.95 mm nozzles the open-packed array produced three times the mass transfer of the close-packed array. The diagram also illustrates the advantages of employing fewer, larger diameter nozzles in terms of restricting liquid phase mass transfer. There appears to be little advantage to using the four 24.40 mm close-packed array over the seven 10.95 mm close-packed array other than the necessity for fewer lances. The small difference in mass transfer between the open-packed and close-packed 24.40 mm array may be attributed to the number of nozzles used (four) being too few to exhibit much

FIGURE 4.5.1 COMPARISON OF LIQUID PHASE MASS TRANSFER FOR CLOSE-PACKED AND OPEN-PACKED ARRAYS OF 2.26mm, 4.95mm, 10.95mm AND 24.4mm NOZZLES ON A JONES CORRELATION

(Q_l=3.7m3/hr, H=0.2m, $\dot{M}$=0.15N, Q_g=1320l/min, Triangular Pitch)

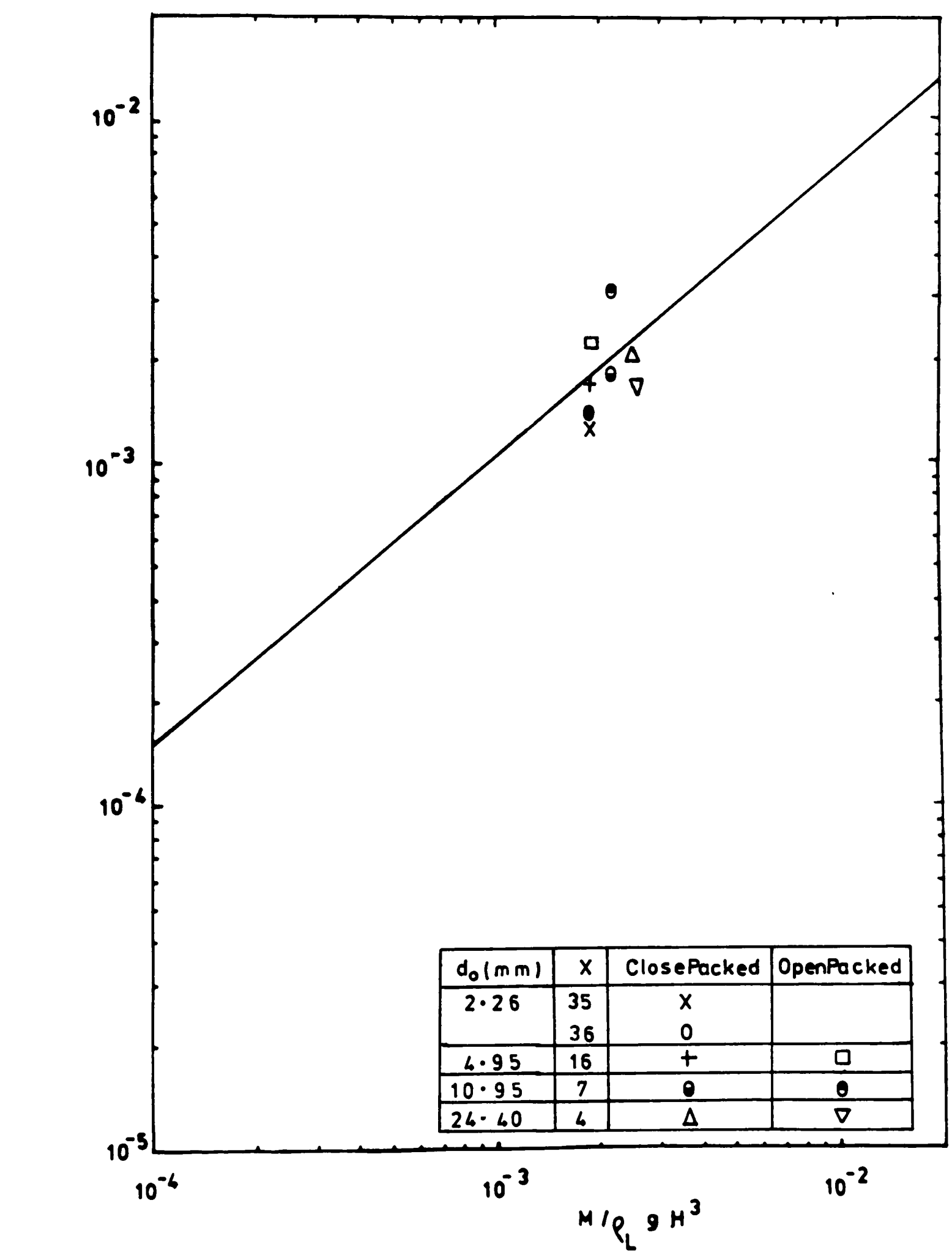

FIGURE 4.5.2 THE EFFECT OF NOZZLE DIAMETER ON LIQUID PHASE MASS TRANSFER FOR OPEN-PACKED ARRAYS

(Q_l=3.7m3/hr, Q_g=1320l/min, H=0.2m, $\dot{M}$=0.15N)

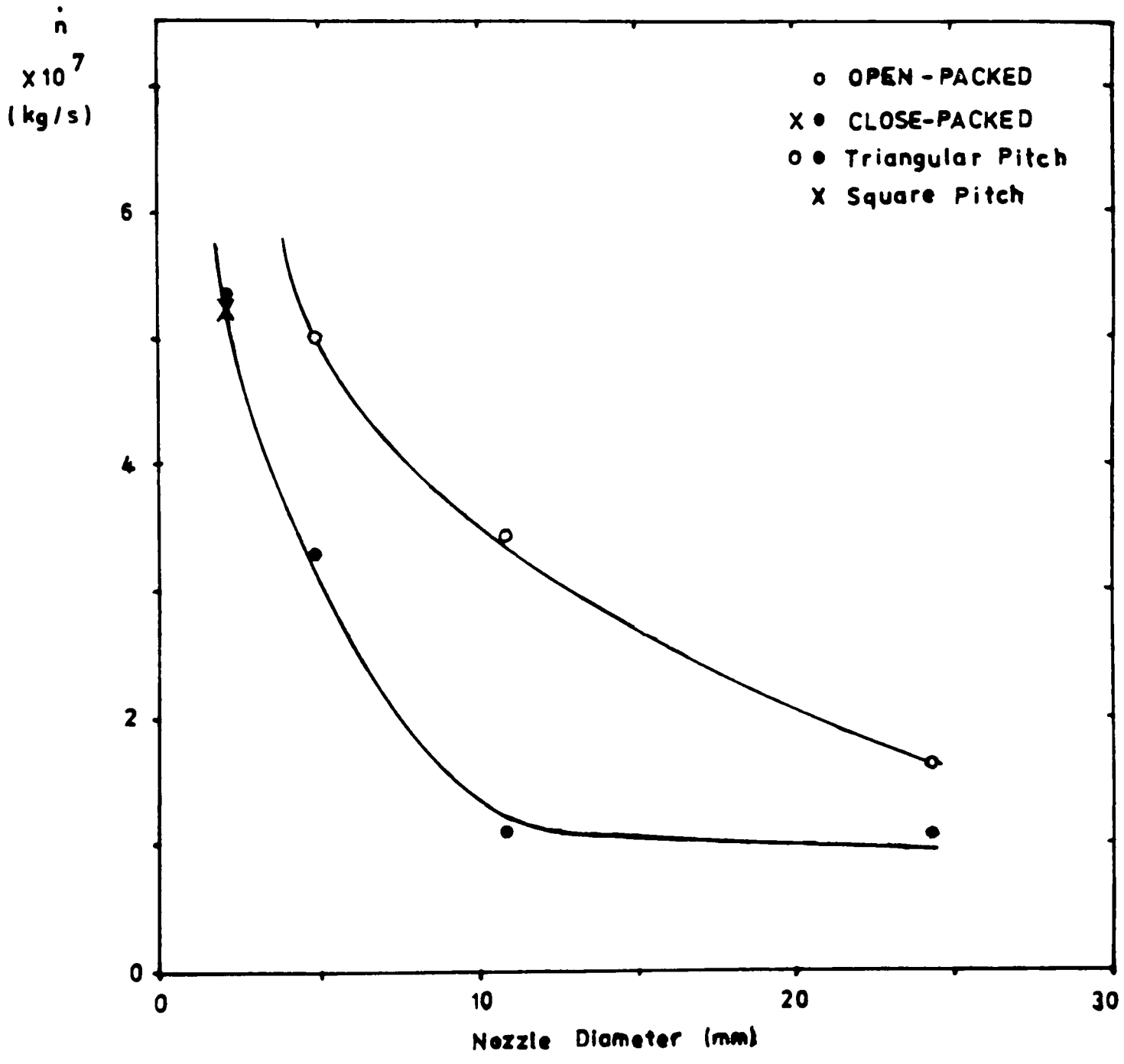

inter-lance interference phenomena.

Plate 4.2 is a photograph of the sixteen 4.95 mm nozzle, close-packed array top-blowing in the channel at a lance height of 20.0 cm (see Figure 3.1.5a). The effect of multiple jet impact areas close together is clearly visible. Cavity lips are higher than for the open-packed arrays. During an experimental run bubbles are seen to burst in the areas between cavities and there is a distinct surface flow of water away from the central cavities to the side walls and then out of the top-blow region in the direction of superimposed channel flow. The cavities at the leading and trailing edges of the close-packed arrays splay out of the top-blow region where there is room to expand. Cavities also oscillate laterally and vertically; the latter case more so when excessive splashing is taking place. At the point of incipient splashing the first drops are thrown out at the leading and trailing edges of the multiple cavity array.

Plates 4.3 and 4.4 depict open-packed arrays of nozzles. Plate 4.3 shows a top-blowing array that used the same lance holding frame as Plate 4.2 except that 12 nozzles were removed to produce the array shown. Each jet in Plate 4.3 is blowing under identical jetting conditions to those in Plate 4.2. It is apparent from comparing Plate 4.2 with Plate 4.3 that once nozzles are in an open packing the impact areas of cavities become larger as they are not constricted by neighbouring cavities. Moreover, surface waves are more evident as illustrated more clearly in Plate 4.4 which shows a series of photographs (viewing left to right, top to bottom) of a three lance open-packed array of 4.95 mm nozzles blowing inside the channel at a height of 20 cm. The first two photographs are of identical conditions, the latter being a close-up of the former. Each jet in the array is blowing at a momentum flux of 0.15 N and clear dimpling is observable together with pronounced

PLATE 4.2

PHOTOGRAPH OF A 16 LANCE CLOSE-PACKED ARRAY OF JET IMPACT CAVITIES; d_o = 4.95 mm, H = 20 cm, $\dot{M}$ = 0.15 N

PLATE 4.3

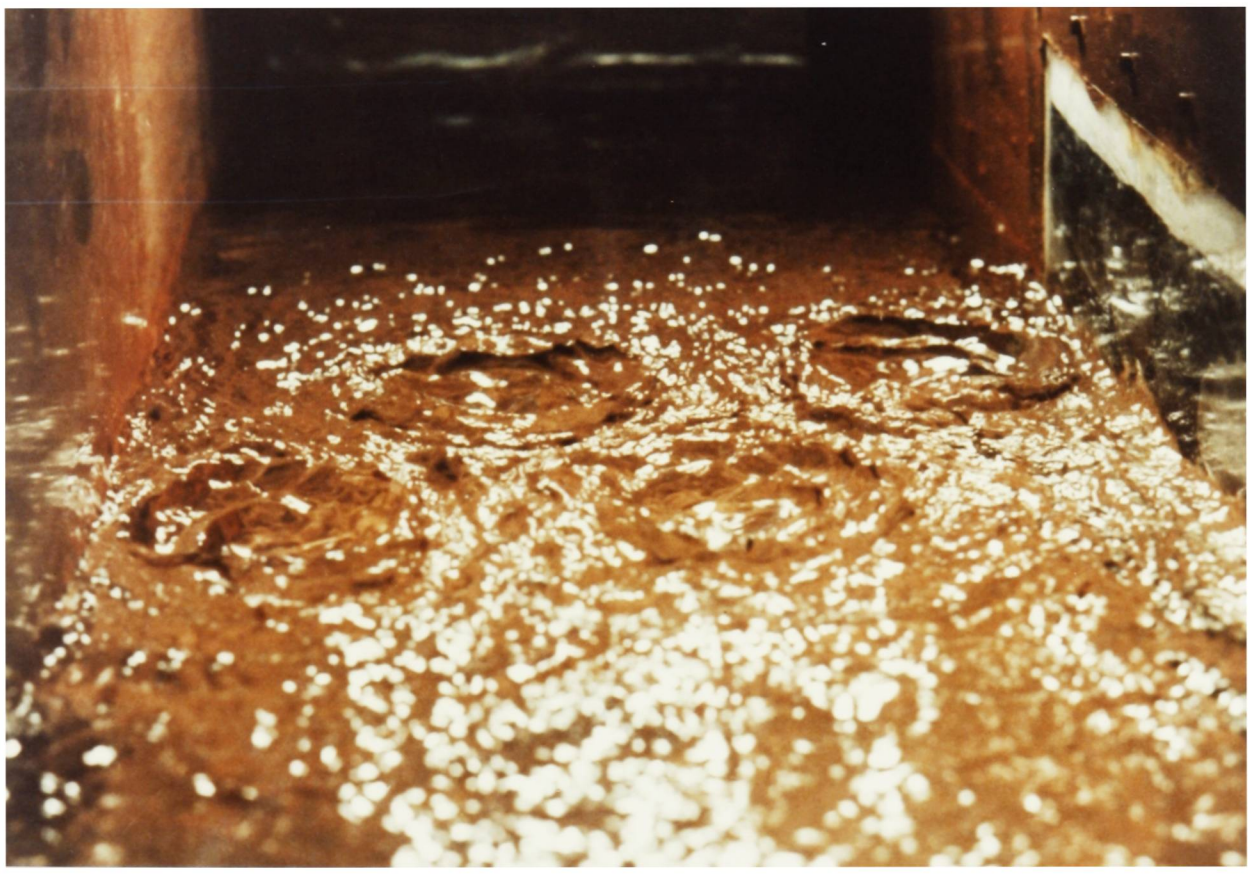

PHOTOGRAPH OF A 4 LANCE CLOSE-PACKED ARRAY OF JET IMPACT CAVITIES; d_o = 4.95 mm, H = 20 cm, $\dot{M}$ = 0.15 N

PLATE 4.4

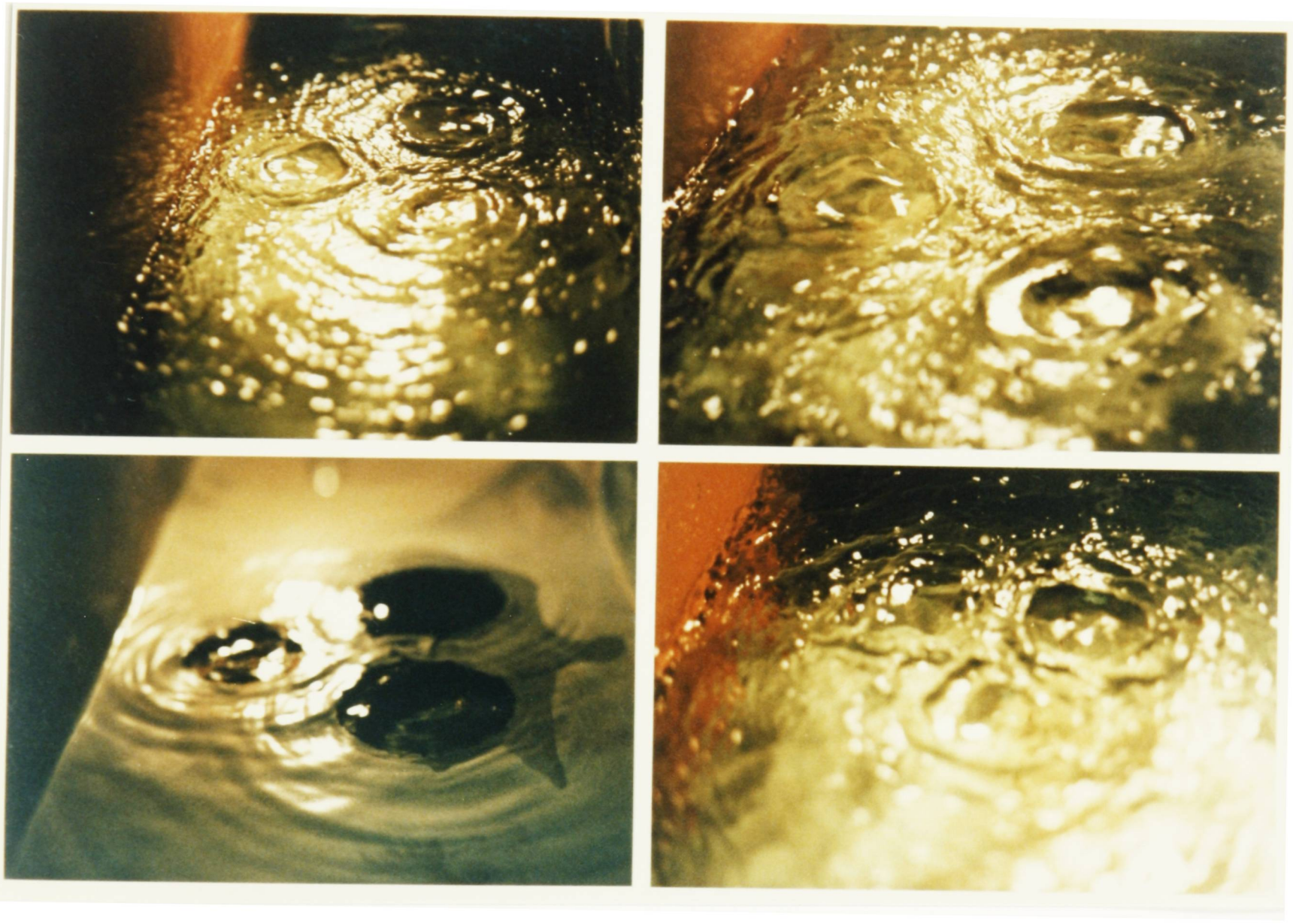

SERIES OF PHOTOGRAPHS OF A 3 LANCE OPEN-PACKED ARRAY OF JET IMPACT CAVITIES; d_o = 4.95 mm, H = 20 cm: a) $\dot{M}$ = 0.15 N b) $\dot{M}$ = 0.15 N c) $\dot{M}$ = 0.15 N PLUS 'SLAG' d) $\dot{M}$ = 0.25 N

rippling of the surface. The ripples are circular, emanating from the lip of each cavity. The third photograph illustrates the same blowing conditions as the previous two except that a simulated slag layer has been added. The fourth photograph illustrates the same array but this time each jet is blowing at 0.25 N. This produces deeper cavities and surface waves of greater amplitude and speed.

4.6 NITROGEN JET OXYGEN DESORPTION EXPERIMENTS

A limited number of multiple nitrogen jet desorption experiments have been carried out (runs NOD.1-2). A modified arrangement of the air jet desorption model was employed as illustrated by Figure 4.6.1 . With this rig a head tank was utilised and no oxygen absorber was necessary. With the nitrogen desorption runs oxygen inherent in the liquid phase was desorbed through displacement by nitrogen from the impinging jets such that a steady state value is obtained in a similar manner to the air jet oxygen desorption from a superoxygenated liquid phase. The results cover two experimental conditions and are plotted in Figure 4.6.2, a Jones correlation. Figure 4.6.3 is a plot of $\dot{n}$ versus Q_l and it compares air jet and nitrogen jet oxygen desorption experiments for identical top-blowing conditions.

Serial numbers NOD.1 and NOD.2 are for a tightly packed array of 35 x 2.26 mm nozzles each blowing at 0.15 N. NOD.1 employed a channel flowrate of 1.0 m^3/hr whereas NOD.2 operated at $Q_l = 3.0\ m^3/hr$. Figure 4.6.2 shows the nitrogen desorption results to lie very close to Jones' correlation line indicating good experimental fit with the predictions. Figure 4.6.3 illustrates similar trends in the nitrogen jet and air jet results for identical conditions. Both sets of data are of the same order of magnitude and are in reasonably close agreement.

For both runs the gas phase oxygen concentration inside the top-blow region was measured by the Beckman probe to be 0.3%. This corresponds to a liquid phase interfacial oxygen concentration, C_L^i, of 0.163 ppm. This figure was used in all the calculations for these runs. As a supplementary confirmatory test for these runs the effect of bulk mixing within the channel was measured using an array of sampler pipes placed in the channel. The

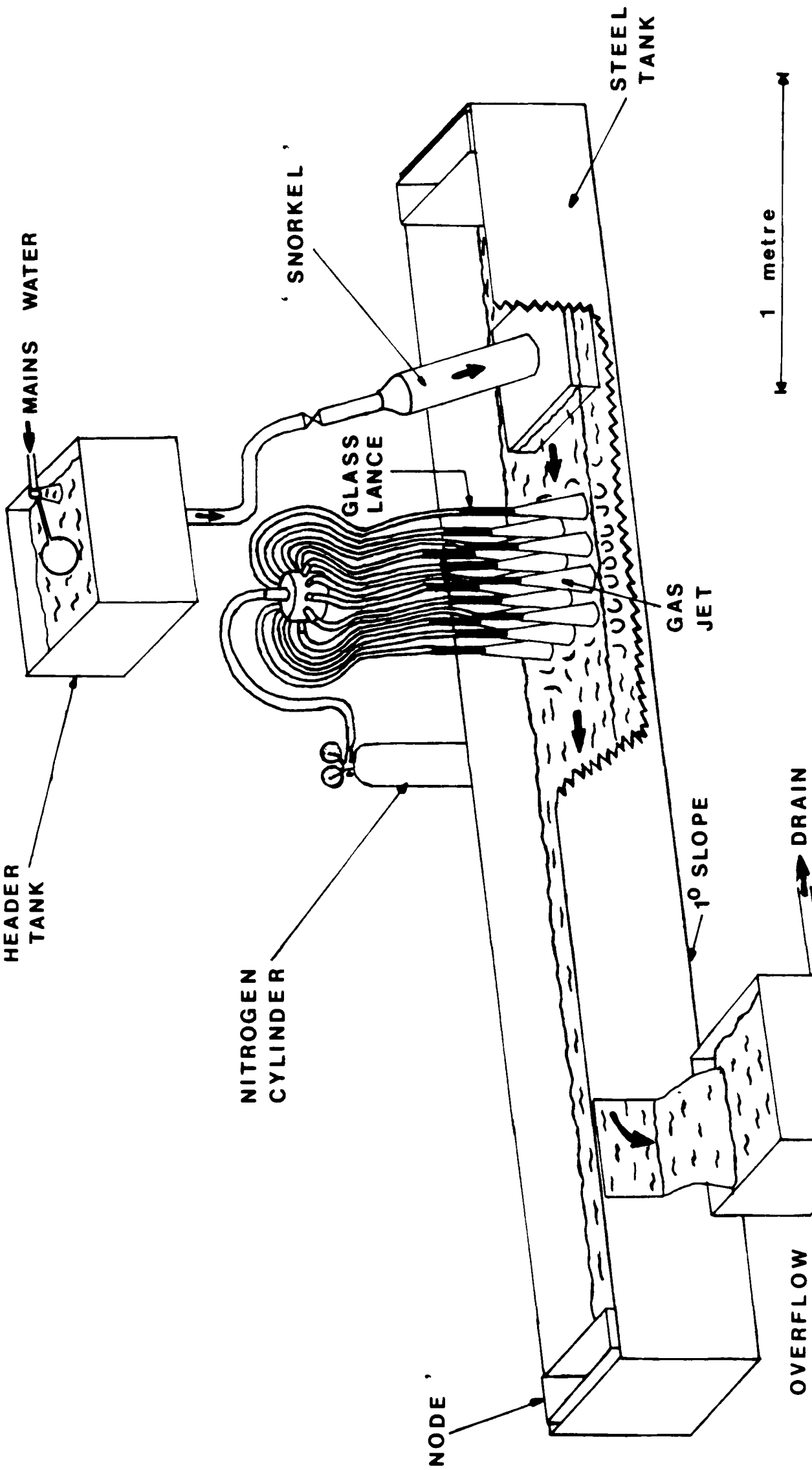

FIGURE 4.6.1 : MODEL OF THE CONVERTING HEARTH FOR NITROGEN DESORPTION TESTS

FIGURE 4.6.2 NITROGEN JET OXYGEN DESORPTION EXPERIMENTS

(Qg=1320l/min, X=35, H=0.2m, $\dot{M}$=0.15N, Close-Packed and Triangular Pitch)

$Sh\, Sc^{-1/2} Ga^{-2/3} (d_b/H)^2 Mo^{0.16}$

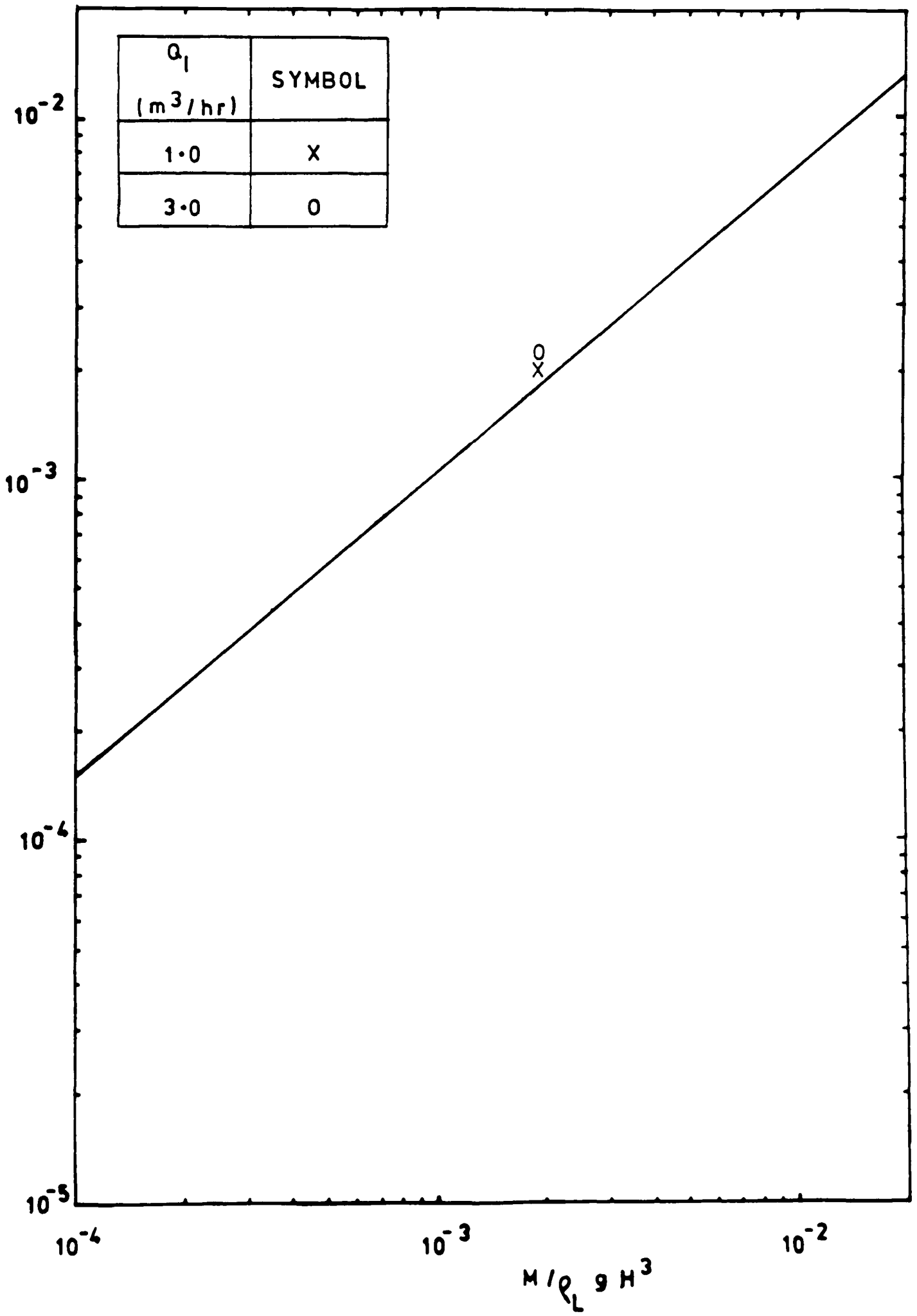

FIGURE 4.6.3 COMPARATIVE PLOT OF NITROGEN JET AND AIR JET OXYGEN DESORPTION EXPERIMENTS

(do=2.26mm;M=0.15N;Qg=13201/min;H=0.2m;X=35;Close-Packed and Triangular Pitch)

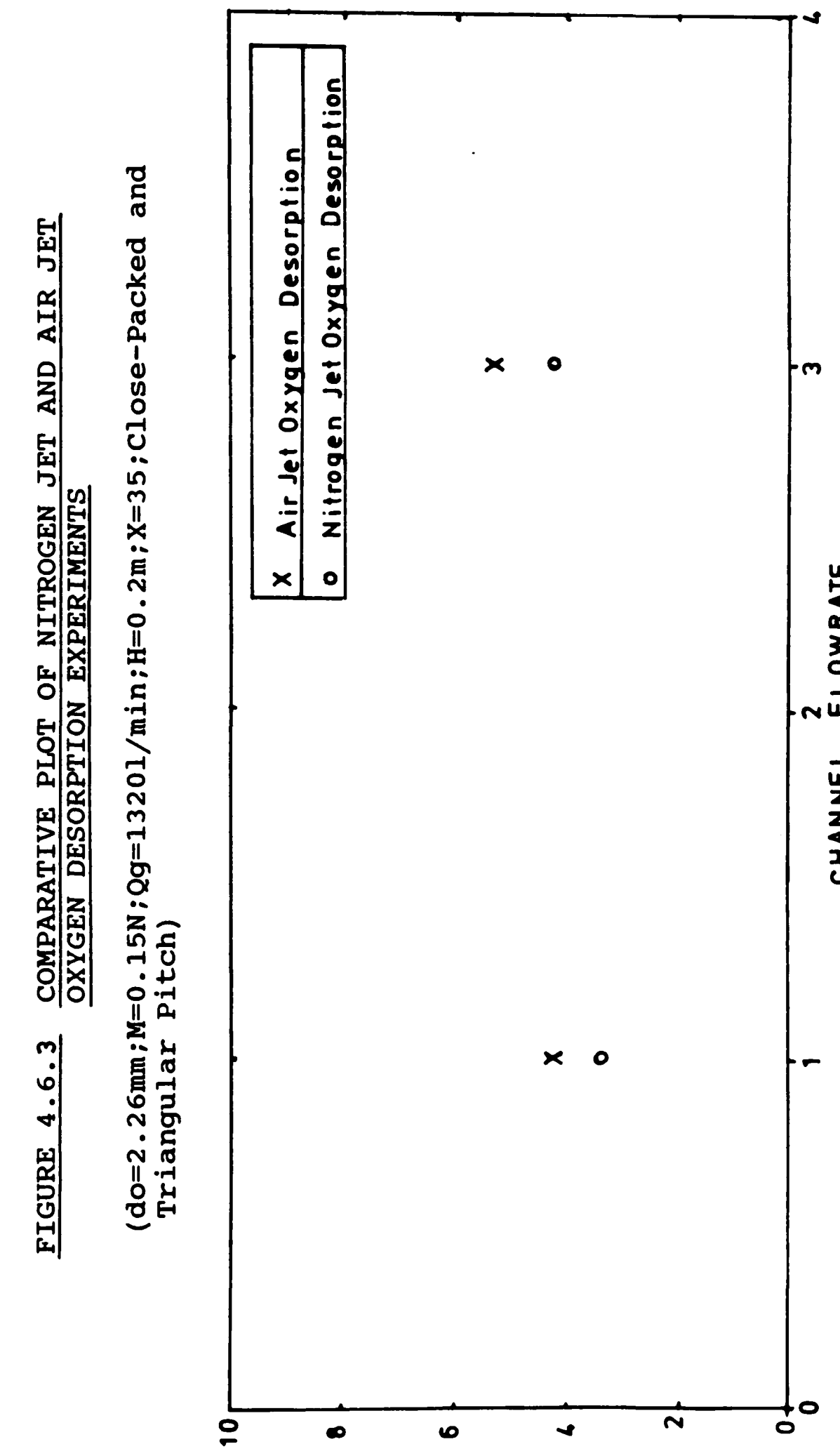

configuration of samples was such that they traversed the channel width and depth. They were placed downstream of the top-blow region. During a top-blow run they could be closed for later analysis out of the channel. It was found that for both low and high channel flowrates complete mixing was taking place as all the samplers registered identical bulk oxygen concentration readings. A similar finding was revealed on placing the configuration upstream of the top-blow region.

4.7 THE CHANGE IN MOMENTUM FLUX OF A JET DUE TO PACKING OF NEIGHBOURING JETS IN AN ARRAY AND CHANNEL WALLS

After the test runs, to provide some indication as to the effect on jet momentum flux of multiple lances close together in an enclosed channel a test was devised. A Sartorius top-loading, electronic balance was placed in the channel with a specially sized plate on top that covered the whole of the top-blow region. Each one of the multiple jet arrays was blown onto the balance and a reading taken. In theory, the reading on the balance should correspond to the combined momentum flux of each individual lance. If it did not then there was obviously some jet/jet and/or jet/wall interaction occurring that was damping or increasing the momentum flux of the jets.

Table 4.7.1 gives the results for the close-packed arrays. $\dot{M}_{eff}$ is the "effective momentum flux" from these tests i.e. the actual momentum flux per lance determined from the Sartorius reading. There is a reduction in momentum flux reading for all 2.26 mm nozzle arrays considered ranging from 7 to 17%. If this new momentum flux per lance, $\dot{M}_{eff}$, is substituted into the Jones-type analysis a new figure for the dimensionless momentum number is obtained. If these values are plotted on Jones' correlation as in Figure 4.7.1 for Serial Nos. AOD.5 and AOD.8-12 then it can be seen that the points shift sideways on the plot. However it only has a nominal effect on the final positions of the points.

When the data for the open-packed arrays are considered then Table 4.7.2 results. Figure 4.7.2 is a comparative plot of the open and close-packed data for the 4.95 mm, 10.95 mm and 24.40 mm nozzles. The reduction in momentum fluxes for the close-packed arrays are seen to be

TABLE 4.7.1: COMPARISON OF ACTUAL AND THEORETICAL MOMENTUM FLUX FOR CLOSE-PACKED ARRAYS

Top-Blowing Conditions			Serial No.	$\dot{M}$ (N)	Theoretical Combined Momentum Flux (N)	Actual Combined Momentum Flux (N)	$\dot{M}_{eff}$ (N)	$(\dot{M}_{eff}/\dot{M}) \cdot 100$ (%)
X	d_o (mm)	H (cm)						
35	2.26	20.0	AOD.1-5	0.150	5.250	4.340	0.124	82.9
"	"	"	NOD.1-2	"	"	4.778	0.140	91.0
"	"	17.5	AOD.9	"	"	4.760	0.136	90.7
"	"	15.0	AOD.10	"	"	4.830	0.138	92.1
"	"	12.5	AOD.11	"	"	"	"	91.8
"	"	10.0	AOD.12	"	"	"	"	91.7
36	"	20.0	AOD.6-8	0.144	5.104	4.608	0.128	88.6
16	4.95	"	AOD.13	0.146	2.336	1.760	0.110	75.5
7	10.95	"	AOD.15	0.159	1.113	0.868	0.124	77.9
4	24.40	"	AOD.17	0.137	0.548	0.364	0.091	66.6

TABLE 4.7.2: COMPARISON OF ACTUAL AND THEORETICAL MOMENTUM FLUX FOR OPEN-PACKED ARRAYS

Top-Blowing Conditions			Serial No.	$\dot{M}$ (N)	Theoretical Combined Momentum Flux (N)	Actual Combined Momentum Flux (N)	$\dot{M}_{eff}$ (N)	$(\dot{M}_{eff}/\dot{M}) \cdot 100$ (%)
X	d_o (mm)	H (cm)						
16	4.95	20	AOD.14	0.146	2.336	1.834	0.115	78.5
7	10.95	"	AOD.16	0.159	1.113	0.956	0.137	85.9
4	24.40	"	AOD.18	0.137	0.548	0.400	0.100	72.9

FIGURE 4.7.1 PLOT OF $\dot{M}_{eff}$ AND $\dot{M}$ FOR 2.26mm NOZZLES IN CLOSE-PACKED ARRAYS ON A JONES CORRELATION

(Q_l=3.7m3/hr, Q_g=1320l/min, H=10-20cm, $\dot{M}$=0.15N, X=35,36 ,Triangular and Square Pitch)

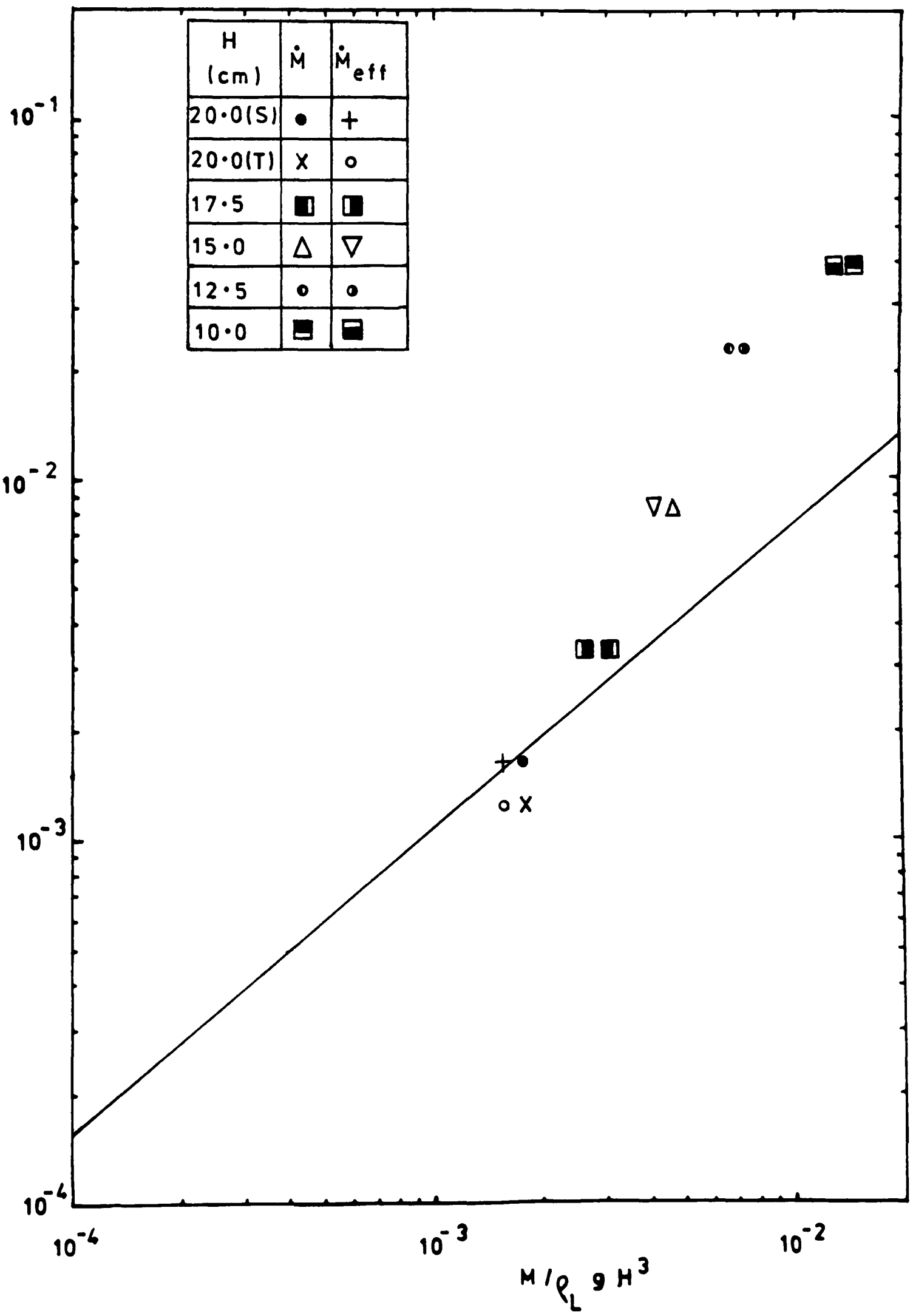

FIGURE 4.7.2 $\dot{M}_{eff}$ AND $\dot{M}$ FOR OPEN AND CLOSE-PACKED ARRAYS OF 4.95mm, 10.95mm AND 24.4mm NOZZLES ON A JONES CORRELATION

(Q_l=3.7m3/hr, Q_g=1320l/min, H=20cm, $\dot{M}$=0.15N, Triangular Pitch)

$Sh\, Sc^{-1/2} Ga^{-2/3} (d_b/H)^2 Mo^{0.16}$

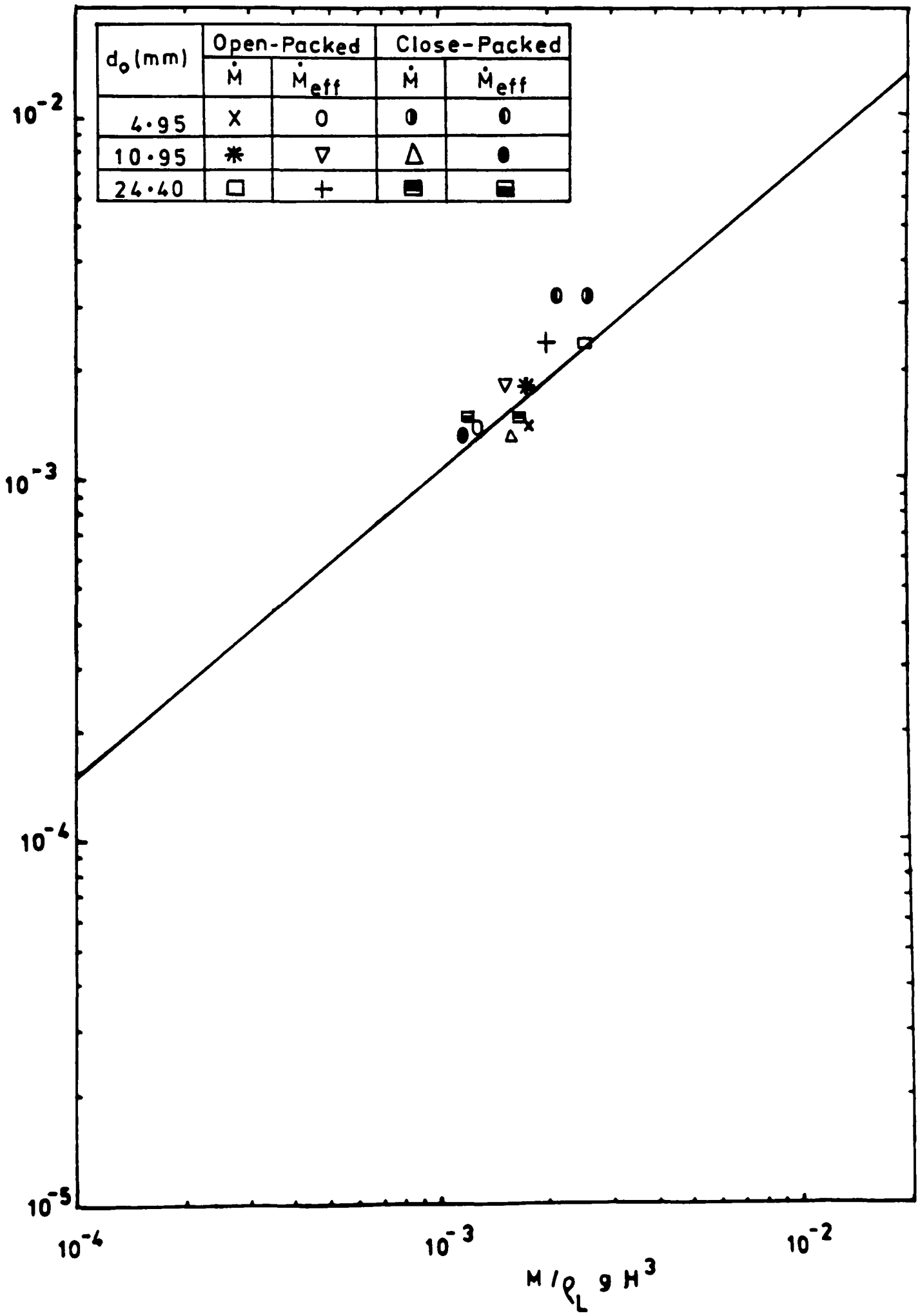

slightly larger than for the comparable open-packed arrays. The greatest reduction in momentum flux occurs for the arrays of fewer, larger diameter nozzles (Serial Nos. AOD.13-18). For these arrays the reduction in $\dot{M}$ is as much as 30% of that expected from a free jet issuing from the same nozzle. This may be attributed partly to the larger geometry of these impinging jets magnifying jet interference and partly to the lower combined momentum flux readings (compared to the 35 or 36 lance arrays, say) on the balance introducing experimental error. Nevertheless, there is a definite shift of points to the left on the Jones correlation plots when $\dot{M}_{eff}$ is used. It is interesting to note that this generally moves points closer to Jones' correlation line.

4.8 TOP-BLOW UNIT DESIGN FOR THE PILOT-SCALE SMELTER

Based on this work and the work of Jones (1986) a top-blow unit has been designed and is currently being constructed so as to be integrated into the pilot-scale smelter commissioning schedule. Even though this work has indicated that fewer, larger diameter nozzles are beneficial in terms of the desired restriction in liquid phase oxygen mass transfer Jones has shown that larger nozzles have lower gas phase mass transfer efficiencies compared to smaller ones. A high gas phase mass transfer efficiency means that improved oxygen utilisation at the jet/liquid interface will result thus producing better chemical reaction stoichiometry in the melt. Dai (1990) is currently expanding on and refining Jones' gas phase jet mass transfer work.

To achieve this fine balance between gas phase and liquid phase oxygen mass transfer the 35 lance, 2.26 mm nozzle, close-packed array (see Figure 3.1.3) has been adopted as the preferred top-blow configuration for the pilot-scale smelter. The top-blow unit design for the smelter requires a compact, relatively small assembly so as to fit onto a prepared flange on top of the pilot-scale smelter - see Figure 4.8.1.

Thermodynamic and chemical calculations have indicated that the air/oxygen lances and the unit as a whole will have to withstand exposure to a converting hearth atmosphere of up to 1100^{o}C. The atmosphere will also be composed of around 65% SO_2 (i.e. very corrosive) during the actual blows. The smelter itself takes a couple of days to reach a melt temperature of 1300^{o}C whereas the circulation and top-blow will only last a few hours. Clearly, the unit will be exposed to an aggressive furnace atmosphere before and after the blow. In terms of construction it was desirable to have a

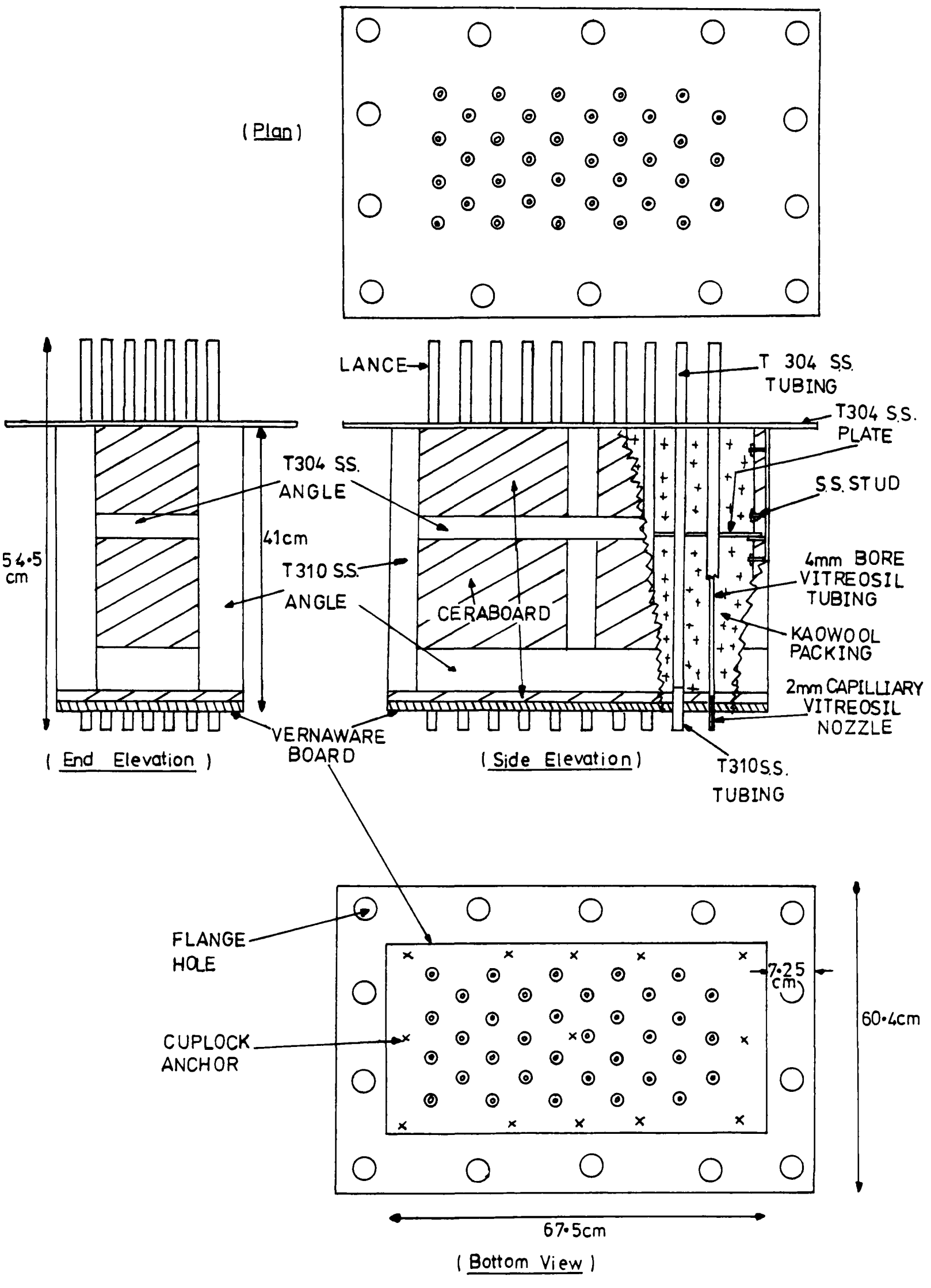

FIGURE 4.8.1 : TOP-BLOW UNIT DESIGN

relatively light, robust unit so that it could easily be removed from the smelter lid for inspection and possible future modifications.

The unit is made from Type 310 (25% Cr, 20% Ni) and Type 304 (18% Cr, 8% Ni) stainless steel angle that acts as a skeletal support for the refractory boards as well as to add rigidity to the structure. Type 310 stainless steel has good strength and corrosion resistance at 1100^{o}C as corrosion tests under an atmosphere similar to that in the converting hearth for 3 hours have verified. Only a surface black oxide film (~ 5 µm thick) was shown to result after microscopic examination. Since the lance tips had to be 2 mm in diameter, capilliary Vitreosil tubing was used for nozzles being fused onto normal bore silica tubing in an effort to decrease pressure drops. Because of the fragility of vitreous silica it is enclosed in a stainless steel sheath for strength - the two together make up the lance. The heavy duty Vernaware Board and the Ceraware Board are secured to the stainless steel frame by a combination of stainless steel studs for the latter and Cuplock Anchors for the former. Cuplock Anchors are a standard industrial method of securing refractory boards in position. Only the Vernaware ceramic fibre board and the lance tips will be directly exposed to the furnace atmosphere during a smelting run and it can be argued that their temperature will not be as high as 1100^{o}C due to the cooling effect of the gas delivered through the lances.

CHAPTER 5: FOG FORMATION DURING VACUUM CONDENSATION

5.1 DEVELOPMENT OF A COMPUTER PROGRAM FOR HIGH TEMPERATURE CONDENSABLE MIXTURES

5.1.1 Consideration of Cooling Curves for Vapour/Gas Mixtures

In order to predict the amount of fog formation to be expected when a given condensable vapour/inert gas mixture is transported past a cooler surface, some indication of the cooling path of the mixture is required. If this cooling curve passes into a supersaturation region then fog could be expected to form (in a "worse case" senario) given favourable nucleation kinetics. From published literature several equations have been derived by various investigators and presented in section 2.2.3.9 of this thesis. The majority of the equations are first order differential equations of the form

$$\frac{dp_v}{dt_v} = f\left(p_v, t_v\right) \qquad (5.1.1)$$

These equations are equally valid at all condenser operating pressures except under molecular distillation conditions. All the equations represent vapour/gas cooling curves for the bulk gas phase during condensation. Three in particular have been examined for the following reasons. The Gardner/Colburn and Drew equation (2.2.23) has been studied in detail because of its sound fundamental basis and the wide applicability claimed by its authors. Since the Warner smelter connected with this work is proposing to condense high vapour content vapour/gas mixtures, the

equations related to these conditions have been considered. Two in particular; namely the Bras equation (2.2.27) and the derived Cairns and Roper equation (2.2.28). Bras gives eqn. 2.2.27 specifically for high initial vapour concentrations whereas the Cairns and Roper equation is empirical based on their experimental work. The equations are reproduced below:

Gardner Equation

$$\frac{dp_v}{dt_v} = \left(\frac{1 - e^{-a}}{a}\right)\left(\frac{P - p_v}{p_{BM}}\right)\left(\frac{Sc}{Pr}\right)^{-2/3}\left(\frac{p_v - p_c}{t_v - t_c}\right) \qquad (2.2.23)$$

Bras Equation

$$\frac{dp_v}{dt_v} = \left(P - p_v\right)\left(\frac{p_v - p_c}{t_v - t_c}\right) \Bigg/ \left[p_{BM}\left(\frac{Sc}{Pr}\right)^{2/3} + \left(p_v - p_c\right)\left(\frac{M_v\, Cp_v}{M\, Cp}\right)\right] \qquad (2.2.27)$$

Cairns and Roper Equation

$$\frac{dp_v}{dt_v} = \left(\frac{1 - e^{-a}}{a}\right)\left(\frac{2}{2+a}\right)\left(\frac{Pr}{Sc}\right)^{2/3}\left(\frac{P - p_v}{p_{BM}}\right)\left(\frac{p_v - p_c}{t_v - t_c}\right)\left(\frac{p_{BM}}{P}\right)^{-0.05} \qquad (2.2.28)$$

5.1.2 Numerical Solution of First Order Differential Equations

Due to the nature of the equations being considered no explicit

integration method can solve them thus a numerical solution is required. A more accurate version of Simpson's Rule was opted for, namely the Runge-Kutta method. It uses a fourth order gradient technique to solve each iteration.

For the solution of

$$\frac{dp_v}{dt_v} = f\left(p_v, t_v\right)$$

the Runge-Kutta method requires the values $t_v = t_{vi}$ and $p_v = p_{vi}$ to be provided before the first integration step in the numerical integration of the differential equation can commence. It then computes the value of p_{vi+1} of the dependent variable p_v that is to be associated with argument $t_{vi+1} = t_{vi} + \Delta t_v$ as follows where Δt_v is the step length:

Let $Q_1 = f(t_{vi}, p_{vi}) \cdot \Delta t_v$

$Q_2 = f(t_{vi} + {}^1/_2\,\Delta t_v, p_{vi} + {}^1/_2\,Q_1) \cdot \Delta t_v$

$Q_3 = f(t_{vi} + {}^1/_2\,\Delta t_v, p_{vi} + {}^1/_2\,Q_2) \cdot \Delta t_v$

$Q_4 = f(t_{vi} + \Delta t_v, p_{vi} + Q_3) \cdot \Delta t_v$

$$\Delta p_v = \frac{1}{6}\left(Q_1 + 2Q_2 + 2Q_3 + Q_4\right)$$

Then the value p_{vi+1} of p_v corresponding to $t_v = t_{vi} + \Delta t_v$ is determined by

$$p_{vi+1} = p_{vi} + \Delta p_v$$

The next point on the curve, p_{v1+2}, is calculated by a similar method

and so on to a specified end-point. The solution outlined above is for a "forward marching technique". For the situation considered in this work where high temperature mixtures are cooled a "backward marching technique" has been adopted. The principle is exactly the same except that the step length, Δt_V is negative. The error involved in the Runge-Kutta calculation is very low. Accuracy increases if smaller step lengths are used.

5.1.3 Solution of the Cooling Curves by a Computer Program

The following simplifying assumptions are inherent in the development of the computer program and in the fog formation model:

i) The equilibrium condition at the condensate interface, (p_C, t_C), is constant along and throughout the condenser. This will be the case if a solid condensate builds up with liquid running off it. t_C will then equal the melting point of the condensate.

ii) The drop in temperature and partial pressure from the bulk mixture to the condensate interface occurs across a gas film - usually the case for turbulent flow.

iii) There is negligible interfacial resistance provided by the metallic condensate such that $p_C = p_{sat}$.

iv) Heat losses through the condenser outer walls are insignificant as is the radiation component of heat transfer from the condensable mixture to the coolant wall.

v) Partial pressures and operating pressures are sufficiently high enough (greater than approximately 0.1 mm Hg) that pressure as conventionally understood (i.e. intermolecular and molecule-wall collisions) is occurring. This should happen in the Warner condenser due to the forced convective vapour/inert gas flow

past the condensation surface inducing such interactions, i.e. bulk gas flow.

vi) The total pressure throughout the condenser (i.e. the operating pressure) remains constant, that is, frictional losses are insignificant.

vii) The carrier gas (the inerts or noncondensables) does not react with the condensable vapour in any way.

viii) The kinetics of fog formation onto an excess of suitable heterogeneous condensation nuclei is such that it is effectively instant once the vapour/gas mixture reaches a state of super-saturation. This is critical with regard to the "worse case" senario adopted in this work - there is no time barrier to fog formation.

ix) All heterogeneous condensation nuclei are taken to be at the same temperature as the condensate interface to compete with the coolant wall on a "worse case" basis.

Assumptions (i), (iii), (v), (viii) and (ix) will tend to overestimate vapour fog formation whereas (ii) and (iv) will underestimate fogging. Assumption (viii) should be the overriding factor thus yielding a cumulative overestimation of fog losses by this "worse case" fog model. It should bepointed out that if assumptions (i) and (iii) are not holding in a given condenser then equilibrium vapour losses will be higher than predicted.

In the solution of the cooling curve equations it is apparent that both the bulk mixture's Schmidt/Prandtl ratio, $k_{mix}/(\rho_{mix} \cdot Cp_{mix} \cdot D_{mix})$, and its specific heat ratio, $M_V.Cp_V/M.Cp$, will vary at each point in the condenser. This is due to the depletion of vapour from the vapour/gas mixture as it cools. Hence, it would be prudent to recalculate both these variables for each point on the cooling curve. Figure 5.1.3.1 shows schematically the format of the

FIGURE 5.1.3.1: SCHEMATIC DETERMINATION OF PROPERTY RATIOS FOR EACH ITERATION OF THE COMPUTER PROGRAM

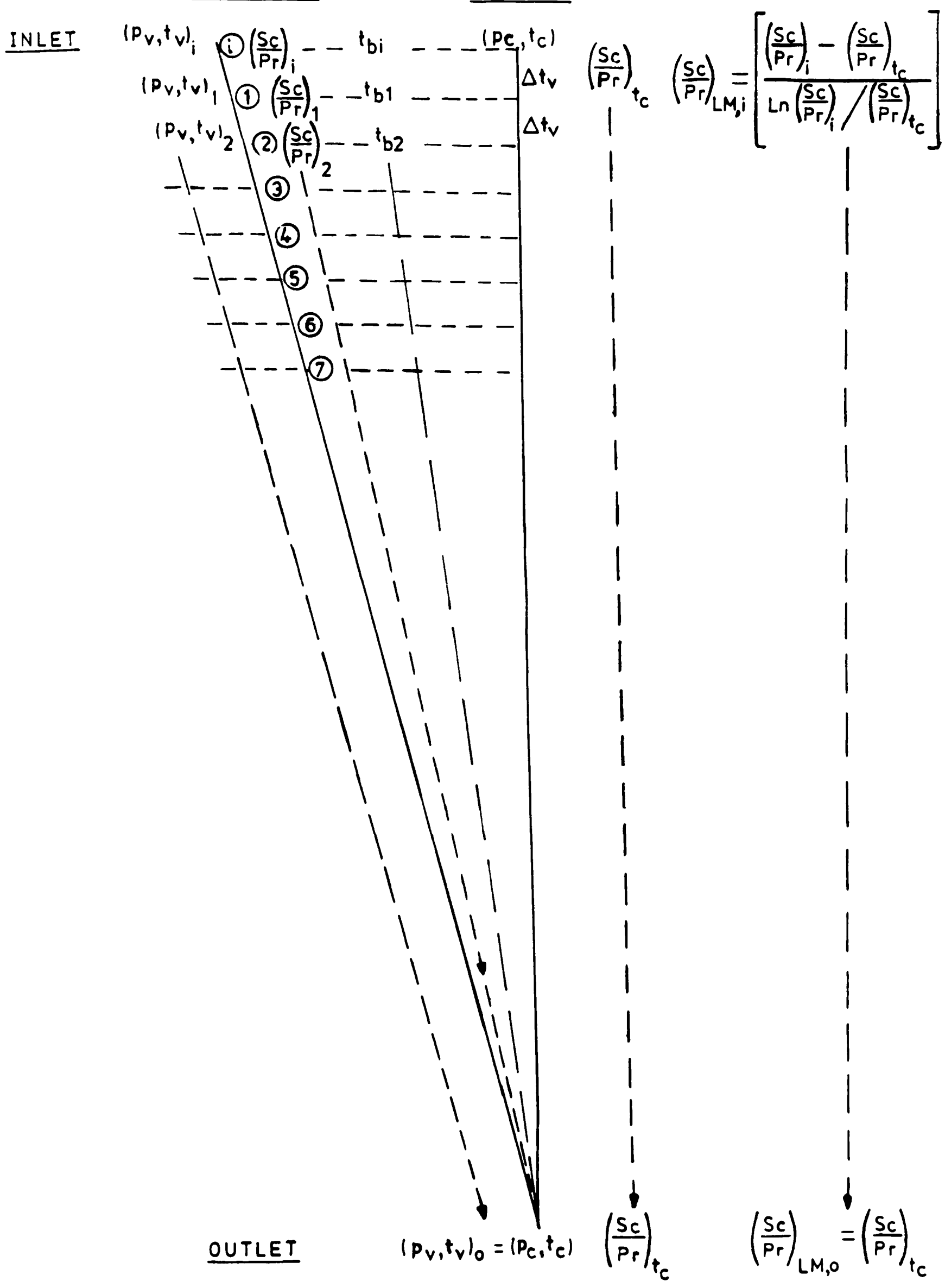

computer program. Point i, the inlet condition for the bulk vapour/gas mixture, is known so a value for $(Sc/Pr)_i$ can be estimated. $(Sc/Pr)_{t_c}$ is constant throughout the program. For the computer solution of the differential equation at each step an arithmetic mean Sc/Pr ratio is used. For instance, the first Sc/Pr ratio utilised was $(Sc/Pr)_{i,AM} = [(Sc/Pr)_i + (Sc/Pr)_{t_c}]/2$ and so on. The ratio $M_v Cp_v/MC_p$ for each step was calculated at the arithmetic mean temperature, t_b, of the incoming mixture. For example, $t_{bi} = (t_{vi} + t_c)/2$ and so on for each point. To estimate each variable in the Sc/Pr ratio for a bulk mixture at temperature t_v(K) the following equations for binary vapour/inert gas mixtures were used:

a) Thermal Conductivity of a Binary Gas Mixture

Bird, Stewart and Lightfoot (1962) give equations 5.1.2 to 5.1.6 by Wilke for a binary mixture of species i and j at low density.

$$k_{mix} = \left(\frac{x_i k_i}{\left[\left(1-x_i\right) \Phi_{ij} + x_i \right]} + \frac{\left(1 - x_i\right) k_j}{\left[x_i \Phi_{ji} + \left(1 - x_i\right) \right]} \right) \qquad (5.1.2)$$

where

$$\Phi_{ij} = \frac{1}{\sqrt{8}} \left(1 + \frac{M_i}{M_j} \right)^{-1/2} \cdot \left[1 + \left(\frac{\mu_i}{\mu_j} \right)^{1/2} \cdot \left(\frac{M_j}{M_i} \right)^{1/4} \right]^2 \qquad (5.1.3)$$

and

$$\Phi_{ji} = \frac{1}{\sqrt{8}}\left(1+\frac{M_j}{M_i}\right)^{-1/2}\cdot\left[1+\left(\frac{\mu_j}{\mu_i}\right)^{1/2}\cdot\left(\frac{M_i}{M_j}\right)^{1/4}\right]^2 \qquad (5.1.4)$$

x_i is the mole fraction of species i in the mixture

μ_i is the viscosity of species i in the mixture from the Chapman-Enskog relationship (see below)

M_i is the molecular weight of species i in grammes.

$$\mu_i = \frac{2.6693 \times 10^{-5}\sqrt{M_i \cdot t_v}}{\left(\sigma_i\right)^2 \cdot \Omega_{\mu,i}} \qquad (5.1.5)$$

and

$$\mu_j = \frac{2.6693 \times 10^{-5}\sqrt{M_j \cdot t_v}}{\left(\sigma_j\right)^2 \cdot \Omega_{\mu,j}} \qquad (5.1.6)$$

where

σ_i is the "collision diameter" of a gas molecule of species i

$\Omega_{\mu,i}$ is the "Omega Mhu, i" function of species i which slowly varies as a function of the dimensionless temperature, $(k/\varepsilon) \cdot t_v$ where k/ε is the particular "force constant" for species i. Bird et al give tables for these functions.

b) Mass Diffusivity of a Binary Gas Mixture

Bird et al give another Chapman-Enskog dimensional equation for mass diffusivity of one species in another at low density:

$$D_{mix} = \frac{0.0018583 \sqrt{t_v^3 \left(\frac{1}{M_i} + \frac{1}{M_j}\right)}}{P \cdot \sigma_{ij}^2 \cdot \Omega_{D,ij}} \qquad (5.1.7)$$

where

σ_{ij} = $1/2(\sigma_i + \sigma_j)$, the "collision diameter": non-polar, non-reacting molecule pairs.

$\Omega_{D,ij}$ = is "Omega D,ij", a varying function of the dimensionless temperature, $(k/\varepsilon)_{ij} \cdot t_v$ where $(k/\varepsilon)_{ij}$ is the force constant for the mixture and equal to $\sqrt{(k/\varepsilon)_i \cdot (k/\varepsilon)_j}$

and P is the system pressure (in atmospheres).

c) Density of a Binary Gas Mixture

For an ideal gas:

$$\rho_i = \frac{M_i}{22.4 \times 10^3} \times \frac{273}{t_v} \times P \qquad (5.1.8)$$

and for a binary mixture

$$\rho_{mix} = x_i \cdot \rho_i + \left(1 - x_i\right) \rho_j \qquad (5.1.9)$$

d) Specific Heat Capacity of a Binary Gas Mixture

$$Cp_{mix} = Cp_i \cdot x_i + Cp_j\left(1 - x_i\right) \qquad (5.1.10)$$

To estimate a value for the ratio $M_V Cp_V / MC_p$ (i.e. H_C) at the bulk mean temperature for the vapour/gas mixture the following equation was used:

$$H_C = \frac{M_v \; Cp_v}{\left[M_v\left(x_m\right) + M_g\left(1 - x_m\right)\right]\left[Cp_v\left(x_m\right) + Cp_g\left(1 - x_m\right)\right]} \qquad (5.1.11)$$

where M_V is the molecular weight of the vapour

M_g is the molecular weight of the inert gas

Cp_v is the specific heat capacity of the vapour at t_b

Cp_g is the specific heat capacity of the gas at t_b

and $x_m = (x_V + x_C)/2$ is the mean mole fraction of the vapour between that at t_V and that at t_C.

To solve these equations at each temperature, data files of several variables are necessary such that they can be called into the main solution of the differential equation at the right juncture. A schematic representation of the computer program is presented in Figure 5.1.3.2 for the specific case of a zinc/nitrogen mixture using the Gardner equation (2.2.23). The actual computer program developed for this problem is presented in Appendix 3 in the BASIC language, version 3.08D for the RM Nimbus computer. The INPUT data files for the program are also in Appendix 3.

As figure 5.1.3.2 illustrates, the program is split up into sections. Lines

FIGURE 5.1.3.2 SCHEMATIC LAYOUT OF THE FOG FORMATION PROGRAMS

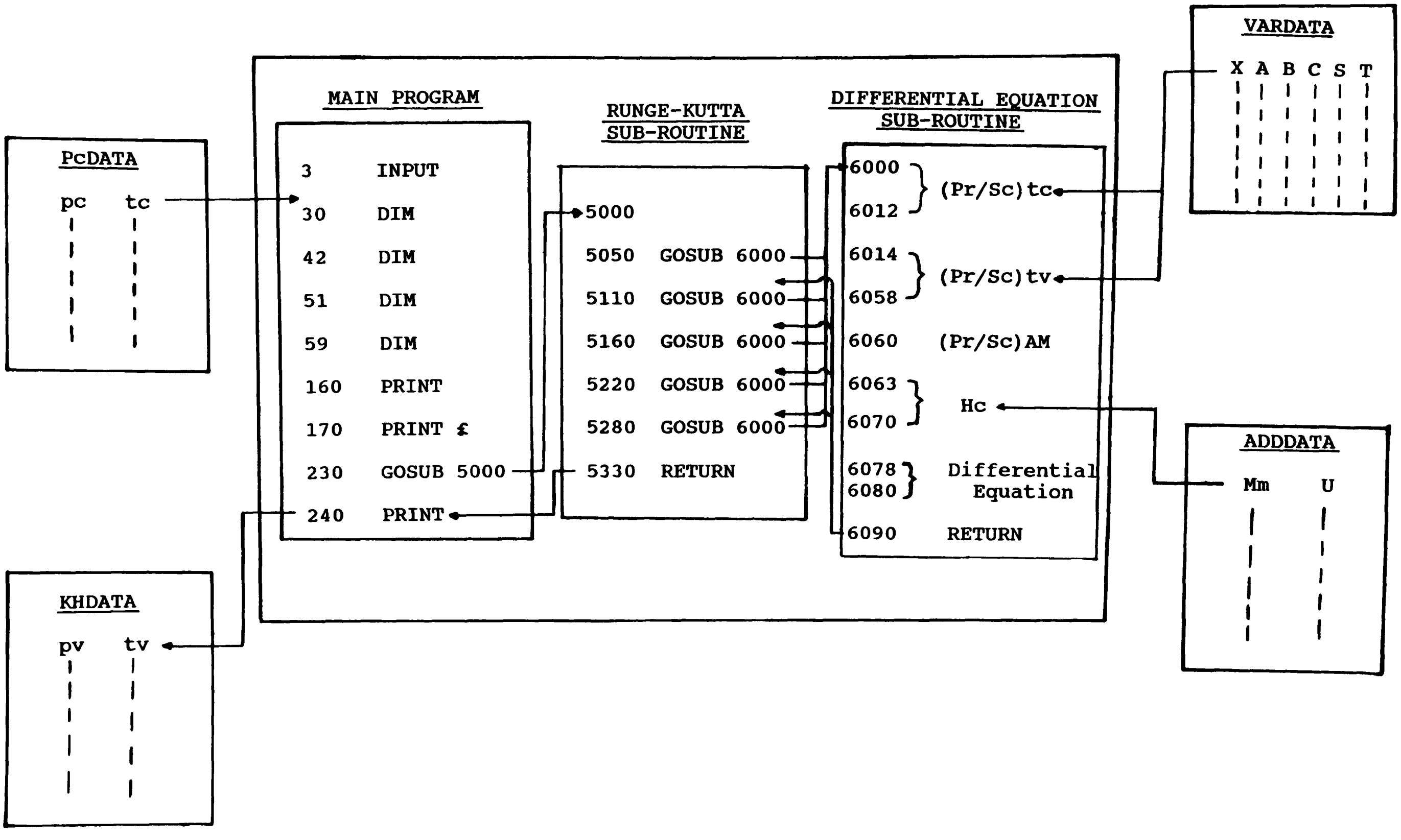

1 to 270 incorporate the INPUT statements; the DIMension statements creating the input files (Vardata, Adddata and Pcdata) and the output file, KHdata; and PRINT statements for the screen and the output file. The program is designed to ask the operator to input condenser operating pressure, P and the mass % zinc in the mixture fed to the condenser. The inlet vapour/gas temperature can be accepted anywhere in the range 420 to 1300^{o}C as long as it is divisible by 5^{o}C (the step length). A condensate temperature, t_c, less than or equal to 420^{o}C (the melting point of zinc) is admissible, here again only if divisible by 5^{o}C.

KHdata is the output data file that holds the numerical solution of the differential equation being solved for the conditions specified by the operator. It also includes an ERROR estimate of the accuracy involved with each calculation. The input data file Vardata holds input variables Omega Mhu, Zn (for eq. 5.1.5), Omega Mhu, N_2 (for eq. 5.1.6), Omega D, ZnN_2 (for eq. 5.1.7), CpN_2 at t_v (for eq. 5.1.10) and kN_2 at t_v (for eq. 5.1.2) calculated over a range of temperature. Adddata is the input data file holding the mean interfacial temperature t_b and the specific heat capacity for N_2 used in eq. 5.1.11. Pcdata is a data file that stores the equilibrium partial pressure of zinc vapour for a range of temperatures. This data can be called into the main program at any point specified by the operator's INPUT data. Special algorithms have been created (lines 215, 6000, 6003, 6014 and 6065) so that data from the files can be read sequentially from the correct point in the files.

Once the operating conditions are given to the main program, the mole fraction of zinc in the feed is calculated (line 16) followed by the inlet partial vapour pressure, p_{vi} (line 150). This value for p_{vi} together with the operator's INPUT t_{vi} are then fed into the Runge-Kutta subroutine (lines

5000 to 5330). At various points in this subroutine (lines 5050, 5100, 5160, 5220 and 5280) the program goes into a further subroutine (lines 6000 to 6100) containing the Gardner equation which is then solved repeatedly.

LInes 6000 to 6012 of the program calculate the Sc/Pr ratio for the interface condition whereas lines 6014 to 6053 calculate the Sc/Pr ratio for the mixture at t_v. The arithmetic mean Sc/Pr ratio is calculated in line 6060. Lines 6063 to 6070 of the subroutine estimate H_C, the specific heat ratio. The actual Gardner differential equation is in lines 6078 to 6080. For solution of the Bras or Cairns and Roper equations these were the only two lines of the program to be changed.

All the variables in the program that are dimensional are calculated in cgs units. The thermal conductivity of zinc at t_v, k_{Zn}, was calculated using the following Chapman-Enskog type equation given by Bird et al. (1962):

$$k_{Zn} = \frac{1.9891 \times 10^{-4} \sqrt{t_v/65.38}}{\left(\sigma_{Zn}\right)^2 \Omega_{k,\,Zn}} \qquad (5.1.12)$$

where $\Omega_{k,\,Zn} = \Omega_{\mu,Zn}$

The dimensional equations 5.1.2 to 5.1.12 incorporate the following constant data for the considered zinc/nitrogen system:

σ_{Zn} = 2.510 Ängstroms

σ_{N_2} = 3.681 Ängstroms

$(\varepsilon/k)_{Zn}$ = 1337

$(\varepsilon/k)_{N2}$ = 91.5

$(Cp)_{Zn}$ = 4.968 cal/mole ^{o}C

M_{Zn} = 65.38 g

M_{N2} = 28.013 g

5.2 TYPICAL COMPUTER PROGRAM PRINTOUT AND SUBSEQUENT ANALYSIS

A typical computer run (G Zn.9) for a 97% zinc/3% nitrogen vapour/gas mixture entering a condenser at 1200^{o}C at total pressure 30 mm Hg is given in Appendix 3. For this run a solid zinc condensate is considered (with liquid running off) since t_c = 420^{o}C(the melting point of zinc). The data from the printout are presented graphically in Figure 5.2.1. Initially the computer program was checked by a hand calculation of the same computer run.

The most apparent observation from the figure is the very pronounced bending of the cooling curve indicating that heat transfer is very much higher than mass transfer during this cooling operation. The cooling curve crosses the equilibrium line for zinc at $(p_V , t_V)_f$ where the mixture becomes saturated. Since this analysis considers a "worse case" fog formation situation then this point of incipient supersaturation is also the point at which zinc will condense as a fog rather than as a condensate on the condenser wall. Clearly, this will be the case if sufficient nuclei are present for the supersaturated vapour to condense on.

If one considers the inlet zinc vapour partial pressure of 27.98 mm Hg this corresponds to a mole fraction of 27.98/30 i.e. 0.93; the mole fraction of N_2 in the mixture being 0.07. Hence, for every kmole of nitrogen entering the condenser there will be 0.93/0.07 kmoles of zinc i.e. 13.85 kmoles. At the point of incipient fog formation the zinc partial vapour pressure, p_{Vf}, is 21.2 mm Hg i.e. a mole fraction of 0.71. At this point in the condenser 1 kmole of N_2 corresponds to 2.41 kmoles of zinc. Thus 11.45 kmoles of zinc have been recovered as condensate. The remaining 2.41 kmoles of zinc are lost from the condenser as a combination of fog and equilibrium vapour

FIGURE 5.2.1: GRAPHICAL PLOT OF COMPUTER RUN GZn9

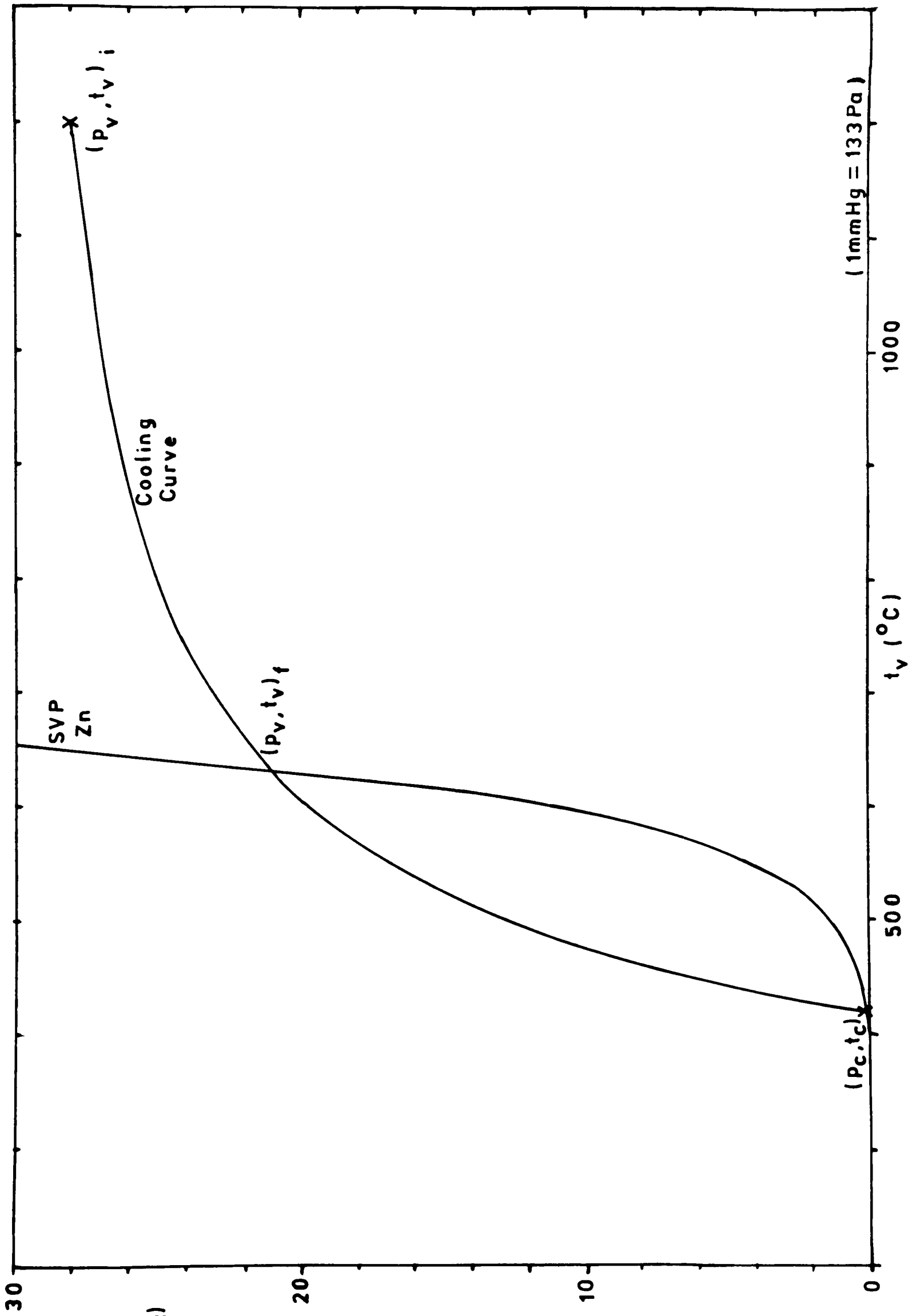

losses. As an extension of this discussion, the following equation gives the percentage of the original feed that ends up as fog exiting the condenser (assuming 100% contacting efficiency in the condenser unit, i.e. the outlet vapour/gas mixture is saturated):

$$\% \text{ Heterogeneous Fog Loss} = \left[\frac{\left(\frac{p_{vf}}{P - p_{vf}} - \frac{p_c}{P - p_c} \right)}{\left(\frac{p_{vi}}{P - p_{vi}} \right)} \right] . \ 100 \qquad (5.2.1)$$

For run G Zn.9 the fog formed amounts to 17.35%. The fraction of the inlet vapour lost due to equilibrium considerations can be estimated using eq. 5.2.2 (again assuming 100% contacting efficiency):

$$\% \text{ Equilibrium Loss} = \frac{\left(\frac{p_c}{P - p_c} \right)}{\left(\frac{p_{vi}}{P - p_{vi}} \right)} . \ 100 \qquad (5.2.2)$$

For run G Zn.9 equilibrium losses amount to a mere 0.04%. Obviously, the lower the operating pressure the greater the equilibrium loss will be. The total losses for a given condensable mixture is a combination of these two component parts. If less than 100% contacting efficiency is achieved in a

condenser then the total losses will remain the same, however the equilibrium loss will be higher and the fog loss consequently lower. The term "loss" is used here merely to indicate vapour not condensed in the condenser. In reality any vapour that passes through the condenser would be captured downstream in the mist extractor and ultimately recirculated to the front end of the smelter. Whatever the contacting efficiency, the outlet gas phase from a zinc condenser where fog is being produced will consist of zinc mist droplets coexisting and in equilibrium with gaseous zinc atoms.

5.3 ASSESSMENT OF THE EFFECT OF STEP LENGTH ON THE PROGRAM ACCURACY

During the early stages of developing the computer program a step length of 20^{o}C between points was chosen. However, later on this was reduced to 5^{o}C so as to improve the accuracy of the technique. Figure 5.3.1 illustrates the advantages graphically of a smaller step length. It is a plot of Run No. G Zn.6 for a 5^{o}C (A) and a 20^{o}C (B) step length. Curve A predicts fog to form at t_{vf} = 430^{o}C; p_{vf} = 0.205 mm Hg i.e. % fog = 0.53%. Curve B on the other hand has a less steep slope and predicts no fog to form at all. Clearly, there is a discrepancy such that the choice of a 5^{o}C increment is merited for this case. At higher total pressures the problem is less pronounced though a similar discrepancy in fog formation is found to be the case. A further decrease in step length to below 5^{o}C produces no further variation in the cooling curve profile.

FIGURE 5.3.1 : TYPICAL GARDNER OPERATING LINE PLOT, $\Delta t_v = 5^oC(A); 20^oC(B)$

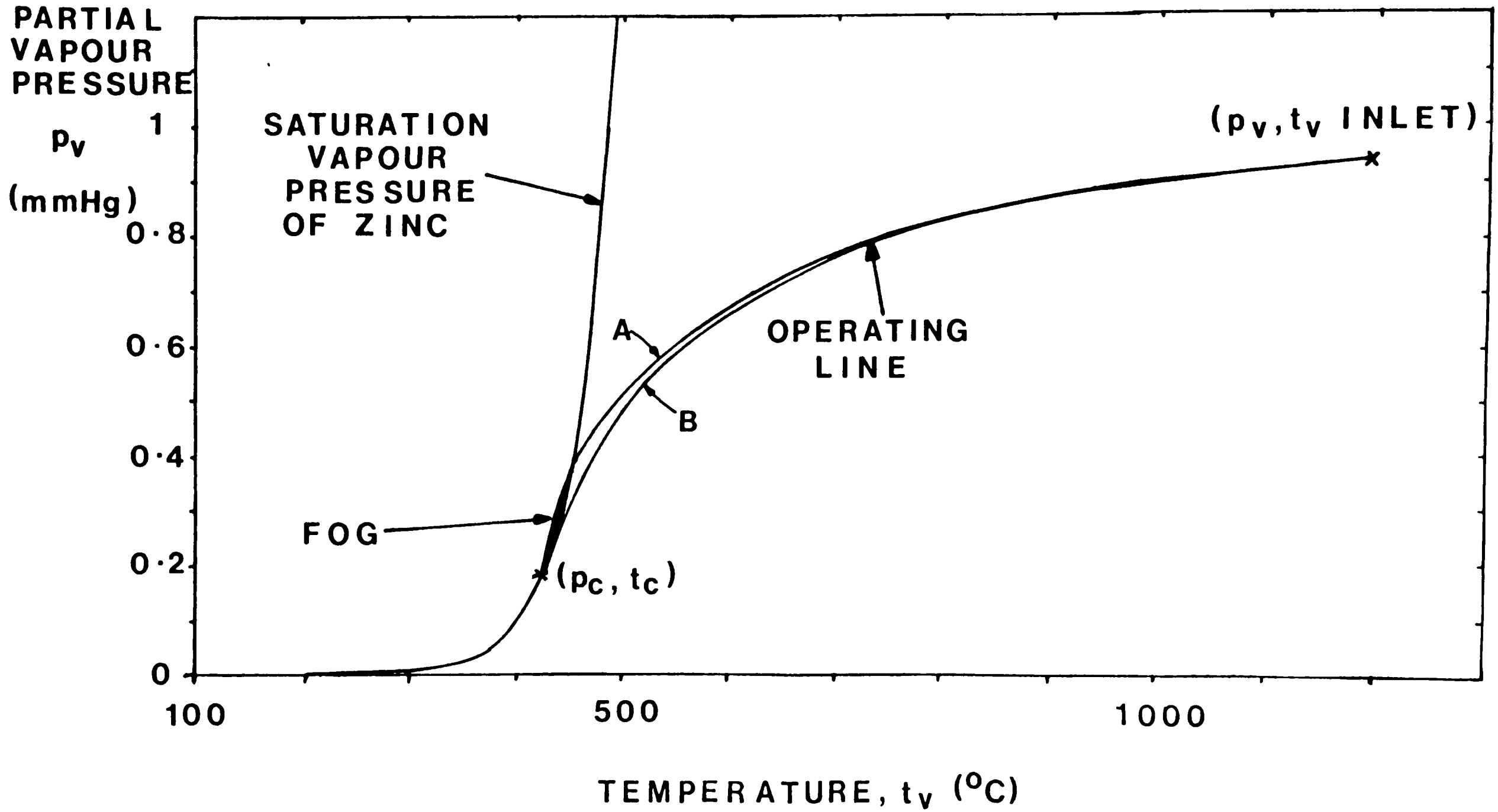

5.4 LOW TEMPERATURE PHYSICAL MODEL OF THE WARNER VACUUM CONDENSER

A low temperature physical model of the Warner Smelter condenser was built to study fog formation under an analogous low temperature mass transport situation. Figure 5.4.1 is a schematic drawing of the condenser model and Plate 5.1 is a photograph of the experimental rig. The condenser model is constructed from glass and is a $^1/_9$th scale model of the actual high temperature condenser. Several low temperature liquids were considered as analogues for zinc condensation under reduced pressure including steam and ethanoic acid. Glycerol was chosen because of its high melting point (18^{o}C), boiling point (290^{o}C) and molecular weight (92.1 g) (Physical Properties of Hydrocarbons, 1966). These physical properties help to ensure good fog formation characteristics at temperatures close to normal room temperature. Glycerol, however, does have an automatic ignition temperature of 429^{o}C and it will flash at temperatures above 160^{o}C if a spark is present. Though not shown in Plate 5.1 the glass model was shielded by a metal mesh in case the glycerol vapour did flash causing the model to shatter.

Referring to Figure 5.4.1, the whole of the apparatus is subjected to reduced pressure conditions via a vacuum pump. Controlled volumes of nitrogen can be metered to the system. Glycerol vapour is generated in a glass boiler where it is kept under a constant head by way of a large glass feed tank. The heating element in the boiler is controlled by a VARIAC transformer that varies the heating rate. Once glycerol vapour is generated at a reduced boiling point in the boiler it is superheated to the required

LEGEND TO FIGURE 5.4.1

A	Nitrogen Cylinder
B	Gas Rotameter
C	Throttling Rotameter
D	Constant Head Tank
E	Reheater
F	Boiler
G	Boiling Nucleator Rod
H	Superheater
I	Crossover
J	Vacustat Pressure Gauge
K	Condenser
L	Perkins Triangle
M	Receiver Flask on a Flexible Retort Stand
N	Cold Traps and Dewer Flask
O	Vacuum Pump
P	Coolant Rotameter
Q	Copper Cooling Coil and Dewer Flask
R	DAB Centrifugal Pump
S	Coolant Head Tank
T	Rockwool Insulation
T/C	Thermocouple (K-Type)
Th	Thermometer
V	Variac
X	Valve

FIGURE 5.4.1 : SCHEMATIC LAYOUT OF THE GLYCEROL CONDENSER MODEL

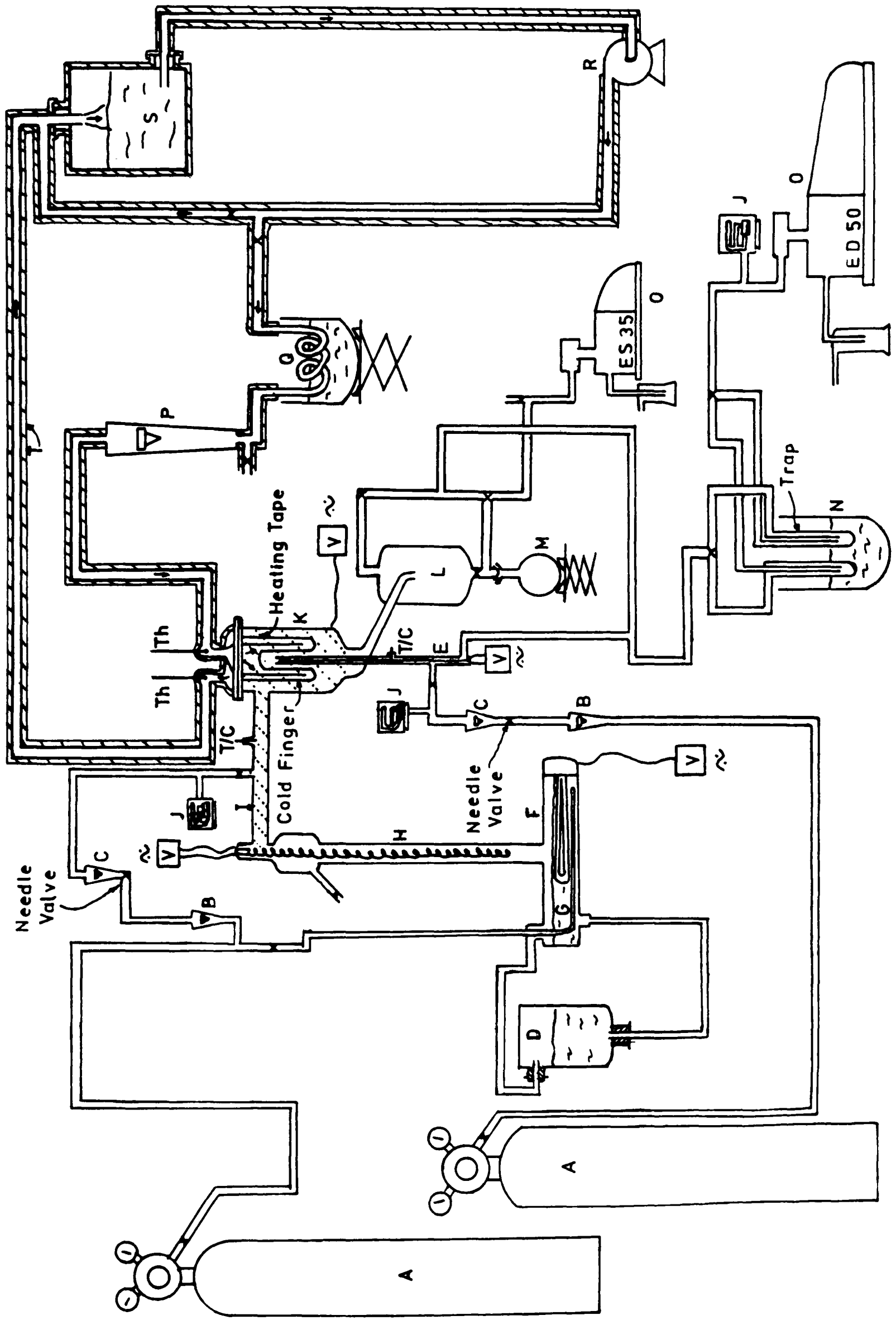

PLATE 5.1

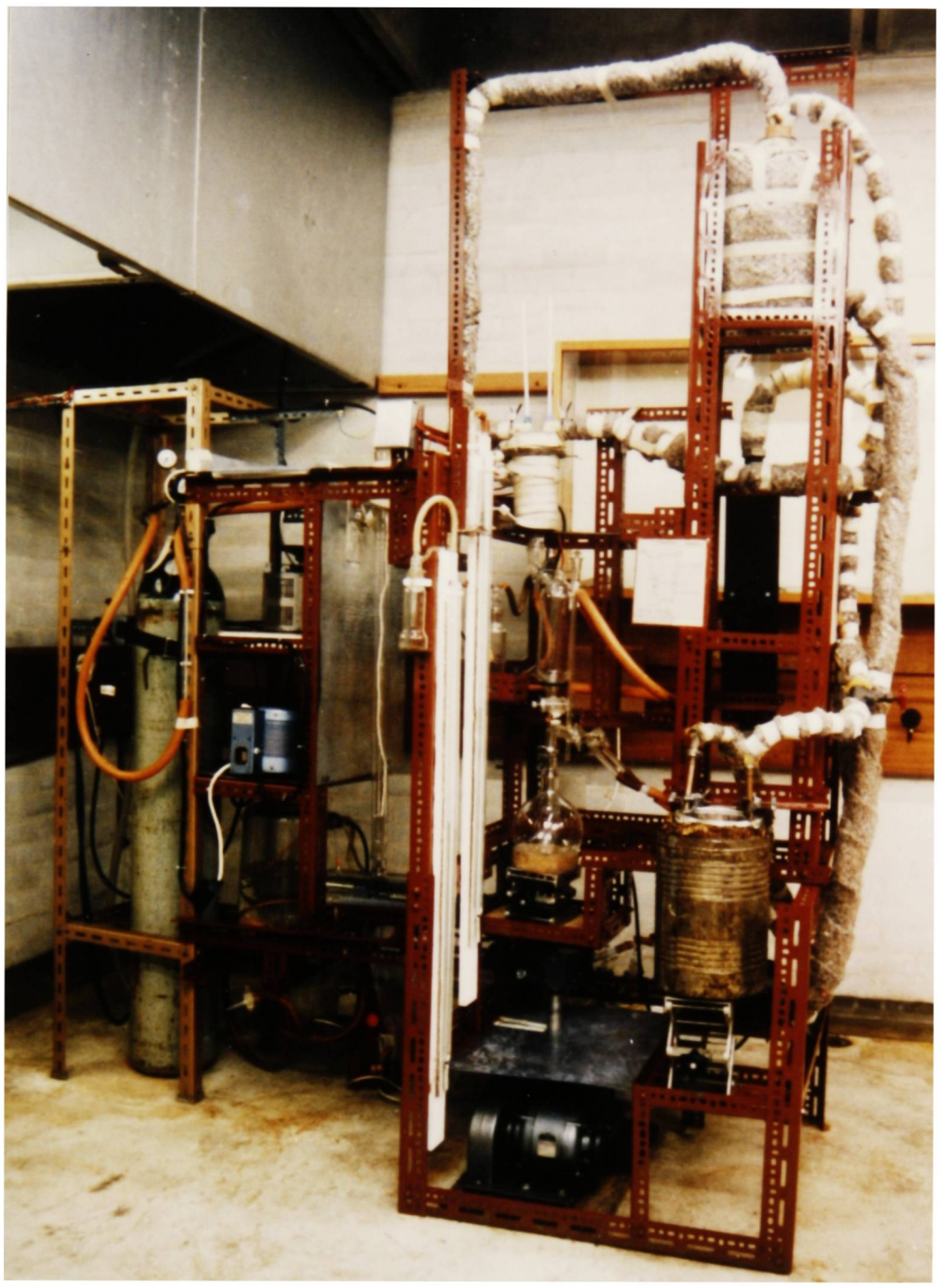

PHOTOGRAPH SHOWING THE GENERAL LAYOUT OF THE CONDENSER MODEL

temperature in a tube with a half metre long Nichrome electrically heated winding located axially in the tube. The vapour is mixed with a controlled quantity of inert gas fed through the pressure tappings or via a bubbler in the boiler. Prior to entering the condenser the mixture passes along a 'crossover' tube similar to that between the RH vessel/zinc condenser region of the Warner Smelter. In the model's crossover tube there is both a thermocouple and a pressure tapping. The crossover feeds a barrel-type condenser that employs a cooling finger to collect the glycerol on. The outer glass walls of the crossover and the condenser have heating tape wound round them to prevent any vapour from condensing on them rather than on the cool surface.

The vapour/gas mixture is stripped of glycerol and passes out of the condenser past a second pressure tapping and back to the fully ballasted Edwards ED50 vacuum pump via a 2-way cold trap system that knocks out any residual vapour in the mixture as a solid glycerol deposit. Downstream of the condenser a reheating coil is used to raise the vapour/gas temperature above the mixture's dewpoint so that it does not condense out prior to the cold trap. Actual quantities of fog formed can be determined from a mass balance over the system at steady state and compared to that predicted from a glycerol/nitrogen computer program utilising the Gardner fog equation. Any liquid condensate that forms in the condenser is collected in a receiver flask that catches the run-off from the cold finger. The receiver flask is below a 'Perkins Triangle' type arrangement consisting of a three-valve system that enables the flask to be isolated during a run. It also allows a quick switch-over from one receiver flask to another during a run. An Edwards ES35 pump is also attached to the Perkins Triangle to re-evacuate the flask prior to exposing it to the reduced pressure system again.

The coolant system consists of a head tank feeding a DAB centrifugal KP30 pump that circulates the cooling liquid through a copper cooling coil immersed in a dewar that is continually topped up with liquid nitrogen. The coolant is metered through a rotameter prior to entering one side of the cooling finger and back to the head tank. The inlet and outlet coolant temperatures of the condenser are measured in side-arm attachments. Because of the need for sub zero temperatures in the testwork, a 25% $CaCl_2$ solution was made up as coolant for the system.

The results from the testwork are presented in Appendix 5. To be a true analogue of the high temperature condenser the glycerol vapour needs to undergo a gas to solid phase change during condensation such that t_c is equal to the melting point of glycerol. The model's cooling system (as described above) is capable of producing a sustainable coolant inlet temperature of -8^{o}C (any lower and the $CaCl_2$ (aq) freezes up in the cooling coil stopping the flow). This cooling temperature limitation equates to a cold wall temperature of -3^{o}C (taking into account the thermal conductivity of glass). Even though the melting point of glycerol is 18^{o}C and all the heat release during condensation is removed by the coolant the cooling finger cold wall temperature needs to be less than -3^{o}C to form a solid deposit. Hence the model had insufficient cooling capacity and it was incapable of producing the desired glycerol phase change necessary to compare the results with the computational model. However, several successful steady state vapour generation runs using glycerol were carried out followed by liquid glycerol condensation under reduced pressure conditions. The runs highlight useful trends and problems associated with condensation under reduced pressure. As such, they are presented in Appendix 5 together with a discussion highlighting experimental difficulties of the technique and possible future avenues to explore.

CHAPTER 6: ZINC CONDENSER COMPUTER PROGRAM FOG PREDICTIONS AND DISCUSSION

6.1 INTRODUCTION

The vapour/gas condensable mixtures considered for fog formation analysis were chosen with the Warner smelter in mind. As such, high zinc vapour concentrations in the feed were of prime importance as well as considering both liquid and solid condensates. A wide range of inlet vapour concentrations were examined to see how concentration influences fog formation. Not only zinc vapour was considered: the inescapable presence of lead in a condensable zinc/nitrogen mixture was examined in terms of lead vapour nucleation and fog formation prior to zinc condensation. The effect of superheat on the inlet vapour/gas mixture in terms of differing quantities of fog formation to be expected was also examined during the series of runs. A wide range of total pressures were considered ranging up to 60 mmHg. The comparative amounts of fog formation to be expected using the three operating lines given by Gardner (eq. 2.2.23), Bras (eq. 2.2.17) and Cairns and Roper (eq. 2.2.18) and their individual merits are assessed. As well as looking at the "worse case" of heterogeneous fog formation, the other extreme of homogeneous fog formation is both delineated and studied in detail. A Gardner type analysis is also used to analyse the fogging potential of two condensation problems: the ISF zinc condenser and the Port Pirie VDZ unit.

6.2 CONSIDERATION OF ZINC VAPOUR HETEROGENEOUS FOG FORMATION IN ZINC/NITROGEN MIXTURES

This main fog analysis is concerned with zinc/nitrogen mixtures. The presence of lead or other possible RH vessel products like zinc oxide and zinc sulphides would manifest itself in terms of nuclei for fog formation in this case. As these computer runs merely require supersaturation to be the criterion for fog formation then a zinc/nitrogen simplification is reasonable. The method of presentation of results adopted here consists of choosing one of the inlet vapour/gas conditions as a variable to be adjusted sequentially whilst the other variables are kept constant. For each computer prediction, the amount of predicted vapour loss as fog loss and as outlet equilibrium loss was determined by the method outlined in Section 5.2. Both the vapour loss as fog and the total vapour loss including fog were then plotted against operating pressure and curves through the predictions drawn. The derived computer run data for each prediction are found in Appendix 4 of this work.

6.2.1 The Effect of Inlet Vapour Concentration on Fog Formation

Figures 6.2.1 to 6.2.4 depict a series of computer predictions using the Gardner equation for zinc/nitrogen mixtures entering a condenser at 1100, 1200 and 1300^{o}C and condensing at 420^{o}C (the melting point of zinc). Five computer printouts go to make up one curve. The data for these diagrams comes from computer runs G Zn.1 to 60 in Appendix 4. The major variable in the figures is zinc vapour concentration. It is varied from 97% to 75% to 50% and to 25%. The first point to make is that the total vapour loss (the dashed line) for all conditions will approach 100% as the operating

FIGURE 6.2.1 PREDICTED ZINC VAPOUR LOSS, 97%Zn/3%N2 MIXTURES; VARYING tvi, GARDNER EQUATION

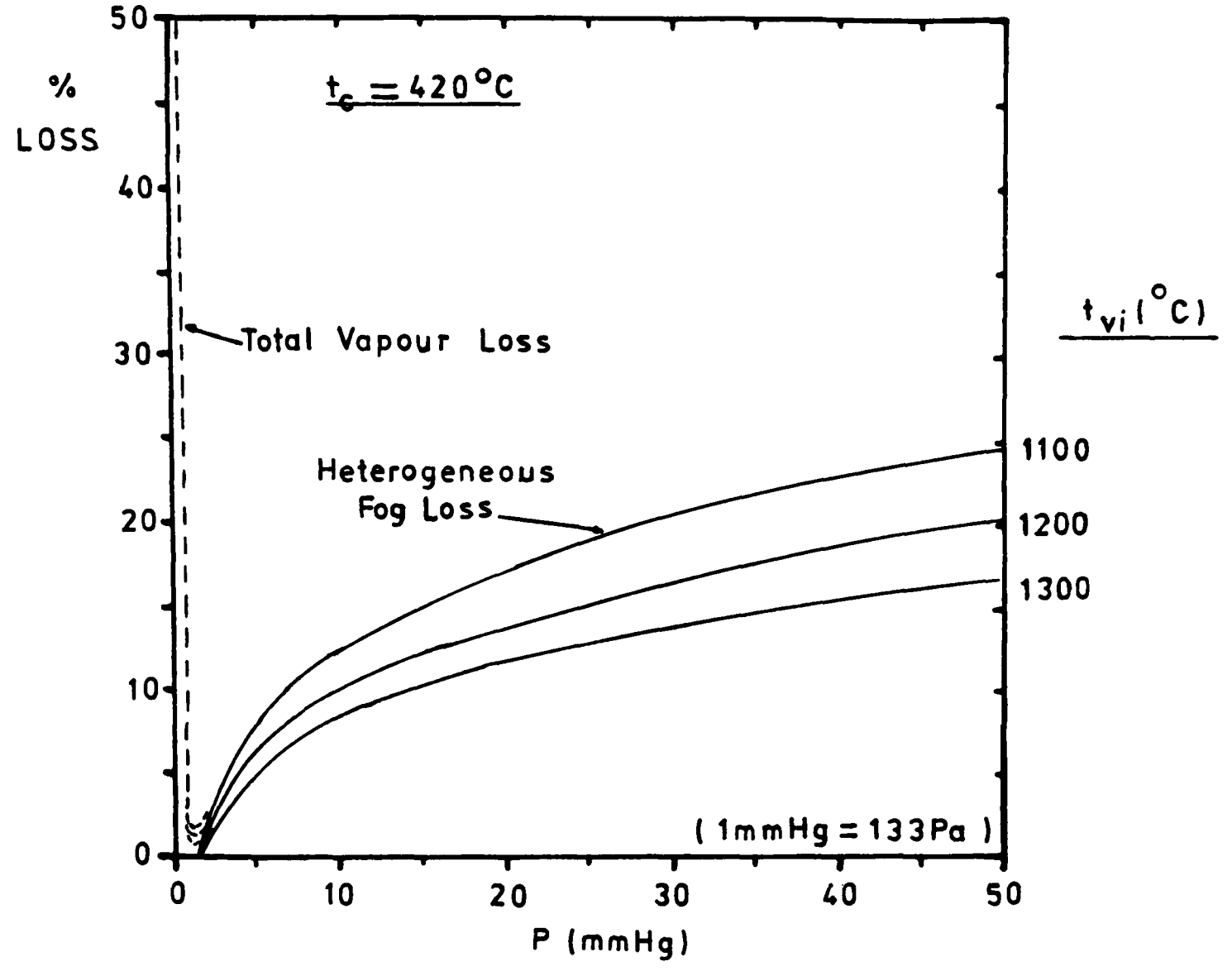

FIGURE 6.2.2 PREDICTED ZINC VAPOUR LOSS, 75%Zn/25%N2 MIXTURES; VARYING tvi, GARDNER EQUATION

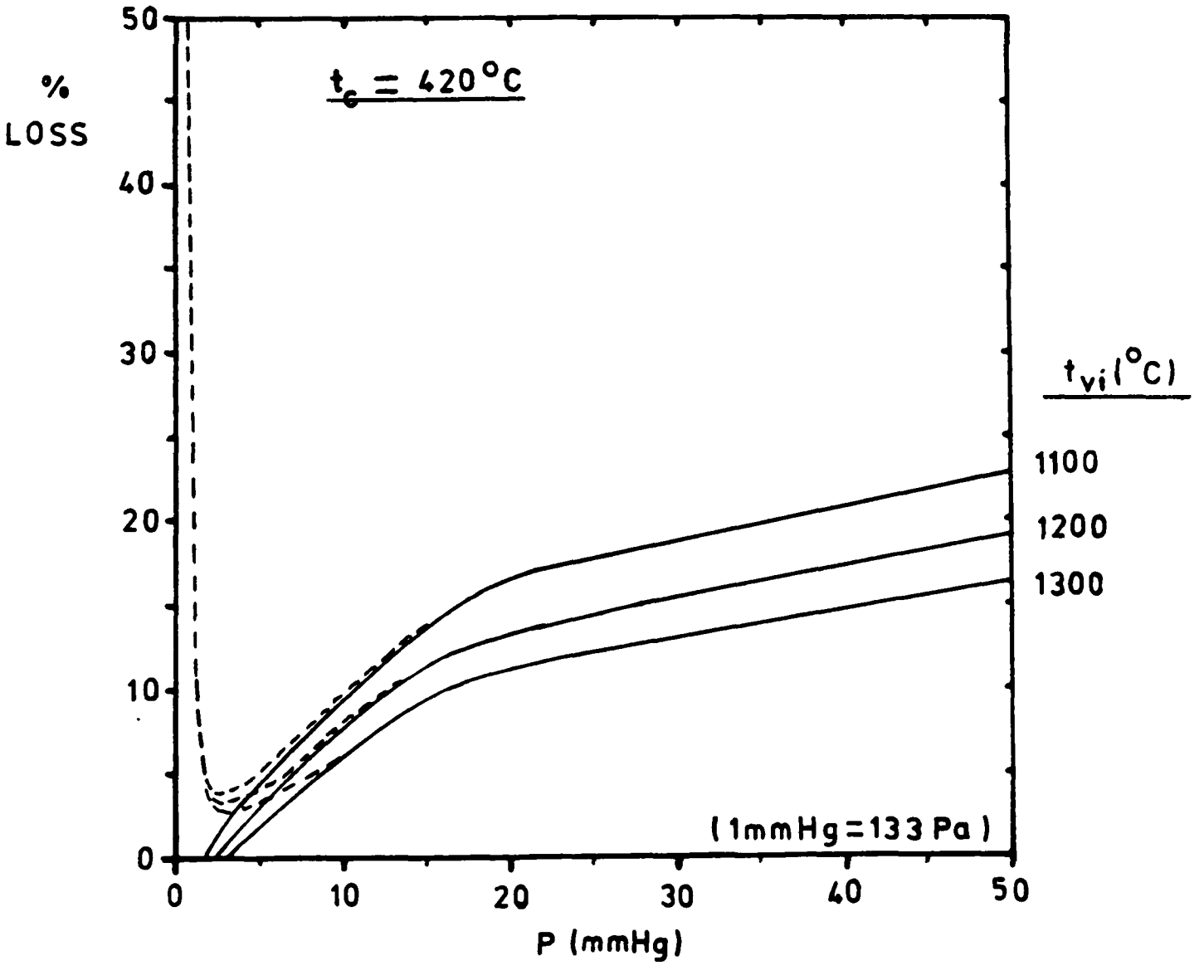

FIGURE 6.2.3 PREDICTED ZINC VAPOUR LOSS, 50%Zn/50%N2 MIXTURES; VARYING tvi, GARDNER EQUATION

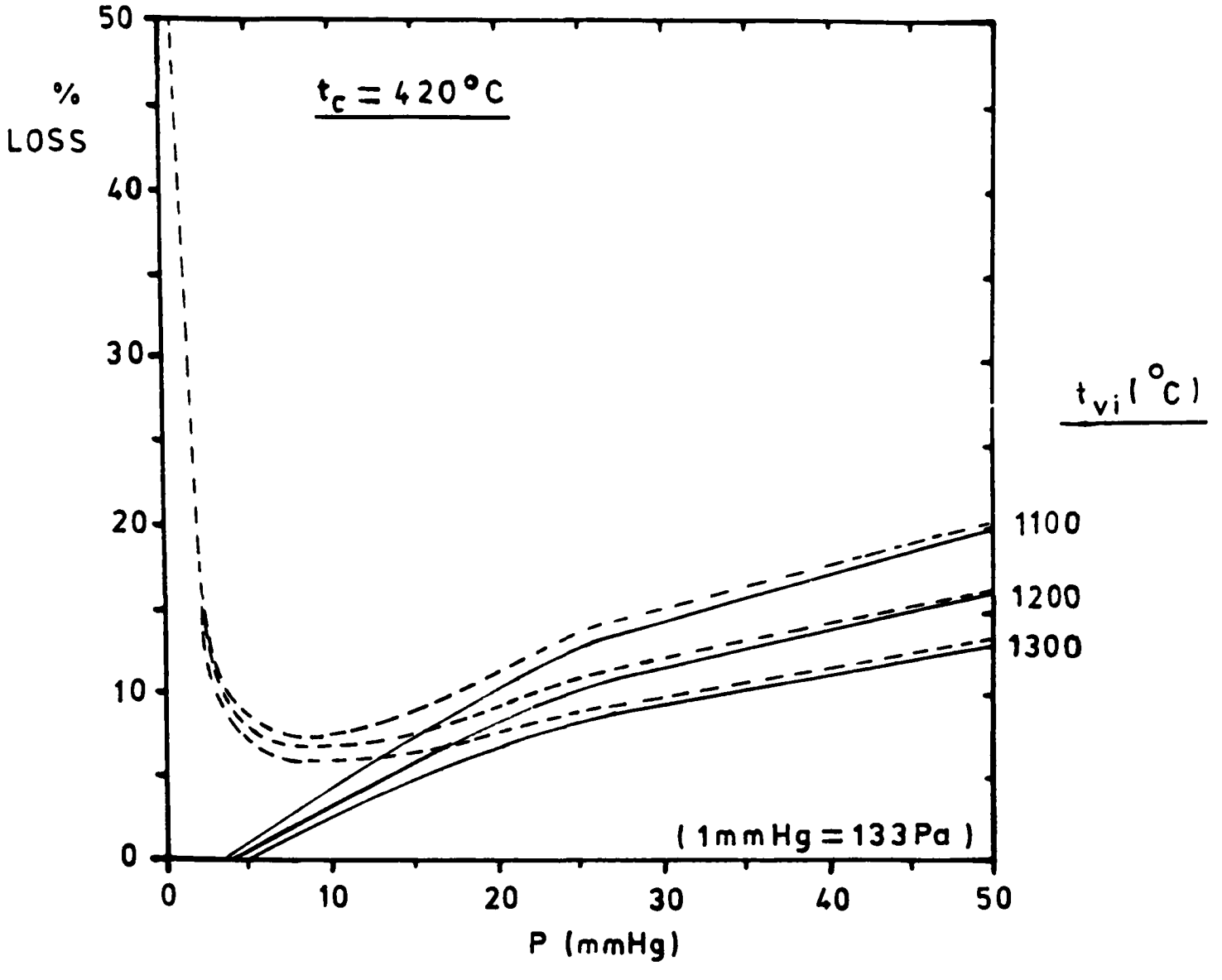

FIGURE 6.2.4 PREDICTED ZINC VAPOUR LOSS, 25%Zn/75%N2 MIXTURES; VARYING tvi, GARDNER EQUATION

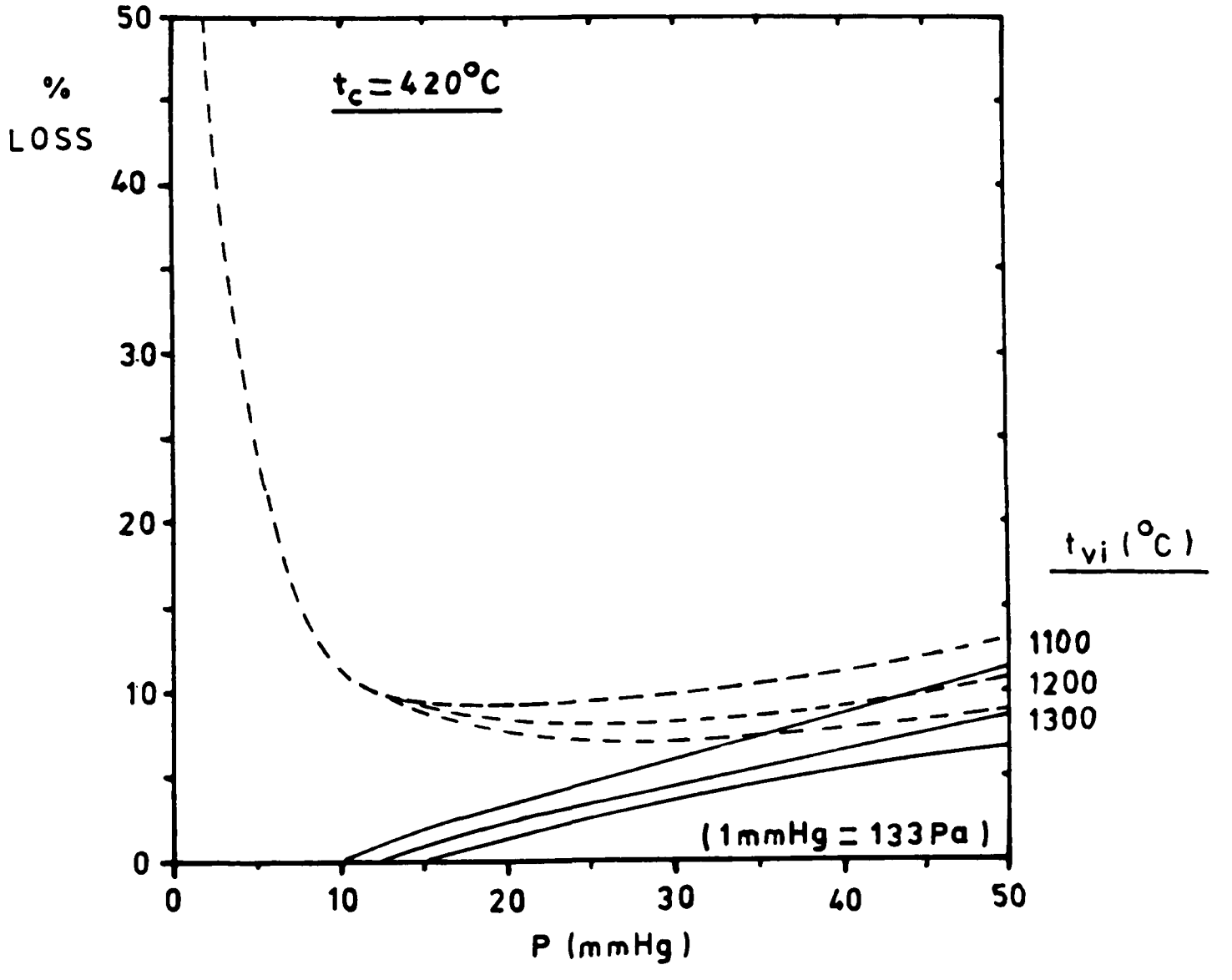

pressure of the system, P, approaches p_c, the condensate partial pressure. The other evident feature of the curves is that fog losses approach zero as P is reduced. There is, however, a penalty to be paid at these low vacuum pressures in terms of equilibrium vapour losses being high and vapour/gas velocity through the RH vessel and condenser being excessive. Equilibrium vapour losses are highest at low vapour concentrations in the feed mixture as indicated by Figures 6.2.3 and 6.2.4. All the curves indicate that the more superheat the vapour/gas mixture fed to the condenser has the less the fog problem will be. This amounts to a 40% lowering in the quantities of fog formed at Zn = 97% for a 200^{o}C increase in superheat from 1100 to 1300^{o}C.

Figures 6.2.5, 6.2.6 and 6.2.7 are computer predictions using the Bras equation for three inlet zinc concentrations; 97%, 86% and 75% (Runs B Zn.1 to 45). Figures 6.2.8 to 6.2.10 are plots of computer predictions for the same zinc concentrations but this time using the Cairns and Roper equation (Runs CR Zn.1-45). For these runs t_c was also 420^{o}C and t_{vi} ranged from 1100 to 1300^{o}C. Only high vapour concentrations were considered for the Bras and Cairns and Roper equations due to their specific applicability range. Figures 6.2.1, 6.2.5 and 6.2.8 are directly comparable as indeed are Figures 6.2.2, 6.2.7 and 6.2.10. The immediate deduction from these figures is the much higher quantities of fog predicted for both the Bras and Cairns and Roper equations compared to that suggested by the Gardner equation. This is highlighted by Figure 6.2.11 that plots predictions for a typical vapour/gas inlet condition of Zn = 97%, t_{vi} = 1200^{o}C, P = 30 mm Hg and t_c = 420^{o}C using all three equations (Runs GZn.9, BZn.9 and CRZn.9). The Cairns and Roper equation predicts twice the amount of fog that the Gardner equation gives. The Bras equation too,

FIGURE 6.2.5 PREDICTED ZINC VAPOUR LOSS, 97%Zn/3%N2 MIXTURES; VARYING tvi, BRAS EQUATION

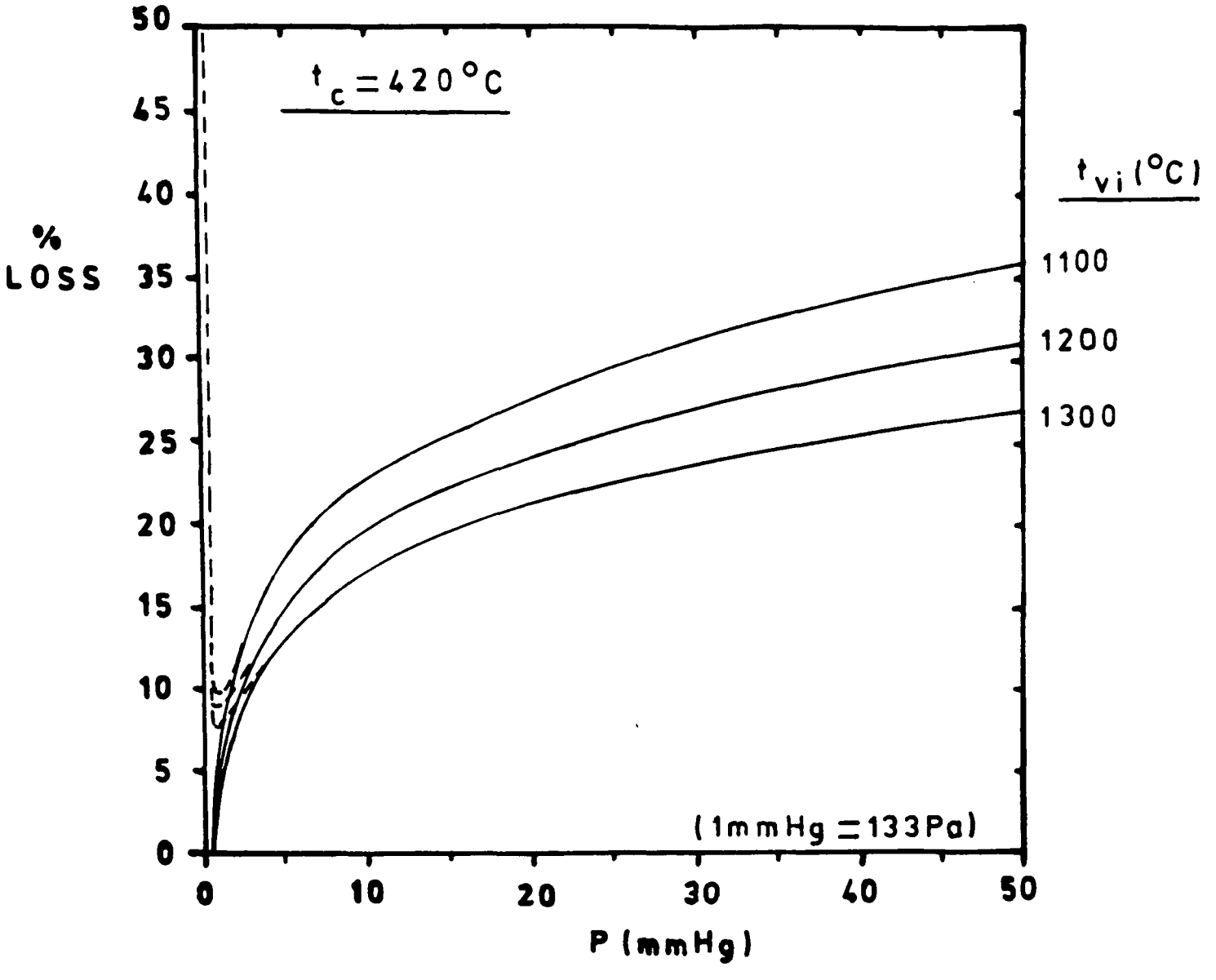

FIGURE 6.2.6 PREDICTED ZINC VAPOUR LOSS, 86%Zn/14%N2 MIXTURES; VARYING tvi, BRAS EQUATION

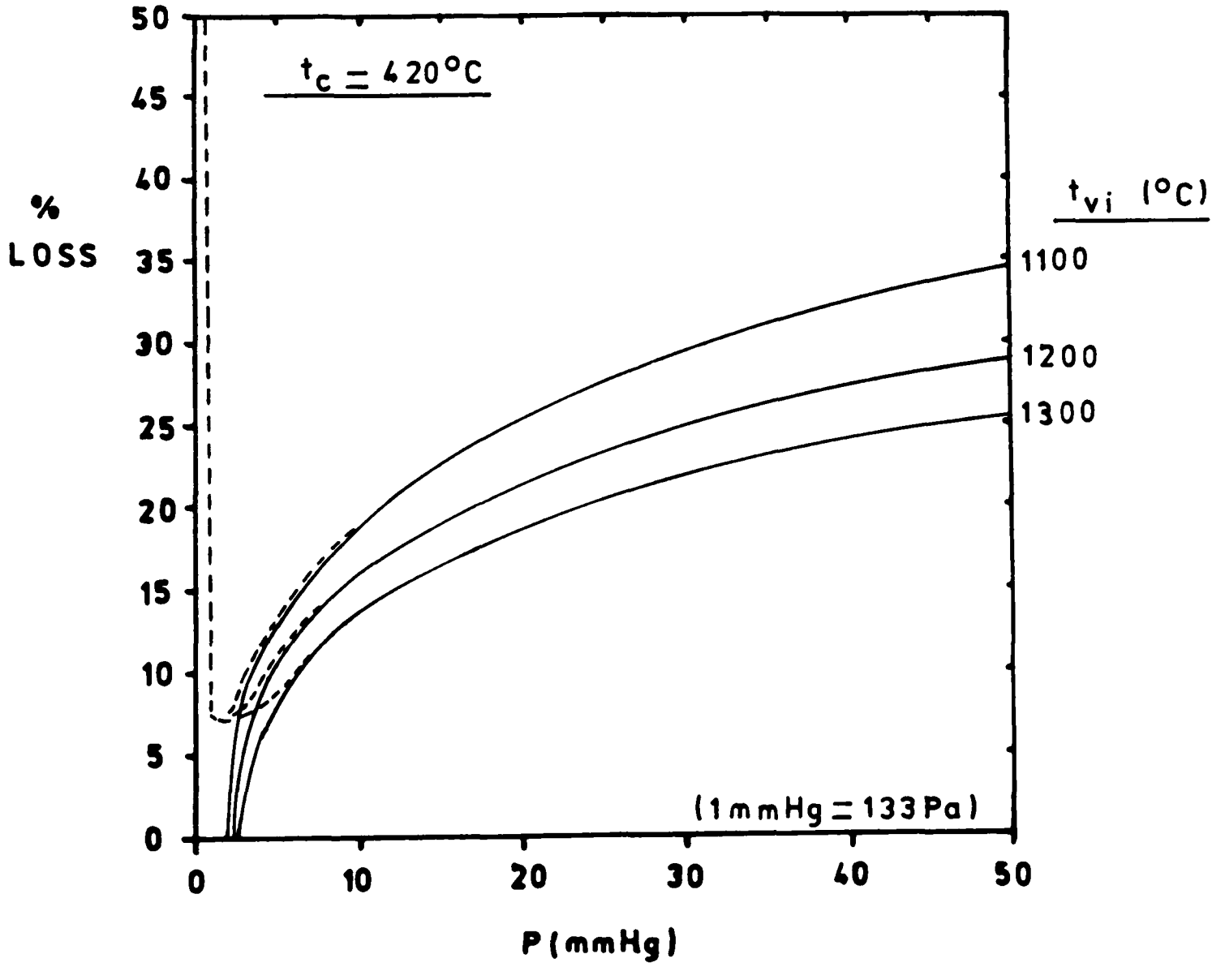

FIGURE 6.2.7 PREDICTED ZINC VAPOUR LOSS, 75%Zn/25%N2 MIXTURES; VARYING tvi, BRAS EQUATION

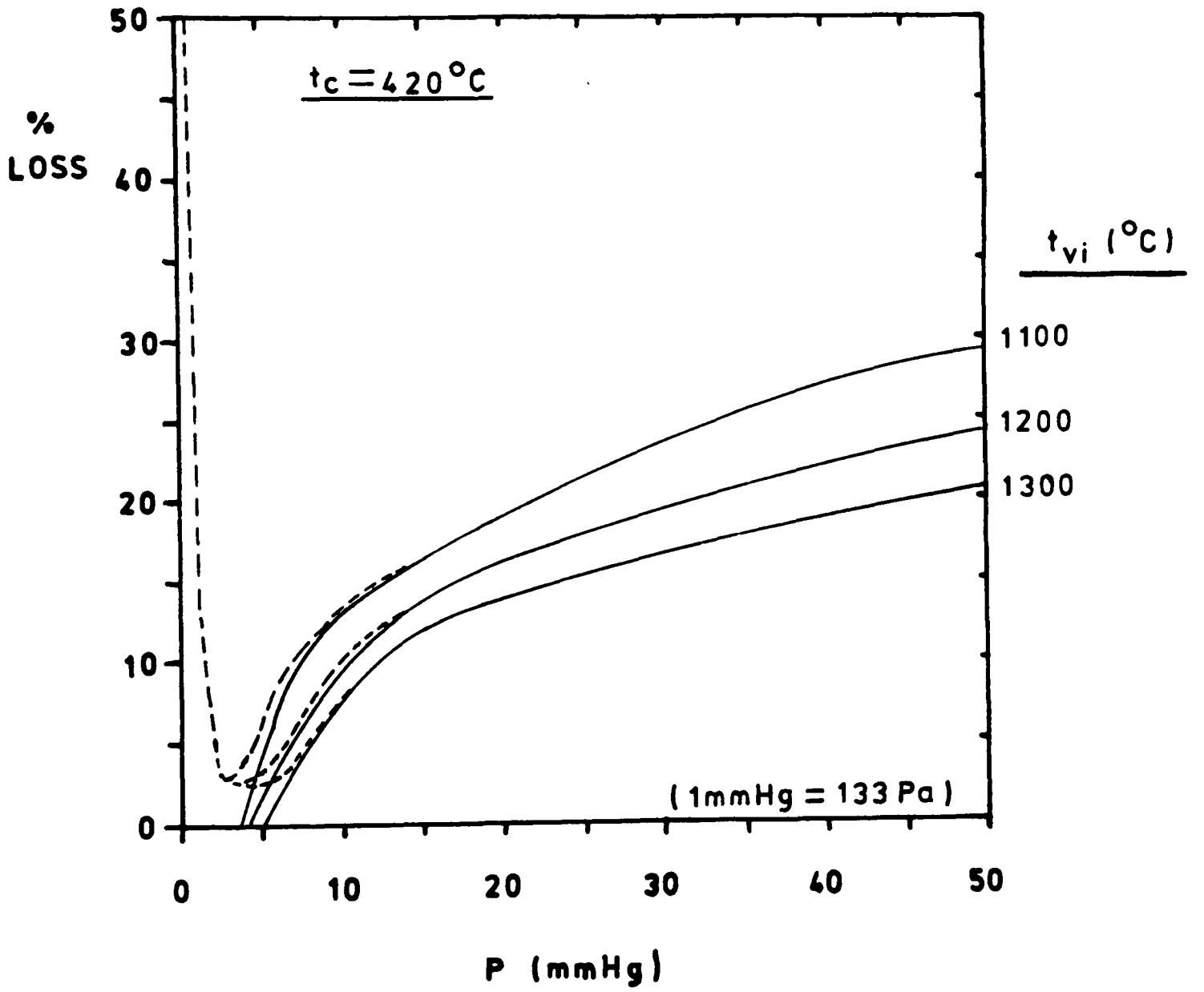

FIGURE 6.2.8 PREDICTED ZINC VAPOUR LOSS, 97%Zn/3%N2 MIXTURES; VARYING tvi, CAIRNS & ROPER EQUATION

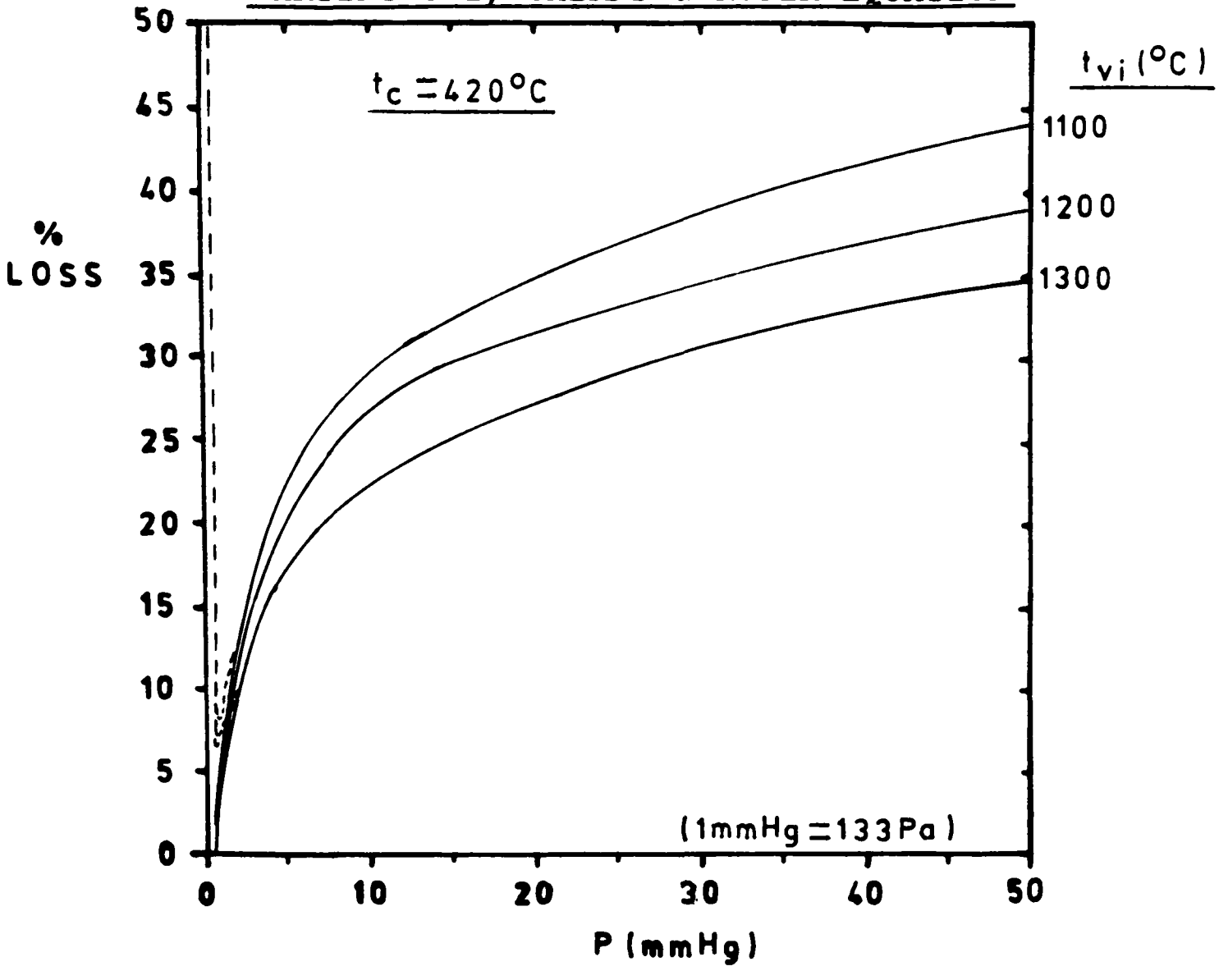

FIGURE 6.2.9 PREDICTED ZINC VAPOUR LOSS, 86%Zn/14%N2 MIXTURES; VARYING tvi, CAIRNS & ROPER EQUATION

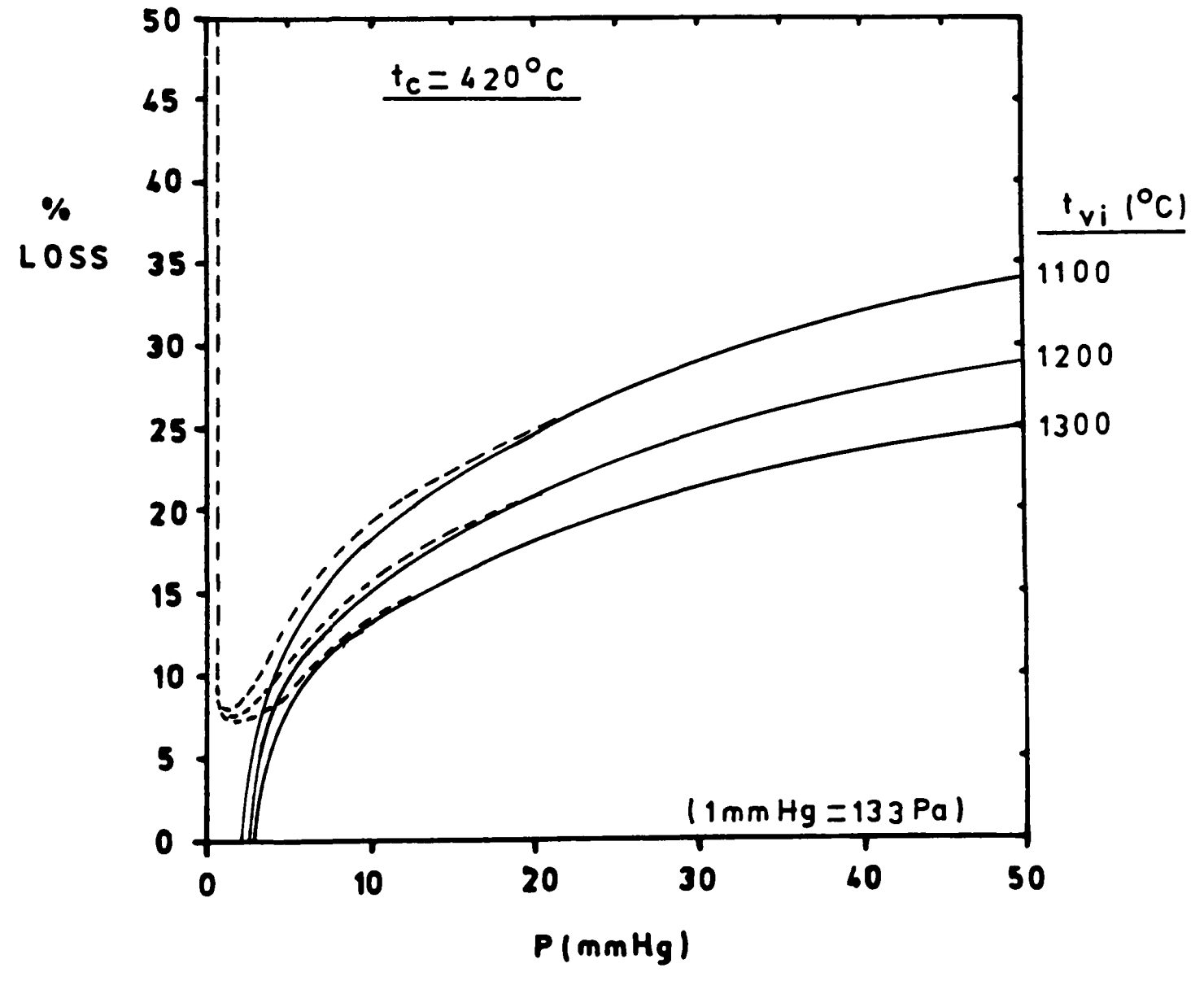

FIGURE 6.2.10 PREDICTED ZINC VAPOUR LOSS, 75%Zn/25%N2 MIXTURES; VARYING tvi, CAIRNS & ROPER EQUATION

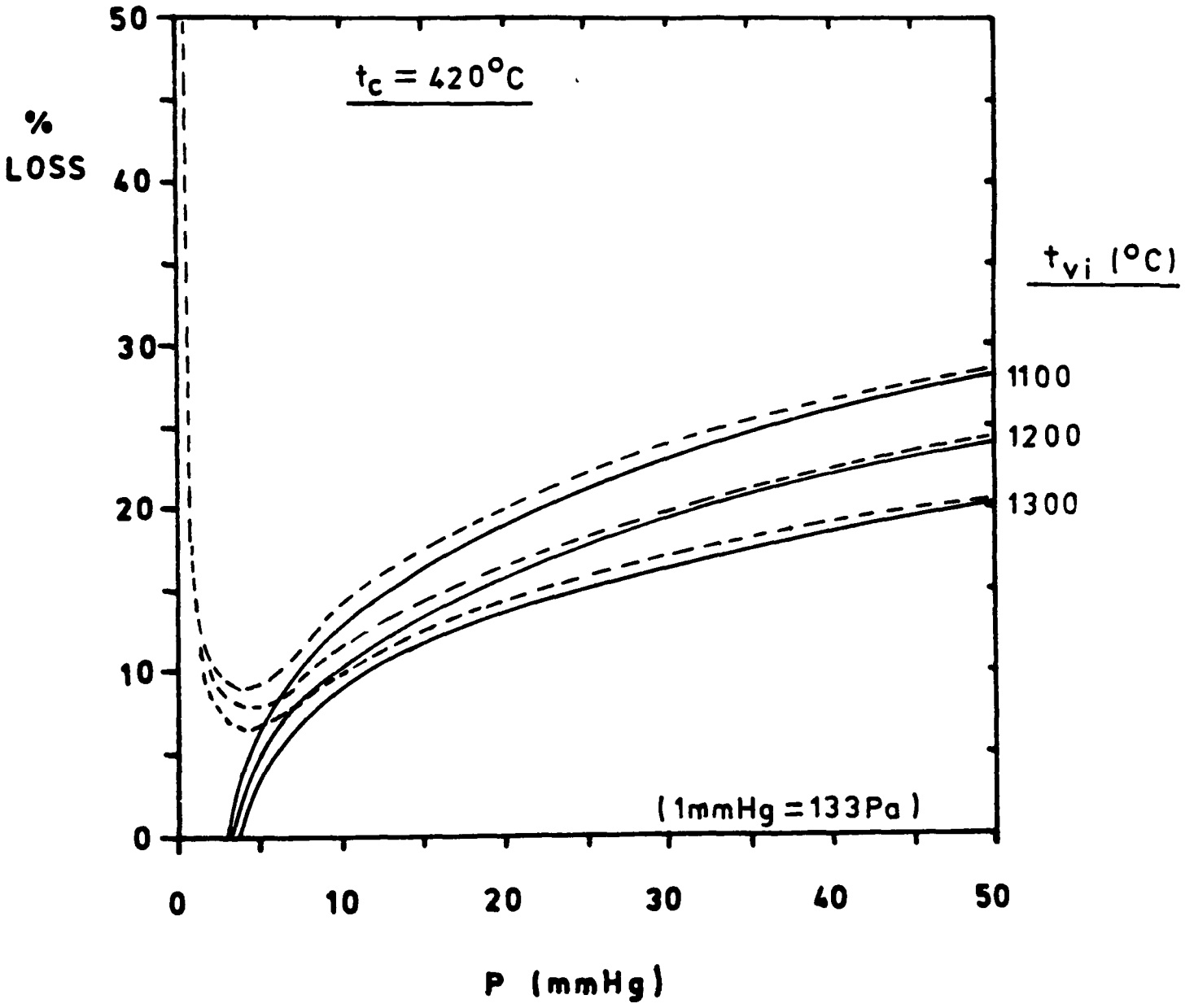

FIGURE 6.2.11: COMPARATIVE PLOT OF THE FOG FORMATION EQUATIONS

(P=30mmHg , t_c= 420°C , t_{vi}= 1200°C , 97%Zn / 3%N_2)

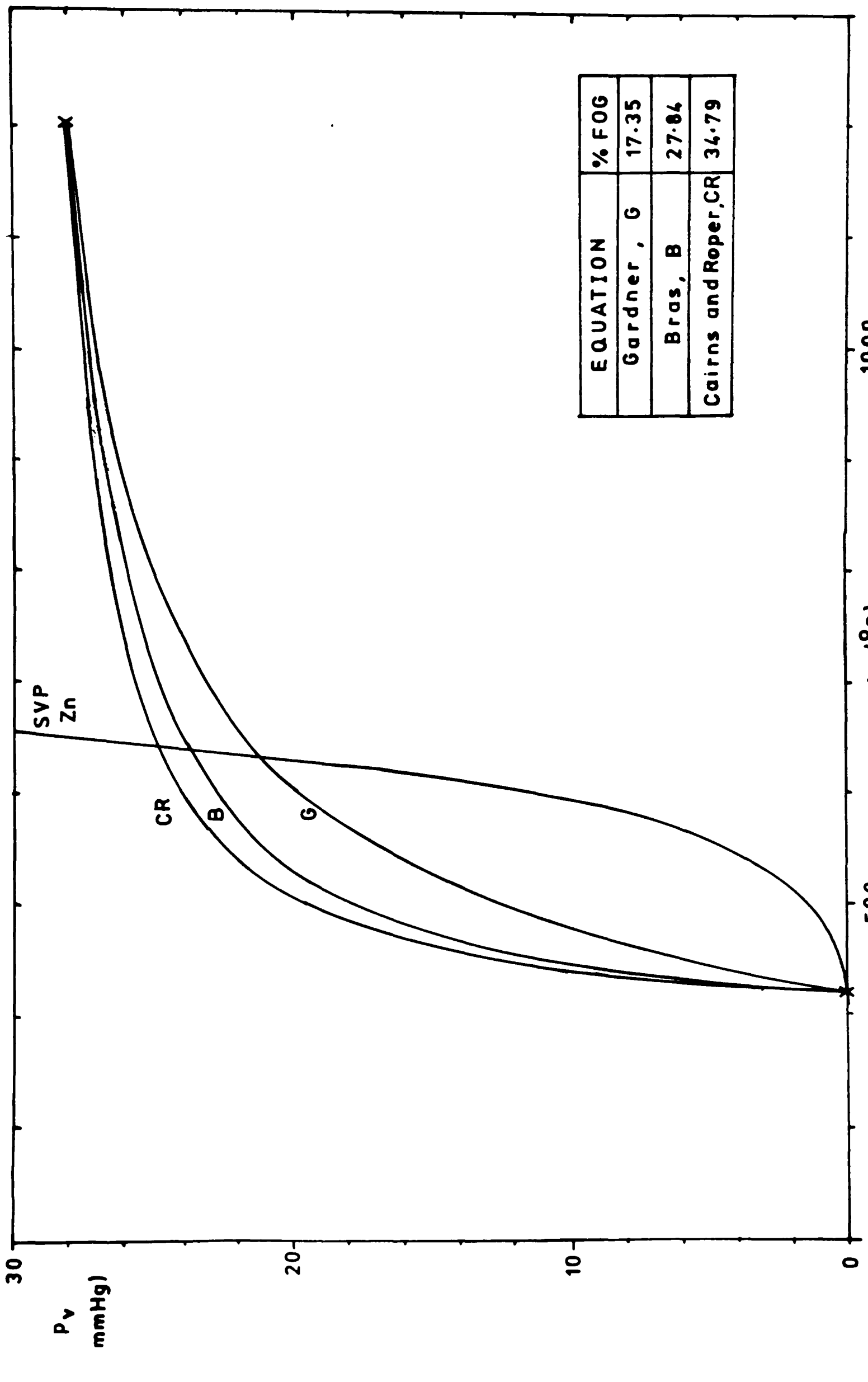

EQUATION	% FOG
Gardner , G	17.35
Bras, B	27.84
Cairns and Roper, CR	34.79

yields large amounts of fog formation. Both the Bras and the Cairns and Roper equations do provide the same general fog formation curves albeit far more pronounced than that produced by the Gardner equation.

All of the equations for all the conditions studied do predict bulk vapour fog formation to occur at temperatures less than 700^{o}C for all inlet conditions. The point of incipient heterogeneous fog formation, t_{vf}, does not vary much with increased superheating of the inlet mixture to the condenser, other parameters being constant.

6.2.2 The Effect of Condensate Interfacial Temperature on Vapour Fog Formation

To study the effect of varying t_c four temperatures were chosen for a constant t_{vi} of 1200^{o}C. Computer runs with t_c = 350, 440 and 460^{o}C, representing a solid zinc condenser for t_c = 350^{o}C and liquid zinc condensers for t_c = 440 and 460^{o}C, were carried out (serial nos. GZn.61-100). These were compared to the t_c = 420^{o}C results discussed earlier for four inlet vapour concentrations of 97%, 75%, 50% and 25%. Only the Gardner equation was used as its fundamental derivation makes it the most appropriate equation for these reduced pressure conditions compared to the more empirical Cairns and Roper and Bras equations. In reality, a condenser operating at t_c = 350^{o}C would not exist for any prolonged time period as it represents an unsteady state, transient solid zinc condenser surface. It has been included in this analysis merely to give an insight into the trends that will occur in heterogeneous zinc fog formation under these so-called 'cold' zinc condensation conditions.

The results are plotted in Figures 6.2.12 to 6.2.15. It can be seen that

FIGURE 6.2.12 PREDICTED ZINC VAPOUR LOSS, 97%Zn/3%N2 MIXTURES; VARYING tc, GARDNER EQUATION

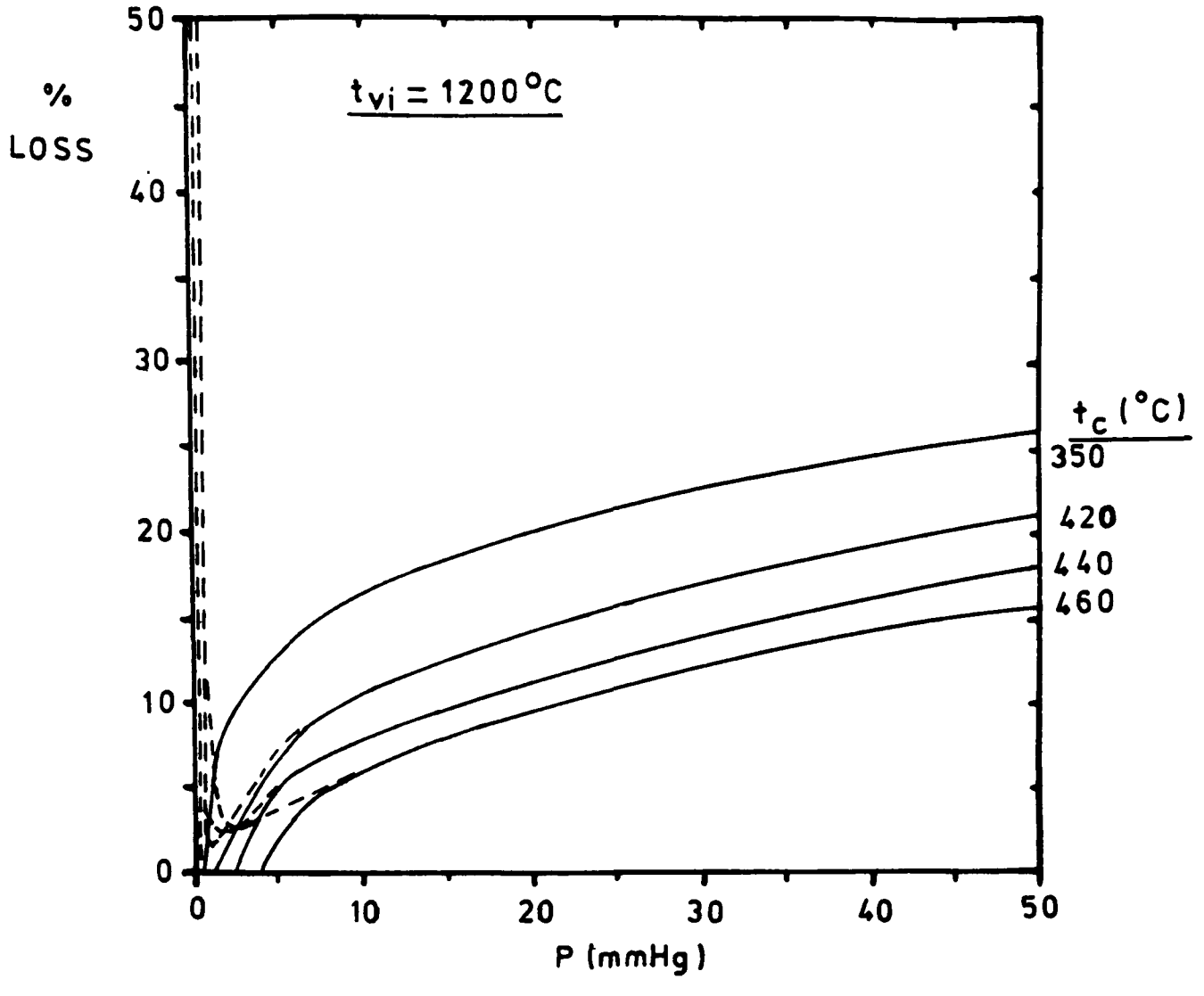

FIGURE 6.2.13 PREDICTED ZINC VAPOUR LOSS, 75%Zn/25%N2 MIXTURES; VARYING tc, GARDNER EQUATION

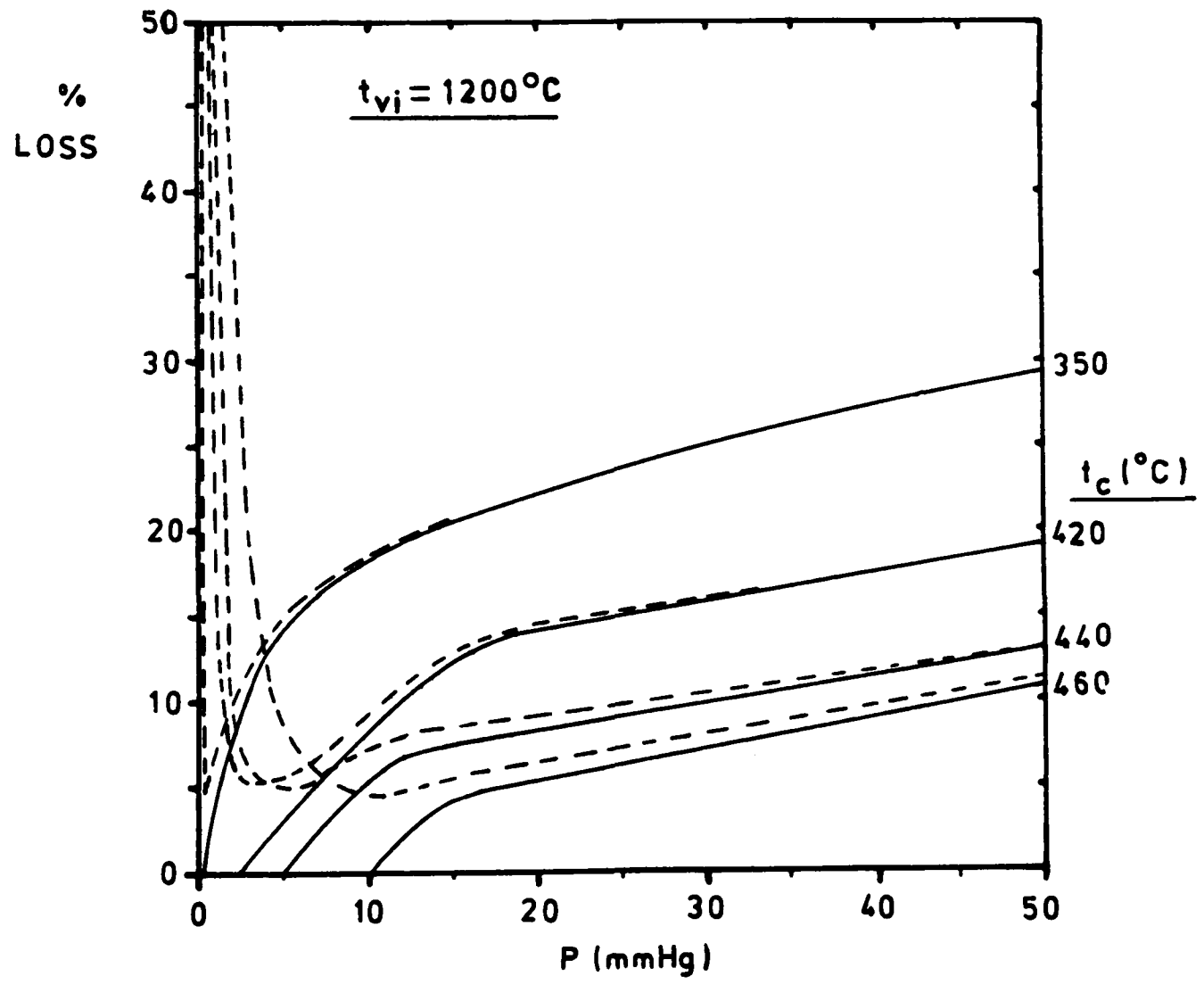

FIGURE 6.2.14 PREDICTED ZINC VAPOUR LOSS, 50%Zn/50%N2 MIXTURES; VARYING tc, GARDNER EQUATION

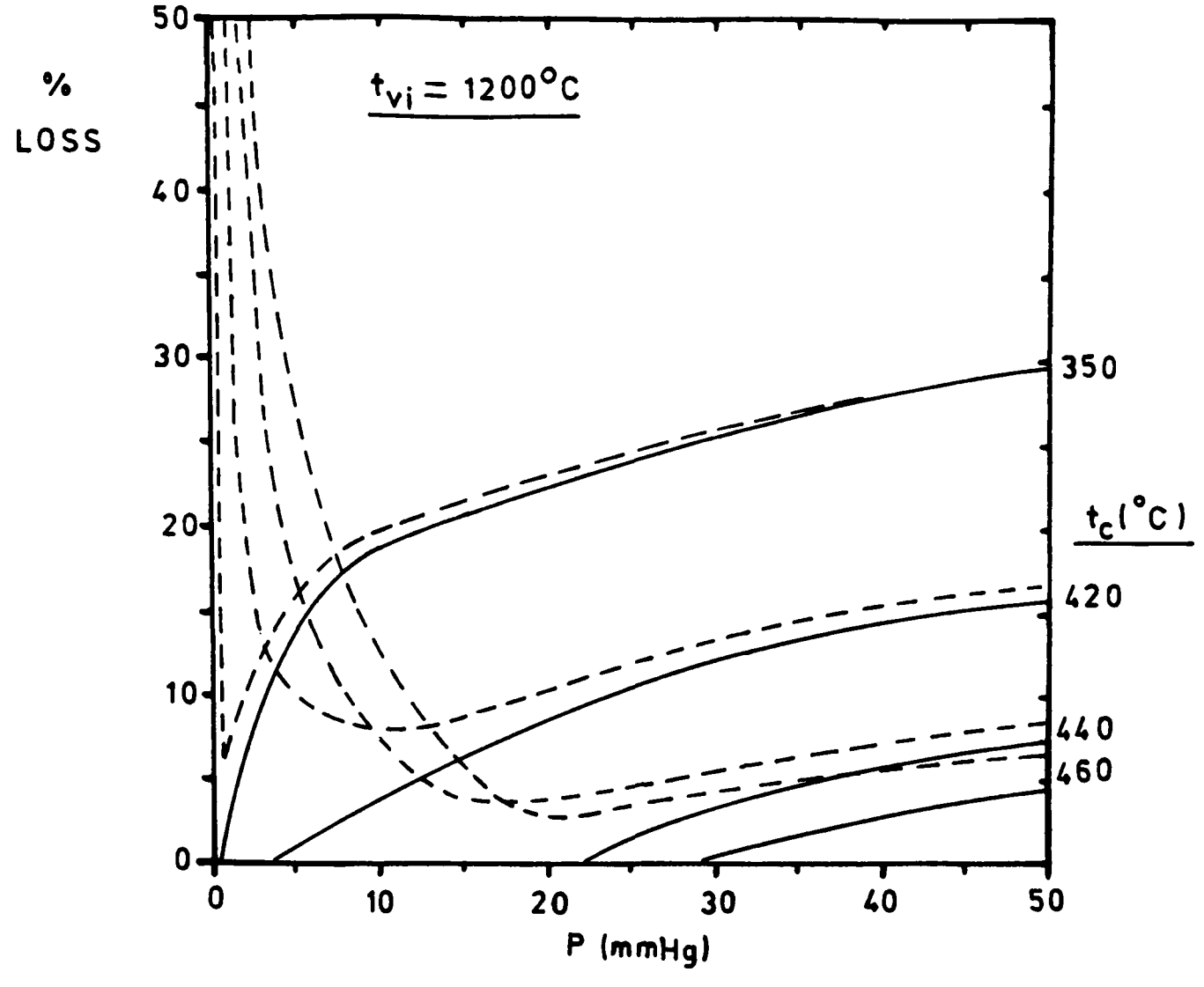

FIGURE 6.2.15 PREDICTED ZINC VAPOUR LOSS, 25%Zn/75%N2 MIXTURES; VARYING tc, GARDNER EQUATION

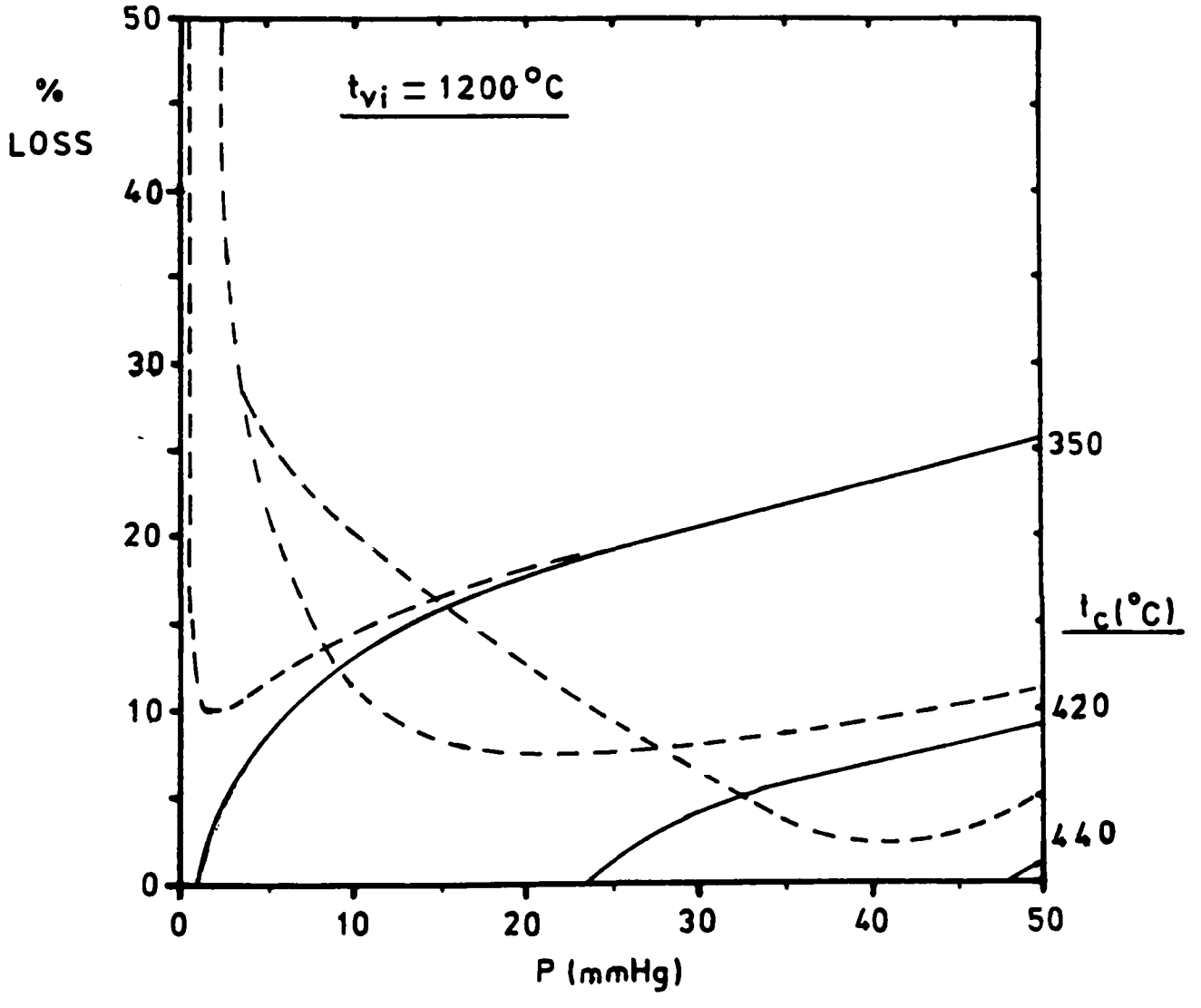

the higher the condensate temperature the less the fog problem will be though equilibrium losses will become more significant. This effect is most pronounced at low total pressures and low vapour concentrations in the mixture. It must be pointed out that higher values of t_c will also result in an undesirable reduction in the quantity of zinc collected in the condenser so a balance between these two conflicting demands must be struck. In the case of the 'cold' condenser with $t_c = 350^oC$, predicted quantities of zinc fog are as much as two-and-a-half times that expected for a liquid zinc condenser at 420^oC.

6.3 CONSIDERATION OF LEAD VAPOUR HETEROGENEOUS FOG FORMATION IN ZINC/LEAD/NITROGEN MIXTURES

A variant of the Gardner computer program for zinc/nitrogen mixtures was developed for the case where lead vapour condensation was present in the mixture. This more realistic multivapour Zn/Pb/N_2 condensation scenario required the modification of input data to include lead in the mixture. As far as this analysis is concerned, zinc vapour acts as a non-condensable carrier gas for the lead together with the inert nitrogen gas. Several runs were carried out (G Pb.1-40, Appendix 4) for a wide range of inlet conditions to elucidate the general fog forming characteristics of lead vapour.

Two possible feed mixtures that could be produced in the Warner smelter and then subsequently condensed are:

i) An Imperial Smelting Furnace (ISF) Zinc/Lead Concentrate Feed

A typical ISF feed consists of 0.4 tonnes of lead per tonne of zinc. A condensable mixture in these proportions plus 3% nitrogen as non-condensable was postulated as a hypothetical feed to be treated in the condenser. Hence, by mass, the condenser feed is composed of:

Zinc; 69.3% Lead; 27.7% Nitrogen; 3.0%

ii) A Zinc Concentrate Feed

Evans and Gray (1971) have reported twenty-six analyses of typical zinc concentrates from ore bodies around the world. If an average feed composition derived from this data is taken then a typical zinc concentrate will contain 49.27% zinc and 1.67% lead. If a condensable mixture is postulated to have these same proportions and if 3% N_2 is again present in

the mixture then the following condenser feed will result:

Zinc; 93.8% Lead; 3.2% Nitrogen; 3.0%

Both these mixtures were fed into the Gardner cooling curve program for lead. An inlet temperature, t_{vi} = 1200°C and a range of four total pressures were considered: P = 1 mm Hg, 5 mm Hg, 15 mm Hg and 30 mm Hg. Several condensate temperatures were considered ranging from 420°C to 800°C. The t_c = 420°C run reflects a condenser operating to collect a liquid zinc condensate such that any lead condensation as either condensate or fog is incidental to its operation. The lead saturation vapour pressure data comes from Kubaschewski and Alcock (1979).

Figure 6.3.1 shows a comparative plot of the p_v, t_v data for both feeds at a total vacuum pressure, P, of 30 mm Hg. Both feeds will produce heterogeneous lead fog in the 80 to 90% range for this inlet condition. The typical ISF feed will produce more fog than the typical zinc concentrate feed at all total pressures and condensing temperatures as illustrated by Figures 6.3.2 and 6.3.3 (data in Appendix 4). For the lowest condensation temperature of 420°C nearly all the lead in the condensable mixture fed to the condenser will form as fog and quite early on in the condensation process. As with the zinc/nitrogen mixtures the same general fog curve profile is evident with the least quantities of fog formation at the lowest total pressures.

As the condensation temperature is raised the quantities of heterogeneous fog predicted for each case fall such that at t_c = 800°C little lead fog forms. This implies that if a two stage condensation process is utilised rather than a simultaneous lead/zinc single stage condensation operation, higher lead recoveries will result. The first stage would operate at t_c = 700-800°C to remove most of the lead from the gas phase (and a little

FIGURE 6.3.1 COMPARATIVE PLOTS OF LEAD COOLING CURVES FOR HETEROGENEOUS FOG FORMATION; COMPUTER RUNS GPb.4 AND GPb.8

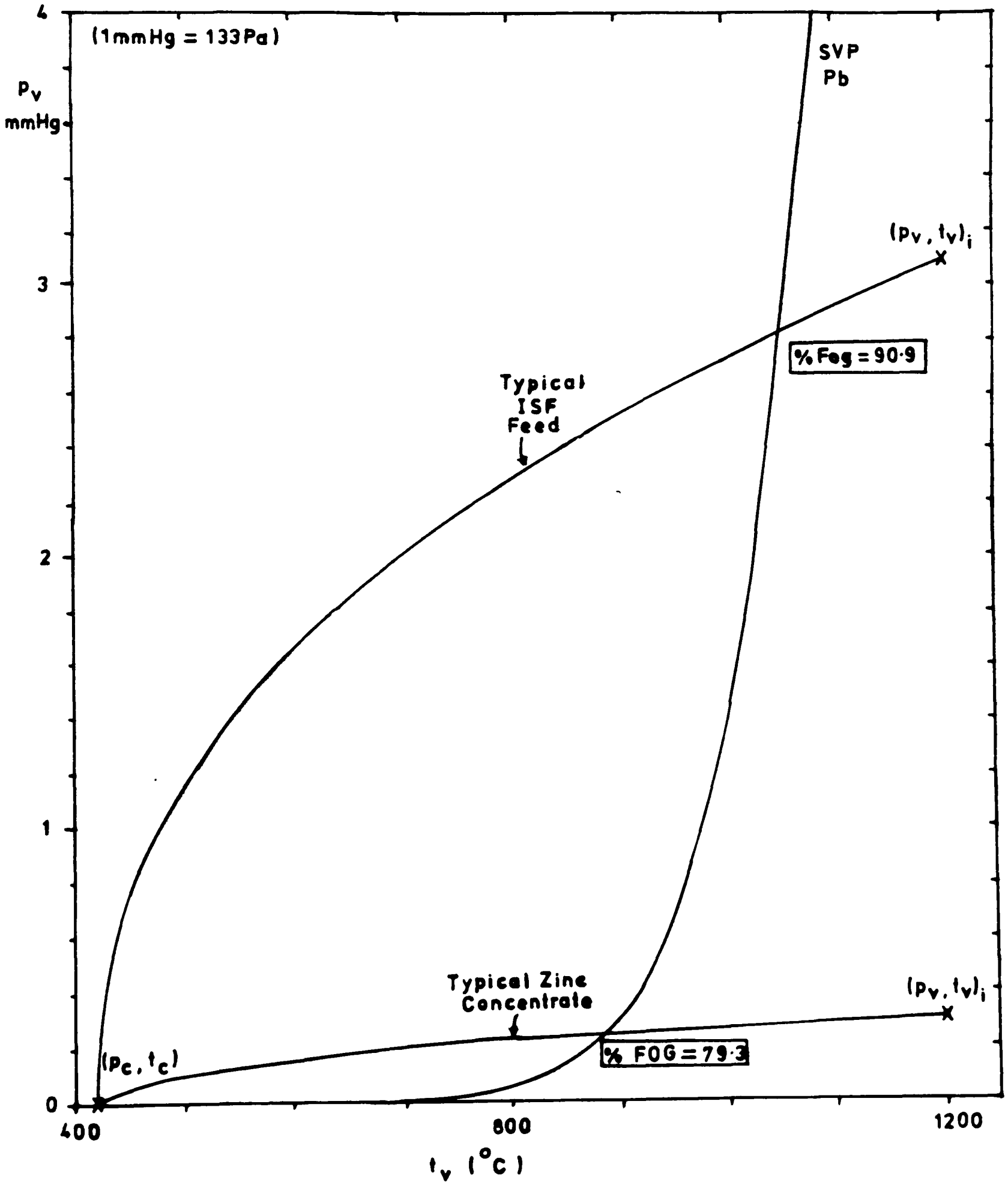

FIGURE 6.3.2 PREDICTED HETEROGENEOUS LEAD FOG LOSSES FOR Zn/Pb/N2 MIXTURES OF AN ISF ZINC/LEAD CONCENTRATE FEED : tvi=1200°C

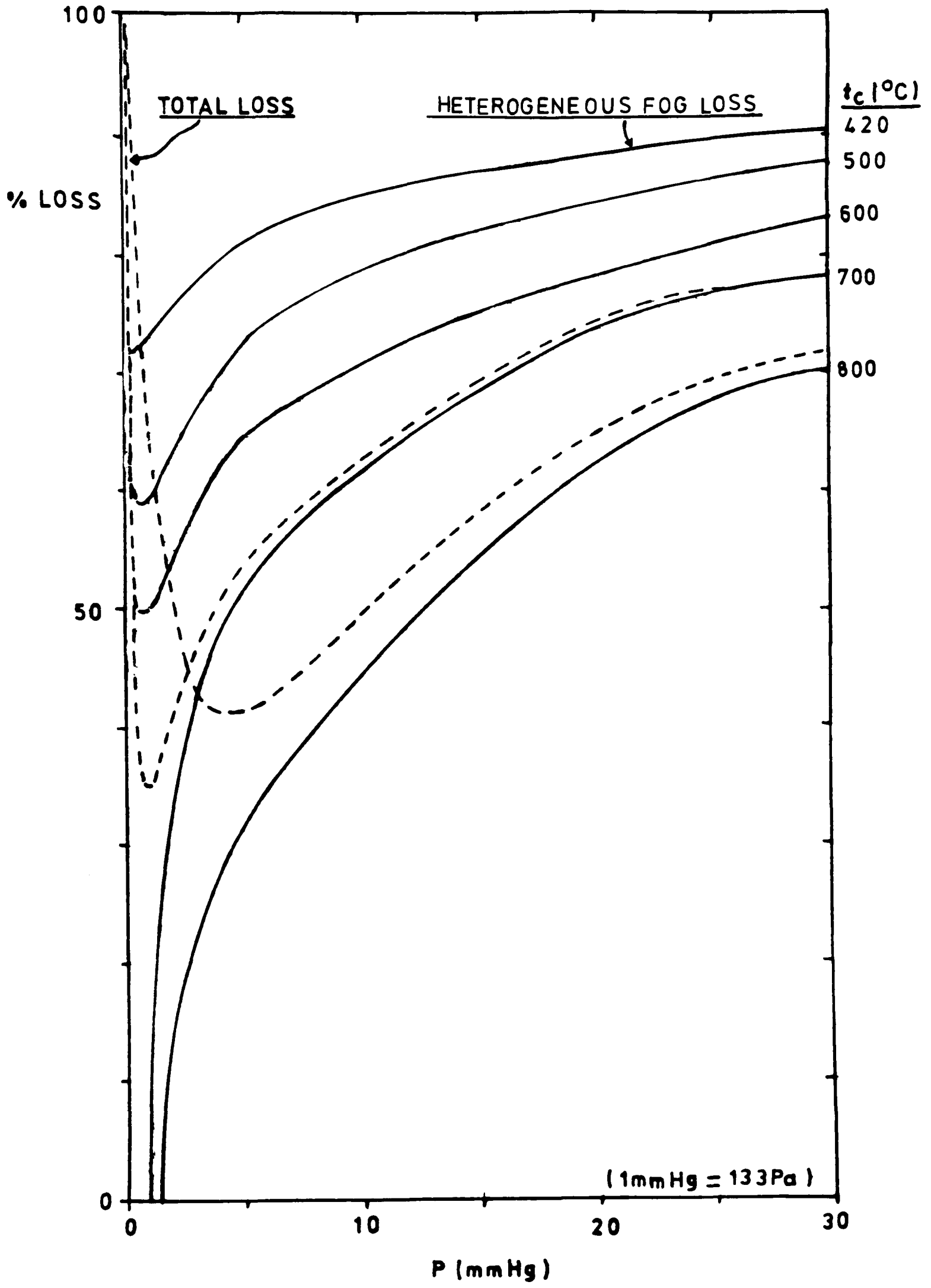

FIGURE 6.3.3 PREDICTED HETEROGENEOUS LEAD FOG LOSSES FOR Zn/Pb/N2 MIXTURES OF A TYPICAL ZINC CONCENTRATE FEED : tvi=1200°C

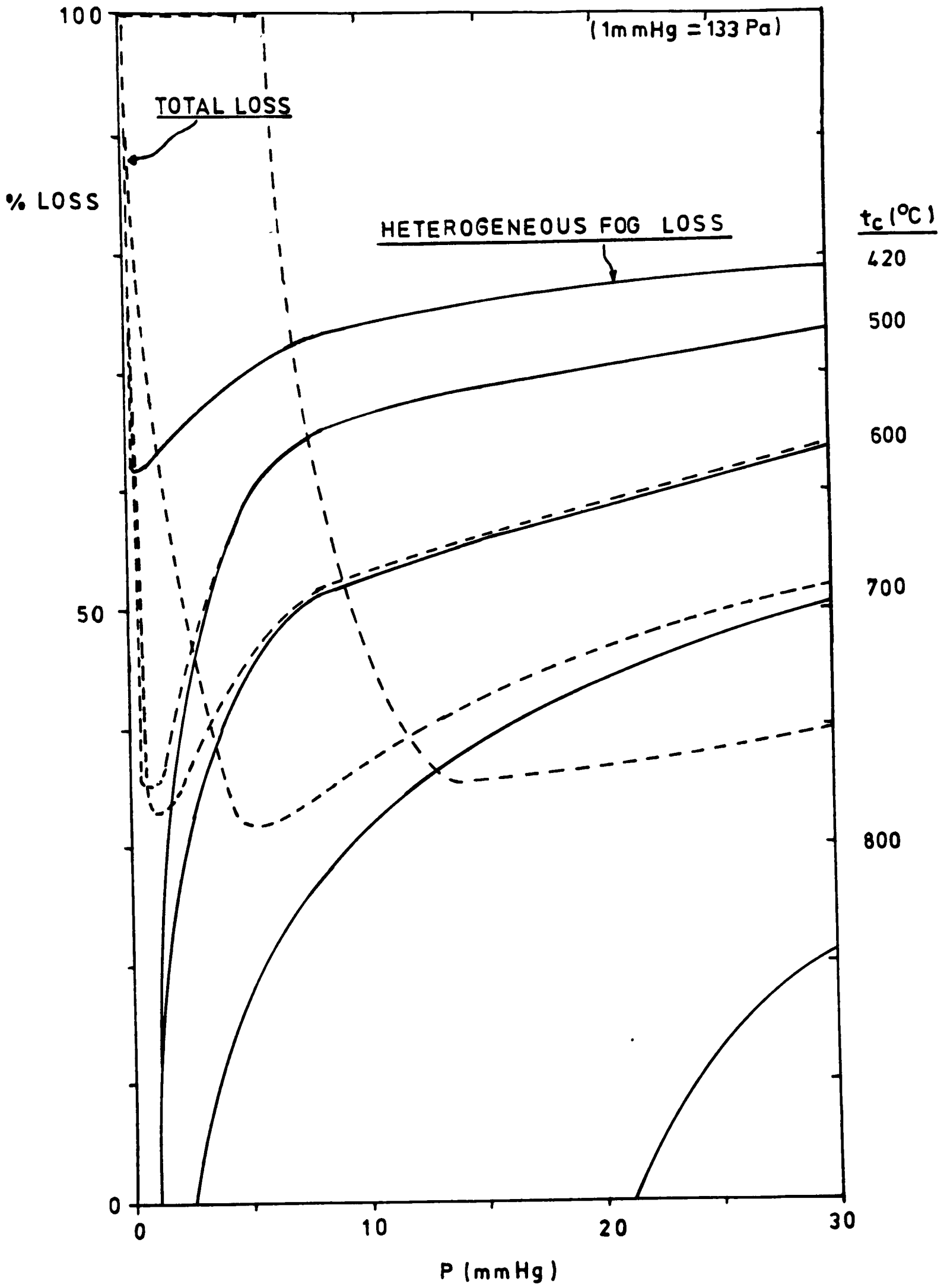

zinc) followed by a second stage operating at 420°C to collect the remaining zinc. This method should ensure lower quantities of lead vapour entering the second stage condenser so that fewer lead fog nuclei will form resulting in higher overall zinc recoveries. This conclusion has been explored in more depth and optimised by Li et al (1990). The temperature at which a lead fog will form varies, being as high as 1055°C for the t_c = 420°C, P = 30 mm Hg run which is remarkably high compared to that expected for zinc (450 to 550°C). Almost certainly, any lead fog droplets that form will, on further cooling, saturate with zinc since they are in a highly reactive state. They will also react with any oxidising species present in the gas phase forming a zinc oxide dust. Both mechanisms will contribute towards the nuclei count necessary for zinc fog particles to grow around in the lower reaches of the condenser.

6.4 ESTIMATING HOMOGENEOUS FOG FORMATION CHARACTERISTICS OF LEAD AND ZINC VAPOURS DURING CONDENSATION

It is of relevance to know the extremes of heterogeneous and homogeneous fog formation conditions for a specific vapour during condensation. The "worse case" basis for heterogeneous fog formation used in this work has been dealt with in detail and is relatively simple to use. If, however, at some stage in the future heterogeneous condensation nuclei could be minimised or eliminated from the gas phase entering a condenser then only homogeneous fog formation would occur. The theoretical Frenkel equations presented in Section 2.2.3.4 of this thesis,are now compared with experimental data and other theoretical work published in the field of lead and zinc critical supersaturation and homogeneous nucleation,to provide an engineering framework for estimating quantities of homogeneous fog formation.

As described in section 2.2.3.1 a critical supersaturation criterion exists to describe the point of homogeneous nucleation of vapours as fog droplets. This S_{crit} as defined by eq. 2.2.11 can be estimated by the equation derived by Frenkel (eq. 2.2.18). In the metallurgical field several studies and theories have been explored in relation to this homogeneous nucleation criterion. The problem of enhanced vaporisation of metals into cold surroundings (in for example BOS steel ladles) involves a fogging mechanism and has been addressed by Turkdogan (1964), Hills and Szekely (1964), and Rosner (1967). Turkdogan does offer an equation of a similar nature to the Frenkel equation. Unfortunately, the equation reproduced in the paper is incorrect though a diagram showing the S_{crit} of

iron versus temperature is accurate.

Frurip and Bauer (1978) have carried out computational and experimental work in this field. In their work they nucleated and captured fogs of iron, lead and bismuth. From their results for lead vapour they empirically produced the following equation for the critical supersaturation criterion:

$$\ln S_{crit} = 69.4 \exp . \left(- 2.79 \times 10^{-3} t_v \right) \qquad (6.4.1)$$

where t_v is in degrees Kelvin.

They do point out that the nucleation rate, I, is immeasurable in their experiments though they estimate typical values using the Becker-Doering nucleation theory.

Solution of the Frenkel Equation for Lead and Zinc

To solve the Frenkel equations for zinc and lead requires knowledge of the surface tension and liquid density of each metal over a range of condensing temperatures. Such data together with the predicted S_{crit} values are summarised in Table 6.4.1 for the temperature range 420-1200^{o}C. The density and surface tension information is taken from a combination of 'best fit' lines through data supplied by Frurip and Bauer (1978) and data from the Handbook of Chemistry and Physics (1971). Good fundamental data on the surface tension of liquid metals are rare due to small amounts of impurities adversely affecting experimentally determined values. The equations used are

TABLE 6.4.1 PREDICTING HOMOGENEOUS CRITICAL SUPERSATURATION RATIOS USING THE FRENKEL, SIMPLIFIED FRENKEL AND THE FRURIP & BAUER EQUATIONS

Gas	Zinc			Lead			
Temp. t_v (°C)	p_{sat} (mmHg)	S_{crit} Frenkel Eq 2.2.18 (α=1,I=1)	S_{crit} Simplified Frenkel Eq 2.2.19	p_{sat} (mmHg)	S_{crit} Frenkel Eq 2.2.18 (α=1,I=1)	S_{crit} Simplified Frenkel Eq 2.2.19	S_{Crit} Frurip & Bauer Eq 6.4.1
420	0.16	4500	1033	5.6e-7	-	507	-
440	0.28	2580	752	1.4e-6	-	384	-
460	0.49	-	561	3.2e-6	-	295	-
480	0.83	-	426	7.5e-6	-	230	-
500	1.36	-	329	1.6e-5	-	184	-
520	2.19	-	258	3.4e-5	3410	149	-
560	5.21	-	-	1.3e-4	991	101	-
600	11.53	-	-	4.6e-4	406	72	-
640	23.54	-	-	1.4e-3	205	53	228
680	45.27	-	-	4.0e-3	117	40	129
720	82.00	-	-	1.0e-2	74	31	77
760	141.10	-	-	2.4e-2	50	25	49
800	234.20	-	-	5.4e-2	36	21	32
840	373.40	-	-	1.1e-1	27	17	22
880	575.80	-	-	2.3e-1	21	15	16
920	-	-	-	4.4e-1	17	13	12
960	-	-	-	7.9e-1	14	11	9
1000	-	-	-	1.4e 0	12	10	7
1040	-	-	-	2.4e 0	10	9	-
1080	-	-	-	3.9e 0	9	8	-
1120	-	-	-	6.2e 0	8	7	-
1160	-	-	-	9.6e 0	7	6	-
1200	-	-	-	1.5e+1	6	6	-

$$\sigma_{Zn} = 935.3 - 0.1897\left(t_v\right) \quad \text{dyne/cm} \tag{6.4.2}$$

$$\sigma_{Pb} = 514 - 0.09\left(t_v\right) \quad \text{dyne/cm} \tag{6.4.3}$$

$$\rho_{Zn} = 6.59 - 0.00097\left(t_v - 419\right) \quad \text{g/cm}^3 \tag{6.4.4}$$

$$\rho_{Pb} = 10.7 - 0.0013\left(t_v\right) \quad \text{g/cm}^3 \tag{6.4.5}$$

where t_v is in degrees Kelvin.

The results from Table 6.4.1 can be plotted on partial pressure-temperature diagrams using eq. 2.2.11. Figure 6.4.1 shows the predicted critical supersaturation lines for zinc vapour and Figure 6.4.2 shows them for lead vapour together with Frurip and Bauer's empirical correlation line.

Some interesting points arise from these predictions. Note that only the S_{crit} values are included that produce $(p_v)_{crit}$ values less than 760 mm Hg (as anything greater than 760 mm Hg is not practicable). For zinc vapour, predicted homogeneous critical supersaturations are so high that they almost certainly would not be reached under the condensing conditions associated with the Warner smelter. This is borne out by the fact that for all the zinc condensation conditions considered in this work ($P < 50$ mm Hg) not one would have a homogeneous fog formation problem. Lead vapour, on the other hand is very susceptible to homogeneous nucleation in the gas phase as illustrated by the proximity of the critical supersaturation lines to the saturation vapour pressure line in Figure 6.4.2. The simplified Frenkel equation (2.2.19) shows a significant deviation from the S_{crit} predictions of the Frenkel equation (2.2.18) for temperatures below about 750^{o}C though

FIGURE 6.4.1 COMPARISON OF CRITICAL SUPERSATURATION EQUATIONS FOR HOMOGENEOUS NUCLEATION OF ZINC VAPOUR

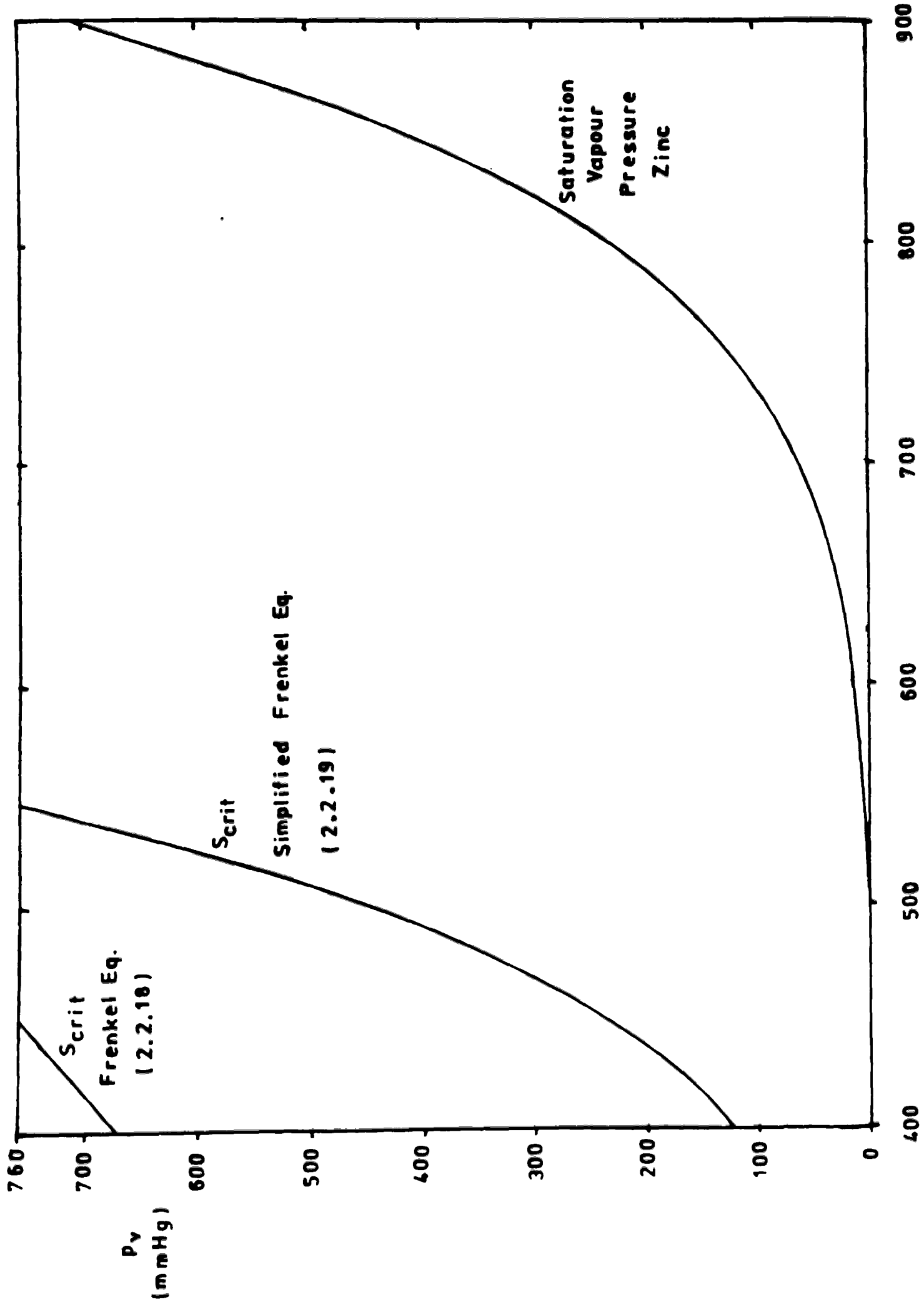

FIGURE 6.4.2 COMPARISON OF CRITICAL SUPERSATURATION EQUATIONS FOR HOMOGENEOUS NUCLEATION OF LEAD VAPOUR

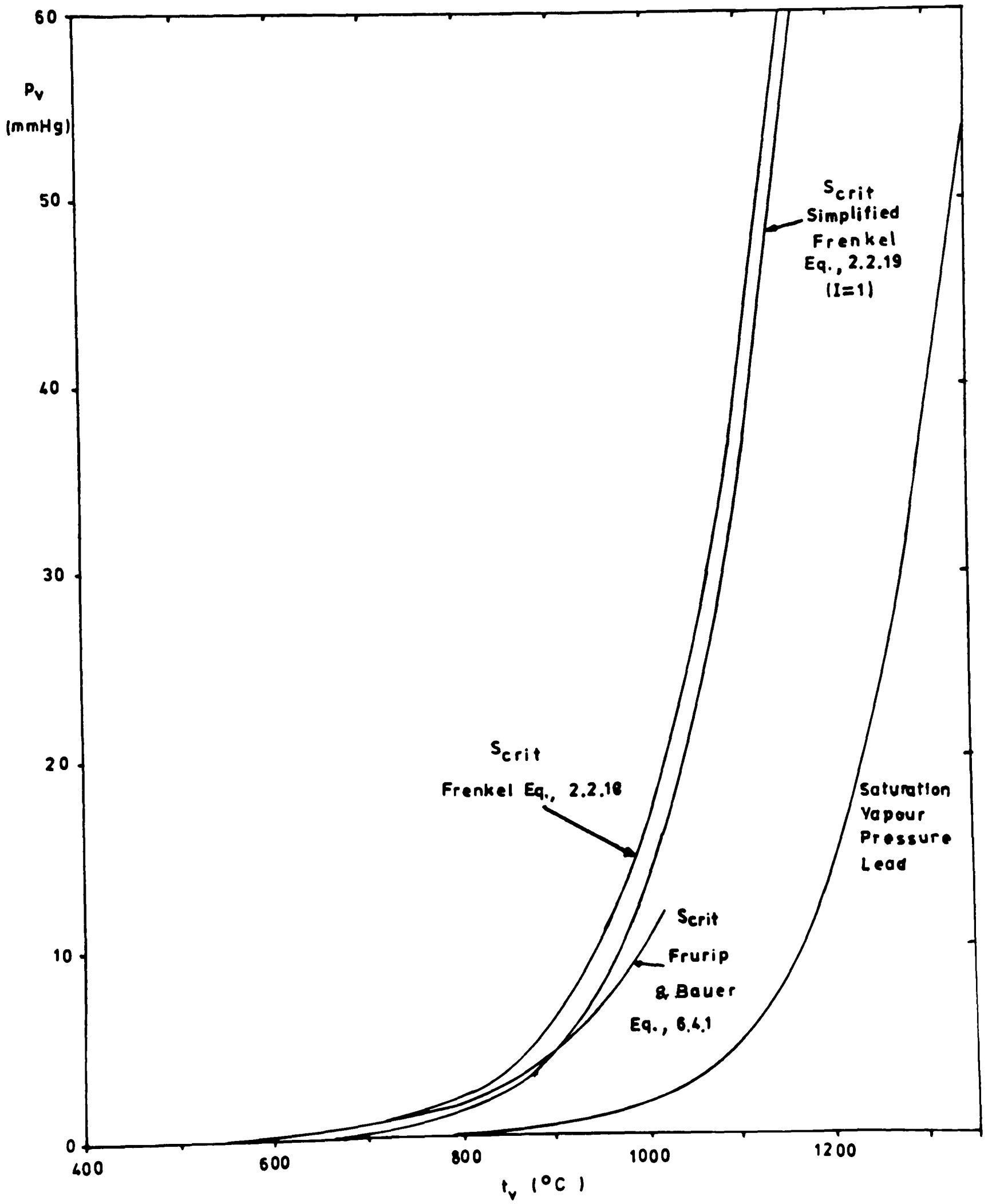

the saturation vapour pressure is so low for lead under these conditions that it is insignificant. There is reasonably good agreement between the Frenkel equations and the experimental results of Frurip and Bauer over their experimental range. This gives a certain degree of confidence in the use of the Frenkel equation for estimating S_{crit} values for metallic vapours.

The Frurip and Bauer homogeneous S_{crit} line for lead vapour can be used as a means of estimating "homogeneous fog losses" by the intersection of cooling curves with this line. For all of the lead condensation predictions for heterogeneous fog formation discussed in section 6.3 (Runs GPb.1-40), corresponding homogeneous fog formation losses have been estimated using this approach and they are detailed in Appendix 4.

For the particular conditions represented by GPb.4 and GPb.8, Figure 6.4.3 is a comparative plot of lead cooling curves showing the predicted quantities of heterogeneous and homogeneous fog losses. Generally, both the ISF and zinc concentrate feed mixtures reveal a significant lowering of lead fog formation predictions by 15-25% for homogeneous fog losses compared with heterogeneous fog losses. Figure 6.4.4 is a plot of Runs GPb.1-8 illustrating the variation in predicted lead fog losses for homogeneous and heterogeneous nucleation over a range of total pressures from 1-30 mm Hg for $t_{vi} = 1200^{o}C$ and $t_c = 420^{o}C$.

A detailed analysis of the homogeneous lead fog formation results in Appendix 4 reveals that no fog is predicted for condensing temperatures greater than $600^{o}C$. Hence, lower lead condensation temperatures are permissible if heterogeneous nuclei can be removed from the gas phase. Moreover, incipient fog formation temperatures for homogeneous nucleation range up to $835^{o}C$ rather than $1055^{o}C$ for heterogeneous fog formation.

FIGURE 6.4.3 COMPARATIVE PLOT OF LEAD COOLING CURVES FOR HOMOGENEOUS AND HETEROGENEOUS FOG FORMATION; COMPUTER RUNS GPb.4 AND GPb.8

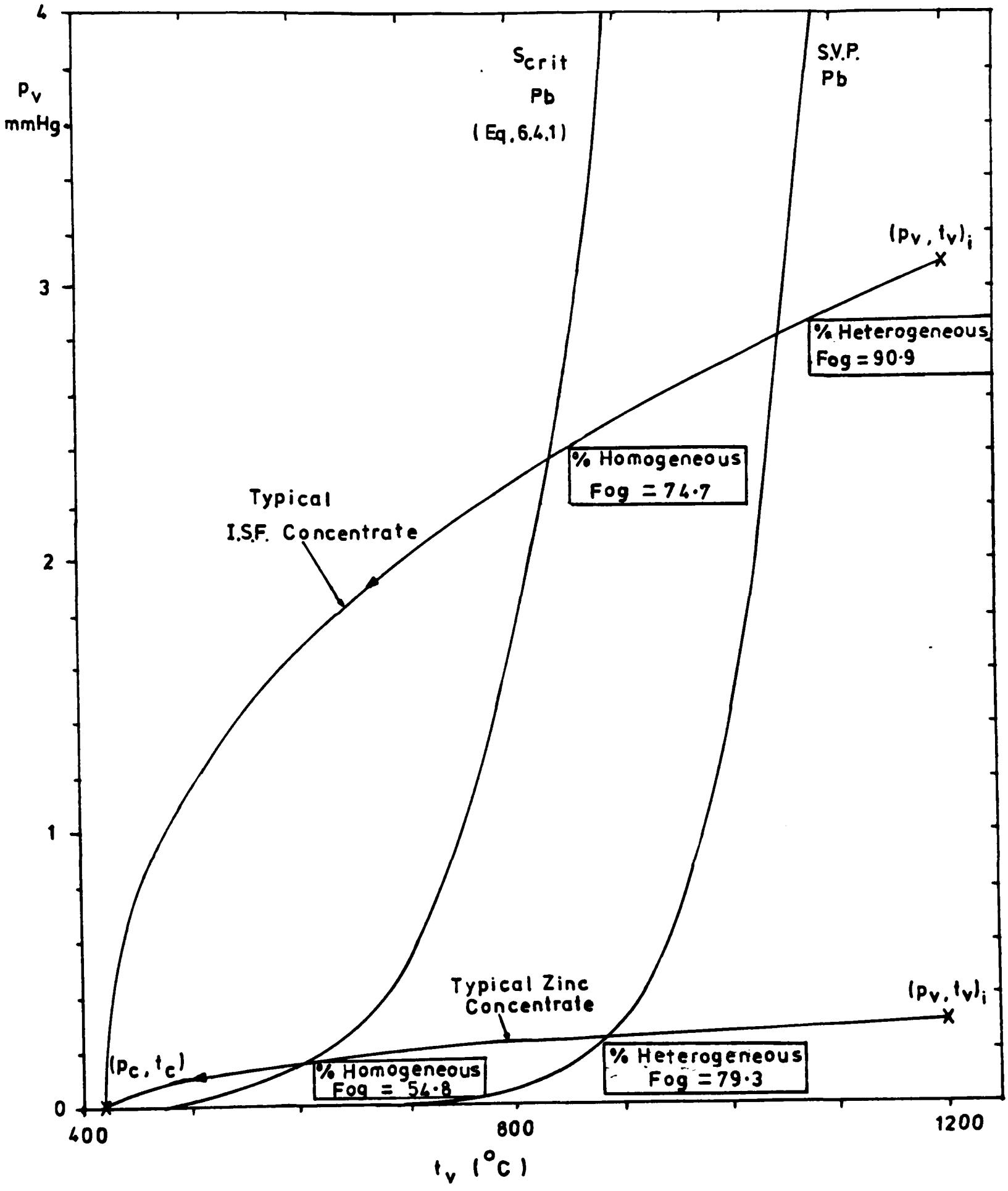

FIGURE 6.4.4 COMPARISON OF PREDICTED LEAD VAPOUR FOG LOSSES FOR HETEROGENEOUS AND HOMOGENEOUS NUCLEATION CONDITIONS ; COMPUTER RUNS GPb.1 TO GPb.8

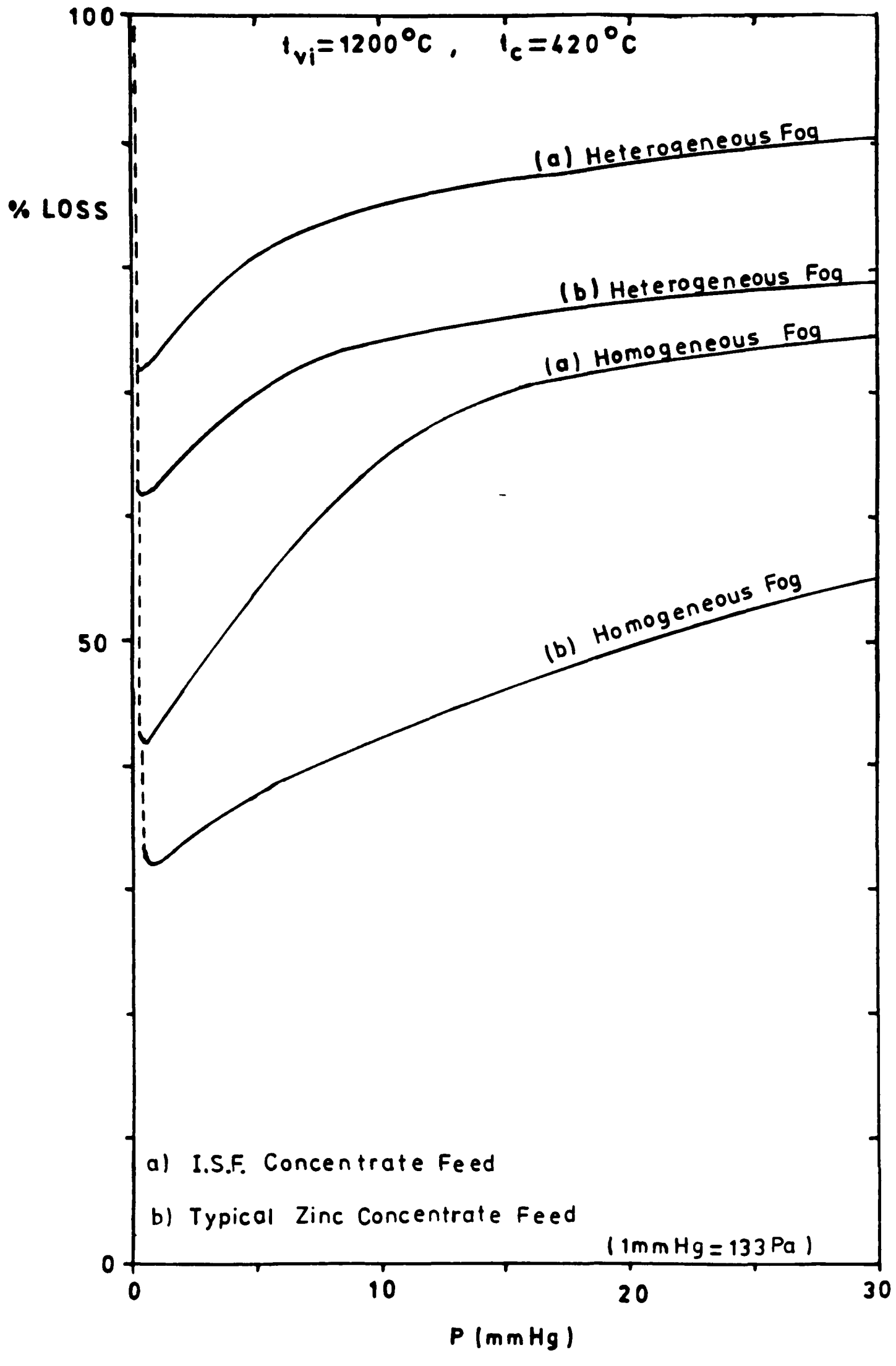

Published Experimental Studies into Homogeneous Fog Formation of Zinc and Lead Vapours

Eversole and Broida (1973) homogeneously nucleated zinc vapour in a heated flowing inert gas stream under vacuum conditions, the total pressure in the system being near 15 mm Hg. Zinc vapour was produced in a small furnace at temperatures just below its melting point of 420^{o}C and rapid cooling (150^{o}C over a height of 2 cm) was allowed to occur by gas conduction to the room-temperature walls. At these low temperatures spontaneous condensation of small solid zinc particles (in the size range 5 nm - 5 μm) was induced and the particles were collected. A 5 nm particle corresponds to approximately 5000 zinc atoms if the bulk density of zinc is used. In all size ranges the particles exhibited simple geometric shapes, no differences being obtained by using different inert gases (N_2, Ar and H_2). The temperatures at the particle collection nozzle were 20-60^{o}C below the evaporation temperature (412 ± 5^{o}C). Gas flow velocities were typically 1-20 cm/s. Estimated zinc particle concentrations produced were up to 5 x 10^{10} particles/cm^3.

The coworkers also note that at total pressures > 35 mm Hg severe turbulence caused difficulties and at low pressures (1-5 mm Hg) the visible light scattering diminished considerably. The maximum light scattering intensity occurred at 15 mm Hg. Increasing the source crucible temperature by 50^{o}C had little visible effect on the light scattering whereas a 150^{o}C temperature rise increased the brightness of the scattered light partially due to the increased volume of particles. A microscopic analysis of the collected zinc particles revealed that the most probable particle shape was a rectangular hexagonal prism. Other shapes also occur, such as triangles, irregular hexagons and pentagons. There was some correlation between

broad, flat particles and low total pressures (< 5 mm Hg). The largest sized particles (0.5 - 5.0 μm diameter) were identifiable as an agglomeration of smaller particles though these larger particles retained the basic hexagonal prism shape. The nucleation time was short compared to the reciprocal of the flow rate so uniform particle size groups at different heights were occurring. When an air leak was introduced into the system there was a pronounced tendency for particles to clump together. The authors suggest that the oxygen molecules coat the nucleated particles epitaxially and thereby prevent further growth except by agglomeration. This suggestion followed from the observation that light scattering from the particles became highly polarised when oxygen was introduced.

Eversole and Broida also estimated the supersaturation ratio for the smallest size of a stable particle to form to be roughly 100-1000 in the region of the collection chamber temperature. These values of supersaturation correspond to a particle consisting of about 10 atoms. The authors also report a limited amount of work on lead nucleation producing small discrete particles rather than sharp-edged geometric shapes.

Hogg and Siberngel (1974) in a parallel study to that done by Eversole and Broida used a similar piece of equipment to investigate zinc, manganese and selenium homogeneous nucleation. They discovered that the average particle size for zinc vapour nucleation increases with increasing zinc vapour pressure. They too noticed striking surface accretion properties of oxidised nuclei when air contamination was allowed.

Buckle (1986) reports from calculations of zinc fog formation that re-evaporation of fog particles in the boundary layer is negligible. He adds that, for zinc, coagulation is important only when condensation is complicated by the oxidation of particles.He also estimates that at reduced

pressures zinc nuclei are a factor of 4-5 times larger in diameter than their corresponding atmospheric counterparts. His work also suggests that the particle sizes increase with rise in atomic mass of the inert supporting gas.

6.5 COMPUTER SOLUTION OF THE GARDNER EQUATION TO ANALYSE ZINC FOG LOSSES IN THE IMPERIAL SMELTING FURNACE CONDENSER

As a validation exercise for the developed Gardner computer program that solves the Gardner equation for bulk vapour condensation, the Imperial Smelting Furnace Zinc Condenser was considered. As described in section 2.2.1.4 the condenser works under atmospheric conditions collecting zinc vapour by an absorption mechanism in a mechanical spray of lead droplets (containing 2.5% zinc). The condensable mixture and the condenser operating conditions may be described by the following:

Feed Mixture (vol %) = Zn (7%), CO(20%), CO_2 (12%), N_2 (61%)

t_{vi} = 1000°C

P = 760 mm Hg

Condensation Stage =	One	Two	Three	Four
t_c =	610°C	520°C	460°C	450°C
p_c =	7.9 mm Hg	1.7 mm Hg	0.5 mm Hg	0.4 mm Hg

Warner (1970) has reported work carried out by Gammon to analyse the ISF condenser for fogging performance. Gammon assumed straight operating lines as a first order approximation for his analysis and an equilibrium transfer efficiency for each condensation stage of 70%. Gammon's predicted zinc operating lines are depicted in Figure 6.5.1 which also highlights his detailed representation of fog formation in the third stage of the condenser. Line CD on the main diagram is the pure zinc saturation vapour pressure line whereas line AB is the equilibrium vapour pressure of

FIGURE 6.5.1 GAMMON FOG ANALYSIS FOR THE ISF CONDENSER

Gas Operating Line In The First Part Of The I.S.F. Condenser

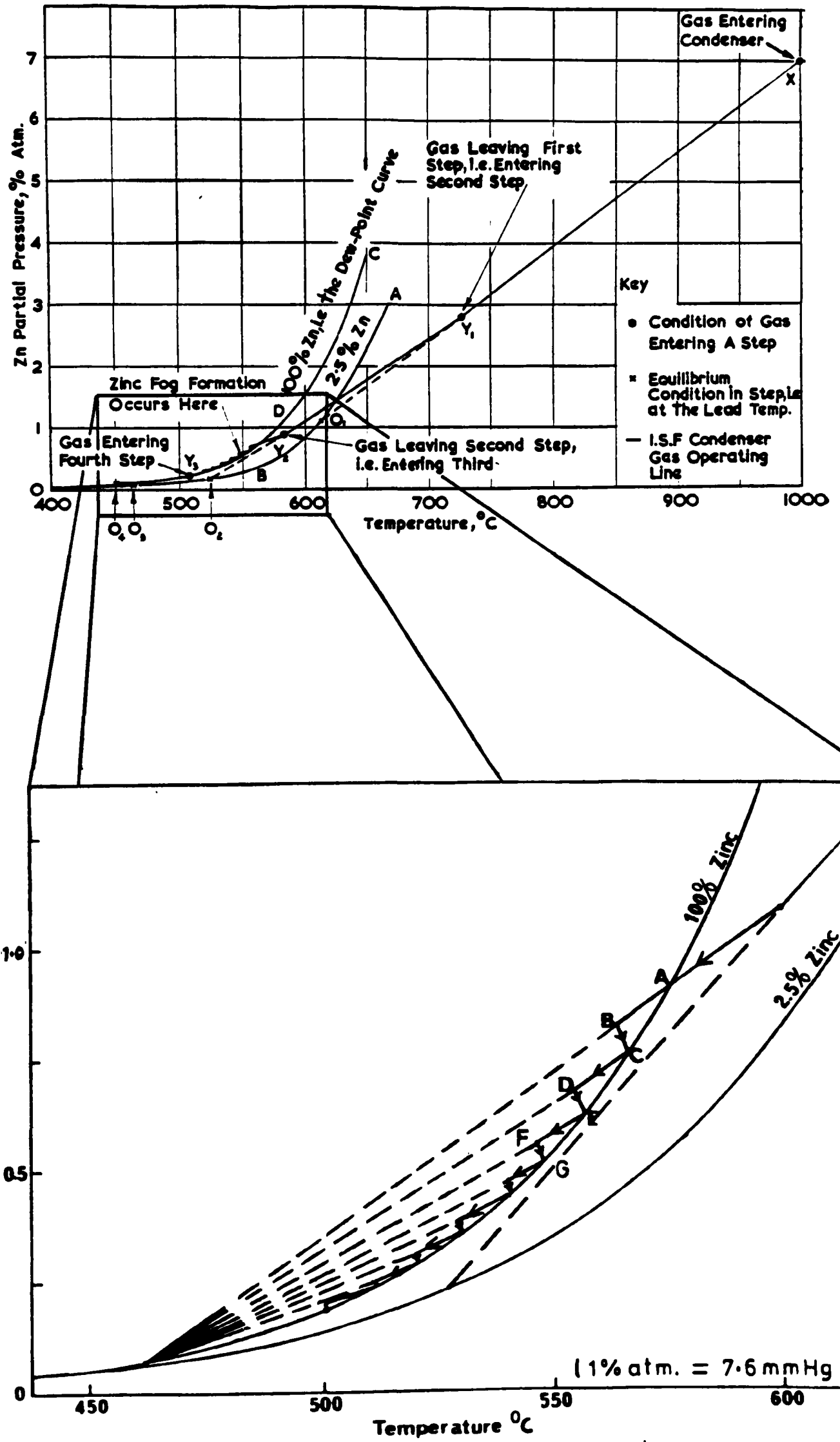

Detailed Representation Of Fog Formation In The Third Stage Of An I.S.F. Condenser

zinc over the zinc-lead spray in the condenser. The operating line for the first stage of the condenser is the line joining the point X, (p_{vi}, t_{vi}) to O_1, representing the liquid spray with which the gas is initially in contact. This operating line represents both the succession of conditions existing in the gas in the layer through which heat and mass is transferred, and the succession of states in time through which the gas would pass if continually scrubbed by the liquids defined as O_1, O_2, O_3 and O_4. The ratio Y_1X/O_1X using abscissa co-ordinates represents the 70% transfer efficiency used in the first stage.

The enlarged detailed representation of fog formation in stage 3 of the ISF condenser was interpreted by Gammon as follows. In the super-saturated region, if nucleation did not occur, the extremity of any operating line (AB, CD etc.) would be the equilibrium condition pertaining to the constant composition and temperature of the lead-zinc solution in the stage under consideration. However, since fog is formed, new operating lines (BC, DE etc.) are followed. When zinc condenses to zinc fog (after nucleation on pre-existing fume) it releases its heat of condensation causing an increase in gas temperature at the same time as effecting a decrease in zinc partial pressure. The amount of zinc which forms as a fog is thus obtained by summing the partial pressure differences between the terminal fog forming positions, i.e. BC, DE etc. Gammon states that the slope of the fog forming lines is constant and can be determined by heat balance. Moreover, he adds that the number of steps in the procedure is arbitrary, the larger the number the more accurate the result. Gammon's analysis estimates zinc fog losses (as a percentage of the zinc volatilised) to be 4.54% in stage 3 of the condenser and 0.34% in stage 4 together with a 1% equilibrium vapour loss of unabsorbed vapour.

The Avonmouth ISF condensers typically produce a blue oxide carry-over dross composed of 38% zinc, 27% lead and 10% carbon, the lead being partly in the form of 1/2 mm lead 'shot' (Gammon, 1989). The overall condenser recovery efficiency is reported to be of the order of 85-91% (sometimes as high as 93-94%) with about 2-4% of these losses being contributed by zinc re-oxidation (reversion).

Several points arise regarding Gammon's work and in connection with this thesis. For totally heterogeneous fog formation in binary vapour/gas mixtures this work adopts the "worse case" basis illustrated by Figure 5.2.1 and quantified by eq. 5.2.1. By implication, once fog forms at $(p_V, t_V)_f$ the vapour/gas mixture remains saturated as it continues to be cooled, the remaining vapour partial pressure differential, $(p_{Vf} - p_C)$ contributing totally to fog formation. In effect the cooling curve should fall along the saturation vapour pressure line. Gammon's approach illustrates what is in effect in-complete heterogeneous fog formation because his cooling mixture on reaching supersaturation (point A, stage 3 condenser) tries to collect in the lead spray (line AB) but on reaching a certain level of supersaturation (point B) nucleates in the gas phase (on foreign nuclei). The nuclei grow and latent heat is removed from the gas phase to the fog droplets (line BC) until the gas phase becomes saturated again (point C). As before, the vapour/gas mixture starts to condense on the zinc-lead coolant spray before nucleating again (point D), and so on. Hence, it appears Gammon is assuming heterogeneous nucleation corresponding to a critical super-saturation line through the points B, D, F etc. His analysis in the super-saturation régime may, however, be a good representation of what actually happens in the ISF condenser. It must be pointed out, though, that choosing points B, D, F etc. must surely depend on a knowledge of foreign nuclei in

the gas phase, especially their number density and size distribution, together with the kinetics of zinc fog droplet growth. These can but be speculated at present. Gammon (1989) notes that his program chose lengths of AB, CD etc. until Y_2 reached Y_3 in ten steps.

If equation 5.2.1 is applied to Gammon's analysis then p_{vf}, t_{vf} occurs in the third stage of the condenser at 7.25 mm Hg and 576^{o}C and 12.8% heterogeneous zinc fog loss is predicted to occur (together with 1% equilibrium vapour loss). A computer solution of the 4 stage ISF condenser conditions outlined above using the Gardner equation produces the cooling curves sketched in Figure 6.5.2 (the Gammon lines are included for comparison). The Gardner analysis clearly produces convex operating lines and predicts fog formation to commence in the second stage of the condenser. There is, however, reasonably close agreement between the cooling curve profiles. Note the less convex nature of the Gardner cooling curves for this atmospheric condenser compared to the predictions for the reduced pressure conditions studied in sections 6.2 and 6.3.

FIGURE 6.5.2 COMPARISON OF THE ISF ZINC CONDENSER OPERATING LINES PRODUCED BY GAMMON AND THOSE USING THE GARDNER EQUATION

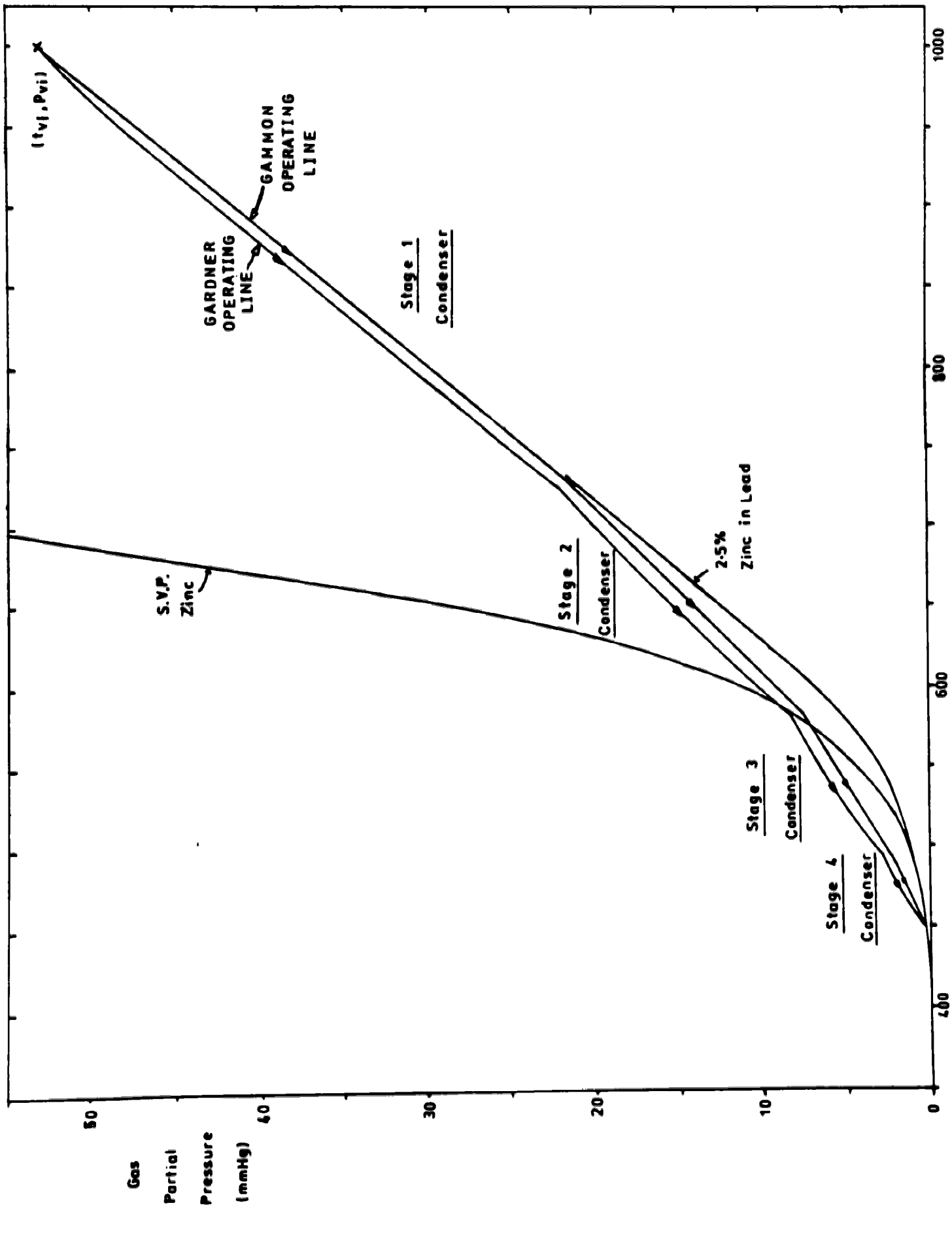

6.6 COMPUTER SOLUTION OF THE GARDNER EQUATION TO ANALYSE FOG FORMATION CHARACTERISTICS IN THE PORT PIRIE VDZ UNIT

Sufficient information is available in the literature (Davey, 1962) to analyse the performance of the Port Pirie VDZ unit described in section 2.2.2.2.2 of this thesis. A Gardner computer solution of the condensing characteristics of zinc and lead vapour under the reduced pressure conditions in the unit may be carried out to check for fog formation characteristics. The problem can be approximately described by the following data given by Davey (for a liquid zinc condenser):

t_{vi} = 600°C

t_c = 420°C

P = 2 mm Hg

p_{vi} = 1.7 mm Hg (Zn), 0.2 mm Hg (Pb), 0.1 mm Hg (N_2)
(assuming a 100 μm vacuum)

Composition of the inlet
gas mixture (mass %) = 71.5% (Zn), 26.7% (Pb), 1.8% (N_2)

p_c = 0.156 mm Hg (Zn), 5.55×10^{-7} mm Hg (Pb)

A computer solution of the Gardner equation (2.2.23) for lead and zinc vapours yields the cooling curves illustrated in Figure 6.6.1. The analysis predicts 43.7% heterogeneous zinc fog formation to occur (together with 1.5% equilibrium zinc losses) if sufficient condensation nuclei are present. If no nuclei are present in the gas phase then no homogeneous zinc fog formation would be expected. The lead cooling curve reveals that once lead vapour evaporates from the bullion at the spreading weir (and all the way

FIGURE 6.6.1 PREDICTED ZINC FOG LOSSES FOR THE PORT PIRIE VDZ UNIT : GARDNER MODEL

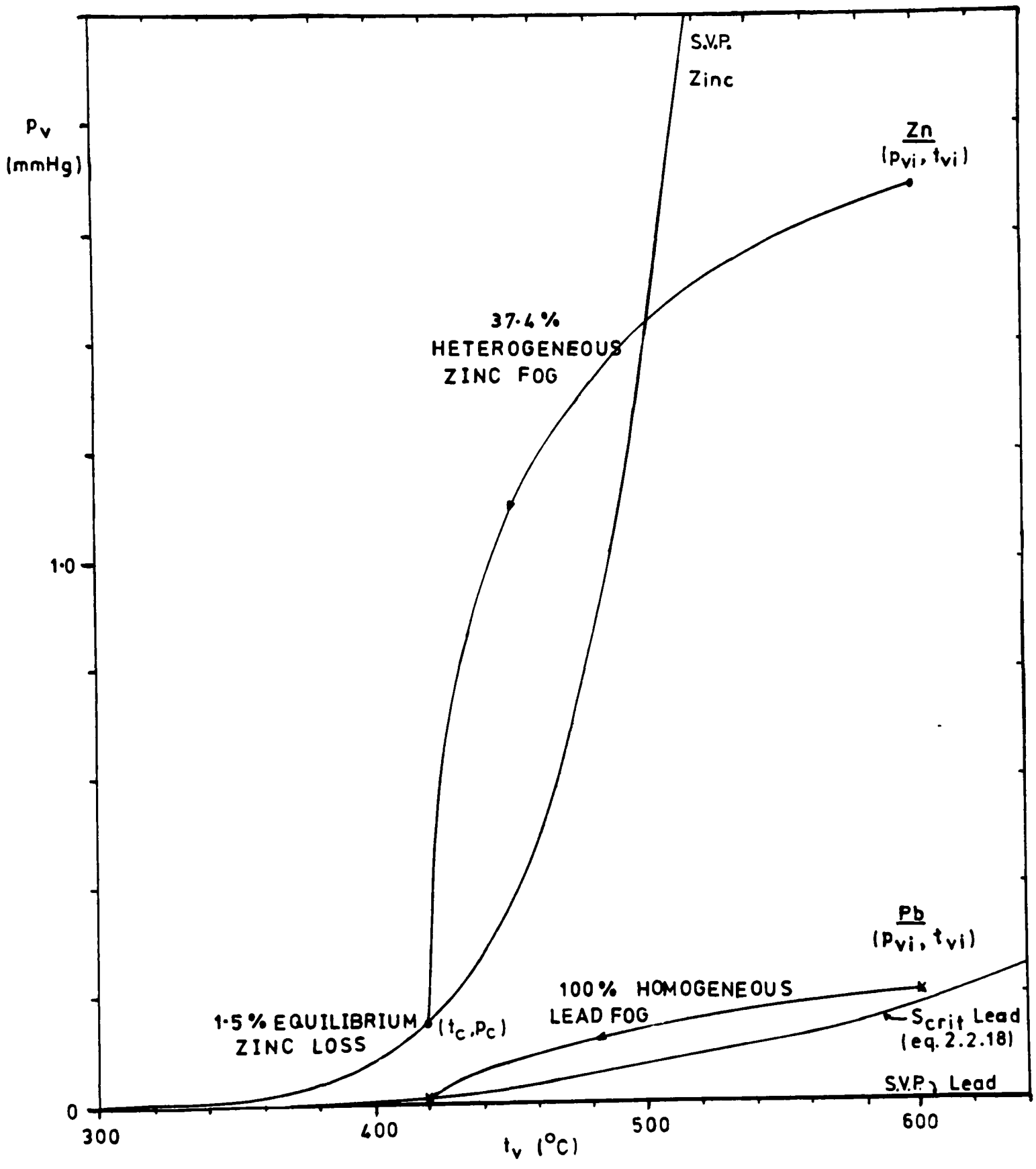

down the spreading surface) it is automatically in a state of supersaturation. Moreover, it is also above its critical supersaturation for homogeneous fog formation such that all of the lead that evaporates should form fog given sufficiently fast kinetics.

Several points arise from these results.

i) The fact that the inerts are present at such a low level should ensure good mass diffusivities towards the condensation surface for the evaporating vapours.

ii) The gas phase under these vacuum conditions should be relatively dust-free compared to the high dust loading in the Warner smelter. Hence, near homogeneous fog formation conditions will prevail for each vapour.

iii) In reality the condensation surface is at a temperature under 100^{o}C and a zinc deposit will build up under unsteady state conditions. During the condensation process a solid zinc deposit builds up slowly. Hence, a Gardner-type analysis for t_c = 100^{o}C, say, would be more applicable albeit it should predict higher quantities of heterogeneous zinc fog formation and similar amounts of lead nucleation to that described by Figure 6.6.1. Note that the cooling curves shown in Figure 6.6.1 are only truly applicable to the bullion condition at the rim of the spreading weir in the VDZ unit.

iv) Calculations by Davey (1962) reveal that the vapour molecules cross the distillation gap at 200 m/s and as the gap is typically of the order of 400 mm this means that a typical residence time in the gas phase is only 2 ms. It could be speculated that this time is insufficient to allow particles to nucleate and grow in the gas phase thus preventing fog formation.

v) Davey also points out that pressure (as normally conceived of) may not be applicable to these uniform vapour flow conditions in one direction. Pressure is usually associated with intermolecular collisions in all directions which may not be occurring in the distillation gap of the Port Pirie VDZ unit. The Gardner equation does, however, rely on conventional partial pressures for its solution.

vi) Davey has also suggested that any lead particles that do form in the gas phase may settle back into the bullion through gravitational forces in a parabolical trajectory. It is also probable that once lead molecules evaporate from the bullion surface they instantly nucleate and to a large extent fall back into the melt.

Partington (1989) reports a typical VDZ zinc deposit to have a composition of 1.54% Pb and 98.34% Zn which indicates nominal lead carry-over to the condensing surface. A dust trap in the vacuum line catches 10-20 kg of dust particles from the condenser over a 300 day vessel operating life. Some dust does carry back to the vacuum pumps ending up in the vacuum oil. Hence, the total amount of dust being carried back to the vacuum pump is a fraction of one percent for a particular 8 hour operation (which is nominal).

It is interesting to note that under a similar vacuum distillation régime Harris (1989) has found that small spherical metallic lead particles appeared in the condensate he collected from his Lift Spray Vacuum Refining Unit (see section 2.2.2.2.2). He suggests that there was probably selective homogeneous nucleation and condensation of lead vapour probably to the solid state in the vacuum chamber. It would seem possible that a similar lead nucleation phenomenon producing small solid lead particles is

occurring in the Port Pirie VDZ unit. It would be of benefit to analyse a typical zinc deposit for these lead nuclei both under an optical microscope and under a scanning electron microscope to prove this hypothesis. In conclusion, a Gardner type analysis under these unsteady state, non-standard pressure, condensing conditions may not be totally applicable. However, homogeneous nucleation of lead vapour droplets in the distillation gap is probably occurring together with the formation of solid lead nuclei. These nuclei either return to the bullion or are convected to the zinc deposit. Some are carried out of the unit back to the vacuum pump and dust trap. Here again, a chemical and microscopic analysis of the particles collected in the dust trap would be of interest - they should be lead rich.

CHAPTER 7: CONCLUSIONS

A new liquid phase mass transfer model for dissolved solute desorption due to impinging top-blown gas jets contacting a moving liquid phase inside a channel has been developed. It utilises log mean bulk liquid concentration differentials across the top-blow region. The analogous situation of oxygen desorption from tap water was used to simulate the mass transfer processes expected to occur during top-blowing gas-liquid contacting in the Warner smelter.

Tests involving multiple lance arrays of both open-packed and close-packed 2.26 mm, 4.95 mm, 10.95 mm and 24.40 mm nozzles have shown liquid phase mass transfer to be independent of channel flowrate. A range of lance heights from 10 to 20 cm, encompassing both gentle blowing and heavy splashing jetting conditions for all the open-packed arrays, indicates good data agreement with the Jones (1987) correlation (for the non-splashing runs). This correlation incorporates both high and low temperature liquid phase mass transfer data. In the case of close-packed arrays of nozzles delivering the same flowrate of gas as an open-packed array of the same nozzles, a significant reduction in liquid phase mass transfer by as much as 75% (in certain cases) was found to occur. For the analogous smelter situation this would entail less oxygen absorption into the matte and subsequent loss of zinc and lead species into the slag as oxides. The larger diameter nozzles with fewer lances in the array, delivering the same quantity of gas as the smaller nozzles, produced much lower liquid phase mass transfer. However, the larger nozzles should only be used if they blow at a momentum flux that is sufficient to clear the surface of the slag produced. They must also provide an acceptable gas phase mass

transfer coefficient to cater for the required chemical reactions on the surface. Dai (1990), in this School is studying this gas phase mass transfer problem as part of an on-going programme of fundamental research in this field.

Additional momentum tests have indicated the presence of jet/jet and/or jet/wall interactions such that the momentum flux of a jet in an array is dampened. In some close-packed arrays this can amount to an effective momentum flux of two-thirds that for each individual free jet in the array. With open-packed configurations of jets the reduction in momentum flux per jet varied from 14% to 27%. The multiple lance liquid phase mass transfer work reported here coupled with work done by Jones (1986) has led to a top-blow unit being designed for the pilot scale Warner smelter. It incorporates a close-packed 35 lance, 2 mm nozzle arrangement and it is currently being constructed for integration into the smelter commissioning schedule.

A computer program has been developed to analyse vapour/gas condensation phenomena and it has revealed general fog formation trends of use to the high temperature Warner smelter. It has highlighted the condenser operating conditions most likely to keep zinc and lead losses down to a minimum during a smelting run. Of these, zinc vapour fog formation will be most marked at high condenser inlet vapour concentrations of greater than 85% zinc. Almost all (70-90%) of the lead present in a condensable zinc/nitrogen mixture will form as a fog quite early on during the condensation process (if sufficient nuclei are present) at temperatures up to 1050^{o}C. These lead fog droplets will almost certainly act as condensation nuclei for the condensing zinc vapour especially if they solidify as dust particles. This lead oxide/sulphide dust will ensure that zinc will form

as a fog upon reaching a state of supersaturation. As much as 40 to 50% of the inlet zinc vapour could be lost as a fog if the conditions in the condenser are not controlled.

The higher the condenser wall temperature the less vapour fog formation will occur though this does not have as pronounced an effect as vapour concentration in the feed mixture. The less superheat a condensable mixture posesses the more likely it is to condense as a fog. The lower the total pressure in the condenser , the less fog will be a problem though equilibrium losses will become more significant. Saturated vapour losses in the outlet from the condenser will also influence total losses quite strongly at lower feed concentrations.

The computer predictions have led to the proposal of a two stage condenser for the Warner smelter; the first stage to recover lead at a temperature of 700-800^{o}C and the second stage at a temperature of 420^{o}C to collect the zinc vapour. Intermediate between the two stages should be a reheater to raise the vapour/gas temperature to around 1200^{o}C.

Of the three fog formation equations studied for the specific case of high vapour content in the feed,there are large variations in predicted amounts of fog. The most conservative fog estimates are given by the Gardner equation (2.2.23) whereas the Cairns and Roper equation (2.2.28) estimates almost twice as much for the same condensable mixture. The Bras equation (2.2.27) also predicts high quantities of fog to be lost from the condenser, though not as much as that from the Cairns and Roper analysis. Ultimately, the only vindication for the use of one of these equations for the high temperature smelter situation will come when the rig is in full production of lead and zinc. Then, the quantities of dust caught in the condenser sump plus the fog trapped in the demister can be related back to zinc and lead

production rates.

The computer program has also been used to analyse fogging characteristics within two industrial condensers using the Gardner equation as the operating line. The Imperial Smelting Furnace zinc condenser performance was shown to be similar to that from the Gardner program prediction and the prediction was also in reasonably good agreement with the simplified approach taken by Gammon. The analysis reveals incomplete heterogeneous fog formation conditions to be existing in the ISF condenser to account for operating condenser efficiencies. The Port Pirie vacuum dezincing unit did not lend itself very well to a Gardner analysis mainly because of the transient nature of the condenser cooling wall temperature and the problem of defining pressure. However, the VDZ unit was shown to be operating in the homogeneous fog forming region such that little or no zinc fog would form coupled with high lead nucleation rates. The lead droplets were postulated to have a tendency to return back to the bullion on the spreading surface due to gravitational effects.

An engineering approach to the development of a method for estimating homogeneous fog formation has also been successfully outlined. It has been used to explain several condensation problems and throw light on others.

A low temperature 1/9th scale model of the Warner condenser made out of glass has revealed useful trends in condensation under reduced pressure conditions for glycerol/nitrogen mixtures. The condenser model was able to collect almost all the glycerol vapour in the feed mixture producing no fog even though the mixtures were supersaturated. This indicates that homogeneous fog nucleation would have been prevalent had the supersaturations been high enough. High condensate temperatures in the collection flasks indicated a variable condensate interfacial temperature which was undesirable in terms of inducing fog formation.

CHAPTER 8: RECOMMENDATIONS FOR FUTURE WORK

This work highlights the need for further research in the two smelting areas considered: multiple lance top-blowing during channel flow and fog formation during condensation under reduced pressure conditions. With the multiple lance top-blowing work there is a need for greater understanding of fluid flow and mixing characteristics in the channel. There is also scope for further studies into the damping effects associated with adjacent jets in an array inside a channel. The effect of slag clearance area during top-blowing is currently being studied in this School by Dai (1990) who is also looking at the gas phase aspects of multiple lance top-blowing. His study into the slag clearing phenomenon should lead to the development of a dimensionless correlation. Clearly, his results must be viewed in the context of this work.

It is feasible to suggest that ultimately the Warner smelter top-blow region will have gas fed to the nozzles via a windbox arrangement with gas smoothing sections. Such an arrangement would be easily assembled and fitted onto a flange on the smelter roof. It would also eliminate the cumbersome multiple tubes and distributor boxes of the present system. It is also well worth considering multiple top-blown plane jets aligned parallel to the channel flow as a much more effective use of top-blow area in the channel. A simple grid or slotted plate fitted to the windbox would then act as an array of multiple nozzles.

There is room for further work on physical modelling of the Warner condenser using the reduced pressure glycerol analogue model. At present, a larger coolant system is needed. Effectively a refrigeration unit is required capable of sustaining a constant coolant flowrate at temperatures down to -20^{o}C ($CaCl_2$ (aq) starts to freeze at these temperatures) and of at

least 1.5 kW cooling capacity. Alternatively, a higher melting point condensable vapour could be used but this could pose a serious flashing hazard and therefore an explosive risk. It may be better to have a condenser model made out of steel for safety and heat transfer reasons rather than the present glass model. If glycerol testwork is successful then a tertiary vapour/ gas model should be considered. The modelling testwork should include heterogeneous nucleation during condensation. Such foreign nuclei when generated must be of a constant size range that is repeatable. It would probably be best to generate such nuclei outside the equipment and to introduce them into the superheater tube via a reduced pressure injection chamber at a slightly higher pressure to that in the model so the particles are sucked in. The alternative of a high temperature nuclei generator inside the superheater would pose an automatic ignition hazard in the equipment. More work also needs to be done in the area of pressure readings in the model as there are difficulties associated with throttling and accurately measuring the nitrogen gas fed to the model (as well as possible back diffusion). It may be best to use pressure transducers as long as the electronics can withstand the model wall temperatures which have to be higher than the vapour's dewpoint. The low temperature model will still provide a useful vehicle for assessing the accuracy of the computer model and the fog formation equations.

The extension of the work reported here on binary vapour/gas mixtures condensing under reduced pressures to tertiary mixtures has already been achieved by Li et al (1990). In his work he solves the Gardner equation simultaneously for each vapour considered, thus eliminating the assumption of one vapour acting as a carrier gas for the other during the solution of the fog formation equations (compare for instance, section 6.3). There is also a

need for the mathematical model to consider the following thermochemical phase changes that will occur during the condensation of zinc/lead/nitrogen condensable mixtures:

$$PbS(g) + Zn(g) = ZnS(s) + Pb(g \text{ or } l)$$

$$\text{and } SO_2(g) + 3Zn(g) = 2ZnO + ZnS(s)$$

These chemical reactions should be amenable (via thermodynamic data) to mathematical modelling iteratively in the computer model of the vapour/gas cooling operation.

Once the Warner smelter is fully operational it would be of use to undertake a fundamental study of the smelter dross/fog carryover to the filters for morphology, chemical composition and size range to ascertain the origins of the particles. Some will be fog particles and some ZnO/ZnS/PbS dross from chemical reactions in the gas phase. This work should also reveal the nature of fog particle coalescence and their settling characteristics. It is also conceivable that a commercial scale Warner condenser unit will be of an Imperial Smelting Furnace type utilising a mechanical spray (of zinc or lead droplets) and a gas absorption mechanism as the mode of vapour collection.

Several refinements and additions to the computer fog formation model are also necessary. They include integrating into each iteration of the cooling process a separate loop that determines the pressure loss in the annulus of the condenser over a set distance. An equation of the Hagen-Poiseuille type for laminar flow should be sufficient. The model should also consider the radiation component of heat transfer in the iterative solution of the Gardner equation. It is best to include it in the heat/mass balance used in the development of the Gardner equation; i.e. develop a new one. Such a balance could also incorporate heat losses through the

condenser walls and possibly Peclet diffusion in the axial direction of the condenser annulus. A true iterative fog formation model would also have to take account of fog droplet growth rates and size distributions. As in Steinmeyer's (1972) approach the heat released on the droplet as vapour condenses should be analysed in terms of heat transfer coefficients. The mathematical model should also incorporate interfacial resistances at the condensate interface.

Another aspect of heterogeneous fog formation still not fully understood and in need of further research is the temperature of the foreign nuclei in the gas phase. This work has assumed a worse case of the nuclei being at the same temperature as the cooling wall. In reality the nuclei should be at temperatures near that of the surrounding gases. Some more experimental work on nuclei to assess which particles are most nucleophilic to a given vapour is a necessity. There may also be scope to study if additions of gases or vapours to the condensable mixture has any effect on deactivating nuclei sites making them nucleophobic.

Another area of heterogeneous fog formation worth studying is the critical supersaturation criterion, S_{crit}, for different levels of condensation nuclei. It seems reasonable that for a profusion of condensation nuclei, S_{crit} for heterogeneous nucleation is equal to unity where S_{crit} is defined as the level of supersaturation that limits nucleation to one particle produced per cm^3 per second. For a given gas temperature there is both a homogeneous S_{crit} (when N, the number of condensation nuclei, equals zero) and a heterogeneous S_{crit} (when N equals infinity). A logical extension of this argument leads to the conclusion that there must be a relationship between S_{crit} and nuclei concentration (if, say, nuclei concentration was defined over narrow size ranges). If these "critical supersaturation lines" are plotted on a

partial pressure-temperature diagram then curves as sketched below should exist.

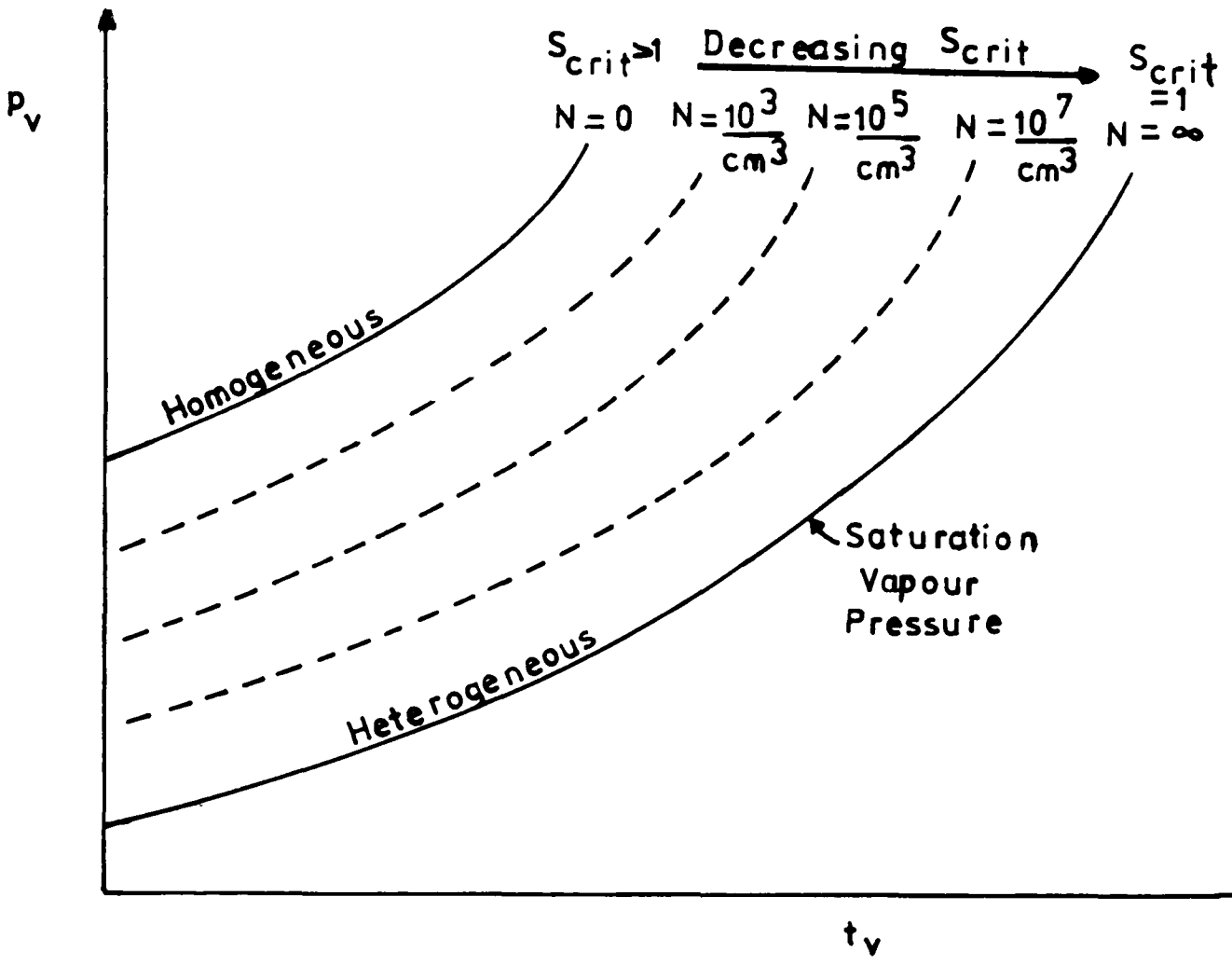

There is obviously a need for a deeper understanding of this problem. With regard to the Warner smelter connected with this work the generation of nuclei spontaneously during cooling such as PbS, ZnS and ZnO should be so pronounced that heterogeneous fog formation in the condenser should be prevalent.

Ultimately, the goal with the computer model is to feed simple on-line smelter readings into the computer such that it will provide an instant indication of the extent of fog formation in the condenser. The operator could then take evasive action. This utilisation of the computer model in a

process control loop will depend on good onstream process readings from instrumentation. Readings that would be desirable to know include total pressure values upstream and downstream of the condenser. At present pressure transducers that provide such readings do not exist due to the aggressive environment in the condenser (high temperatures and corrosive gases) but eventually they probably will become available. Note that a pressure transducer downstream of the condenser (operating at temperatures around 450^{o}C) should provide a reading similar to that present upstream (ignoring frictional pressure losses). Another onstream reading that should also be available is a downstream fog/particulate number density and size distribution. Such values should be obtainable via laser or tomographical techniques such that they will also provide the process operator with a direct estimate of fog formation in the condenser.

APPENDIX 1: TOP BLOWING CALIBRATION DATA

TABLE A.1.1: SATURATION CONCENTRATION OF OXYGEN IN FRESH WATER (PERRY, 1984)

Water Temp. (°C)	Saturation Concentration (ppm)	Water Temp. (°C)	Saturation Concentration (ppm)
6.0	12.50	13.2	10.56
6.2	12.44	13.4	10.50
6.4	12.38	13.6	10.46
6.6	12.31	13.8	10.42
6.8	12.26	14.0	10.37
7.0	12.20	14.2	10.32
7.2	12.14	14.4	10.28
7.4	12.07	14.6	10.24
7.6	12.02	14.8	10.20
7.8	11.95	15.0	10.16
8.0	11.90	15.2	10.11
8.2	11.84	15.4	10.07
8.4	11.78	15.6	10.02
8.6	11.72	15.8	9.99
8.8	11.65	16.0	9.95
9.0	11.60	16.2	9.91
9.2	11.54	16.4	9.87
9.4	11.48	16.6	9.84
9.6	11.42	16.8	9.79
9.8	11.36	17.0	9.75
10.0	11.30	17.2	9.71
10.2	11.26	17.4	9.67
10.4	11.21	17.6	9.63
10.6	11.16	17.8	9.60
10.8	11.11	18.0	9.55
11.0	11.06	18.2	9.52
11.2	11.02	18.4	9.48
11.4	10.96	18.6	9.44
11.6	10.92	18.8	9.40
11.8	10.87	19.0	9.36
12.0	10.82	19.2	9.32
12.2	10.78	19.4	9.28
12.4	10.73	19.6	9.24
12.6	10.69	19.8	9.20
12.8	10.64	20.0	9.16
13.0	10.60	20.2	9.12

TABLE A.1.2: MOMENTUM FLUX AND MASS FLOWRATE CALIBRATION

Measured Flowrate ($L.min^{-1}$)	Rotameter Reading ($L.min^{-1}$)	Upstream pressure (mm Hg)	Upstream Density (g/cm^3) x 10^3	Measured Mass Flow ($g.s^{-1}$)	Theoretical Mass Flow ($g.s^{-1}$)	Discharge Coefficient (C_d)	Calculated Momentum (N) (eq. 3.2.4)	Measured Momentum (N)	% Difference
19.23	21.0	42	1.258	0.3879	0.4664	0.8317	0.0378	0.0373	1.1
23.56	25.0	62	1.268	0.4707	0.5618	0.8380	0.0556	0.0564	1.4
28.57	30.1	95	1.316	0.5763	0.6919	0.8329	0.0833	0.0829	0.1
37.69	38.8	174	1.402	0.7603	0.9195	0.8269	0.1459	0.1511	3.9
44.56	45.0	247	1.465	0.8903	1.0757	0.8277	0.2009	0.2157	6.9
50.56	50.1	324	1.544	1.0102	1.2131	0.8327	0.2571	0.2726	5.7

Mean C_d = 0.8317

TABLE A.1.3 : Density (kg/m³) of Water from 0 to 100°C (Perry, 1984)

t, °C	ρ_L kg/m³									
	0.0	0.1	0.2	0.3	0.4	0.5	0.6	0.7	0.8	0.9
0	999.839	999.846	999.852	999.859	999.865	999.871	999.877	999.882	999.888	999.893
1	999.898	999.903	999.908	999.913	999.917	999.921	999.925	999.929	999.933	999.936
2	999.940	999.943	999.946	999.949	999.952	999.954	999.956	999.958	999.961	999.962
3	999.964	999.966	999.967	999.968	999.969	999.970	999.971	999.971	999.972	999.972
4	999.972	999.972	999.972	999.971	999.971	999.970	999.969	999.968	999.967	999.965
5	999.964	999.962	999.960	999.958	999.956	999.954	999.951	999.949	999.946	999.943
6	999.940	999.937	999.934	999.930	999.926	999.923	999.919	999.915	999.910	999.906
7	999.901	999.897	999.892	999.887	999.882	999.877	999.871	999.866	999.860	999.854
8	999.848	999.842	999.836	999.829	999.823	999.816	999.809	999.802	999.795	999.788
9	999.781	999.773	999.765	999.758	999.750	999.742	999.734	999.725	999.717	999.708
10	999.699	999.691	999.682	999.672	999.663	999.654	999.644	999.635	999.625	999.615
11	999.605	999.595	999.584	999.574	999.563	999.553	999.542	999.531	999.520	999.509
12	999.497	999.486	999.474	999.462	999.451	999.439	999.426	999.414	999.402	999.389
13	999.377	999.364	999.351	999.338	999.325	999.312	999.299	999.285	999.272	999.258
14	999.244	999.230	999.216	999.202	999.188	999.173	999.159	999.144	999.129	999.114
15	999.099	999.084	999.069	999.054	999.038	999.022	999.007	998.991	998.975	998.958
16	998.943	998.926	998.910	998.894	998.877	998.860	998.843	998.826	998.809	998.792
17	998.775	998.757	998.740	998.722	998.704	998.686	998.668	998.650	998.632	998.614
18	998.595	998.577	998.558	998.539	998.520	998.502	998.482	998.463	998.444	998.425
19	998.405	998.385	998.366	998.346	998.326	998.306	998.286	998.265	998.245	998.224
20	998.204	998.183	998.162	998.141	998.120	998.099	998.078	998.057	998.035	998.014
21	997.992	997.971	997.949	997.927	997.905	997.883	997.860	997.838	997.816	997.793
22	997.770	997.747	997.725	997.702	997.679	997.656	997.632	997.609	997.585	997.562
23	997.538	997.515	997.491	997.467	997.443	997.419	997.394	997.370	997.345	997.321
24	997.296	997.272	997.247	997.222	997.197	997.172	997.146	997.121	997.096	997.070
25	997.045	997.019	996.993	996.967	996.941	996.915	996.889	996.863	996.836	996.810
26	996.783	996.757	996.730	996.703	996.676	996.649	996.622	996.595	996.568	996.540
27	996.513	996.485	996.458	996.430	996.402	996.374	996.346	996.318	996.290	996.262
28	996.233	996.205	996.176	996.148	996.119	996.090	996.061	996.032	996.003	995.974
29	995.945	995.915	995.886	995.856	995.827	995.797	995.767	995.737	995.707	995.677
30	995.647	995.617	995.586	995.556	995.526	995.495	995.464	995.433	995.403	995.372
31	995.341	995.310	995.278	995.247	995.216	995.184	995.153	995.121	995.090	995.058
32	995.026	994.997	994.962	994.930	994.898	994.865	994.833	994.801	994.768	994.735
33	994.703	994.670	994.637	994.604	994.571	994.538	994.505	994.472	994.438	994.405
34	994.371	994.338	994.304	994.270	994.236	994.202	994.165	994.134	994.100	994.066

FIGURE A.1.1 : THE DIFFUSIVITY OF OXYGEN IN WATER (Si-Denis and Fell, 1971)

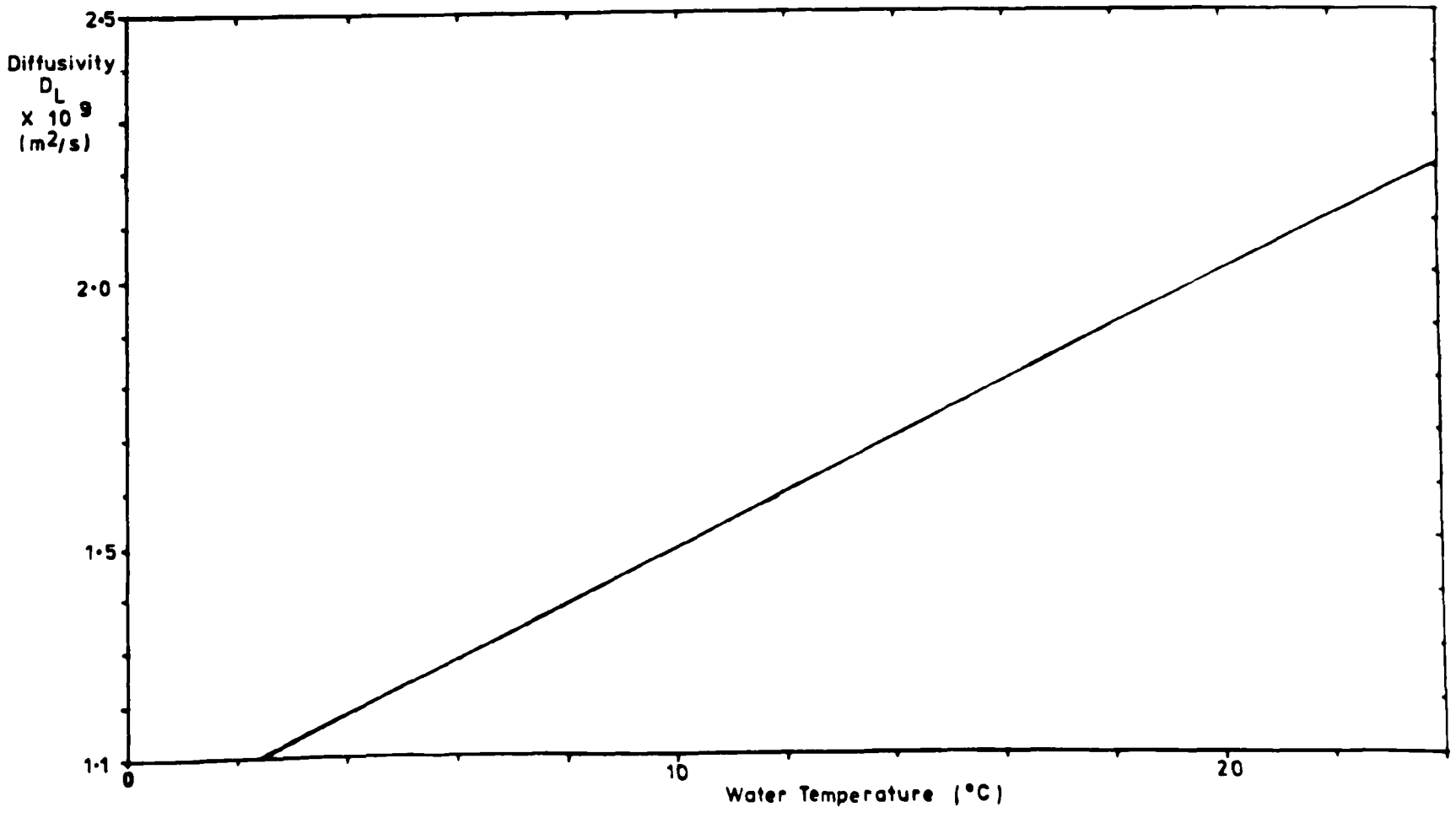

FIGURE A.1.2 : SURFACE TENSION OF WATER AGAINST AIR
(Handbook of Physics and Chemistry, 1971)

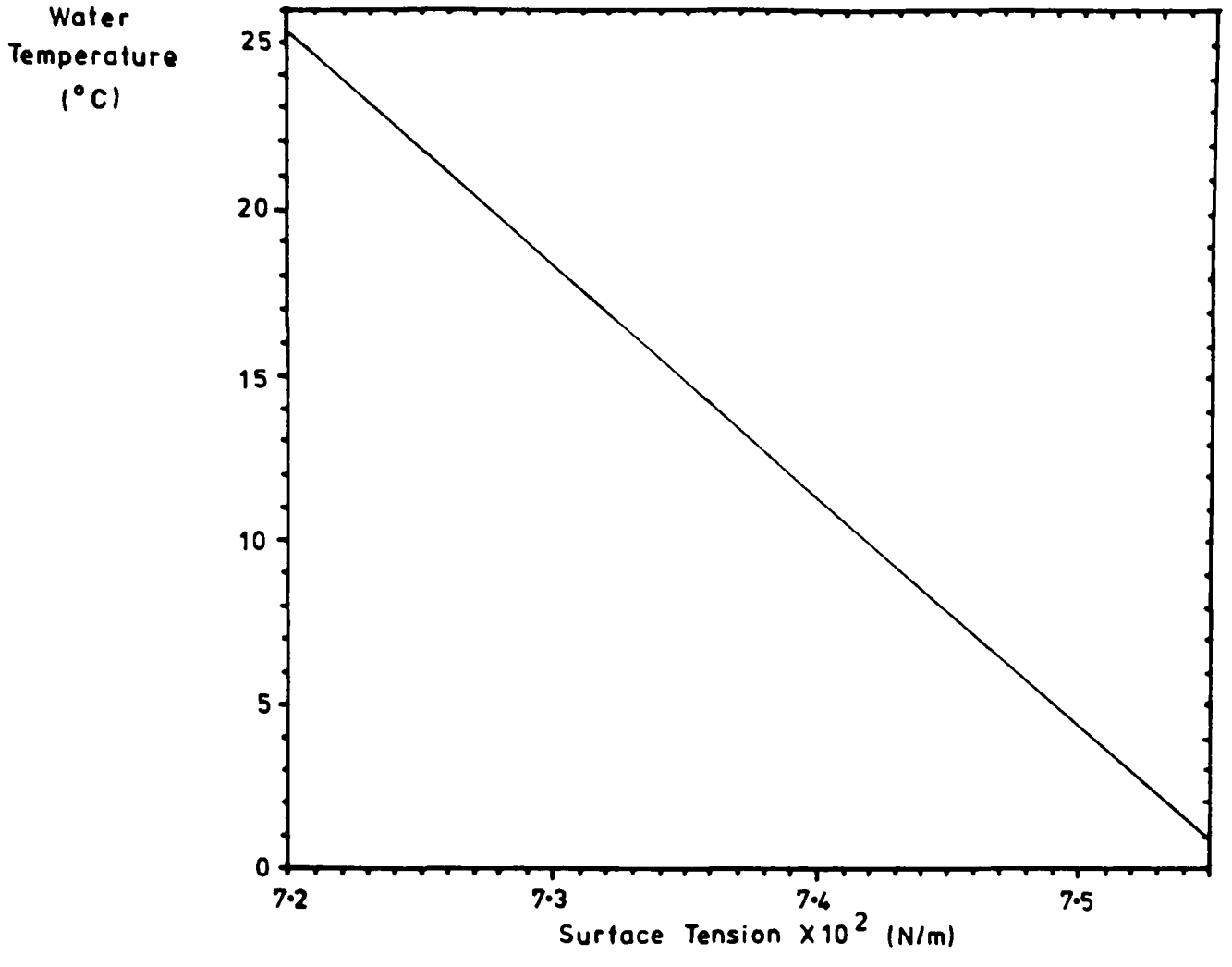

FIGURE A.1.3 : THE VISCOSITY OF WATER
(Handbook of Physics and Chemistry, 1971)

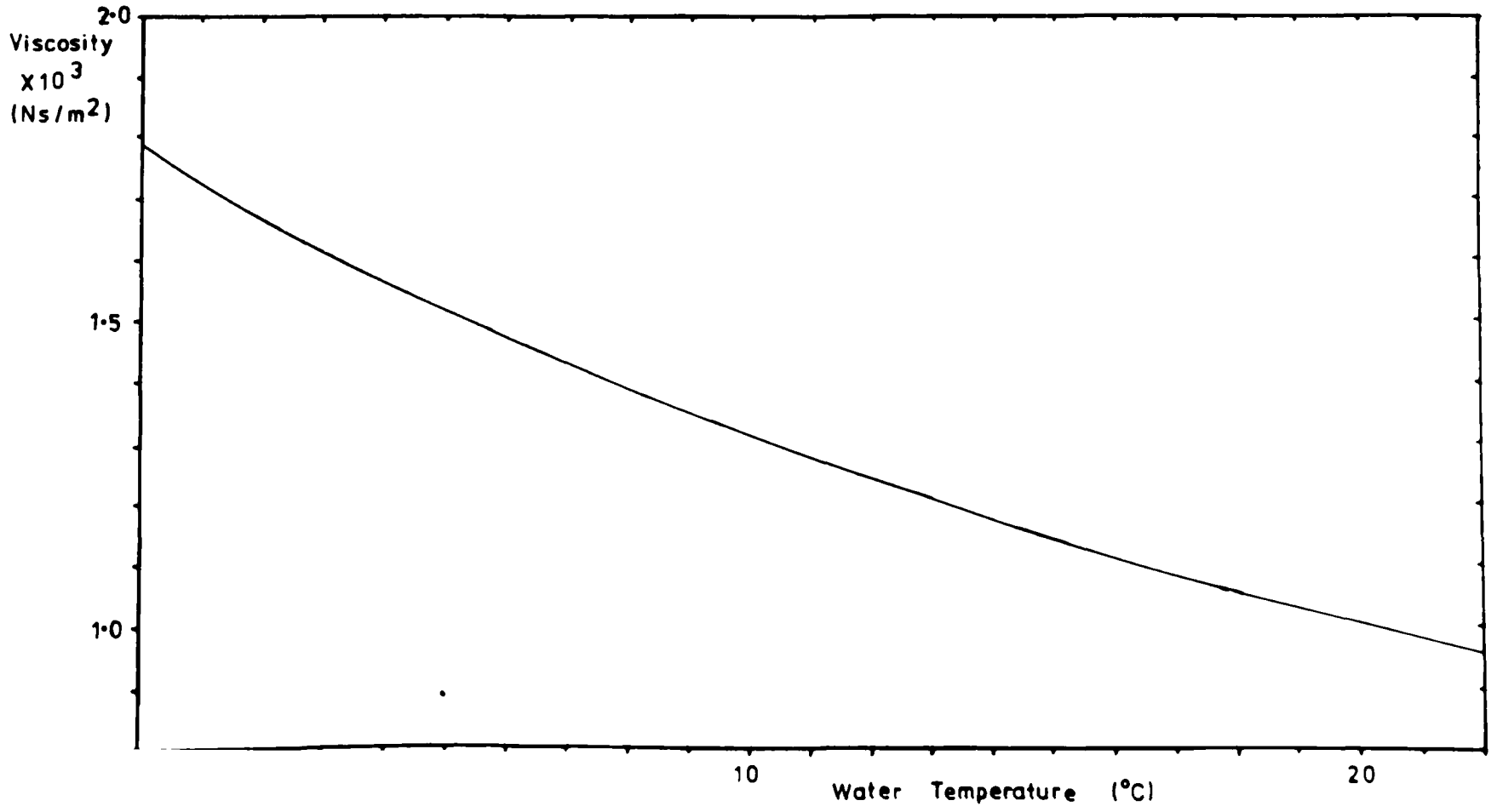

Key:
AOD ; Air Jet Oxygen Desorption
NOD ; Nitrogen Jet Oxygen Desorption
O ; Open Packing
C ; Close Packing
Tr ; Triangular Pitch
Sq ; Square Pitch
st. st. ; Steady State

Serial No.	d_o (mm)	$\dot{M}$ (N)	X	H (m)	Q (m^3/hr)	t_{av} (°C)	$C_L^b i$ T=0 (ppm)	$C_L^b o$ T=0 (ppm)	$C_L^b i$ st. st. (ppm)	$C_L^b o$ st. st. (ppm)	Lance Packing and Pitch	k_{Lj} x 10^4 (m/s) (Eq. 3.4.1)	$\dot{n}$ x 10^7 (kg/s) (Eq. 2.1.36)
AOD.1a	2.26	0.150	35	0.20	1.03	19.0	30.2	29.7	30.4	27.4	O, Tr	2.45	4.02
AOD.1b	"	"	"	"	1.03	19.0	32.2	31.8	32.2	29.15	"	2.38	4.27
AOD.2a	"	"	"	"	1.76	20.4	22.3	22.0	22.6	21.35	"	2.40	3.85
AOD.2b	"	"	"	"	1.76	20.4	23.35	23.05	23.4	21.95	"	2.77	3.99
AOD.3a	"	"	"	"	2.40	19.3	25.6	25.4	25.6	24.0	"	4.00	4.97
AOD.3b	"	"	"	"	2.40	19.3	28.2	28.0	28.2	26.75	"	3.05	4.31
AOD.4a	"	"	"	"	3.02	20.1	32.55	32.45	32.55	31.35	"	2.68	5.20
AOD.4b	"	"	"	"	3.02	20.1	33.0	32.9	33.0	31.75	"	2.75	5.43
AOD.5a	"	"	"	"	3.71	20.1	32.1	32.0	32.0	31.0	"	2.75	5.22
AOD.5b	"	"	"	"	3.71	20.1	32.1	32.0	32.0	31.0	"	2.75	5.51
AOD.6a	"	0.144	36	"	1.00	20.7	30.3	29.8	30.6	27.8	O, Sq	2.06	3.59
AOD.6b	"	"	"	"	1.00	20.7	32.95	32.45	33.0	29.7	"	2.27	4.38
AOD.7a	"	"	"	"	2.40	20.7	32.7	32.45	32.7	31.0	"	2.73	5.43
AOD.7b	"	"	"	"	2.40	20.7	31.65	31.35	31.7	30.1	"	2.56	4.87
AOD.8a	"	"	"	"	3.71	20.5	28.45	28.35	28.4	27.4	"	3.17	5.22
AOD.8b	"	"	"	"	3.71	20.5	28.85	28.75	28.8	27.8	"	3.11	5.22
AOD.9a	2.26	0.150	35	0.175	3.72	20.2	31.1	31.0	30.9	29.05	C, Tr	5.74	10.2
AOD.9b	"	"	"	0.175	3.75	20.2	30.85	30.75	31.25	29.4	"	5.68	10.3
AOD.10a	"	"	"	0.150	3.68	20.2	28.35	28.25	28.35	25.7	"	9.65	14.6
AOD.10b	"	"	"	0.150	3.68	20.2	28.35	28.25	28.35	25.75	"	9.43	14.3
AOD.11a	"	"	"	0.125	3.70	20.2	27.15	27.05	27.0	22.6	"	18.80	24.9
AOD.11b	"	"	"	0.125	3.69	20.2	27.05	26.95	27.15	22.85	"	18.12	24.3
AOD.12a	"	"	"	0.100	3.69	20.2	26.85	26.75	26.85	21.8	"	22.32	28.5
AOD.12b	"	"	"	0.100	3.66	20.2	26.85	26.75	26.85	21.75	"	22.41	28.6
AOD.13a	4.95	0.146	16	0.200	3.72	20.2	31.5	31.45	31.55	30.95	C, Tr	2.93	3.19
AOD.13b	"	"	"	"	3.69	20.2	32.25	32.2	32.2	31.55	"	3.09	3.46
AOD.14a	"	"	"	"	3.67	20.2	28.8	28.7	28.8	27.85	O, Tr	3.58	4.87
AOD.14b	"	"	"	"	3.71	20.2	28.75	28.65	29.0	28.0	"	3.78	5.21
AOD.15a	10.95	0.159	7	"	3.70	19.2	24.15	24.10	24.1	23.85	C, Tr	2.78	1.16
AOD.15b	"	"	"	"	3.71	19.2	24.6	24.55	24.4	24.15	"	2.73	1.16
AOD.16a	"	"	"	"	3.73	19.2	23.6	23.5	23.6	22.9	O, Tr	2.66	3.50
AOD.16b	"	"	"	"	3.70	19.2	23.8	23.7	23.8	23.1	"	2.61	3.48
AOD.17a	24.4	0.137	4	"	3.70	19.6	27.4	27.35	27.3	27.05	C, Tr	2.42	1.16
AOD.17b	"	"	"	"	3.70	19.6	27.65	27.60	27.65	27.4	"	2.37	1.16
AOD.18a	"	"	"	"	3.70	19.6	25.0	24.95	25.0	24.65	O, Tr	1.01	1.73
AOD.18b	"	"	"	"	3.68	19.6	25.35	25.30	25.5	25.2	"	0.81	1.44
NOD.1	2.26	0.150	35	0.20	0.99	8.8	11.4	11.4	11.4	9.4	C, Tr	3.58	3.11
NOD.2	"	"	"	0.20	2.97	6.1	14.0	14.0	14.0	23.15	"	3.46	3.95

THE 'GARDNER' COMPUTER PROGRAM FOR ZINC/NITROGEN VAPOUR/GAS MIXTURES

```
1 REM SOLUTION OF THE GARDNER OPERATING LINE FOR A ZINC/NITROGEN VAPOUR/GAS
2 REM MIXTURE ;0/04 (NB NO LEAD PRESENT)
3 PRINT "THIS WILL ERASE THE OLD DATAFILE 'Hbdata.DAT' .TO KEEP FILE PRESS"
4 PRINT "(Ctl BREAK) AND Use(RENAME) Command "
5 INPUT "CONDENSER OPERATING (TOTAL) PRESSURE,P (mmHg):"; P
6 INPUT "CONDENSER VAPOUR/GAS INLET TEMP.(<OR= 1300C IN 5C STEPS)Tv(K):"; Tv
8 INPUT "CONDENSATE TEMPERATURE ( < OR = TO 420C IN 5C STEPS),Tc(K):"; Tc
12 INPUT
15 INPUT "MASS % ZINC IN THE VAPOUR/GAS MIXTURE,Z:"; Z
16 Q := ((Z     * 28.013) / (( 28.013 * Z     ) + ( 65.38 * (100 - Z)    )))
17 REM Q IS THE MOLE FRACTION OF ZINC IN THE GAS PHASE ENTERING THE CONDENSER
18 REM file channel numbers need to be greater than 10 on nimbus
19 IF LOOKUP("hbdata.dat") THEN ERASE "hbdata.dat"
20 CREATE #11, "HBDATA.dat"
22 REM "HBDATA.dat" IS THE OUTPUT pv,Tv DATA FILE
25 OPEN #12, "VARDATA2.dat"
26 REM "VARDATA2.dat"IS THE INPUT DATA FILE HOLDING THE VARIABLES I,A,B,C,S,T
27 REM ALL PHYSICAL VARIABLE DATA IN THIS PROGRAM IS IN c.g.s. SYSTEM UNITS
30 DIM I(241), A(241), B(241), C(241), S(241), T(241)
32 FOR I := 241 TO 1 STEP - 1
34   INPUT #12, I(I), A(I), B(I), C(I), S(I), T(I)
36 NEXT I
40 CLOSE #12
41 OPEN #13, "ABDDATA2.DAT"
42 DIM Hm(305), H(305)
43 FOR I := 305 TO 1 STEP - 1
44   INPUT #13, Hm(I), H(I)
45 NEXT I
46 CLOSE #13
47 REM THAT ABDDATA2 IS THE INPUT DATA FILE HOLDING THE VARIABLES Hm AND H
48 REM WHERE Hm IS THE MEAN INTERFACIAL TEMPERATURE AND H IS THE SPECIFIC
49 REM HEAT CAPACITY OF NITROGEN AT THIS TEMPERATURE.
50 OPEN #14, "PCDATA2.DAT"
51 DIM Tc(65), M(65)
52 FOR I := 65 TO 1 STEP - 1
54   INPUT #14, Tc(I), M(I)
55 NEXT I
56 CLOSE #14
57 REM THAT "PCDATA2" IS THE INPUT DATA FILE HOLDING VALUES OF Tc AND M
58 REM WHERE M IS THE CONDENSATE ZINC SATURATION VAPOUR PRESSURE (pc)
59 DIM Y(1), B(1), H(4, 1)
60 REM Y IS EQUIVALENT TO pv, THE PARTIAL VAPOUR PRESSURE OF ZINC IN THE GAS
61 REM PHASE; B(1) IS dpv/dTV,THE GRADIENT OF THE OPERATING LINE
63 REM X IS EQUIVALENT TO Tv, THE ABSOLUTE TEMPERATURE OF THE VAPOUR/GAS
64 REM MIXTURE
70 REM N IS THE NUMBER OF DIFFERENTIAL EQUATIONS (IN THIS CASE ONE ).
110 N := 1
120 X := Tv
125 REM THAT THIS FIRST VALUE OF X IS THE CONDENSER ENTRANCE VAPOUR/GAS
126 REM TEMPERATURE.
130 X1 := - 5
131 REM TOO HUST USE SK INTERVALS AS THE VARIABLE DATA IS CALCULATED IN SUCH
132 REM INCREMENTS.
140 REM X1=STEP LENGTH IN KELVINS, HERE THE CALCULATION IS WORKING BACKWARDS
141 REM FROM A HIGH TEMPERATURE TO A LOW ONE.
150 Y(1) := Q * P
160 PRINT "TOTAL PRESSURE:"; P, "mmHg"
162 PRINT "INLET VAPOUR/GAS TEMPERATURE :"; Tv, "K"
166 PRINT "CONDENSATE TEMPERATURE :"; Tc; "K"
169 PRINT "MASS % ZINC IN THE VAPOUR/GAS MIXTURE :"; Z; "%"
170 PRINT #11, "TOTAL PRESSURE:"; P; "mmHg"
172 PRINT #11, "INLET VAPOUR/GAS TEMPERATURE :"; Tv; "K"
176 PRINT #11, "CONDENSATE TEMPERATURE :"; Tc; "K"
178 PRINT #11,
179 PRINT #11, "MASS % ZINC IN THE VAPOUR/GAS MIXTURE :"; Z; "%"
180 PRINT "Temp.,Tv", "pressure,pv",, "Error"
190 PRINT #11, "Temp.,Tv", "pressure,pv",, "Error"
200 PRINT X, Y(1),, B(1, 1)
210 PRINT #11, X, Y(1),, B(1, 1)
215 Ir := ((1573 - Tv) / 5) + 1
220 FOR J := 1 TO (241 - Ir)
230   GOSUB 5000
240   PRINT X, Y(1),, B(1, 1)
250   PRINT #11, X, Y(1),, B(1, 1)
260 NEXT J
265 CLOSE #11
270 STOP
5000 FOR I := 1 TO N
5010   H(1, I) := Y(I)
5020 NEXT I
5030 Q1 := X
5040 Q2 := X1 / 3
5050 GOSUB 6000
5060 FOR I := 1 TO N
5070   H(2, I) := B(I) * Q2
5080   Y(I) := Y(I) + H(2, I)
5090 NEXT I
5100 X := X + Q2
5110 GOSUB 6000
5120 FOR I := 1 TO N
5130   H(3, I) := B(I) * Q2
5140   Y(I) := H(1, I) +  0.5 * (H(2, I) + H(3, I))
5150 NEXT I
5160 GOSUB 6000
5170 FOR I := 1 TO N
5180   H(3, I) := B(I) * Q2
5190   Y(I) := H(1, I) +  0.375 * (H(2, I) + 3 * H(3, I))
5200 NEXT I
5210 X := Q1 +  1.5 * Q2
5220 GOSUB 6000
5230 FOR I := 1 TO N
5240   H(4, I) := B(I) * Q2
5250   Y(I) := H(1, I) +  1.5 * (H(2, I) - 3 * H(3, I) + 4 * H(4, I))
5260 NEXT I
5270 X := Q1 + X1
5280 GOSUB 6000
5290 FOR I := 1 TO N
5300   Y(I) := H(1, I) +  0.5 * (H(2, I) + B(I) * Q2 + 4 * H(4, I))
5310   H(1, I) :=  0.1 * (2 * H(2, I) - 9 * H(3, I) + 8 * H(4, I) - B(I) * Q2)
5320 NEXT I
5330 RETURN
6000 Ic := ((693 - Tc) / 5) + 1
6002 Ma := M(Ic) / P
6003 Id := 177 + ((693 - Tc) / 5)
6004 Ca := ( 4.968 * Ma /  65.38) * S(Id) * (1 - Ma)
6005 Ka := ( 1.04844e-03 * Ma / Tc) + ( 4.49221e-04 * (1 - Ma) / Tc)
6006 Da :=  3.32722e-02 * (Tc) ^  1.5 / C(Id)
6007 Ba :=  3.28703 * (M(Id) / A(Id))
6008 Bc :=  ( 3.9045e-06 * (Tc) ^  0.5) / A(Id)
6009 Bd :=  0.19363 * (1 + (Ma ^  0.5 *  0.88906)) ^ 2
6010 Be :=  0.29582 * (1 + ((1 / Ma) ^  0.5 *  1.23601)) ^ 2
6011 Ka := (Ba * Bc) / ((Bd * (1 - Ba)) + Ba) + ((1 - Ba) * T(Id)) / ((Be * Ba) + (1 - Ba))
6012 Psc := (Ca * Ka * Da / Ka)
6013 REM LINES 6000 - 6012 ARE TO CALC. THE Pr/Sc RATIO AT THE INTERFACE.
6014 Ib := ((1573 - X) / 5) + 1
6015 Aa := Y(1) / P : REM Aa IS THE MOLE FRACTION OF ZINC IN THE GAS PHASE
6016 C := ( 4.968 * Aa /  65.38) + (S(Ib) * (1 - Aa))
6017 REM C IS THE SPECIFIC HEAT CAPACITY OF THE VAPOUR/GAS MIXTURE AT Tv-cal/gC
6018 REM S(IB) IS THE CALCULATED SPECIFIC HEAT CAPACITY DATA FOR PURE NITROGEN
6019 REM GAS AT Tv (FROM COULSON AND RICHARDSON V1) - cal/gC.
6020 R := (( 1.04844e-03 * Aa * P) / (X)) + (( 4.49221e-04 * (1 - Aa) * P) / (X))
6021 REM R IS THE DENSITY OF THE VAPOUR/GAS MIXTURE AT Tv - g/cm^3
6030 D := ( 3.32722e-02 * X ^  1.5) / (C(Ib) * P)
6031 REM D IS THE DIFFUSIVITY OF THE VAPOUR/GAS MIXTURE AT Tv - cm/s
6032 REM C(IB) IS THE ' OMEGA D Za/N2 ' CONSTANT DATA FOR THE MIXTURE AT Tv
6040 N :=  3.28703 * (B(Ib) / A(Ib))
6041 REM N IS THE RATIO OF THE VISCOSITY OF ZINC TO THAT OF NITROGEN AT Tv
6042 REM B(IB) IS THE 'OMEGA MMU N2' CONSTANT DATA FOR NITROGEN AT Tv
6043 REM A(IB) IS THE 'OMEGA MMU Za' CONSTANT DATA FOR ZINC AT Tv
6046 Bb := ( 3.9045e-06 * X ^  0.5) / A(Ib)
6047 Cc :=  0.19363 * (1 + (N ^  0.5 *  0.88906)) ^ 2
6048 Dd :=  0.29582 * (1 + ((1 / N) ^  0.5 *  1.23601)) ^ 2
6050 K := (Aa * Bb) / ((Cc * (1 - Aa)) + Aa) + ((1 - Aa) * T(Ib)) / ((Dd * Aa) + (1 - Aa))
6051 REM K IS THE THERMAL CONDUCTIVITY OF THE VAPOUR/GAS MIXTURE AT Tv-cal/cmsC
6052 REM A(IB) HERE IS THE 'OMEGA MMU Za' CONSTANT DATA FOR THERMAL
6053 REM CONDUCTIVITY (THE SAME AS THE VISCOSITY OMEGA VALUES)
6054 REM T(Ib) HERE IS THE CALCULATED THERMAL CONDUCTIVITY DATA FOR PURE
6055 REM NITROGEN GAS AT Tv (FROM C&R V1) - cal/cmsC
6060 Ps := (((C * R * D / K) + Psc) / 2)
6061 REM PS IS THE BULK MEAN PRANDTL/SCHMIDT RATIO ACROSS THE GAS FILM FOR
6062 REM THE VAPOUR/GAS MIXTURE.
6063 Hm := (X + Tc) / 2
6065 Ia := ((1133 - Hm) /  2.5) + 1
6066 Ma :=  65.38 * (Aa + Ba) / 2
6067 Ff :=  28.013 * (1 - ((Aa + Ba) / 2))
6068 Gg :=  7.599e-02 * (Aa + Ba) / 2
6069 Hh := H(Ia) * (1 - ((Aa + Ba) / 2))
6070 N :=  4.968 / ((Ma + Ff) * (Gg + Hh))
6071 REM N IS THE RATIO OF THE SPECIFIC HEAT CAPACITY OF THE VAPOUR TO THAT OF
6072 REM THE MIXTURE CALCULATED AT Tb, THE MEAN INTERFACIAL TEMPERATURE,
6073 REM Hm OR Tb = (Tv + Tc)/2
6074 REM H(Ia) IS THE SPECIFIC HEAT CAPACITY OF PURE NITROGEN GAS AT Tb-cal/gC
6076 IF X = Tc THEN Y(1) = M(Ic) : GOTO 6100
6078 Gr = (1 / N) * ((P - Y(1)) / (X - Tc))
6080 B(1) := (1 - EXP(Ps ^ (2 / 3) * N * LN((P - Y(1)) / (P - M(Ic))))) * Gr
6081 REM B(1) IS THE GARDNER DIFFERENTIAL EQUATION FOR THE BULK VAPOUR/GAS
6082 REM CONDITION.
6085 REM THAT Ia, Ib, Ic, Id, Ir ARE ALGORITHMS USED SO THAT INTERMEDIATE ARRAY
6086 REM VARIABLE DATA MAY BE EXTRACTED FROM THE DATA FILES IN ACCORDANCE WITH
6087 REM THE STIPULATED INPUT VARIABLE FIGURES.
6090 RETURN
6100 END
```

ADDDATA DATA FILE

Tc	E											
373	0.24910	508	0.25270	643	0.25920	778	0.26700	913	0.27460	1048	0.28066
375.5	0.24913	510.5	0.25280	645.5	0.25935	780.5	0.26715	915.5	0.27475	1050.5	0.28073
378	0.24915	513	0.25290	648	0.25950	783	0.26730	918	0.27495	1053	0.28080
380.5	0.24918	515.5	0.25302	650.5	0.25965	785.5	0.26745	920.5	0.27505	1055.5	0.28087
383	0.24920	518	0.25314	653	0.25980	788	0.26760	923	0.27520	1058	0.28094
385.5	0.24925	520.5	0.25327	655.5	0.25992	790.5	0.26775	925.5	0.27532	1060.5	0.28102
388	0.24930	523	0.25340	658	0.26004	793	0.26790	928	0.27544	1063	0.28110
390.5	0.24935	525.5	0.25350	660.5	0.26017	795.5	0.26805	930.5	0.27557	1065.5	0.28120
393	0.24940	528	0.25360	663	0.26030	798	0.26820	933	0.27570	1068	0.28130
395.5	0.24925	530.5	0.25370	665.5	0.26045	800.5	0.26835	935.5	0.27582	1070.5	0.28140
398	0.24950	533	0.25380	668	0.26060	803	0.26850	938	0.27594	1073	0.28150
400.5	0.24955	535.5	0.25390	670.5	0.26075	805.5	0.26865	940.5	0.27607	1075.5	0.28158
403	0.24960	538	0.25400	673	0.26090	808	0.26880	943	0.27620	1078	0.28165
405.5	0.24965	540.5	0.25410	675.5	0.26102	810.5	0.26895	945.5	0.27632	1080.5	0.28172
408	0.24970	543	0.25420	678	0.26114	813	0.26910	948	0.27644	1083	0.28180
410.5	0.24975	545.5	0.25432	680.5	0.26127	815.5	0.26922	950.5	0.27657	1085.5	0.28187
413	0.24980	548	0.25444	683	0.26140	818	0.26934	953	0.27670	1088	0.28194
415.5	0.24987	550.5	0.25457	685.5	0.26155	820.5	0.26947	955.5	0.27680	1090.5	0.28202
418	0.24995	553	0.25470	688	0.26170	823	0.26960	958	0.27690	1093	0.28210
420.5	0.25003	555.5	0.25480	690.5	0.26185	825.5	0.26975	960.5	0.27700	1095.5	0.28215
423	0.25010	558	0.25490	693	0.26200	828	0.26990	963	0.27710	1098	0.28220
425.5	0.25015	560.5	0.25500	695.5	0.26215	830.5	0.27005	965.5	0.27722	1100.5	0.28225
428	0.25020	563	0.25510	698	0.26230	833	0.27020	968	0.27734	1103	0.28230
430.5	0.25025	565.5	0.25522	700.5	0.26245	835.5	0.27035	970.5	0.27747	1105.5	0.28237
433	0.25030	568	0.25534	703	0.26260	838	0 .27050	973	0.27760	1108	0.28245
435.5	0.25035	570.5	0.25547	705.5	0.26275	840.5	0.27065	975.5	0.27772	1110.5	0.28253
438	0.25040	573	0.25560	708	0.26290	843	0.27080	978	0.27784	1113	0.28260
440.5	0.25045	575.5	0.25572	710.5	0.26305	845.5	0.27095	980.5	0.27797	1115.5	0.28265
443	0.25050	578	0.25584	713	0.26320	848	0.27110	983	0.27810	1118	0.28270
445.5	0.25054	580.5	0.25597	715.5	0.26335	850.5	0.27125	985.5	0.27820	1120.5	0.28275
448	0.25065	583	0.25610	718	0.26350	853	0.27140	988	0.27830	1123	0.28280
450.5	0.25073	585.5	0.25622	720.5	0.26365	855.5	0.27152	990.5	0.27840	1125.5	0.28285
453	0.25080	588	0.25634	723	0.26380	858	0.27164	993	0.27850	1128	0.28290
455.5	0.25088	590.5	0.25647	725.5	0.26392	860.5	0.27177	995.5	0.27860	1130.5	0.28295
458	0.25095	593	0.25660	728	0.26404	863	0.27190	998	0.27870	1133	0.28300
460.5	0.25103	595.5	0.25672	730.5	0.26417	865.5	0.27205	1000.5	0.27880		
463	0.25110	598	0.25684	733	0.26430	868	0.27220	1003	0.27890		
465.5	0.25122	600.5	0.25697	735.5	0.26445	870.5	0.27235	1005.5	0.27900		
468	0.25134	603	0.25710	738	0.26460	873	0.27250	1008	0.27910		
470.5	0.25147	605.5	0.25722	740.5	0.26475	875.5	0.27262	1010.5	0.27920		
473	0.25160	608	0.25734	743	0.26490	878	0.27274	1013	0.27930		
475.5	0.25165	610.5	0.25747	745.5	0.26505	880.5	0.27287	1015.5	0.27940		
478	0.25170	613	0.25760	748	0.26520	883	0.27300	1018	0.27950		
480.5	0.25175	615.5	0.25772	750.5	0.26535	885.5	0.27315	1020.5	0.27960		
483	0.25180	618	0.25784	753	0.26550	888	0.27330	1023	0.27970		
485.5	0.25190	620.5	0.25797	755.5	0.26565	890.5	0.27345	1025.5	0.27980		
488	0.25200	623	0.25810	758	0.26580	893	0.27360	1028	0.27990		
490.5	0.25210	625.5	0.25825	760.5	0.26595	895.5	0.27372	1030.5	0.28000		
493	0 25220	628	0.25840	763	0.26610	898	0.27384	1033	0.28010		
495.5	0.25228	630.5	0.25855	765.5	0.26625	900.5	0.27397	1035.5	0.28020		
498	0.25235	633	0.25870	768	0.26640	903	0.27410	1038	0.28030		
500.5	0.25243	635.5	0.25882	770.5	0.26655	905.5	0.27422	1040.5	0.28040		
503	0.25250	638	0 25894	773	0.26670	908	0.27434	1043	0.28050		
505.5	0.25260	640.5	0.25907	775.5	0.26685	910.5	0.27447	1045.5	0.28058		

PCDATA DATA FILE

Tc(E)	pc(mmHg)		
373	7.20e-10	538	2.40e-04
378	1.15e-09	543	3.17e-04
383	1.95e-09	548	4.20e-04
388	3.30e-09	553	5.40e-04
393	5.60e-09	558	7.20e-04
398	9.10e-09	563	9.20e-04
403	1.50e-08	568	1.14e-03
408	2.40e-08	573	1.42e-03
413	4.00e-08	578	1.78e-03
418	6.80e-08	583	2.30e-03
423	1.00e-07	588	2.80e-03
428	1.50e-07	593	3.50e-03
433	2.20e-07	598	4.55e-03
438	3.40e-07	603	5.60e-03
443	5.00e-07	608	6.90e-03
448	7.50e-07	613	8.50e-03
453	1.08e-06	618	1.03e-02
458	1.55e-06	623	1.28e-02
463	2.20e-06	628	1.53e-02
468	3.10e-06	633	2.18e-02
473	4.50e-06	638	2.22e-02
478	6.50e-06	643	2.72e-02
483	9.20e-06	648	3.35e-02
488	1.20e-05	653	4.10e-02
493	1.63e-05	658	4.90e-02
498	2.26e-05	663	5.90e-02
503	3.10e-05	668	7.20e-02
508	4.15e-05	673	8.20e-02
513	5.80e-05	678	9.50e-02
518	8.20e-05	683	0.110
523	1.05e-04	688	0.128
528	1.39e-04	693	0.156
533	1.80e-04		

VARDATA DATA FILE

I	A	B	C	S	T
373	2.8594	0.9661	1.3959	0.2491	7.489e-05
378	2.8461	0.9644	1.3872	.24918	7.523e-05
383	2.8329	0.9628	1.3786	.24926	7.595e-05
388	2.8197	0.9612	1.3700	.24933	7.667e-05
393	2.8065	0.9596	1.3614	0.2494	7.743e-05
398	2.7941	0.9562	1.3535	0.2495	7.818e-05
403	2.7818	0.9528	1.3457	0.2496	7.905e-05
408	2.7694	0.9493	1 3379	0.2497	8.025e-05
413	2.7571	0.9458	1.3301	0.2498	8.078e-05
418	2.7452	0.9435	1.3231	.24982	8.128e-05
423	2.7334	0.9413	1.3160	.25004	8.240e-05
428	2.7217	0.9391	1.3089	.25016	8.312e-05
433	2.7101	0.9369	1.3018	0.2503	8.365e-05
438	2.6983	0.9348	1.2951	.25042	8.431e-05
443	2.6865	0.9328	1.2885	.25054	8.479e-05
448	2.6748	0.9307	1.2819	.26066	8.574e-05
453	2.6631	0.9287	1.2753	0.2508	8.651e-05
458	2.6516	0.9269	1.2695	0.2510	8.718e-05
463	2.6403	0.9252	1.2637	0.2512	8.789e-05
468	2.6290	0.9235	1.2579	0.2514	8.861e-05
473	2.6177	0.9217	1.2521	0.2516	8.962e-05
478	2.6076	0.9201	1.2464	.25175	9.028e-05
483	2.5974	0.9184	1.2408	.25198	9.100e-05
488	2.5872	0.9167	1.2352	.25205	9.195e-05
493	2.577	0.915	1.2296	0.2522	9.252e-05
498	2.5670	0.9134	1.2945	.25238	9.315e-05
503	2.5568	0.9117	1.2894	.25256	9.386e-05
508	2.5466	0.9100	1.2845	.25274	9.458e-05
513	2.5364	0.9083	1.2894	0.2529	9.536e-05
518	2.5262	0.9067	1.2847	.25312	9.601e-05
523	2.5159	0.9050	1.2800	.25334	9.673e-05
528	2.5058	0.9034	1.1952	.25356	9.744e-05
533	2.4957	0.9017	1.1904	0.2538	9.798e-05
538	2.4864	0.9001	1.1858	.25402	9.864e-05
543	2.4770	0.8985	1.1815	.25424	9.936e-05
548	2.4676	0.8969	1.1771	.25446	1.001e-04
553	2.4582	0.8953	1.1727	0.2547	1.008e-04
558	2.4488	0.8940	1.1686	.25492	1.015e-04
563	2.4397	0.8927	1.1645	.25514	1.020e-04
568	2.4304	0.8914	1.1604	.25536	1.029e-04
573	2.4211	0.8901	1.1563	0.2556	1.035e-04
578	2.3118	0.8889	1.1526	.25585	1.041e-04
583	2.3025	0.8876	1.1488	0.2561	1.046e-04
588	2.2933	0.8863	1.1450	.25635	1.053e-04
593	2.2841	0.885	1.1412	0.2566	1.058e-04
598	2.2753	0.8837	1.1378	.25685	1.065e-04
603	2.2666	0.8824	1.1343	0.2571	1.075e-04
608	2 2579	0.8810	1.1309	.25735	1.080e-04
613	2.2492	0.8798	1.1274	0.2576	1.086e-04
618	2.2408	0.8785	1.1241	.25787	1.092e-04
623	2.2326	0.8772	1.1207	.25814	1.089e-04
628	2 2243	0.8759	1.1173	.25841	1.106e-04
633	2 2160	0.8746	1.1139	0.2587	1.112e-04
638	2.2076	0.8735	1.1108	.25897	1.118e-04
643	2.2993	0 8723	1.1076	.25924	1.123e-04
648	2 2910	0.8712	1 1045	.25951	1.127e-04
653	2.2827	0.8701	1.1013	0.2598	1.133e-04
658	2.2746	0.8691	1.0982	.26007	1.139e-04
663	2.2664	0.8681	1.0952	.26034	1.146e-04
668	2.2583	0.8670	1.0922	.26061	1.151e-04
673	2.2502	0.8660	1.0892	0.2609	1.157e-04
678	2.2426	0.8657	1.0865	.26117	1.163e-04
683	2.2351	0.8645	1.0838	.26144	1.170e-04
688	2.2275	0.8632	1.0811	.26171	1.175e-04
693	2.2200	0.8619	1.0784	0.2620	1.178e-04
698	2.2125	0.8611	1.0759	0.2623	1.182e-04
703	2.2049	0.8603	1.0733	0.2626	1.192e-04
708	2.1973	0.8595	1.0707	0.2629	1.197e-04
713	2.1897	0.8588	1.0681	0.2632	1.207e-04
718	2.1822	0.8575	1.0656	.26347	1.216e-04
723	2.1756	0.8562	1.0630	.26374	1.218e-04
728	2.1671	0.8549	1.0604	.26401	1.224e-04
733	2.1596	0.8536	1.0578	0.2643	1.231e-04
738	2.1527	0.8527	1.0555	0.2646	1.238e-04
743	2.1458	0.8519	1.0532	0.2649	1.244e-04
748	2.1389	0.8510	1.0509	0.2652	1.249e-04
753	2.1320	0.8501	1.0486	0.2655	1.258e-04
758	2.1251	0.8492	1.0453	0.2658	1.266e-04
763	2.1183	0.8484	1.0431	0.2661	1.271e-04
768	2.1115	0.8475	1.0410	0.2664	1.275e-04
773	2.1047	0.8467	1.0389	0.2667	1.282e-04
778	2.0979	0.8458	1.0373	0.2670	1.290e-04
783	2.0911	0.8450	1.0352	0.2673	1.297e-04
788	2.0843	0.8441	1.0331	0.2676	1.304e-04
793	2.0775	0.8432	1.0310	0.2679	1.310e-04
798	2.0710	0.8473	1.0289	0.2682	1.316e-04
803	2.0646	0.8414	1.0268	0.2685	1.328e-04
808	2.0581	0.8405	1.0247	0.2688	1.330e-04
813	2.0516	0.8397	1.0226	0.2691	1.335e-04
818	2.0454	0.8391	1.0206	.26837	1.339e-04
823	2.0392	0.8383	1.0186	.26864	1.347e-04
828	2.0330	0.8374	1.0166	.26891	1.357e-04
833	2.0268	0.8365	1.0146	0.2702	1.360e-04
838	2.0205	0.8358	1.0137	0.2705	1.364e-04
843	2.0143	0.8350	1.0119	0.2708	1.376e-04
848	2.0081	0.8342	1.0090	0.2711	1.381e-04
853	2.0019	0.8335	1.0072	0.2714	1.384e-04
858	1.9959	0.8328	1.0044	.27167	1.388e-04
863	1.9898	0.8320	1.0036	.27194	1.395e-04
868	1.9837	0.8302	1.0019	.27221	1.404e-04
873	1.9776	0.8305	1.0001	0.2725	1.409e-04
878	1.9720	0.8298	0.9985	.27277	1.416e-04
883	1.9665	0.8291	0.9968	.27304	1.421e-04
888	1.9610	0.8283	0.9951	.27331	1.431e-04
893	1.9555	0.8275	0.9934	0.2736	1.435e-04
898	1.9498	0.8268	0.9917	.27385	1.440e-04
903	1.9442	0.8261	0.9901	.27410	1.450e-04
908	1.9386	0.8253	0.9884	.27435	1.457e-04
913	1.9330	0.8245	0.9867	0.2746	1.464e-04
918	1.9275	0.8240	0.9841	.27487	1.467e-04
923	1.9221	0.8236	0.9835	.27514	1.476e-04
928	1.9167	0.8231	0.9820	.27541	1.481e-04
933	1.9113	0.8226	0.9805	0.2757	1.486e-04
938	1.9061	0.8221	0.9790	.27595	1.495e-04
943	1.9010	0.8217	0.9775	.27520	1.502e-04
948	1.8959	0.8212	0.9760	.27545	1.507e-04
953	1.8908	0.8208	0.9746	0.2767	1.512e-04
958	1.8858	0.8203	0.9732	.27692	1.518e-04
963	1.8808	0.8199	0.9718	.27718	1.526e-04
968	1.8758	0.8195	0.9704	0.2774	1.529e-04
973	1.8708	0.8191	0.9690	0.2776	1.536e-04
978	1.8658	0.8186	0.9677	.27782	1.545e-04
983	1.8608	0.8182	0.9663	.27804	1.550e-04
988	1.8558	0.8178	0.9649	.27826	1.555e-04
993	1.8508	0.8173	0.9635	0.2785	1.560e-04
998	1.8460	0.8168	0.9622	0.2787	1.567e-04
1003	1.8412	0.8163	0.9608	0.2789	1.572e-04
1008	1.8364	0.8159	0.9594	0.2791	1.579e-04
1013	1.8316	0.8155	0.9580	0.2793	1.582e-04
1018	1.8270	0.8150	0.9567	0.2795	1.591e-04
1023	1.8225	0.8146	0.9555	0.2797	1.600e-04
1028	1.8179	0.8142	0.9543	0.2799	1.603e-04
1033	1.8134	0.8138	0.9530	0.2801	1.610e-04
1038	1.8089	0.8134	0.9417	0.2819	1.618e-04
1043	1.8043	0.8130	0.9405	0.2847	1.622e-04
1048	1.7997	0.8125	0.9493	0.2865	1.627e-04
1053	1.7951	0.8120	0.9481	0.2888	1.636e-04
1058	1.7906	0.8116	0.9469	.28887	1.643e-04
1063	1.7862	0.8111	0.9457	.28114	1.648e-04
1068	1.7818	0.8107	0.9445	.28131	1.653e-04
1073	1.7773	0.8102	0.9433	0.2815	1.663e-04
1078	1.7732	0.8097	0.9332	.28165	1.667e-04
1083	1.7690	0.8093	0.9310	.28180	1.674e-04
1088	1.7649	0.8089	0.9399	.28195	1.679e-04
1093	1.7608	0.8084	0.9387	0.2821	1.687e-04
1098	1.7566	0.8079	0.9376	.28223	1.693e-04
1103	1.7525	0.8075	0.9364	.28236	1.698e-04
1108	1.7484	0.8071	0.9353	.28249	1.703e-04
1113	1.7443	0.8067	0.9342	0.2826	1.714e-04
1118	1.7402	0.8063	0.9332	0.2827	1.720e-04
1123	1.7361	0.8059	0.9322	0.2829	1.722e-04
1128	1.7320	0.8054	0.9311	0.2829	1.732e-04
1133	1.7279	0.8050	0.9300	0.2830	1.739e-04
1138	1.7241	0.8045	0.9290	.28300	1.746e-04
1143	1.7202	0.8040	0.9280	.28316	1.751e-04
1148	1.7164	0.8035	0.9269	.28323	1.758e-04
1153	1.7125	0.8031	0.9259	0.2833	1.765e-04
1158	1.7088	0.8027	0.9249	.28335	1.770e-04
1163	1.7051	0.8023	0.9239	0.2834	1.775e-04
1168	1.7014	0.8019	0.9229	.28345	1.784e-04
1173	1.6977	0.8014	0.9219	0.2835	1.791e-04
1178	1.6940	0.8010	0.9209	.28355	1.796e-04
1183	1.6902	0.8005	0.9199	0.2836	1.801e-04
1188	1.6865	0.8001	0.9189	.28365	1.810e-04
1193	1.6827	0.7996	0.9179	0.2837	1.815e-04
1198	1.6791	0.7992	0.9170	.28375	1.822e-04
1203	1.6755	0.7987	0.9160	0.2838	1.827e-04
1208	1.6719	0.7983	0.9151	.28375	1.834e-04
1213	1.6683	0.7978	0.9141	0.2837	1.839e-04
1218	1.6649	0.7974	0.9132	0.2836	1.844e-04
1223	1.6615	0.7970	0.9123	.28365	1.851e-04
1228	1.6580	0.7966	0.9114	.28363	1.858e-04
1233	1.6546	0.7961	0.9105	0.2836	1.863e-04
1238	1.6512	0.7956	0.9096	.28355	1.870e-04
1243	1.6477	0.7951	0.9087	0.2835	1.875e-04
1248	1.6443	0.7947	0.9078	.28345	1.884e-04
1253	1.6408	0.7943	0.9069	0.2834	1.889e-04
1258	1.6374	0.7939	0.9061	.28333	1.894e-04
1263	1.6340	0.7935	0.9052	.28324	1.906e-04
1268	1.6306	0.7931	0.9044	.28317	1.911e-04
1273	1.6272	0.7925	0.9035	0.2831	1.915e-04
1278	1.6241	0.7921	0.9026	0.2830	1.923e-04
1283	1.6209	0.7917	0.9017	0.2829	1.930e-04
1288	1.6178	0.7912	0.9008	0.2828	1.935e-04
1293	1.6146	0.7907	0.9000	0.2827	1.939e-04
1298	1.6115	0.7903	0.8992	.28255	1.947e-04
1303	1.6083	0.7899	0.8984	0.2824	1.951e-04
1308	1.6052	0.7894	0.8976	.28225	1.958e-04
1313	1.6020	0.7890	0.8968	0.2821	1.966e-04
1318	1.5989	0.7886	0.8960	.28195	1.970e-04
1323	1.5958	0.7882	0.8952	0.2818	1.978e-04
1328	1.5926	0.7777	0.8944	.28165	1.982e-04
1333	1.5895	0.7872	0.8936	0.2815	1.987e-04
1338	1.5866	0.7868	0.8928	.28128	1.997e-04
1343	1.5837	0.7863	0.8920	.28106	2.004e-04
1348	1.5808	0.7858	0.8913	.28184	2.009e-04
1353	1.5779	0.7854	0.8905	0.2806	2.016e-04
1358	1.5751	0.7850	0.8897	.28035	2.023e-04
1363	1.5723	0.7846	0.8890	0.2801	2.030e-04
1368	1.5694	0.7842	0.8883	0.2785	2.035e-04
1373	1.5666	0.7837	0.8875	0.2796	2.040e-04
1378	1.5638	0.7833	0.8867	.27935	2.049e-04
1383	1.5609	0.7828	0.8860	0.2791	2.054e-04
1388	1.5581	0.7824	0.8852	.27885	2.057e-04
1393	1.5552	0.7819	0.8845	0.2786	2.066e-04
1398	1.5525	0.7817	0.8838	0.2783	2.076e-04
1403	1.5497	0.7815	0.8831	0.2780	2.080e-04
1408	1.5470	0.7812	0.8824	0.2776	2.085e-04
1413	1.5442	0.7810	0.8817	0.2773	2.090e-04
1418	1.5416	0.7804	0.8811	.27695	2.097e-04
1423	1.5390	0.7798	0.8804	0.2766	2.102e-04
1428	1.5363	0.7791	0.8797	.27625	2.107e-04
1433	1.5337	0.7784	0.8790	0.2759	2.119e-04
1438	1.5312	0.7780	0.8783	0.2755	2.123e-04
1443	1.5288	0.7775	0.8776	0.2751	2.128e-04
1448	1.5263	0.7771	0.8769	0.2747	2.134e-04
1453	1.5238	0.7766	0.8762	0.2743	2.142e-04
1458	1.5211	0.7762	0.8746	0.2739	2.150e-04
1463	1.5184	0.7757	0.8749	0.2735	2.157e-04
1468	1.5156	0.7752	0.8742	0.2731	2.165e-04
1473	1.5129	0.7748	0.8735	0.2726	2.171e-04
1478	1.5105	0.7744	0.8729	0.2721	2.176e-04
1483	1.5081	0.7740	0.8722	0.2716	2.183e-04
1488	1.5057	0.7735	0.8716	0.2711	2.190e-04
1493	1.5033	0.7730	0.8709	0.2707	2.195e-04
1498	1.5009	0.7726	0.8703	0.2702	2.200e-04
1503	1.4986	0.7722	0.8696	0.2697	2.204e-04
1508	1.4962	0.7718	0 8689	0.2692	2.212e-04
1513	1.4938	0.7713	0.8683	0 2686	2.221e-04
1518	1.4914	0.7709	0.8677	.26805	2.224e-04
1523	1.4890	0.7705	0.8671	0.2675	2.233e-04
1528	1.4866	0.7701	0.8665	.26695	2.240e-04
1533	1.4842	0.7695	0.8659	0.2664	2.245e-04
1538	1.4819	0.7691	0.8653	0.2658	2.250e-04
1543	1.4797	0.7686	0.8647	0.2652	2.255e-04
1548	1.4774	0.7681	0.8641	0.2646	2.263e-04
1553	1.4751	0.7677	0.8635	0.2639	2.269e-04
1558	1.4729	0.7673	0.8629	.26325	2.274e-04
1563	1.4706	0.7668	0.8623	0.2626	2.286e-04
1568	1.4684	0.7664	0.8617	.26195	2.293e-04
1573	1.4661	0.7660	0.8611	0.2613	2.295e-04

TOTAL PRESSURE= 30 cmHg
INLET VAPOUR/GAS TEMPERATURE = 1473 K
CONDENSATE TEMPERATURE = 693 K
MASS FLOWRATE OF THE VAPOUR/GAS MIXTURE= 50 kg/hr
MASS % ZINC IN THE VAPOUR/GAS MIXTURE = 97 %

Temp.,Tv	pressure,pv	Error
1473	27.9003	0
1468	27.96257	6.211922e-08
1463	27.94459	8.586795e-08
1458	27.92636	1.9297e-07
1453	27.90786	-2.635643e-08
1448	27.8891	4.484318e-08
1443	27.87006	3.348185e-08
1438	27.85075	2.193265e-08
1433	27.83116	2.844253e-08
1428	27.81128	1.006294e-07
1423	27.79111	5.927868e-08
1418	27.77064	7.096678e-08
1413	27.74986	9.974464e-08
1408	27.72876	8.172356e-08
1403	27.70735	9.220894e-08
1398	27.68561	-3.236346e-08
1393	27.66354	2.090353e-07
1388	27.64112	9.033829e-08
1383	27.61836	1.876615e-08
1378	27.59525	5.867332e-08
1373	27.57177	7.897616e-08
1368	27.54793	-1.264736e-07
1363	27.52371	2.330168e-07
1358	27.4991	7.720665e-08
1353	27.47409	7.188497e-08
1348	27.44869	2.129884e-07
1343	27.42286	-6.845221e-08
1338	27.39663	-1.379888e-06
1333	27.36999	1.594331e-06
1328	27.34288	1.489428e-07
1323	27.31531	-2.449378e-08
1318	27.28729	1.178673e-07
1313	27.25879	6.853597e-08
1308	27.2298	1.384783e-07
1303	27.20033	1.110137e-07
1298	27.17035	7.884483e-08
1293	27.13984	1.388682e-07
1288	27.10881	7.850112e-08
1283	27.07723	5.783514e-08
1278	27.0451	1.138626e-07
1273	27.0124	1.288951e-07
1268	26.97912	2.244488e-08
1263	26.94523	7.189811e-08
1258	26.91074	2.181157e-07
1253	26.87561	9.84488e-08
1248	26.83984	6.165356e-08
1243	26.80341	1.584886e-07
1238	26.7663	8.642673e-08
1233	26.7285	1.287884e-07
1228	26.68999	1.2042e-07
1223	26.65074	1.878478e-07
1218	26.61074	1.598689e-07
1213	26.56997	1.574867e-07
1208	26.52841	7.981435e-08
1203	26.48603	1.798002e-07
1198	26.44282	7.24569e-08
1193	26.39876	1.798384e-07
1188	26.35381	9.369165e-08
1183	26.30797	2.226792e-07
1178	26.26119	1.287888e-07
1173	26.21346	1.143664e-07
1168	26.16474	1.881178e-07
1163	26.11502	2.719462e-07
1158	26.06425	1.367182e-07
1153	26.01242	1.445413e-07
1148	25.95948	1.944602e-07
1143	25.90542	2.717589e-07
1138	25.85019	-3.390814e-08
1133	25.79376	1.966953e-07
1128	25.7361	2.741814e-07
1123	25.67717	5.237758e-07
1118	25.61692	1.192893e-08
1113	25.55532	3.324822e-07
1108	25.49232	5.995855e-07
1103	25.42788	1.797453e-07
1098	25.36196	1.758337e-07
1093	25.29451	3.352761e-07
1088	25.22548	3.142282e-07
1083	25.15481	5.819276e-06
1078	25.0823	-3.015623e-07
1073	25.00811	-5.333871e-06
1068	24.93226	7.431954e-07
1063	24.85454	2.624467e-07
1058	24.77492	3.023073e-07
1053	24.69333	5.700007e-07
1048	24.60965	6.854534e-06
1043	24.52366	5.697887e-06
1038	24.43536	-2.93348e-06
1033	24.34492	-8.751824e-06
1028	24.25235	5.777825e-07
1023	24.15737	1.248522e-07
1018	24.05987	1.181568e-06
1013	23.95977	1.182313e-06
1008	23.85685	-4.954636e-08
1003	23.75136	7.029623e-07
998	23.64287	3.255904e-07
993	23.53138	8.806586e-07
988	23.41677	3.937632e-07
983	23.31396	-3.002664e-03
978	23.26982	3.059434e-03
973	23.14537	1.595542e-06
968	23.01848	1.114234e-06
963	22.88763	4.135072e-08
958	22.75211	1.425296e-06
953	22.61312	9.726733e-07
948	22.46992	-1.734495e-06
943	22.3224	6.988645e-07
938	22.17031	4.334748e-06
933	22.01338	2.469495e-06
928	21.85146	7.662922e-07
923	21.6844	8.683652e-07
918	21.51195	4.301965e-06
913	21.33383	-1.798943e-06
908	21.14995	1.899153e-06
903	20.95994	2.016872e-06
898	20.76356	4.149973e-06
893	20.56046	1.139194e-06
888	20.35045	1.631677e-07
883	20.13322	4.643947e-06
878	19.90835	1.166016e-06
873	19.67559	3.21269e-06
868	19.43452	1.747161e-06
863	19.18481	5.271286e-06
858	18.92596	6.362796e-06
853	18.65755	-1.978874e-06
848	18.37937	-3.427267e-07
843	18.09092	-1.297146e-06
838	17.79169	1.121536e-05
833	17.48088	3.960729e-06
828	17.15817	-1.15484e-06
823	16.82307	1.016334e-05
818	16.47471	7.578731e-06
813	16.11256	9.141863e-07
808	15.73611	2.367795e-06
803	15.34468	-3.799796e-06
798	14.93758	1.519769e-05
793	14.51363	8.709729e-06
788	14.07215	6.076694e-06
783	13.61231	9.371341e-06
778	13.13311	1.017749e-05
773	12.63354	1.35392e-05
768	12.11245	1.078397e-05
763	11.56803	6.483495e-06
758	11.00156	5.264581e-06
753	10.40934	1.121163e-05
748	9.790503	2.373904e-05
743	9.143215	5.748868e-06
738	8.466864	1.155883e-05
733	7.756761	1.022116e-05
728	7.012633	1.769364e-05
723	6.230649	7.551909e-06
718	5.407141	-7.390976e-06
713	4.536696	4.132986e-05
708	3.609833	5.450845e-05
703	2.612559	2.277493e-05
698	1.515197	1.567453e-04
693	0.156	0

APPENDIX 4: COMPUTER PROGRAM PREDICTIONS

Key:
G = Gardner Equation (No. 2.2.23)
B = Bras Equation (No. 2.2.27)
CR = Cairns and Roper Equation (No. 2.2.28)
Zn = Zinc
Pb = Lead
N = Nitrogen
Het. = Heterogeneous
Homo. = Homogeneous

A) Zinc Condensation in Zinc/Nitrogen Mixtures

Serial No.	P (mm Hg)	t_{vl} (°C)	p_{vl} (mm Hg)	Zn (%)	N (%)	t_c (°C)	p_c (mm Hg)	t_{vl} (°C)	Heterogeneous p_{vl} (mm Hg)	Fog Loss (%)	Equilibrium Loss (%)
GZn.1	1	1300	0.93	97.0	3.0	420	0.156	425	0.18	0.23	1.33
GZn.2	5	"	4.67	"	"	"	"	522	2.33	6.04	0.23
GZn.3	10	"	9.33	"	"	"	"	565	5.62	9.16	0.11
GZn.4	30	"	28.00	"	"	"	"	630	20.06	14.53	0.04
GZn.5	50	"	46.67	"	"	"	"	664	35.50	17.65	0.02
GZn.6	1	1200	0.93	"	"	"	"	430	0.21	0.53	1.33
GZn.7	5	"	4.67	"	"	"	"	527	2.56	7.34	0.23
GZn.8	10	"	9.33	"	"	"	"	568	6.05	10.94	0.11
GZn.9	30	"	28.00	"	"	"	"	634	21.20	17.35	0.04
GZn.10	50	"	46.67	"	"	"	"	667	37.20	20.96	0.02
GZn.11	1	1100	0.93	"	"	"	"	435	0.24	0.93	1.33
GZn.12	5	"	4.67	"	"	"	"	530	2.80	8.91	0.23
GZn.13	10	"	9.33	"	"	"	"	572	6.51	13.35	0.11
GZn.14	30	"	28.00	"	"	"	"	637	22.41	21.28	0.04
GZn.15	50	"	46.67	"	"	"	"	670	38.97	25.48	0.02
GZn.16	1	1300	0.56	75.0	25.0	"	"	NO	FOG	0.00	14.38
GZn.17	5	"	2.81	"	"	"	"	440	0.28	2.16	2.51
GZn.18	10	"	5.63	"	"	"	"	483	0.89	6.37	1.23
GZn.19	30	"	16.88	"	"	"	"	552	4.45	13.14	0.41
GZn.20	50	"	28.13	"	"	"	"	585	8.80	16.38	0.24
GZn.21	1	1200	0.56	"	"	"	"	NO	FOG	0.00	14.38
GZn.22	5	"	2.81	"	"	"	"	445	0.32	2.95	2.51
GZn.23	10	"	5.63	"	"	"	"	490	1.05	7.89	1.23
GZn.24	30	"	16.88	"	"	"	"	558	5.09	15.49	0.41
GZn.25	50	"	28.13	"	"	"	"	593	10.05	19.33	0.24
GZn.26	1	1100	0.56	"	"	"	"	NO	FOG	0.00	14.38
GZn.27	5	"	2.81	"	"	"	"	452	0.40	4.17	2.51
GZn.28	10	"	5.63	"	"	"	"	496	1.23	9.63	1.23
GZn.29	30	"	16.88	"	"	"	"	567	5.95	18.84	0.41
GZn.30	50	"	28.13	"	"	"	"	600	11.53	23.07	0.24
GZn.31	1	1300	0.30	50.0	50.0	"	"	NO	FOG	0.00	43.14
GZn.32	5	"	1.50	"	"	"	"	NO	FOG	0.00	7.52
GZn.33	10	"	3.00	"	"	"	"	435	0.27	2.73	3.70
GZn.34	30	"	9.00	"	"	"	"	500	1.36	9.86	1.22
GZn.35	50	"	15.00	"	"	"	"	530	2.83	13.26	0.73
GZn.36	1	1200	0.30	"	"	"	"	NO	FOG	0.00	43.14
GZn.37	5	"	1.50	"	"	"	"	426	0.18	1.20	7.52
GZn.38	10	"	3.00	"	"	"	"	442	0.31	3.64	3.70
GZn.39	30	"	9.00	"	"	"	"	507	1.60	11.93	1.22
GZn.40	50	"	15.00	"	"	"	"	540	3.35	16.00	0.73
GZn.41	1	1100	0.30	"	"	"	"	NO	FOG	0.00	43.14
GZn.42	5	"	1.50	"	"	"	"	427	0.19	1.45	7.52
GZn.43	10	"	3.00	"	"	"	"	448	0.35	4.64	3.70
GZn.44	30	"	9.00	"	"	"	"	515	1.90	14.55	1.22
GZn.45	50	"	15.00	"	"	"	"	545	3.87	18.86	0.73

GZn.46	2	1300	0.13	25.0	75.0	420	0.156	NO FOG / NO CONDENSATION			100.00
GZn.47	5	"	0.63	"	"	"	"	NO	FOG	0.00	22.55
GZn.48	10	"	1.25	"	"	"	"	NO	FOG	0.00	11.10
GZn.49	30	"	3.75	"	"	"	"	445	0.29	3.15	3.66
GZn.50	50	"	6.25	"	"	"	"	470	0.66	7.18	2.19
GZn.51	2	1200	0.13	"	"	"	"	NO FOG / NO CONDENSATION			100.00
GZn.52	5	"	0.63	"	"	"	"	NO	FOG	0.00	22.55
GZn.53	10	"	1.25	"	"	"	"	NO	FOG	0.00	11.10
GZn.54	30	"	3.75	"	"	"	"	446	0.34	4.37	3.66
GZn.55	50	"	6.25	"	"	"	"	477	0.80	9.19	2.19
GZn.56	2	1100	0.13	"	"	"	"	NO FOG / NO CONDENSATION			100.00
GZn.57	5	"	0.63	"	"	"	"	NO	FOG	0.00	22.55
GZn.58	10	"	1.25	"	"	"	"	NO	FOG	0.00	11.10
GZn.59	30	"	3.75	"	"	"	"	447	0.39	5.63	3.66
GZn.60	50	"	6.25	"	"	"	"	485	0.95	11.38	2.19
GZn.61	1	1200	0.93	97.0	3.0	350	0.013	465	0.52	7.66	0.093
GZn.62	5	"	4.67	"	"	"	"	535	3.25	13.28	0.018
GZn.63	10	"	9.33	"	"	"	"	575	7.02	16.79	0.009
GZn.64	30	"	28.00	"	"	"	"	640	22.91	23.11	0.003
GZn.65	50	"	46.67	"	"	"	"	670	39.30	26.23	0.002
GZn.66	1	1200	0.93	"	"	440	0.285	NO	FOG	0.00	2.88
GZn.67	5	"	4.67	"	"	"	"	520	2.20	5.24	0.44
GZn.68	10	"	9.33	"	"	"	"	560	5.27	7.82	0.21
GZn.69	30	"	28.00	"	"	"	"	630	19.89	14.14	0.07
GZn.70	50	"	46.67	"	"	"	"	665	36.05	18.61	0.04
GZn.71	1	1200	0.93	"	"	460	0.493	NO	FOG	0.00	7.02
GZn.72	5	"	4.67	"	"	"	"	505	1.54	2.44	0.79
GZn.73	10	"	9.33	"	"	"	"	555	4.67	5.96	0.37
GZn.74	30	"	28.00	"	"	"	"	627	19.05	12.44	0.12
GZn.75	50	"	46.67	"	"	"	"	662	34.50	16.00	0.07
GZn.76	1	1200	0.56	75.0	25.0	350	0.013	405	0.10	7.14	1.007
GZn.77	5	"	2.81	"	"	"	"	480	0.84	15.43	0.200
GZn.78	10	"	5.63	"	"	"	"	515	2.01	19.40	0.100
GZn.79	30	"	16.88	"	"	"	"	580	7.58	26.23	0.033
GZn.80	50	"	28.13	"	"	"	"	610	13.76	29.51	0.020
GZn.81	1	"	0.56	"	"	440	0.285	NO	FOG	0.00	31.01
GZn.82	5	"	2.81	"	"	"	"	NO	FOG	0.00	4.70
GZn.83	10	"	5.63	"	"	"	"	485	0.93	5.70	2.28
GZn.84	30	"	16.88	"	"	"	"	540	3.42	9.25	0.75
GZn.85	50	"	28.13	"	"	"	"	575	7.28	12.80	0.45
GZn.86	1	"	0.56	"	"	460	0.493	NO	FOG	0.00	75.65
GZn.87	5	"	2.81	"	"	"	"	NO	FOG	0.00	8.51
GZn.88	10	"	5.63	"	"	"	"	NO	FOG	0.00	4.03
GZn.89	30	"	16.88	"	"	"	"	530	2.75	6.56	1.30
GZn.90	50	"	28.13	"	"	"	"	568	6.35	10.54	0.78
GZn.91	1	"	0.30	50.0	50.0	350	0.013	375	0.03	4.69	3.025
GZn.92	5	"	1.50	"	"	"	"	440	0.29	13.72	0.599
GZn.93	10	"	3.00	"	"	"	"	475	0.73	18.10	0.299
GZn.94	30	"	9.00	"	"	"	"	535	2.95	25.37	0.100
GZn.95	50	"	15.00	"	"	"	"	570	5.62	29.48	0.060

GZn.96	1	1200	0.30	50.0	50.0	440	0.285	NO	FOG	0.00	93.03
GZn.97	5	"	1.50	"	"	"	"	NO	FOG	0.00	14.11
GZn.98	10	"	3.00	"	"	"	"	NO	FOG	0.00	6.85
GZn.99	30	"	9.00	"	"	"	"	466	0.68	3.13	2.24
GZn.100	50	"	15.00	"	"	"	"	518	1.85	7.63	1.34
GZn.101	1	"	0.30	"	"	460	0.493	NO FOG / NO CONDENSATION			100.00
GZn.102	5	"	1.50	"	"	"	"	NO	FOG	0.00	25.53
GZn.103	10	"	3.00	"	"	"	"	NO	FOG	0.00	12.10
GZn.104	30	"	9.00	"	"	"	"	465	0.56	0.52	3.90
GZn.105	50	"	15.00	"	"	"	"	500	1.39	4.33	2.32
GZn.106	1	"	0.13	25.0	75.0	350	0.013	355	0.02	1.58	9.076
GZn.107	5	"	0.63	"	"	"	"	400	0.08	9.44	1.80
GZn.108	10	"	1.25	"	"	"	"	430	0.21	13.83	0.90
GZn.109	30	"	3.75	"	"	"	"	482	0.89	21.11	0.30
GZn.110	50	"	6.25	"	"	"	"	520	1.80	25.95	0.18
GZn.111	1	"	0.13	"	"	440	0.285	NO FOG / NO CONDENSATION			100.00
GZn.112	5	"	0.63	"	"	"	"	NO	FOG	0.00	23.93
GZn.113	10	"	1.25	"	"	"	"	NO	FOG	0.00	20.54
GZn.114	30	"	3.75	"	"	"	"	NO	FOG	0.00	6.72
GZn.115	50	"	6.25	"	"	"	"	448	0.35	0.92	4.01
GZn.116	1	"	0.13	"	"	460	0.493	NO FOG / NO CONDENSATION			100.00
GZn.117	5	"	0.63	"	"	"	"	NO	FOG	0.00	76.59
GZn.118	10	"	1.25	"	"	"	"	NO	FOG	0.00	36.31
GZn.119	30	"	3.75	"	"	"	"	NO	FOG	0.00	11.70
GZn.120	50	"	6.25	"	"	"	"	NO	FOG	0.00	6.97

BZn.1	1	1300	0.93	97.0	3.0	420	0.156	460	0.48	5.39	1.33
BZn.2	5	"	4.67	"	"	"	"	537	3.29	13.59	0.23
BZn.3	10	"	9.33	"	"	"	"	576	7.12	17.73	0.11
BZn.4	30	"	28.00	"	"	"	"	639	23.15	24.36	0.04
BZn.5	50	"	46.67	"	"	"	"	671	39.70	27.80	0.02
BZn.6	1	1200	0.93	"	"	"	"	461	0.51	6.09	1.33
BZn.7	5	"	4.67	"	"	"	"	540	3.44	15.67	0.23
BZn.8	10	"	9.33	"	"	"	"	578	7.40	20.43	0.11
BZn.9	30	"	28.00	"	"	"	"	641	23.83	27.84	0.04
BZn.10	50	"	46.67	"	"	"	"	673	40.72	31.65	0.02
BZn.11	1	1100	0.93	"	"	"	"	464	0.55	7.63	1.33
BZn.12	5	"	4.67	"	"	"	"	543	3.61	18.51	0.23
BZn.13	10	"	9.33	"	"	"	"	579	7.65	23.38	0.11
BZn.14	30	"	28.00	"	"	"	"	642	24.50	32.12	0.04
BZn.15	50	"	46.67	"	"	"	"	675	41.79	36.72	0.02
BZn.16	1	1300	0.73	86.0	14.0	"	"	NO	FOG	0.00	7.02
BZn.17	5	"	3.62	"	"	"	"	486	0.99	8.16	1.22
BZn.18	10	"	7.25	"	"	"	"	530	2.72	13.59	0.60
BZn.19	30	"	21.74	"	"	"	"	597	10.95	21.64	0.20
BZn.20	50	"	36.23	"	"	"	"	631	20.20	25.64	0.12
BZn.21	1	1200	0.73	"	"	"	"	NO	FOG	0.00	7.02
BZn.22	5	"	3.62	"	"	"	"	493	1.17	10.38	1.22
BZn.23	10	"	7.25	"	"	"	"	535	3.05	16.07	0.60
BZn.24	30	"	21.74	"	"	"	"	602	12.00	25.13	0.20
BZn.25	50	"	36.23	"	"	"	"	636	21.90	29.49	0.12

BZn.26	1	1100	0.73	86.0	14.0	420	0.156	NO	FOG	0.00	7.02
BZn.27	5	"	3.62	"	"	"	"	500	1.36	12.97	1.22
BZn.28	10	"	7.25	"	"	"	"	540	3.43	19.23	0.60
BZn.29	30	"	21.74	"	"	"	"	607	13.18	29.57	0.20
BZn.30	50	"	36.23	"	"	"	"	641	23.85	34.53	0.12
BZn.31	1	1300	0.56	75.0	25.0	"	"	NO	FOG	0.00	14.38
BZn.32	5	"	2.81	"	"	"	"	430	0.21	0.97	2.51
BZn.33	10	"	5.63	"	"	"	"	490	1.06	8.00	1.23
BZn.34	30	"	16.88	"	"	"	"	560	5.36	16.53	0.41
BZn.35	50	"	28.13	"	"	"	"	596	10.70	20.94	0.24
BZn.36	1	1200	0.56	"	"	"	"	NO	FOG	0.00	14.38
BZn.37	5	"	2.81	"	"	"	"	435	0.26	1.73	2.51
BZn.38	10	"	5.63	"	"	"	"	497	1.26	9.98	1.23
BZn.39	30	"	16.88	"	"	"	"	567	6.15	19.65	0.41
BZn.40	50	"	28.13	"	"	"	"	603	12.10	24.59	0.24
BZn.41	1	1100	0.56	"	"	"	"	NO	FOG	0.00	14.38
BZn.42	5	"	2.81	"	"	"	"	445	0.45	5.10	2.51
BZn.43	10	"	5.63	"	"	"	"	506	1.55	13.04	1.23
BZn.44	30	"	16.88	"	"	"	"	575	7.17	24.03	0.41
BZn.45	50	"	28.13	"	"	"	"	610	13.81	29.43	0.24
CRZn.1	1	1300	0.93	97.0	3.0	"	"	460	0.48	5.41	1.33
CRZn.2	5	"	4.67	"	"	"	"	542	3.57	17.79	0.23
CRZn.3	10	"	9.33	"	"	"	"	578	7.60	22.74	0.11
CRZn.4	30	"	28.00	"	"	"	"	642	24.32	30.87	0.04
CRZn.5	50	"	46.67	"	"	"	"	674	41.46	35.02	0.02
CRZn.6	1	1200	0.93	"	"	"	"	464	0.53	6.94	1.33
CRZn.7	5	"	4.67	"	"	"	"	545	3.70	20.40	0.23
CRZn.8	10	"	9.33	"	"	"	"	580	7.91	27.21	0.11
CRZn.9	30	"	28.00	"	"	"	"	643	24.85	34.79	0.04
CRZn.10	50	"	46.67	"	"	"	"	675	42.23	39.20	0.02
CRZn.11	1	1100	0.93	"	"	"	"	466	0.57	8.23	1.33
CRZn.12	5	"	4.67	"	"	"	"	546	3.83	23.40	0.23
CRZn.13	10	"	9.33	"	"	"	"	581	8.04	29.50	0.11
CRZn.14	30	"	28.00	"	"	"	"	644	25.38	39.62	0.04
CRZn.15	50	"	46.67	"	"	"	"	676	43.02	44.47	0.02
CRZn.16	1	1300	0.73	86.0	14.0	"	"	NO	FOG	0.00	7.02
CRZn.17	5	"	3.62	"	"	"	"	487	0.99	8.16	1.22
CRZn.18	10	"	7.25	"	"	"	"	528	2.63	12.96	0.60
CRZn.19	30	"	21.74	"	"	"	"	596.5	10.75	21.02	0.20
CRZn.20	50	"	36.23	"	"	"	"	630	19.92	25.03	0.12
CRZn.21	1	1200	0.73	"	"	"	"	NO	FOG	0.00	7.02
CRZn.22	5	"	3.62	"	"	"	"	492	1.12	9.74	1.22
CRZn.23	10	"	7.25	"	"	"	"	533	2.94	15.22	0.60
CRZn.24	30	"	21.74	"	"	"	"	602	11.82	24.50	0.20
CRZn.25	50	"	36.23	"	"	"	"	635	21.63	28.84	0.12
CRZn.26	1	1100	0.73	"	"	"	"	NO	FOG	0.00	7.02
CRZn.27	5	"	3.62	"	"	"	"	497	1.29	11.92	1.22
CRZn.28	10	"	7.25	"	"	"	"	540	3.34	18.46	0.60
CRZn.29	30	"	21.74	"	"	"	"	606	12.97	28.74	0.20
CRZn.30	50	"	36.23	"	"	"	"	640	23.58	33.79	0.12

CRZn.31	1	1300	0.56	75.0	25.0	420	0.156	NO	FOG	0.00	14.38
CRZn.32	5	"	2.81	"	"	"	"	450	0.38	3.86	2.51
CRZn.33	10	"	5.63	"	"	"	"	495	1.19	9.28	1.23
CRZn.34	30	"	16.88	"	"	"	"	560	5.46	16.89	0.41
CRZn.35	50	"	28.13	"	"	"	"	595	10.70	20.93	0.24
CRZn.36	1	1200	0.56	"	"	"	"	NO	FOG	0.00	14.38
CRZn.37	5	"	2.81	"	"	"	"	455	0.44	4.97	2.51
CRZn.38	10	"	5.63	"	"	"	"	500	1.36	11.01	1.23
CRZn.39	30	"	16.88	"	"	"	"	567	6.20	19.86	0.41
CRZn.40	50	"	28.13	"	"	"	"	602	12.05	24.46	0.24
CRZn.41	1	1100	0.56	"	"	"	"	NO	FOG	0.00	14.38
CRZn.42	5	"	2.81	"	"	"	"	462	0.53	6.62	2.51
CRZn.43	10	"	5.63	"	"	"	"	506	1.58	13.37	1.23
CRZn.44	30	"	16.88	"	"	"	"	575	7.11	23.74	0.41
CRZn.45	50	"	28.13	"	"	"	"	609	13.59	28.79	0.24

B) Lead Condensation in Zinc/Lead/Nitrogen Mixtures

69.3% Zn/27.7% Pb = AN IMPERIAL SMELTING FURNACE CONCENTRATE
93.8% Zn/3.2% Pb = A TYPICAL ZINC CONCENTRATE

Serial No.	P (mm Hg)	t_{vi} (°C)	p_{vi} (mm Hg)	Zn (%)	Pb (%)	N (%)	t_c (°C)	p_c (mm Hg)	t_{vf} (°C) (Het.)	t_{vf} (°C) (Homo.)	p_{vf} (mm Hg) (Het.)	p_{vf} (mm Hg) (Homo.)	Fog Loss (%) (Het.)	Fog Loss (%) (Homo.)	Equilibrium Loss (%)
GPb.1	1	1200	0.103	69.3	27.7	3.0	420	5.6×10^{-7}	820	540	0.077	0.046	73.2	42.0	1×10^{-3}
GPb.2	5	"	0.514	"	"	"	"	"	920	632	0.427	0.295	81.4	54.7	1×10^{-4}
GPb.3	15	"	1.542	"	"	"	"	"	1000	760	1.362	1.090	87.2	68.4	3×10^{-5}
GPb.4	30	"	3.083	"	"	"	"	"	1055	835	2.830	2.365	90.9	74.7	2×10^{-5}
GPb.5	1	"	0.010	93.8	3.2	"	"	"	698	485	0.006	0.003	62.6	32.1	1×10^{-2}
GPb.6	5	"	0.050	"	"	"	"	"	778	515	0.035	0.019	70.4	37.8	1×10^{-3}
GPb.7	15	"	0.149	"	"	"	"	"	838	560	0.113	0.069	75.6	45.8	4×10^{-4}
GPb.8	30	"	0.298	"	"	"	"	"	886	625	0.236	0.164	79.3	54.9	2×10^{-4}
GPb.9	1	"	0.103	69.3	27.7	"	500	1.6×10^{-5}	806	-	0.063	-	58.8	-	1.4×10^{-2}
GPb.10	5	"	0.514	"	"	"	"	"	912	596	0.385	0.170	72.8	30.7	2.8×10^{-3}
GPb.11	15	"	1.542	"	"	"	"	"	996	732	1.290	0.864	82.1	53.2	9.5×10^{-4}
GPb.12	30	"	3.083	"	"	"	"	"	1052	816	2.732	2.050	87.5	63.9	4.7×10^{-4}
GPb.13	1	"	0.010	93.8	3.2	"	"	"	586	-	2.9×10^{-3}	-	29.0	-	0.16
GPb.14	5	"	0.050	"	"	"	"	"	768	-	2.9×10^{-2}	-	59.3	-	3.2×10^{-2}
GPb.15	15	"	0.149	"	"	"	"	"	834	520	1.0×10^{-1}	0.024	68.2	15.9	1.1×10^{-2}
GPb.16	30	"	0.298	"	"	"	"	"	876	570	2.2×10^{-1}	0.093	72.9	30.8	5.4×10^{-3}
GPb.17	1	"	0.103	69.3	27.7	"	600	4.6×10^{-4}	798	-	0.053	-	48.7	-	4×10^{-1}
GPb.18	5	"	0.514	"	"	"	"	"	906	-	0.345	-	64.6	-	8×10^{-2}
GPb.19	15	"	1.542	"	"	"	"	"	990	676	1.195	0.439	75.6	26.3	2.7×10^{-2}
GPb.20	30	"	3.083	"	"	"	"	"	1050	790	2.621	1.603	83.6	49.2	1.3×10^{-2}
GPb.21	1	"	0.010	93.8	3.2	"	"	"	676	-	3.3×10^{-3}	-	28.1	-	4.56
GPb.22	5	"	0.050	"	"	"	"	"	756	-	2.3×10^{-2}	-	44.5	-	0.91
GPb.23	15	"	0.149	"	"	"	"	"	820	-	8.3×10^{-2}	-	54.9	-	0.30
GPb.24	30	"	0.298	"	"	"	"	"	870	-	1.9×10^{-1}	-	63.5	-	0.15
GPb.25	1	"	0.103	69.3	27.7	"	700	6.4×10^{-3}	780	-	0.038	-	28.8	-	5.62
GPb.26	5	"	0.514	"	"	"	"	"	900	-	0.295	-	53.6	-	1.12
GPb.27	15	"	1.542	"	"	"	"	"	986	-	1.098	-	68.6	-	0.37
GPb.28	30	"	3.083	"	"	"	"	"	1046	-	2.484	-	78.6	-	0.19
GPb.29	1	"	0.010	93.8	3.2	"	"	"	NO		FOG				64.2
GPb.30	5	"	0.050	"	"	"	"	"	740	-	1.6×10^{-2}	-	19.5	-	12.8
GPb.31	15	"	0.149	"	"	"	"	"	806	-	6.3×10^{-2}	-	38.1	-	4.3
GPb.32	30	"	0.298	"	"	"	"	"	856	-	1.5×10^{-1}	-	49.0	-	2.1
GPb.33	1	"	0.103	69.3	27.7	"	800	5.4×10^{-2}	NO		FOG				50.0
GPb.34	5	"	0.514	"	"	"	"	"	880	-	0.225	-	31.6	-	9.6
GPb.35	15	"	1.542	"	"	"	"	"	970	-	0.944	-	55.5	-	3.2
GPb.36	30	"	3.083	"	"	"	"	"	1040	-	2.290	-	70.6	-	1.6
GPb.37	1	"	0.010	93.8	3.2	"	"	"	NO FOG / NO CONDENSATION						100.0
GPb.38	5	"	0.050	"	"	"	"	"	NO FOG / NO CONDENSATION						100.0
GPb.39	15	"	0.149	"	"	"	"	"	NO		FOG				36.2
GPb.40	30	"	0.298	"	"	"	"	"	840	-	0.116	-	20.8	-	18.1

APPENDIX 5: CONDENSER MODEL RESULTS

Four glycerol condensation runs under reduced pressure were carried out using the glass model described in section 5.4 of this work. Nitrogen was the inert carrier gas added in each experiment. For three of the experiments the cooling medium was mains water at temperatures of 14 and 17^{o}C fed on a once-through basis. The final experiment used the cooling system outlined in section 5.4 with a coolant temperature of -5^{o}C. The experimental procedure for a typical run is outlined below together with results followed by a discussion of all the experimental findings.

Referring to Figure 5.4.1 and A.5.1 the following experimental procedure was followed for Run GG.2. The whole of the vacuum side of the apparatus was evacuated using the Edwards ED50 vacuum pump after the addition of liquid nitrogen to the cold trap dewar to collect residual moisture in the equipment during the pumpdown. The two-way valve system before and after the cold traps had been adjusted so that the whole flow was directed through either trap A or B. One of the three receiver flasks was in position under the Perkins Triangle network. Coolant (water for this run) was passed through the cold finger at a flowrate of 13.6 l/min and allowed to stabilise. All of the heater elements were switched on and allowed to reach temperature. Both upstream and downstream temperature readings were taken via K-type thermocouples leading to a Foster Box Model 3156 Portable Potentiometer. Pressure readings were taken via a tilting mercury Vacustat gauge near the pump. For all four experiments residual inert gas pressures in the system were of the order of 100-200 μm. Glycerol does not boil or evaporate instantly (like water) when a vacuum is applied to the boiler at room temperature. As Figure A.5.1 illustrates, it takes about 30 minutes for the first glycerol vapour to pass through the crossover to the cooling finger. During condensation no liquid droplets form on the outer walls of the condenser vessel or on the crossover due to the heating tape windings keeping the glass at a temperature above the dewpoint of the glycerol vapour.

Over the next 60 minutes of the run the condenser collects glycerol vapour and the liquid condensate runs down into the receiver flask. Once a steady glycerol flow was running off the condenser the upstream pressure tapping's glass valve was opened and nitrogen was bled into the system. The rotameter upstream of the throttling needle valve in the inert gas line meters the nitrogen flowrate to the system and on calibration it provides an estimate of inert gas flowrate to the system. The throttling needle valve was adjusted to the point where the float in the throttling rotameter was barely moving. This corresponds to the incoming nitrogen flowrate being just higher than the combined nitrogen plus glycerol flowrate in the crossover tube. The pressure reading in the upstream vacustat gauge then registers the total pressure of the vapour/gas mixture entering the condenser. This technique also ensures that no glycerol vapour back-diffuses up the pressure tapping and condenses in the tapping or in the vacustat. If a downstream pressure tapping is required then a similar procedure is followed for that tapping. For Run GG.2 the upstream pressure tapping registered a total pressure of 1.05 mm Hg during steady state operation whereas a downstream reading of 1.00 mm Hg was recorded - the difference represents frictional pressure losses throughout the condenser.

Prior to a stable steady state condensation situation occurring the reheater was switched on to reheat the outlet vapour/gas stream (to keep it above its dewpoint) before it was captured in the cold trap. At steady state a

second receiver flask was exchanged for the first one after the vacuum line was diverted through the other cold trap. The new receiver vessel was evacuated separately through the Perkins Triangle via the ES35 vacuum pump. The second receiver flask collected glycerol condensate for 20 minutes before a third receiver flask was inserted into the system (so that the mean of two steady state condensate mass flowrates could be obtained). After a further 20 minutes the vacuum line was again switched to the other trap and the third receiver removed from the line. The boiler and electrics were switched off and the system allowed to cool down under vacuum - there is an explosive risk with glycerol under these conditions. The coolant flow was switched off and the system opened to atmosphere. The collected condensate in the receiver flask was weighed and its temperature taken along with the cold trap residue weights. For Run GG.2 the steady state experimental conditions were identical for receiver flasks 2 and 3. They were:

t_{vi}	=	136°C
t_{vo}	=	30°C
t_{cm}(Inlet)	=	14.3°C
t_{cm}(Outlet)	=	14.5°C
Coolant Water Flowrate	=	13.6 l/min
$t_{condensate}$	=	38°C
P	=	1.05 mm Hg
Condenser Inlet Mass Flowrates (g/s)	=	1.55×10^{-1} (glycerol), 1.02×10^{-3} (nitrogen)
Condenser Outlet Mass Flowrates (g/s)	=	8.3×10^{-5} (glycerol), 1.02×10^{-3} (nitrogen)
Mass % Glycerol in the Receiver Flask	=	99.95%
Mass % Glycerol in the Cold Trap	=	0.05%

These results together with a visual inspection during the run indicated that no glycerol fog formation was occurring. A Gardner computer solution of the condensation run was carried out and the predicted cooling curve is illustrated in Figure A.5.2. The computational analysis assumes a condensate interfacial temperature of 20°C. A critical supersaturation line for homogeneous nucleation is also plotted on the diagram based on a solution of the simplified Frenkel Equation (eq. 2.2.19). Also plotted on the diagram is the probable cooling curve path for the condensable mixture (glycerol being the object vapour) for this run. This deduction comes from the recorded condensate temperature of the collected condensate in the receiver flask. A condensate temperature of 38°C implies that the glycerol vapour probably condensed at 50°C, say, at the inlet region to the condenser (t_{c1}) and as the vapour/gas mixture passed down the cold finger t_c progressively fell. Here, values of t_{c2} = 42°C, t_{c3} = 33°C and t_{c4} = 24°C are chosen to illustrate the point. Hence, though the Gardner computer model predicts the cooling curve to pass into the homogeneous fog formation region, the actual cooling profile did not for the reasons cited above. Note that the simplified Frenkel equation has incorporated into it a value of the condensation coefficient, α, of 1. There is evidence in Amelin's (1967) work that for glycerol α = 0.05 under these conditions. For low values of α the derived critical supersaturations are higher than those for α = 1 thus reducing the possibility of homogeneous fog formation.

Table A.5.1 is a comparative table of the four glycerol condensation runs carried out during the testwork. For each run no fog formation was observed to occur and no solid glycerol deposits were formed though the deposit for Run GG.4 was very viscous. Some general conclusions can be drawn from these results. In all cases high glycerol recovery efficiencies in

TABLE A.5.1 SUMMARY OF TESTWORK FOR THE GLYCEROL CONDENSER MODEL

Serial Number	tvi (°C)	tvo (°C)	tcm Inlet (°C)	tcm Outlet (°C)	t Condensate (°C)	Q (coolant) (l/min)	P mmHg	Composition (Mass %) Inlet Glyc.	Inlet N2	Outlet Glyc.	Outlet N2	Mass Flowrate (g/s) Inlet Glyc.	Inlet N2	Outlet Glyc.	Outlet N2	Mass % Glycerol Receiver	Mass % Glycerol Trap
GG.1	165	30	16.85	17.00	41	14.4	3.6	97.8	2.2	6.1	93.9	1.4 e-1	3.1 e-3	2.0 e-4	3.1 e-3	99.85	0.15
GG.2	136	30	14.30	14.50	38	13.6	1.05	99.4	0.6	7.8	92.2	1.6 e-1	1.0 e-3	1.3 e-5	1.0 e-3	99.95	0.05
GG.3	138	30	14.10	14.30	39	13.6	0.95	99.5	0.5	13.7	86.3	1.6 e-1	8.7 e-4	1.7 e-4	8.7 e-4	99.90	0.10
GG.4	138	24	-5.5	-4.0	26	8.7	0.8	99.3	0.7	12.1	87.9	1.3 e-1	7.3 e-4	1.0 e-4	7.3 e-4	99.93	0.07

the condenser were found (99.8 + %) This is probably due to the condenser geometry. The bulk of the glycerol vapour condensed at the inlet region to the barrel condenser and down the inlet barrel wall. Droplets were seen to be blown away from the condenser inlet region in parabolic trajectories down the condensing wall.

This work has led to the high temperature Warner condenser installing a distributor plate at the condenser inlet to redistribute the vapour/gas mixture more evenly around the barrel condenser circumference. This also prevents the preferential build-up of a solid deposit at the crossover inlet region. For run GG.1 both upstream and downstream pressure tappings had nitrogen gas bled in. The condenser upstream pressure was 3.6 mm Hg and the downstream pressure was 3.4 mm Hg. In this run the feed mixture was more dilute and the lowest glycerol recovery efficiency of the four runs occurred. The actual contact thermal efficiency for each run was around 90% as the outlet vapour/gas mixtures were about 10°C above their dewpoint temperatures. Calculations reveal that for Gun GG.3, the Reynolds Number of the gas phase entering the condenser is 900 (i.e. laminar flow) with an inlet gas velocity of 110 m/s. The residence time of the vapour/gas mixture in the condenser is therefore very low.

FIGURE A.5.1 EXPERIMENTAL RESULTS FOR GLYCEROL CONDENSATION RUN GG.2

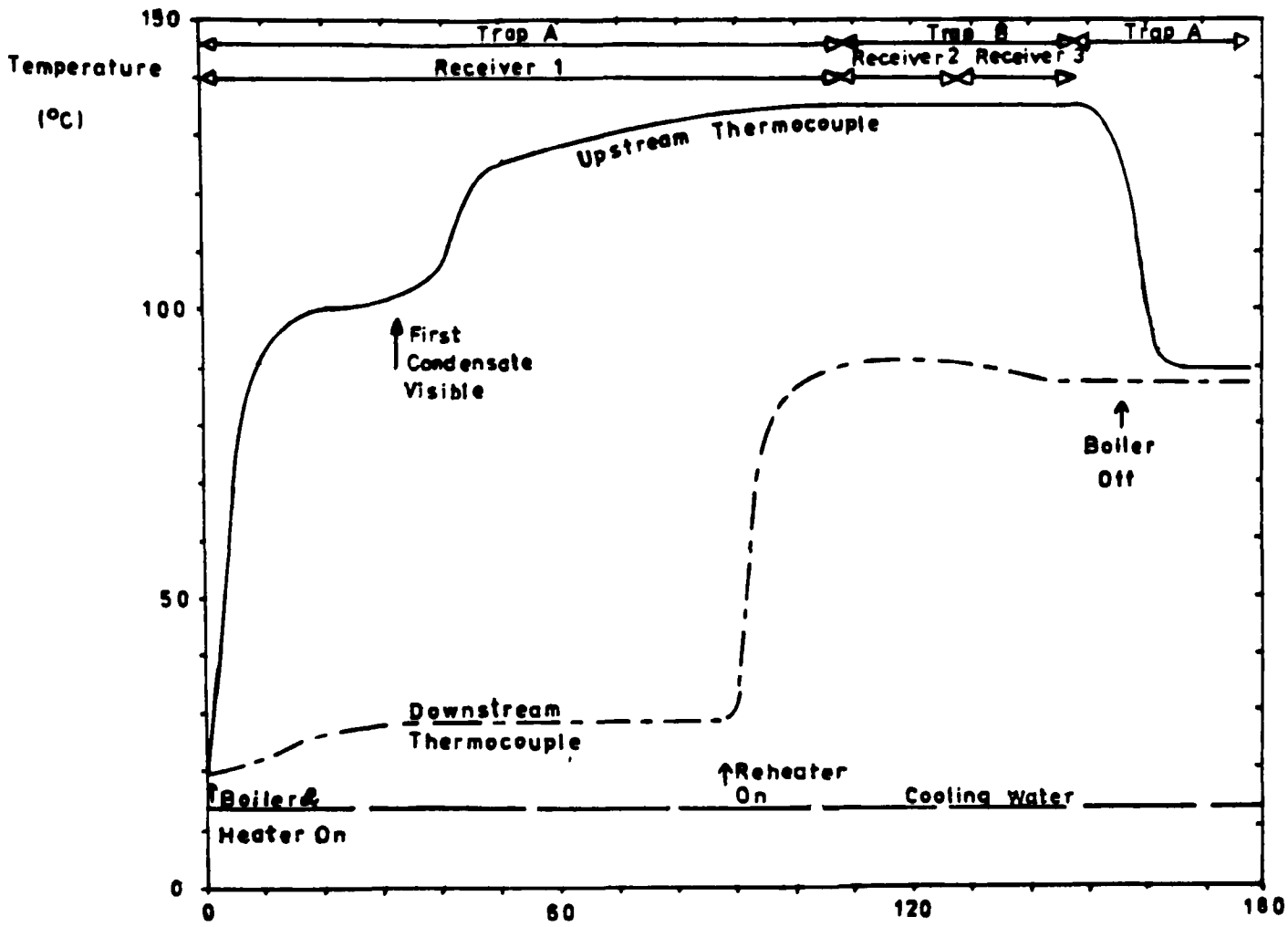

FIGURE A.5.2 COMPARISON OF THE PREDICTED COMPUTER MODEL COOLING CURVES FOR RUN GG.2 TO THE PROBABLE EXPERIMENTAL COOLING CURVE

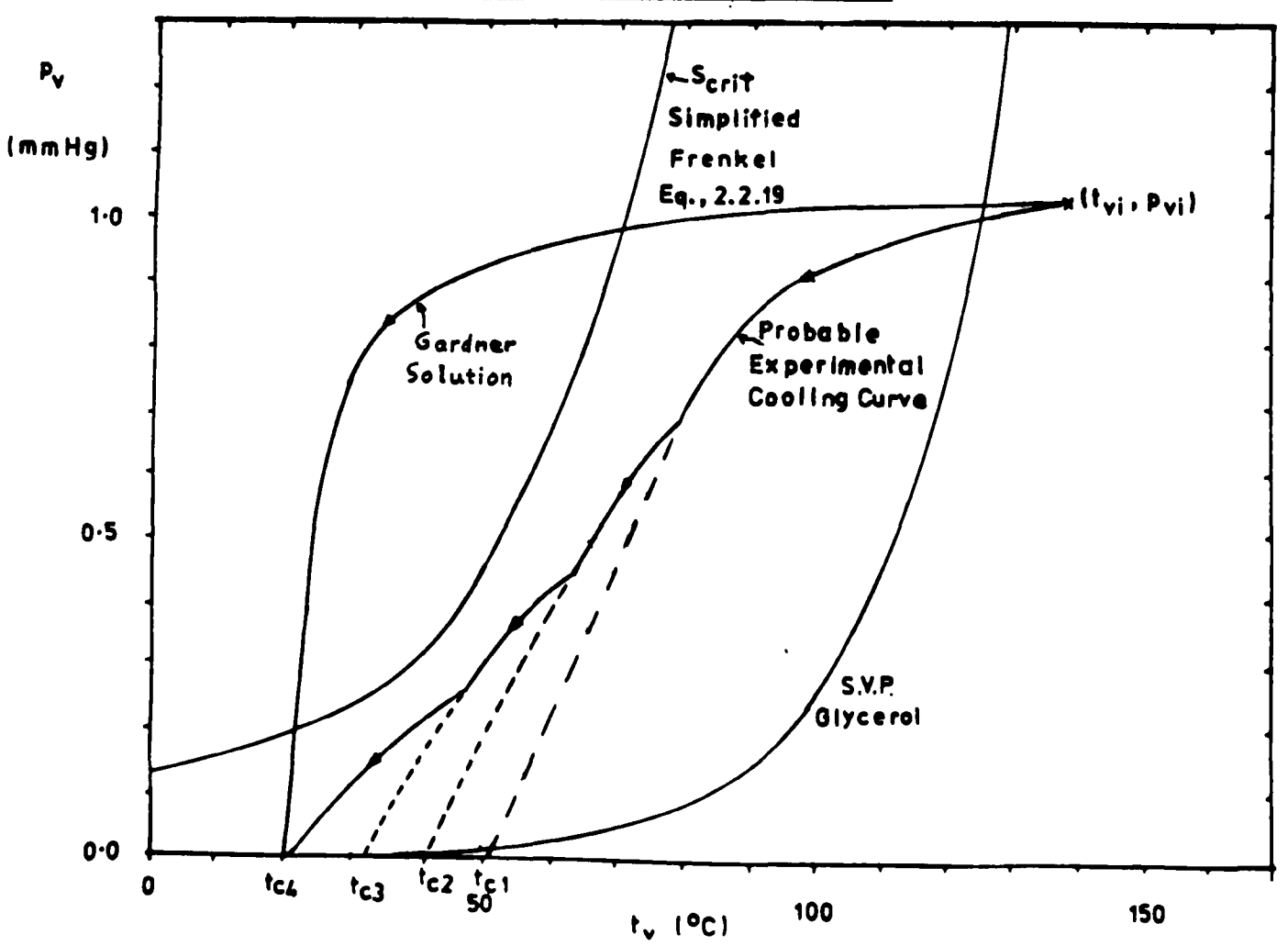

Process Requirements for the Direct Condensation of Both Zinc and Lead as Metals in the Polymetallic Smelting of Zn-Pb-Cu Sulphides

R K HANNA[1] and N A WARNER[2]

ABSTRACT

There is an inherent problem in producing simultaneously lead, zinc and copper as metals in a single polymetallic smelting furnace. It relates to the condensation of lead and zinc from the gas phase under vacuum conditions such that metals in bulk form, either solid or liquid, are obtained as products rather than a fume or dust containing both metallic and non-metallic components. To understand this phenomenon, it has been necessary to establish mathematical models with computer simulation to identify the process requirements for effecting the objective of maximum bulk metal production with minimum fog formation. The theoretical framework of simultaneous heat and mass transfer involved in condensation from gas mixtures containing a non-condensable gas has been extended to the high temperature and reduced pressure conditions. These apply to new technology for polymetallic smelting now being developed in a project currently funded jointly by the Commission of the European Communities and the Mineral Industry Research Organisation. Under the right conditions it is theoretically possible to condense out both lead and zinc with minimal fume formation, but in all practical cases it is anticipated that some circulating load for reversion back to the smelter will be needed.

INTRODUCTION

Current research into the development of a polymetallic Pb-Zn-Cu smelter to treat complex sulphide minerals (Warner, 1989a, 1989b, 1986, 1985) has led to further consideration of an age-old metallurgical problem. It has long been recognised that metallic vapours on cooling show a propensity to condense in the gas phase rather than as a condensate. This will manifest itself as metallic vapour fog formation and subsequent fume and dust problems in outlet gas streams from condensers. This pernicious problem usually necessitates the introduction of spray towers, filters or particulate entrainment systems downstream of the condensation stage to trap the resultant particles and droplets. As well as resulting in low metal recovery efficieacies and the need for a reversion operation such dusts can introduce corrosion problems downstream and constitute both an environmental and a health hazard in the surrounding regions. It would be desirable to know the point of incipient fog formation in a system thus giving an indication of the amount of metallic fog to be expected. Then, if the process operating variables can be manipulated the potential would be available to maximise or possibly eliminate a fog problem.

The possibility of metallic fog formation has been suggested by Kroll (1951) for aluminium, magnesium, zinc, lead and tin vapours condensing under vacuum. The problem has been referred to for zinc and lead vapours by Morgan (1957), Davey (1962, 1953), Alcock and Howitt (1987) and addressed by Warner (1970) following work at Avonmouth zinc smelter (*Gammon, unpublished report, 1970*). *Indeed, there are many* metallurgical operations where the mechanism of fog formation is most probably a contributing factor towards reported low metal recoveries though it is often not suspected or simply ignored until losses become too high. Moreover, the mechanism proposed by Turkdogan (1964) to explain the enhanced vaporisation of steel and subsequent red oxide fume formation is also a fogging phenomenon.

Fog and mist formation is not restricted to the metallurgical industry; it is also the bane of many processing operations in the chemical industries. Fog problems have been reported during the condensation of sulphuric acid, phosphoric acid, sulphur, steam, alcohols, ammonium compounds and various hydrocarbon compounds (Colburn and Edison, 1941; Johnstone, Kelley and McKinley, 1950; Hampson and Furman, 1953; Schuler and Abell, 1956; Sikchi, 1956; Olander, 1961; Lewin and Dalin, 1965; Amelin, 1967; Hayashi, Takimoto and Kanbe, 1976; Lekae, Kutnetsov and Myagkov, 1981; Lo Pinto, 1982). Indeed, any condensation process that involves relatively high molecular weight condensables coupled with non-condensable gases is liable to fog problems as such molecules will have low mass diffusivities in the gas phase. This will result in low rates of mass transfer relative to heat transfer; a requisite for vapour fog formation (Colburn and Edison, 1941). It is the presence of the inert gases that enhances the fogging problem since the condensable molecules must also diffuse through a boundary layer of non-condensable gas to condense on any cold surface.

DIRECT POLYMETALLIC SMELTING

A pilot-scale direct polymetallic smelter has been constructed at Birmingham University and is currently undergoing commissioning trials. The process has been well documented elsewhere (Warner, 1989a, 1989b, 1986, 1985) such that a brief outline is included here.

The smelter will treat complex Pb-Zn-Cu sulphide ore feeds producing each metal simultaneously. Figure 1 is a schematic drawing of the smelter illustrating its dual hearth nature. The two hearths are sitting side-by-side and linked by an overflow weir at one end and an RH vessel the other. Forced circulation of the matte feed in a closed loop through the 4m long hearths is induced by inert gas injection into the uplift snorkel leg when the RH vessel is dipped into the matte. The melt itself, at 1200°C, is subjected to chemical changes as it passes through an oxidation zone in the converting hearth of the smelter when it is top-blown by multiple lance oxygen jets. This produces blister copper by the following reaction:

$$Cu_2S_{(l)} + O_{2(g)} = 2Cu_{(l)} + SO_{2(g)} \qquad (1)$$

[1] Research Student

[2] Professor of Chemicals Engineering University of Birmingham PO Box 363, Edgbaston Birmingham B15 2TT United Kingdom

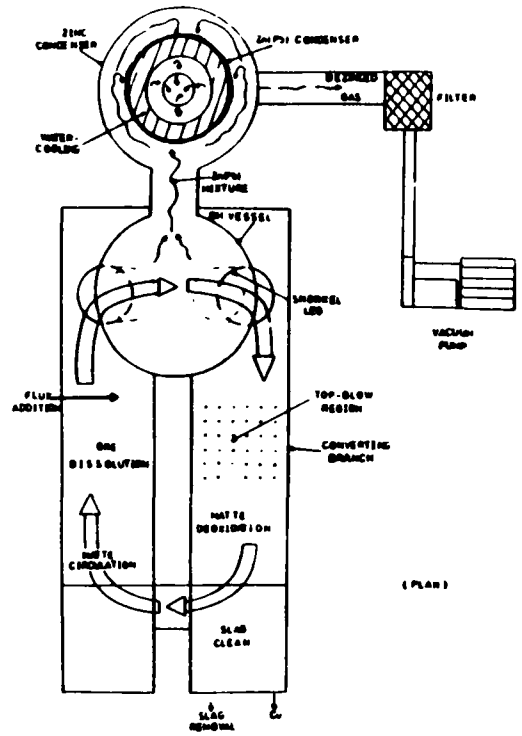

Fig 1. Schematic Layout of the Smelter

Solid charge is assimilated into the circulating matte under neutral or reducing conditions in the other hearth.

As the copper-saturated matte passes through the RH vessel it is subjected to a moderately high vacuum such that zinc and lead vapours are flashed off according to the following reactions:

$$ZnS + 2Cu = Cu_2S + Zn_{(g)} \qquad (2)$$

$$PbS + 2Cu = Cu_2S + Pb_{(g)} \qquad (3)$$

Some PbS will also be flashed off. The vapours at around 1200°C together with any inert gases from the RH vessel are cooled and collected in an adjacent water-cooled barrel condenser. Equations 2 and 3 reveal that copper matte is regenerated in the RH vessel such that the solvent is self-sustaining. Excess copper and slag from the top-blowing zone will be tapped off periodically from the smelter.

Other equilibrium changes expected to occur in the cross-over between the RH vessel and the condenser should include the following:

$$PbS_{(l,s)} + Zn_{(g)} = ZnS_{(s)} + Pb_{(l)} \qquad (4)$$

$$SO_2 + 3Zn_{(g)} = 2ZnO_{(s)} + ZnS \qquad (5)$$

These reaction products together with other particulates carried over from the RH vessel will ultimately end up in the condenser sump.

The key to the smelter lies in the forced circulation of matte resulting in the transfer of heat from sites of exothermic production to those of endothermic absorption. Thermodynamic calculations on the vacuum dezincing of matte (Warner, 1983) have indicated that the equilibrium partial pressure of zinc vapour in the RH vessel will be in the region of 60 mm Hg compared to the practical 1 - 2 mm Hg reported (Herbertson and Warner, 1974) for vacuum dezincing (VDZ) of lead in the Imperial Smelting Furnace. The significance of this is that VDZ of matte in the presently considered smelter is kinetically much more favourable than VDZ of lead. However, the mode of circulation in the proposed smelter whereby inert gas lift is utilised will ensure a higher inert gas concentration in the feed to the condenser compared to the relatively low residual inert gas concentrations associated with VDZ of lead. Calculations have also indicated that a typical condensable mixture to be treated in the condenser will have a greater than 90% zinc vapour content.

THEORETICAL BACKGROUND TO FOG FORMATION

The condensation of a vapour as droplets in the gas phase rather than on a surface is known as fog or mist formation. A fog is a suspension of fine droplets ranging from less than 1 micron up to about 10 microns in diameter (Steinmayer, 1972; Lo Pinto, 1982; Perry and Green, 1984). These droplets are sufficiently small such that they behave as a gas and are not captured by impingement devices. Globules which may be formed by the growth of fog particles, or spray that is created by the entrainment of liquid into a gas stream from the tube walls of an industrial condenser because of excessive gas speeds are classed as mists. Mists may range in size from 10 microns to a few millimeters in diameter. In terms of opacity, fogs are optically more dense than mists reducing the visual range appreciably.

Fog particles will grow because of excess saturation in a vapour/gas mixture. Sometimes this means that the gas phase is supersaturated, ie. it is below the vapour's dewpoint. At other times fog can grow on foreign nuclei at partial pressures below saturation. Either way, fogging results from an increase in the relative saturation, provided sufficient nuclei are present.

Amelin (1967) defines six different means of achieving supersaturation and subsequent formation of fog:

i) Fog formation by eddy and molecular diffusion and thermal conduction i.e. forced convective cooling, the usual industrial condensation situation.

ii) Fog formation by radiative cooling, i.e. of very high temperature condensable mixtures. (t_{vi} >2000K) (Chan, Cho and Condiff, 1980). This form of fogging is enhanced for polyatomic vapours and gases e.g. SO_3 ,H_20, NH_3 that exhibit pronounced radiation heat transfer components.

iii) Fog formation as a result of chemical reactions by vapours in a condensable mixture resulting in a product of lower vapour pressure than the reactants, e.g. in industrial sulphuric acid production.

iv) Fog formation due to the turbulent mixing of vapour/gas streams, e.g. in large scale atmospheric fog formation and also in mist formation associated with turbulent free jets.

v) Fog formation in an adiabatically expanding vapour/gas mixture, e.g. in the Wilson Cloud Chamber.

vi) Fog formation by molecular diffusion and thermal conduction, e.g. radiative fogs that form at the end of a cloudless night in regions of stagnant air (in troughs or forest clearings).

Of the six types of fog formation, types (i) to (iii) are industrially of the most relevance with type (i) being noteworthy for the extensive research devoted to it. It is also the mode of fogging considered here.

During the condensation of vapour/gas mixtures the possibility of fog formation will exist dependent upon the relative rates of vapour depletion from the gas phase and temperature decrease. Theoretically, fog can only form once the mixture becomes supersaturated. Supersaturation occurs whenever the heat transfer rate from the vapour/gas mixture to the condensation surface is too high relative to the mass transfer rate. One of the contributing factors towards this will be a high Sc/Pr ratio greater

than one. The degree of supersaturation is measured by the ratio of the actual vapour pressure of the condensable vapour in the mixture to the saturation (or equilibrium) vapour pressure at the same temperature:

$$S = \left| \frac{p_v}{p_{sat}} \right|_{t_v} \qquad (6)$$

Two different modes of fog formation can occur, namely homogeneous and heterogeneous vapour condensation:

a) Homogeneous Fog Formation

This consists of 3 distinct stages:

i) The formation of supersaturated vapour.

ii) The spontaneous nucleation of vapour embryos.

iii) The condensation of vapour onto the embryonic surfaces and the growth of the embryos to the size of fog droplets.

b) Heterogeneous Fog Formation

This can be divided into two stages:

i) The formation of supersaturated vapour.

ii) The condensation of vapour onto residual nuclei or gaseous ions present in the gas phase. These particles grow to the size of fog droplets.

Before fog can become visible by a light-scattering test, the mixture must reach a certain level of supersaturation. This level of visible fog formation is called the critical saturation ratio, S_{crit}. S_{crit} is defined as the amount of supersaturation at which embryos capable of further growth form at a rate of one per ml per second (Bras, 1955). For example, with water vapour having values of S equal to 3, 4 and 5, the time required for the formation of 1 nucleus $ml^{-1}s^{-1}$ amounts to an average of about 100,000 years, 10 seconds and 10^{-6} second respectively. S_{crit} for heterogeneous nucleation can range from the homogeneous value to $S_{crit} = 1$, i.e. the saturation criterion, for a certain level of condensation nuclei.

Amelin (1967) offers Frenkel's Formula for estimating values of homogeneous critical supersaturations:

$$s_{crit} = \exp\left\{0.56 \frac{M_v}{\rho_L}\left(\frac{\sigma_L}{t_v}\right)^{3/2}\right\} \qquad (7)$$

where

ρ_L = the liquid density at t_v (g/cm^3)

σ_L = the surface tension of the liquid at t_v (dyne/cm)

M_v = the molecular weight of the vapour (g)

and t_v = the vapour/gas temperature (K)

S_{crit} will decrease with increasing temperature and a particular value is characteristic of the specific vapour/inert gas mixture. Amelin has also shown that if free electrically charged gaseous ions are present in a mixture then droplets of fog may form even when S<1 in unsaturated mixtures. Due to the lack of uniformity of some gas mixtures in condensers S_{crit} may be reached in isolated parts of the equipment due to local temperature gradients. This will result in some local fog formation.

Foreign nuclei necessary for heterogeneous fog formation can come from various sources (Steinmayer, 1972):

1) Solids External to the Process

The obvious source is dust particles in process air streams. Air typically contains 1000 particles/ml in the 0.1 to 1.0 micron range suitable for condensation nuclei. When dust particles are completely wettable by the condensing liquid they will act like liquid droplets of the same radius.

2) Ions in Air or the Vapour/Gas Stream

Gas streams with large multiply charged ions are the most susceptible to fog condensation. Typical ordinary air contains up to 60,000 ions per cm^3 compared to a few thousand in clean air. Ions will generally decrease S_{crit} values by 10 - 20 %.

3) Entrained Liquid

The production of small droplets is inherent in evaporation and bubbling processes. Typical number densities in the 0.1 to 1.0 micron range within evaporators will be about $100/cm^3$.

4) Upstream Reactions

Probably the easiest way of ensuring an adequate nuclei count for a fog problem is to have an upstream reaction between two vapours that yields a liquid or solid of much lower vapour pressure.

5) Solids Produced by Upstream Combustion and Corrosion Products

During combustion, poor mixing of partially burned gases produces enormous amounts of foreign nuclei for downstream equipment. Moreover, any corrosion or erosion products from the process lines, if sufficiently small enough, will act as nuclei sites.

The number density of fog, N, is measured by the number of droplets/cm^3. In atmospheric air a slight fog is observed when N = 50 - 100/cm^3. A heavy fog with a visibility of less than 200m has N = 500 - 600/cm^3. Atmospheric fog has a mean drop size of 7-15 microns, N always being variable with time. The level of foreign condensation nuclei necessary to promote complete heterogeneous fog formation at $S_{crit} = 1$ will vary from system to system. Steinmayer (1972) estimates that for N = $1x10^6$ - $1x10^7$ /cm^3 in his cited examples such a threshold is reached. Beyond this threshold nuclei concentration has no further effect on the quantities of fog produced. He also estimates that for vacuum condensation operations calculated equilibrium fog droplet diameters can be expected to be smaller than those estimated for atmospheric condensation processes (4μm as opposed to 15 - 25micron).

Nusselt (1916) in his pioneering treatise on the condensation of a pure, quiescent, saturated vapour outlined the ideal situation with heat conduction through the condensate being the controlling step. Practically, forced convective heat transfer is used and the presence of a non-condensable gas such as air is almost inescapable during vapour condensation. This introduces a mass diffusion component for heat transfer above and beyond the conduction-convection component. This situation was first studied theoretically by Colburn and Drew in 1937 and subsequently by Colburn and Edison (1941). The presence of an inert gas makes vapour diffusion the rate-controlling step during condensation.

Figure 2 is a schematic representation of the overall condensation situation being considered. Colburn and Drew in their analysis derived from first principles an equation that relates the rate of change of bulk vapour composition in a vapour/gas mixture to temperature change during condensation. Their equation was subsequently modified slightly by Bras (1955) and Gardner (1957). Gardner's equation is presented below. It is a complex first order differential equation:

$$\frac{dp_v}{dt_v} = \left(\frac{1-e^{-a}}{a}\right)\left(\frac{P-p_v}{p_{BM}}\right)\left(\frac{Sc}{Pr}\right)^{-2/3}\left(\frac{p_v-p_c}{t_v-t_c}\right) \qquad (8)$$

where

$$a = \left(\frac{Pr}{Sc}\right)^{2/3}\left(\frac{M_v C p_v}{MCp}\right)\ln\left(\frac{P-p_c}{P-p_v}\right)$$

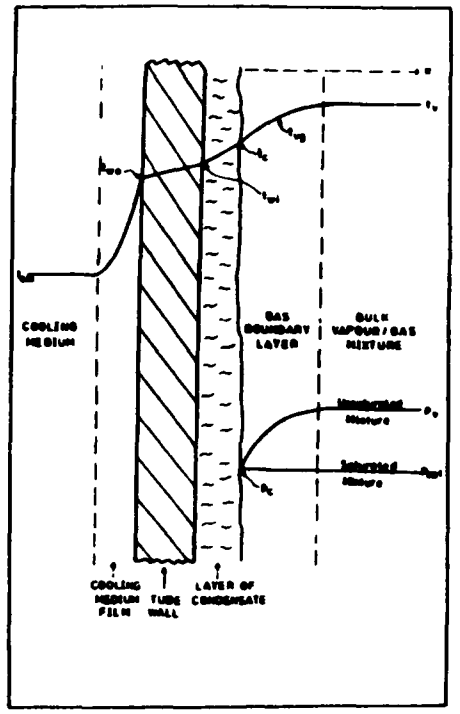

Fig 2. Schematic Diagram of Typical Profiles of Partial Vapour Pressure and Temperature near a Condenser Wall when condensing a Vapour/Gas Mixture

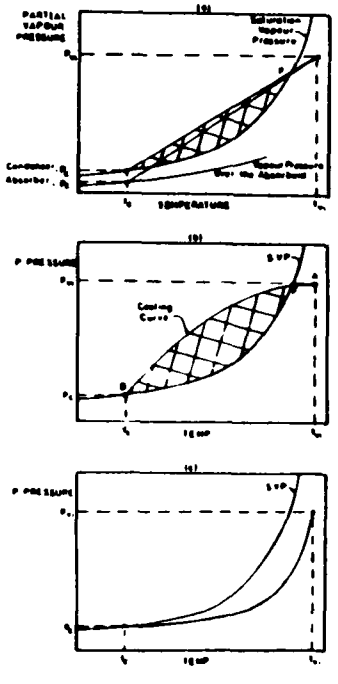

Fig 3 Different types of Vapour/Gas Cooling Curves

A solution of this equation will yield a cooling curve or operating line for a specific condensable mixture that traces the relationship between vapour pressure and temperature during the course of vapour condensation along a cold surface. Colburn and Edison have outlined the three possible cooling paths a vapour/gas mixture can follow inside a condenser or absorber. Figure 3 illustrates the general principles involved. Figure 3(a) shows the comparative effect of using a cooler absorber that uses a solvent as the cooling surface for collecting the vapour. As the solvent will have a solute vapour pressure that is lower than the saturation vapour pressure the point of incipient heterogeneous fog formation, F, will be lower than the comparable condenser situation. In Figure 3(b) the temperature and partial vapour pressure differentials between points A and B are the driving forces for the transfer of heat and mass from the vapour/gas mixture to the condenser wall. Point A represents the inlet conditions for the mixture entering the condenser whereas point B is typical of the interfacial vapour/gas conditions at the condensate interface. All points to the left of the saturation vapour pressure lines represent the regions of vapour supersaturation and conversely to the right of the lines unsaturated vapour mixtures will exist. If 100% equilibrium is reached during a condensation process then the outlet vapour/gas condition from a condenser will also be at the saturated condition, i.e. (p_{sat} ,t_{sat}).

In Figure 3(a) the cooling curves or operating lines represent the case where the heat transfer rate equals the mass transfer rate. In Figure 3(b) the heat transfer rate is greater than the mass transfer rate hence the curve bows to the left whereas in Figure 3(c) the mass transfer rate is greater than the heat transfer rate making the operating line concave. All the cross-hatched regions represent the parts of the cooling curves that are supersaturated and as such the potential for fog formation will exist given favourable nucleation kinetics. In the presence of sufficient levels of suitable condensation nuclei maximum quantities of fog formation can be expected to begin at point F on the cooling curves in Figure 3(a) and (b) where they cross the dewpoint curves. This method utilises a "worse case" approach to fogging in these systems.

Other workers in the fog field (Johnstone, Kelley and McKinley, 1950; Bras, 1955; Amelin, 1967; Rosner and Epstein, 1968) have theoretically proven that incipient homogeneous fog formation in dilute vapour/gas mixtures will always be a boundary layer phenomenon near the condenser cooling surface. This would seem to be borne out experimentally by Hampson and Furman (1953) who observed that the first sign of fog was just below pendant drops of condensate for a horizontal condenser. Toor (1971a,b) has studied fog formation in boundary value problems. With simplifying assumptions he uses the equations of energy and diffusion state to determine local rates of fog formation. He also postulates equations that illustrate the discontinuous nature of the fog formed in the boundary layer. At the interface between clear and fog regions he deduces that the fog vaporises discontinuously in parallel with continuous droplet condensation in the fog region. Quite separately, Turkdogan (1964), Hayashi, Takimoto and Kanbe (1976) and Buckle (1989) have reinforced the predictions of Toor's model in their experimental studies of induced fog condensation during the forced evaporation of vapours from sink liquids (the opposite situation to that considered in this work). The condensed metallic fog droplets produced by Buckle's experiments are collected as powders that have much wider size distributions than powders produced by atomisation techniques.

Bettelheim, Forster and Kyte (1980) have studied the localised rates of fog formation in flue gas washing plants (cooler absorbers). Here again, dilute vapour/gas mixtures were considered and predicted fog losses were of the order of 1-2%. They discovered that though fog condensation in the boundary layer has little effect on the overall rates of heat and mass

transfer, neglecting its effect in their fog models underestimated the amount of fog formed by a factor of up to three. Hence, most fog must have formed in the boundary layer. They point out that the transition from fog condensation in the boundary layer alone to full fog condensation in the bulk mixture is very rapid.

Amelin (1967) has shown that once fog forms near the surface of a tubular condenser during the condensation of a turbulent vapour/gas mixture the droplets are incapable of penetrating the turbulent core (Re>10000). They will settle out on the tube wall due to a combination of the diffusive current of vapour from the core to the condensate interface (thermophoresis) and Stefan flow (a vapour pressure gradient that causes a dynamic flow towards the wall). In laminar flows or when fog forms in the bulk and grows into a mist some of the droplets will experience Stokesian gravitational settling onto the condenser walls (Schuler and Abell, 1956, Toor, 1971 b). Davey (1953) has considered this settling effect for the zinc/lead problem and has remarked that it would have a significant effect in reducing fog losses for vertical condensation surfaces compared to horizontal ones.

In tests, Alexander and Coldren (1951) report that between 30-60% of water droplets (mean diameter 27micron) in an aerosol will attach to duct walls depending upon the superimposed gas phase velocity. The main resistance to attachment lies with the gas film near the duct walls. Hutchinson, Hewitt and Dukler (1971) have developed a stochastic attachment model for droplets in the 0.8 - 125mm range in gas flows of Re = 8×10^3 - 3×10^5. In the lower droplet size ranges low attachment to the walls was predicted. Hence, it can be said that, dependent upon the condenser geometry, a sizeable proportion of the fog formed in a condenser will be convected out whereas mist attachment near the outlet can be expected. This mist attachment effect will help to reduce overall vapour losses.

DEVELOPMENT OF A COMPUTER PROGRAM TO SOLVE THE GARDNER EQUATION

The Gardner equation, (8), cannot be solved by any explicit integration method. Instead, a numerical solution of the equation by a fourth order Runge-Kutta technique was used. The method merely requires knowledge of the inlet vapour/gas composition, the system operating pressure, P, the condensing surface conditions (p_c ,t_c), and transport properties for the condensable mixture over the cooling temperature range. The equation is solved iteratively over a specified step length decrease in temperature in the form of a "backward-marching" technique until a predetermined end-point is reached; usually (p_o, t_c). After the solution of the Gardner equation over the first iteration has been determined a new vapour composition and temperature will result. This second point is then used to again solve the Gardner equation to provide a third point on the cooling curve and so on. The error involved with a Runge-Kutta solution is very low. An optimum step length of 5°C produced the least variation in the cooling curve profile.

During the solution of the Gardner Equation both the bulk vapour/gas mixture's Sc/Pr ratio, (k/pCpD), and its specific heat ratio, (M_v .Cp_v /M.Cp), will vary at each point in the condenser. This is due to the depletion of vapour from the vapour/gas mixture as it is cooled. For the computer solution of the differential equation at each point a logarithmic mean Sc/Pr ratio across the gas film was used. The Sc/Pr ratio at t_c , the condensate interfacial temperature is assumed constant throughout the condenser, i.e. it is at steady state. The specific heat ratio for each step in the program was calculated at the arithmetic mean temperature, t_b , of the vapour/gas mixture entering the step. For example, $t_{b1} = (t_{vi} + t_c)/2$ and so on for each subsequent step. Transport properties for individual vapours and then vapour/gas mixtures at a given temperature were determined using Chapman - Enskog/Wilke equations found in textbooks like Bird, Stewart and Lightfoot (1962).

THE ANALYSIS OF A COMPUTER PROGRAM RUN

A typical computer printout will provide a list of vapour composition and temperature data. This can be plotted as a cooling curve on a partial vapour pressure/temperature axis as in Figure 4. The plot is of a computer run considering a 97% Zinc/3% nitrogen vapour/gas mixture entering a condenser at 1200°C under a total pressure of 30 mm Hg. For this run t_c =420°C i.e. the condensate interface is at the melting point of zinc. If the condenser is operating under steady state conditions this could represent a solid zinc deposit with liquid zinc running off the solid condensate.

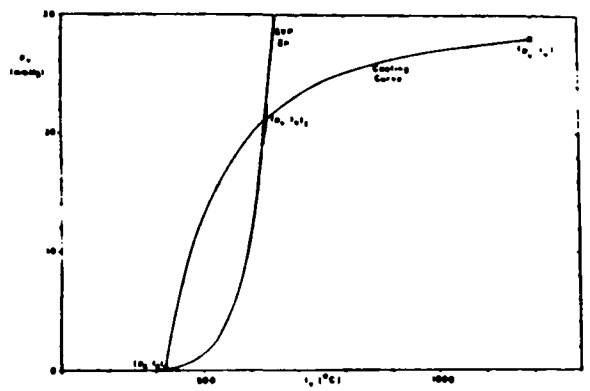

Fig 4. Graphical Plot of a Typical Computer Run

The most apparent observation from Figure 4 is the very pronounced convex nature of the cooling curve indicating that heat transfer is very much higher than mass transfer during this cooling operation. The cooling curve crosses the equilibrium line for zinc at (p_v , t_v)$_f$ where the mixture becomes saturated. This point of incipient supersaturation is also the point at which maximum heterogeneous zinc fog formation will begin as opposed to further zinc condensation on the coolant surface.

On consideration of the inlet zinc vapour partial pressure of 28 mm Hg, this corresponds to a mole fraction of 28/30 i.e. 0.93; the mole fraction of nitrogen in the mixture being 0.07. Hence, for every mole of nitrogen entering the condenser there will be 0.93/0.07 moles of zinc, i.e. 13.3 moles. The quantity of nitrogen in the condenser will not change as it is non-condensable. If it is used as a basis then at the point of incipient heterogeneous fog formation where the zinc partial vapour pressure, p_{vf} , is 21.2 mm Hg or a mole fraction of 0.7, one mole of nitrogen corresponds to 2.3 moles of zinc. Thus 11 moles of zinc have been recovered as condensate. The remaining 2.3 moles of zinc are lost from the condenser as a combination of fog and equilibrium vapour losses. The above discussion results in the following equation that gives the percentage of the original feed that ends up as fog exiting from the condenser:

$$\text{Heterogeneous Fog Loss} = \frac{\left[\frac{p_{vf}}{P-p_{vf}}\right] - \left[\frac{p_c}{P-p_c}\right]}{\left[\frac{p_{vi}}{P-p_{vi}}\right]} \times 100 \qquad (9)$$

For the 97%Zn/3%N_2 run the amount of heterogeneous fog loss amounts to 17.2%. The fraction of the inlet vapour lost due

to equilibrium considerations can be estimated as follows:

$$\text{\% Equilibrium Loss} = \frac{\left[\frac{p_c}{P-p_c}\right]}{\left[\frac{p_{vi}}{P-p_{vi}}\right]} \times 100 \qquad (10)$$

For the 97%Zn/3%N_2 run equilibrium losses amount to a mere 0.04 %. Obviously, the lower the system operating pressure is, the greater the equilibrium vapour loss will be. The total vapour loss for a given condensing system is a combination of these two constituent components. In other words the outlet gas phase from the condenser will consist of zinc mist droplets coexisting and in equilibrium with gaseous zinc atoms.

COMPUTER PREDICTIONS FOR ZINC FOG FORMATION IN ZINC/NITROGEN MIXTURES

The relatively ideal situation of zinc/nitrogen condensable mixtures was considered to help elucidate general condensing principles for high temperature mixtures under vacuum. High zinc vapour concentrations in the feed mixtures were of prime importance with the proposed smelter in mind. Initially, a range of inlet vapour temperatures were examined to assess the effect of superheat on vapour fog formation over a wide range of operating pressures up to 60mmHg. Vapour concentration in the feed mixtures was another variable that was manipulated to establish its influence on fog formation. Three different condensing temperatures were considered, namely 420, 440 and 460°C.

This main fog analysis is concerned with zinc/nitrogen mixtures. The presence of lead or possible RH vessel solid products like zinc oxides, zinc sulphides and lead sulphides would manifest themselves in terms of nuclei for heterogeneous fog formation. The method of presentation of predictions adopted here consists of choosing several inlet vapour/gas conditions in a series where only one system parameter is adjusted. Both the vapour loss as fog and the total vapour loss including fog were then plotted against the operating pressure and curves through the computer predictions drawn.

The Effect of Inlet Vapour Concentration on Fog Formation

Figures 5 to 8 depict a series of computer predictions using the Gardner Equation for Zn/N_2 condensable mixtures entering a

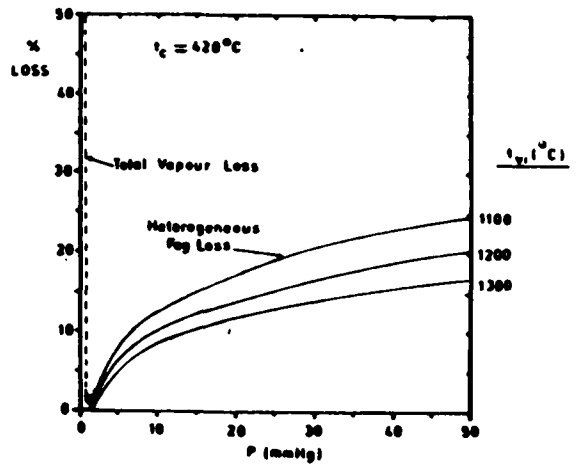

Fig 5. Predicted Zinc Vapour Loss, 97%Zn/3%N_2 Mixtures; Varying t_{vi}

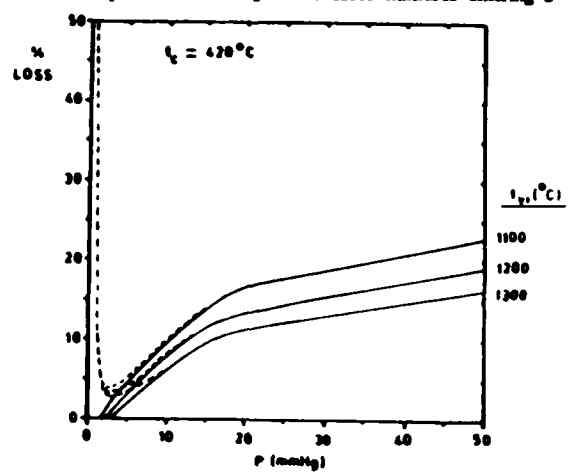

Fig 6. Predicted Zinc Vapour Loss, 75%Zn/25%N_2 Mixtures; Varying t_{vi}

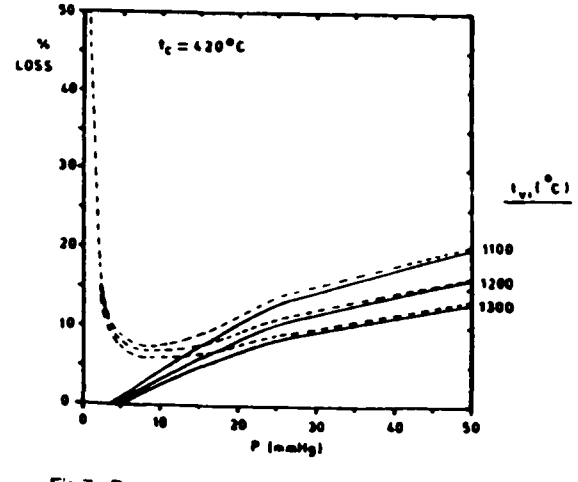

Fig 7. Predicted Zinc Vapour Loss, 50%Zn/50%N_2 Mixtures; Varying t_{vi}

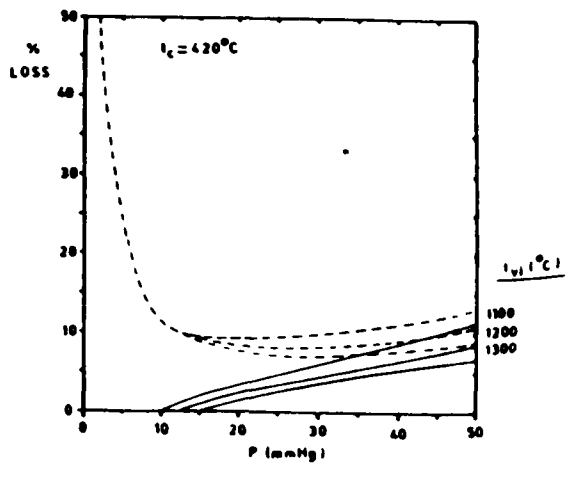

Fig 8. Predicted Zinc Vapour Loss, 25%Zn/75%N_2 Mixtures; Varying t_{vi}

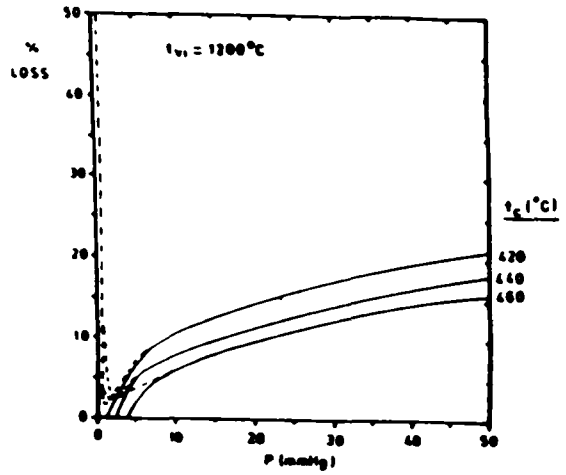

Fig 9. Predicted Zinc Vapour Loss, 97%Zn/3%N_2 Mixtures; Varying t_c

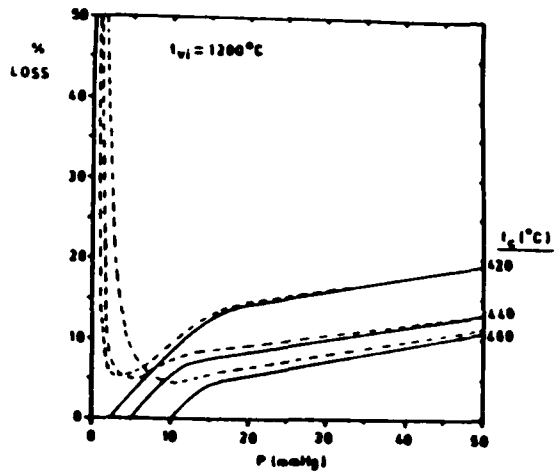

Fig 10. Predicted Zinc Vapour Loss, 75%Zn/25%N_2 Mixtures; Varying t_c

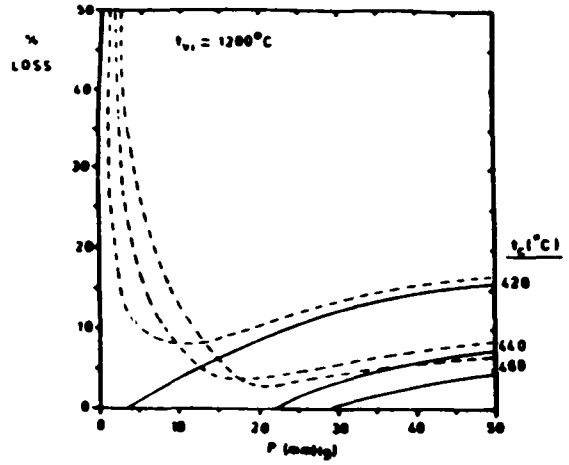

Fig 11. Predicted Zinc Vapour Loss, 50%Zn/50%N_2 Mixtures; Varying t_c

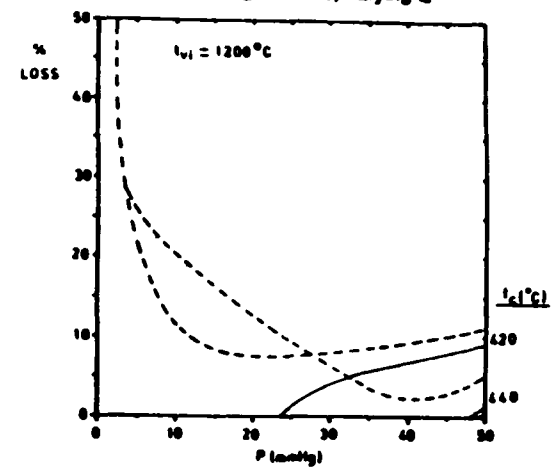

Fig 12. Predicted Zinc Vapour Loss, 25%Zn/75%N_2 Mixtures; Varying t_c

condenser at 1100, 1200 and 1300°C and condensing at 420°C. Five computer runs constitute one curve drawn through them. The major variable in the figures is zinc vapour concentration. It is varied from 97% to 75% to 50% and to 25% (Zinc, by mass).

The first point to make is that the total vapour loss (the dashed line) for all conditions will approach 100% as the total vacuum pressure, P of the system approaches p_c , the condensate interfacial partial pressure. The other evident feature of the curves is that fog losses approach zero as P is reduced. There is, however, a penalty to be paid at these low vacuum pressures in terms of equilibrium losses being high and vapour/gas velocity through the RH vessel and condenser being excessive. Equilibrium vapour losses are highest at low vapour concentrations in the feed mixture as indicated by Figures 7 and 8. All of the curves indicate that the more superheat the vapour/gas mixture fed to condenser has the less the fog problem will be. This can amount to a 40% lowering in the quantities of fog formed at Zn=97% for a 200°C increase in superheat from 1100 - 1300oC. For all of the conditions studied the computer predictions suggest that bulk vapour fog formation will occur at temperatures less than 670°C. The point of incipient fog formation, t_{vf} , does not vary much with increased superheating of the inlet mixture to the condenser, other parameters being equal. For 97% Zn/3%N_2 mixtures t_{vf} extends up to 670°C compared to 480°C for 25% Zn/75% N_2 mixtures, over the operating pressures considered.

THE EFFECT OF CONDENSATE INTERFACIAL TEMPERATURE ON VAPOUR FOG FORMATION

To study the effect of varying t_c three temperatures were chosen for a constant t_{vi} of 1200°C. Computer runs with t_c = 440 and 460°C representing liquid zinc condensers were carried out. These were compared to the t_c =420°C results discussed earlier for the four inlet vapour concentrations of 97%, 75%, 50% and 25% zinc.

The predictions are plotted in Figures 9 to 12. The diagrams reveal that the higher the condensate temperature the less the fog problem will be though equilibrium losses will become more significant. This effect is most pronounced at low vacuum pressures and low vapour concentrations in feed mixtures. Over the range of pressures considered t_{vf} stretched from 667°C for Zn=97%, t_c =420°C to 448°C at Zn = 25%, t_c =440°C.

COMPUTER PREDICTIONS FOR LEAD FOG FORMATION IN ZINC/LEAD/NITROGEN MIXTURES

As a more realistic multivapour condensation situation, a Zn/Pb/N_2 condensable mixture was considered for lead fogging characteristics. For this analysis, the simplification that zinc acts as a carrier vapour for the lead was adopted. Two hypothetical condensable mixtures were considered to throw light on the general fog forming characteristics of lead vapour in a complex mixture. Two possible feed mixtures that could be produced in the proposed smelter and subsequently condensed are:

i) An Imperial Smelting Furnace (ISF) Zinc/Lead Concentrate Feed

A typical ISF feed consists of 0.4 tonnes of lead per tonne of zinc. A condensable mixture in these proportions plus 3% nitrogen as non-condensable was postulated as a hypothetical feed to the condenser. Hence, by mass, the feed composition is:

Zinc 69.3% Lead 27.7% Nitrogen 3.0%

ii) A Zinc Concentrate Feed

Evans and Gray (1971) have reported twenty-six analyses of typical zinc concentrates from ore bodies around the world. If an average feed composition derived from this data is taken then a typical zinc concentrate will contain 49.27% zinc and 1.6% lead. If a condensable mixture is postulated to have these same proportions and if 3% inerts is again present in the mixture, then the following condenser feed will result:

Zinc 93.8% Lead 3.2% Nitrogen 3.0%

Both these feed mixtures were considered for condensation at an inlet condenser temperature, t_{vi} of 1200°C and a range of four operating pressures; P = 1mmHg, 5mmHg, 15mmHg and 30mmHg. A condensate interfacial temperature, t_c , of 420°C was chosen. This temperature reflects the fact that the condenser would be operating to collect zinc condensate such that any lead condensation as either condensate or fog is incidental to its operation.

Figure 13 is a comparative plot of the p_v, t_v data for both feed mixtures on solving the Gardner equation at an operating pressure of 30mmHg Both feeds will produce quantities of heterogeneous lead fog in the 60 to 90% range. It is therefore reasonable to state that nearly all the lead in the condensable mixture fed to the condenser will form as fog quite early on in the condensation process. The typical ISF feed will result in more fog than the typical zinc concentrate feed at all operating pressures as illustrated by Figure 14. In a similar way to the zinc/nitrogen condensation system the same general fog prediction profile is evident with the least amounts of fog expected at the lowest operating pressures. The temperature at which a lead fog will begin to form varies for each computer run extending up to 1055°C. This is very much higher than the predicted fog forming temperatures for zinc under similar condensing conditions (t_{vf} = 450 to 550°C). Almost certainly, the lead fog droplets produced early on in the condenser will saturate with zinc on further cooling since they are in a highly reactive state. They will also react with any oxidising species in the gas phase (such as SO_2) form a lead oxide dust. This mechanism will help to contribute towards the nuclei count necessary for zinc fog droplets to grow around in the lower reaches of the condenser.

CONCLUSIONS

The computer program developed to analyse the condensation characteristics of vapour/gas mixtures has revealed general fog formation trends. It has highlighted the condenser operating conditions most likely to keep zinc and lead losses down to a minimum. Of these, zinc vapour fog formation will be most

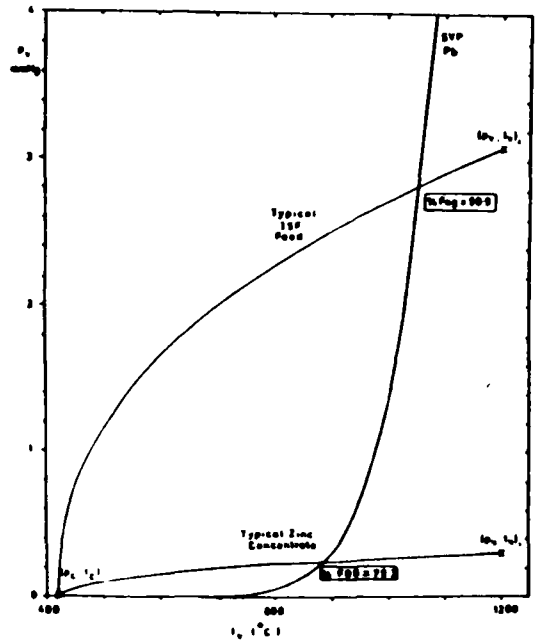

Fig 13. Comparative Plot of Lead Cooling Curves

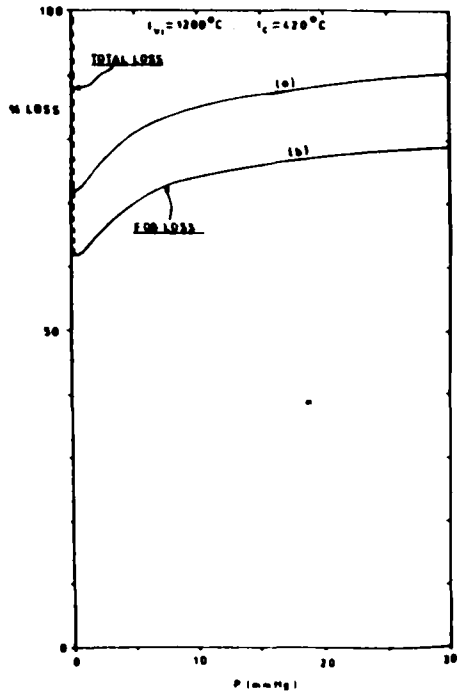

Fig 14. Predicted Lead Vapour Losses
a) An ISF Zinc/Lead Concentrate Feed
b) A Typical Zinc Concentrate Feed

marked at high condenser inlet vapour concentrations of greater than 85% zinc, by mass. Almost all (60-90%) of the lead present in a condensable Zn/Pb/N_2 mixture will form as a fog quite early on during the condensation process at temperatures up to and beyond 1000°C. These lead fog droplets will almost certainly act as condensation nuclei for the condensing zinc vapour especially if they solidify as dust particles on cooling. This lead oxide/sulphide dust will help to ensure that zinc will form fog heterogeneously upon reaching a state of supersaturation. As much as 40-50% of the inlet zinc vapour could be lost as a fog if the conditions in the condenser are not controlled. In general, the higher the condenser wall temperature the less vapour fog formation will occur though this does not have as pronounced an effect as vapour concentration in the feed mixture. The less superheat a condensable mixture possesses the more likely it is to condense as a fog. The lower the total operating pressure in a condenser the less fog will be a problem though equilibrium losses will become more significant. Saturated vapour losses in the outlet from a condenser will also influence total losses quite strongly at the lowest feed vapour concentrations.

This computer modelling work has led the smelter project to consider the possibility of a two-stage condensation unit with a preliminary condenser operating at, say, 900°C to knock out most of the lead as condensate. The formation of some lead fog is unavoidable and it will necessitate a lead reversion stage. An intermediate reheating stage would then be necessary followed by a secondary zinc condensation stage at 420°C to remove zinc from the vapour phase as a liquid deposit. This two stage condensation process would enhance recoveries of the two metals. On the other hand, for low lead levels in the feed mixture or for practical considerations, the bulk condensation could be in a single stage condenser with simultaneous lead and zinc condensation as a solid or liquid condensate.

ACKNOWLEDGEMENTS

The Department of Education for Northern Ireland is acknowledged for providing financial support during the period of this research. The Institution of Mining and Metallurgy has kindly made available to Mr R K Hanna a Travel Award from the Bosworth Smith Trust Fund. The assistance of Mr A B Roberts during the development of the computer program is also gratefully recognised.

NOMENCLATURE

a = Ackermann constant (as defined in the text)

C_p = Specific heat capacity of a gaseous mixture

C_{pv} = Specific heat capacity of a vapour

D = Diffusivity of a vapour in a gaseous mixture

k = Thermal conductivity of a gaseous mixture

M_v = Mean molecular weight of a gaseous mixture

M = Molecular weight of a vapour

N = Number Density of a fog (No. of droplets/cm^3)

P = Total pressure in a condensing system

p_{BM} = log mean partial pressure of an inert gas in a gas film

$$p_{BM} = \frac{(P-p_v) - (P-p_c)}{\ln[(P-p_v)/(P-p_c)]}$$

p_c = Condensate interfacial partial vapour pressure

p_{sat} = Saturation vapour pressure

p_{vf} = Partial vapour pressure at incipient heterogeneous fog formation

p_{vg} = Partial vapour pressure in a gas film

p_{vi} = Partial vapour pressure in a bulk vapour/gas mixture entering a condenser

p_{vo} = Partial vapour pressure in a bulk vapour/gas mixture leaving a condenser

S = Degree of vapour saturation (as defined by eq. 6.)

S_{crit} = Critical degree of vapour saturation (as defined by eq. 7.)

t_b = Vapour/gas bulk interfacial temperature, $t_b = (t_v + t_c)/2$

t_c = Condensate interfacial vapour temperature

t_{cm} = Condenser cooling medium temperature (see Figure 2)

t_{sat} = Saturation vapour temperature

t_{vf} = Vapour/gas temperature at incipient heterogeneous fog formation

t_{vg} = Vapour/gas temperature in a gas film

t_{vi} = Vapour/gas temperature in a bulk gas phase entering a condenser

t_{vo} = Vapour/gas temperature in a bulk gas phase leaving a condenser

t_{wi}, t_{wo} =Condenser wall inside, outside temperatures (see Figure 2)

x = Distance from a condenser wall

ρ = Density of a gaseous mixture

Pr = Prandtl No. for a gaseous mixture ($Pr = C_p\mu/k$)

Sc = Schmidt No. for a gaseous mixture ($Sc = \mu/\rho D$)

Sc/Pr= Schmidt/Prandtl ratio for a gaseous mixture $Sc/Pr = (k/C_p.D.\rho)$

Re = Reynolds No. for a gaseous mixture
$Re = du\rho/\mu$ where d is a characteristic dimension, u is the velocity of the mixture and μ is the viscosity of the mixture

REFERENCES

Alcock, C.B. and Howitt, I., *Pyrometallurgy '87*, Institution of Mining and Metallurgy, London, p.1., 1987

Alexander, L.G. and Coldren, C.L., *Industrial and Engineering Chemistry*, 1951, 43(6), 1326.

Amelin, A.G., *Theory of Fog Condensation*, 2nd Edition, Jerusalem, Israel Program for Scientific Translations, 1967.

Bettelheim, J., Forster, P.M. and Kyte, J.S., *Transactions of the Institution of Chemical Engineers*, 1980, 58, (Jan), 3.

Bird, R.D., Stewart, W.E. and Lightfoot, E.N., *Transport Phenomena*, New York and London, Wiley International, 1962.

Brus, G.H.P., *The Industrial Chemist*, 1955, January, 22.

Buckle, E.R., *Chemistry in Britain*, Jan. 1989, p.57.

Chan, C.H., Cho, D.H. and Condiff, D.W., *International Journal of Heat and Mass Transfer*, 1980, 23(1), 63.

Colburn, A.P. and Drew, T.B., *Transactions of the American Institute of Chemical Engineers*, 1937, 33, 197.

Colburn, A.P. and Edison, A.G., *Industrial and Engineering Chemistry*, 1941, 33(4), 457.

Davey, T.R.A., *Vacuum*, 1962, 12, 83.

Davey, T.R.A., *Trans. AIME, Journal of Metals*, 1953, 197, 991.

Evans, C.J.G. and Gray, P.M.J., *Advances in Extractive Metallurgy*, Institution of Mining and Metallurgy, London, 1971, p.565.

Gardner, C.G., *British Chemical Engineering*, 1957, 2 (6), 296.

Hampson, H. and Furman, T., *National Engineering Laboratory Heat Division*, Paper No. 50, Sept. 1953.

Hayashi, Y., Takimoto, A. and Kambe, M., *Trans. of the American Society of Mechanical Engineers, Journal of Heat Transfer*, 1976, February, 114.

Herbertson, J.G. and Warner, N.A., *Trans. of the Institution of Mining and Metallurgy*, 1973, 82, C16, 1974, 83, C126.

Hutchinson, P., Hewitt, G.F. and Dukler, A.E., *Chemical Engineering Science* 1971, 26, 419.

Johnstone, H.F., Kelley, M.D. and McKinley, D.L., *Industrial and Engineering Chemistry*, 1950, 42(11), 2298.

Kroll, W.J., *Vacuum*, 1951, 1(3), 163.

Lekae, V.M., Kutnetsov, V.M. and Myagkov, L.V., *Chemische Technik (Leipzig)*, 1981, 33(4), 179.

Lewin, S.W. and Dalin, G.A., *Journal of Chemical Education*, 1965, 42(1), A5.

Morgan, S.W.K., *Trans. of the Institution of Mining and Metallurgy*, 1957, 66, 553.

Nusselt, W., *Zeitschrift Ver. Deut. Ing.*, 1916, 60, 541, 569.

Olander, D.R., *Industrial and Engineering Chemistry*, 1961, 53(2) 121.

Perry, R.H. and Green, D.W. (Ed.), *Chemical Engineers' Handbook*, 6th Edition, McGraw Hill, 1984.

Lo Pinto, L. *Chemical Engineering*, 1982, 89, May 17, 111.

Rosner, D.E. and Epstein, M., *Journal of Colloid and Interface Science*, 1968, 28(1), 60.

Schuler, R.W. and Abell, J.B., *Chemical Engineering Symposium Series, Heat Transfer*, 1956, 52(18), 51.

Siktchi, K.K.G., *Ph.D. Thesis*, Carnegie Institute of Technology College of Engineering and Science, 1956.

Steinmayer, D.E. *Chemical Engineering Progress*, 1972, 68(7), 64.

Toor, H.L., *American Institute of Chemical Engineering Journal*, 1971, 17(1), 5.

Toor, H.L., *Industrial and Engineering Chemistry Fundamentals*, 1971, 10(1), 121.

Turkdogan, E.T., *Trans. of the Metallurgical Society of the American Institute of Mechanical Engineers*, 1964, 230(6), 740.

Warner, N.A., "Coal-based Iron Making via Melt Circulation", *International Symposium on Metallurgical Processes for the Year 2000 and Beyond*, Las Vegas, Nevada, U.S.A., 1989.

Warner, N.A., "Advanced Technology for Smelting McArthur River Ore", *Minerals Engineering*, 1989, 2(1), 3.

Warner, N.A., "Innovative Smelting with Slag Heat Recovery", *Reinhardt Schuhmann International Symposium on Innovative Reactor Design in Extractive Metallurgy*, Colorado Springs, Colorado, U.S.A., 1986.

Warner, N.A., "Towards Polymetallic Smelting", *American Institute of Metallurgical Engineering Symposium on Complex Sulphides*, San Diego, Proceedings, p847, 1985.

Warner, N.A., *Trans. of the Institution of Mining and Metallurgy*, 1983, 92, C147.

Warner, N.A., *Extraction and Refining, Institution of Metallurgists Review Course*, Nov. 1970, Series 2, Number 4, 3.2.

LIST OF SYMBOLS

Symbol	Meaning	Units
A	Area of top-blow region or interfacial condensation area	m^2
A_b	Area of a circle of diameter d_b	m^2
A_j	Jet impact area	m^2
a	Ackermann Constant	dim.less
	$a = \left(\frac{Pr}{Sc}\right)^{2/3} \left(\frac{M_v Cp_v}{M Cp}\right) \ln\left(\frac{P - p_c}{P - p_v}\right)$	
	or as defined in the text	
a_o	Area of nozzle orifice	m^2
a_1	Area of pipe behind the nozzle	m^2
C_d	Nozzle discharge coefficient	dim.less
$Cp; Cp_{mix}$	Mean specific heat capacity of a gaseous mixture	J/kg^oC
Cp_g	Specific heat capacity of an inert gas	J/kg^oC
Cp_v	Specific heat capacity of a vapour	J/kg^oC
C_L^b	Bulk liquid phase solute concentration	ppm
$C_L^b\ i$	Bulk liquid phase solute concentration at the inlet of the top-blow region	ppm
$C_L^b\ o$	Bulk liquid phase solute concentration at the outlet of the top-blow region	ppm
C_L^i	Interfacial Liquid Phase Oxygen Concentration	ppm
$D_L; D_{O_2-H_2O}$	Diffusivity of solute (oxygen) in liquid (water)	m^2/s
D_{mix}	Diffusivity of a gaseous mixture	m^2/s
d_o	Nozzle diameter	m
d_b	Bath diameter (stationary baths) or interlance spacing (channel flow)	m
d_H	Hydraulic mean diameter	m
d_s	Diameter of equivalent square (eq. 2.1.24)	m
d_T	Diameter of equivalent hexagon (eq. 2.1.23)	m
f	Constant defined by equation 2.1.25	dim.less
g	Acceleration due to gravity	m^2/s
G	Vapour/Gas Mass Velocity	$kg/m^2\ s$
H	Lance height from nozzle tip to liquid surface	m
H'	Lance height from jet pole to liquid surface	m
H_c	Specific heat capacity ratio at t_b $H_C = M_V Cp_V / M Cp$	dim.less
h_{comb}	Combined heat transfer coefficient for the cooling medium film, tube wall, condensate and dirt plus scale layers	$W/m^2\ K$
h_g	Heat transfer coefficient for the gas film	$W/m^2\ K$
h_{Nu}	Nusselt heat transfer coefficient	$W/m^2\ K$
I	Rate of Nucleation	$cm^{-3}\ s^{-1}$
j_D	Chilton-Colburn j-factor for mass transfer	dim.less
j_H	Chilton-Colburn j-factor for heat transfer	dim.less
K	Nucleation Constant	dim.less

K1	Jet Constant for momentum (eq. 2.1.1)	dim.less
K2	Jet Constant for mass entrainment (eq. 2.1.9)	dim.less
K_C	The Coalescence/Coagulation Constant	dim.less
k	Boltzmann Constant	As defined in the text
k/ε	Molecular force constant	$^oC^{-1}$
k_g	Gas phase mass transfer coefficient	m/s
k_L	Liquid phase mass transfer coefficient	m/s
k_{Lj}	Liquid phase mass transfer coefficient per jet	m/s
k_{mix}	Thermal conductivity of a gaseous mixture	W/m K
$\ddot{M}$	Momentum flux of a gas jet	N
$\ddot{M}_{eff}$	Effective momentum flux of a gas jet	N
M	Molecular weight of a gaseous mixture	g
M_g	Molecular weight on an inert gas	g
M_v	Molecular weight of a vapour	g
$\dot{m}_o$	Nozzle mass flowrate of a gas	kg/s
$\dot{m}_x$	Downstream mass flowrate of a gas in a jet	kg/s
N	Number Density of fog; no. of droplets/cm^3	-
$\dot{n}$	Volumetric rate of solute mass transfer	m^3/s
n	Radial depth of a liquid cavity below the surface	m
n_o	Maximum cavity depth	m
n_c	Critical depth of cavity at onset of splashing	m
n_p	Crest height of a liquid cavity	m
P	Total pressure in the condenser	mm Hg
P_o	Atmospheric pressure/Downstream nozzle pressure	mm Hg
P_1	Upstream nozzle pressure	mm Hg
P_s	Impact jet pressure at U_s	mm Hg
p_{BM}	Log mean partial pressure of the inert gas in the gas film: $$p_{BM} = \frac{(P - p_v) - (P - p_c)}{\ln\left[(P - p_v)/(P - p_c)\right]}$$	mm Hg
p_c	Condensate interfacial partial vapour pressure	mm Hg
p_G^i	Interfacial gas phase solute partial pressure	N/m^2
p_r	Vapour pressure of a droplet	mm Hg
p_{sat}	Saturation vapour pressure	mm Hg
p_v	Partial vapour pressure	mm Hg
p_{vf}	Partial vapour pressure at incipient fog formation	mm Hg
p_{vg}	Partial vapour pressure in the gas film	mm Hg
p_{vi}	Partial vapour pressure in the bulk vapour/gas mixture entering a condenser	mm Hg
Q_g	Volumetric gas flowrate	m^3/s
Q_L	Channel water volumetric flowrate	m^3/s

q_c	Rate of heat transfer due to condensation	J/S
q_l	Rate of heat transfer due to latent heat	J/S
q_s	Rate of heat transfer due to sensible heat	J/S
q_T	Total rate of heat transfer	J/S
R_o	Liquid cavity diameter during jetting	m
R	Gas Constant	J/K.mole
r	Jet radial distance (top-blowing)	m
r	Radius of a fog droplet (condensation)	m
r_o	Nozzle diameter	m
$r_{1/2}$	Jet radius at which $U_r = U_x/2$	m
r_b	Stationary bath radius	m
r_j	Jet impact radius	m,
S	Degree of Vapour Supersaturation (eq. 2.2.11)	dim.less
S_{crit}	Critical degree of Vapour Supersaturation	dim.less
T	Time	seconds
t	Temperature	^oC
t_{av}	Average water temperature during a top-blow run	^oC
t_b	Vapour/gas bulk mean temperature $t_b = (t_v + t_c)/2$	^oC
t_c	Condensate interfacial temperature	^oC
t_{cm}	Cooling Medium temperature	^oC
t_{sat}	Saturation vapour temperature	^oC
t_v	Vapour temperature	^oC
t_{vf}	Vapour temperature at incipient fog formation	^oC
t_{vg}	Vapour temperature in the gas film	^oC
t_{vi}	Vapour temperature in the bulk vapour/gas mixture entering a condenser	^oC
t_w	Condenser wall temperature; i = inner, o = outer	^oC
U	Overall heat transfer coefficient	W/m^2K
U_o	Nozzle velocity	m/s
$U_{g\infty}$	Gas velocity parallel to a liquid surface	m/s
U_H	Jet centreline velocity at height H	m/s
$U_L; U_{H_2O}$	Water velocity in the channel	m/s
U_r	Radial gas velocity in a jet	m/s
U_s	Surface velocity of an impinged liquid	m/s
U_x	Jet downstream centreline velocity	m/s
V_j	Jet velocity	m/s
W	Work required to form a fog embryo	J
X	Number of lances in an array	-
x	Downstream distance from a nozzle	m
x'	Downstream distance from a jet pole	m
x_c	Vapour mole fraction at condensate interface	-
x_i	Bulk vapour mole fraction at the inlet to a condenser	-
x_m	Bulk mean vapour mole fraction across the gas film, $x_m = (x_v + x_c)/2$	-
x_v	Bulk vapour mole fraction	-

GREEK SYMBOLS

α	Jet spreading angle (Top-blowing)	Degrees
α	Condensation coefficient	dim. less
γ	Ratio of specific heats at constant pressure and temperature for a gas	dim.less
Δt_{ov}	Overall temperature drop between a vapour/gas mixture and the cooling medium, $\Delta t_{ov} = t_v - t_{cm}$	^oC
Δt_v	Change in bulk vapour/gas temperature; computer program step length	^oC
Δp_v	Change in bulk vapour/gas partial pressure	mm Hg
λ	Latent heat of condensation	J/kg
λ_1	Wavelength of gravity waves	m
λ_2	Wavelength of capillary waves	m
μ_L	Liquid viscosity	Ns/m^2
μ_{mix}	Viscosity of a gaseous mixture	Ns/m^2
ν_g	Kinematic viscosity of a gas	m^2/s
ν_L	Kinematic viscosity of a liquid	m^2/s
ρ_1	Density of environmental gas	kg/m^3
ρ_o	Density of gas in a jet	kg/m^3
ρ_{mix}	Density of a gaseous mixture	kg/m^3
ρ_L	Density of a liquid	kg/m^3
σ_L	Surface tension of a liquid	N/m
σ_r	Surface tension of a droplet	N/m
σ_i	Collision diameter of species i	m
σ_{ij}	Collision diameter of species i and j	m
$\Omega_{k,i}$	"Omega k" constant for species i	*dim.less*
$\Omega_{\mu,i}$	"Omega μ" constant for species i	dim.less

DIMENSIONLESS GROUPS

Ga	Galileo No. $\left(d_b^3 \cdot g \cdot \rho_L^2 / \mu_L^2\right)$	(Top-Blowing)
Mo	Morton Number $\left(\sigma_L^3 \cdot \rho_L / g \cdot \mu_L^4\right)$	(Top-Blowing)
Pr	Prandtl Number $\left(\frac{Cp_{mix}\,\mu_{mix}}{k_{mix}}\right)$	(Condensation)
Sc	Schmidt Number $\left(\frac{\mu_L}{\rho_L\,D_L}\right)$	(Top-Blowing)
	$\left(\frac{\mu_{mix}}{\rho_{mix}\,D_{mix}}\right)$	(Condensation)
Sh	Sherwood Number $\left(\frac{k_{Lj}\,d_b}{D_L}\right)$	(Top-Blowing)
Re	Reynolds Number $\left(\frac{d_H\,U_L\,\rho_L}{\mu_L}\right)$	(Top-Blowing)

All other symbols are defined in the text.

REFERENCES

ABRAMOVICH, G.N., BAKULEV, V.I., GOLUBEV, V.A. and SMOLIN, G.G., International Journal of Heat Mass Transfer, 1966, 9, 1047.

ABRAMOVICH, M.L., The Theory of Turbulent Jets, Massachusetts Institute of Technology Press, Cambridge, Massachusetts, 1963.

ALBERTSON, M.L., DAI, Y.B., JENSEN, R.A. and ROUSE, H., Trans. of the American Society of Civil Engineering, 1950, 115, 639.

ALCOCK, C.B. and HOWITT, I., Pyrometallurgy '87, Institution of Mining and Metallurgy, London, p. 1, 1987.

ALEXANDER, L.G. and COLDREN, C.L., Industrial and Engineering Chemistry, 1951, 43 (6), 1326.

AMELIN, A.G., Theory of Fog Condensation, 2nd Edition, Jerusalem, Israel Program for Scientific Translations, 1967.

ANON, "New Zinc Purification Process", Metallurgia, 1967, Dec. p. 250.

AXE, J.R., D.Eng. Thesis, The Catholic University of America, 1972.

BACON, N.P., CHESTERS, J.H. and HALLIDAY, I.M.D., Journal of the Iron and Steel Institute, 1960, July, 286.

BAKER, A.R., Ph.D. Thesis, University of London, 1977.

BAKER, A.R. and RAJAKUMAR, V., Transactions of the Institution of Mining and Metallurgy, 1983, 92, C179.

BALEKJIAN, G. and KATZ, D.L., American Institute of Chemical Engineering Journal, 1958, 4 (1), 43.

BANDROWSKI, J. and KUBACZKA, D., International Journal of Heat and Mass Transfer, 1981, 24, 147.

BANKS, R.B., Conference on Hydraulics and Fluid Mechanics, Univ. of Western Australia, Nedlands, 1962, Ed. R. Silvester, Oxford: Pergamon Press, p. 111.

BANKS, R.B. and BAHAVAMAI, A., Journal of Fluid Mechanics, 1965, 23 (2), 229.

BANKS, R.B. and CHANDRASEKHARA, D.V., Journal of Fluid Mechanics, 1963, 15 (1), 13.

BARCHILON, M. and CURTET, R., Journal of Basic Engineering, Transactions of the American Society of Mechanical Engineers, 1964, December, 777.

BARRETT, K.R. and KNIGHT, R.P., I.M.M. Conference on Extractive Metallurgy, 1985, London, Proceedings, p. 683.

BARTON, R.G. and BRIMACOMBE, J.K., Metallurgical Transactions B, 1977, 8B (Sept), 417.

BELTAOS, S. and RAJARATNAM, N., Journal of the Hydraulics Division, American Society of Civil Engineers, 1974, 100, (10), 1313.

BETTELHEIM, J., FORSTER, P.M. and KYTE, W.S., Trans. of the Institute of Chemical Engineers, 1980, 58, (Jan), 3.

BIN, A.K., American Institute of Chemical Engineering Journal, 1985, 31, (8), 1397.

BIRD, R.D., STEWART, W.E. and LIGHTFOOT, E.N., Transport Phenomena, New York and London, Wiley International, 1962.

BRADSHAW, A.V. and CHATTERJEE, A., Chemical Engineering Science, 1971, 26, 767.

BRAS, G.H.P., Petroleum Refiner, 1956, 35 (6), 177.

BRAS, G.H.P., The Industrial Chemist, 1955, January, 22.

BRAS, G.H.P., Chemical Engineering, 1954, 61 (5), 190.

BRAS, G.H.P., Chemical Engineering, 1953, 60 (5), 238.

BRAS, G.H.P., Chemical Engineering, 1953, 60 (4), 223.

BRIMACOMBE, J.K. and GRAY, N.B., Bulletin of the Proceedings of the Australasian Institute of Mining and Metallurgy, 1985, 290 (4), June, 59.

BRIMACOMBE, J.K. and WEINBURG, F., Metallurgical Transactions, 1972, 3, 2298.

BUCKLE, E.R., Department of Metallurgy, University of Sheffield, Personal Correspondence, May 1989.

BUCKLE, E.R., Chemistry in Britain, Jan. 1989, p. 57.

BUCKLE, E.R., Proceedings of the Royal Society London, 1986, A406, 227.

BUCKLE, E.R. and POURING, A.A., Nature, 1965, Oct. 23, p. 367.

BURNET, G. and BUCHANAN, W., United States Atomic Energy Commission, Report IS-273, Ames Laboratory, Feb. 1961.

CAIRNS, R.C., Chemical Engineering Science, 1954, 3, 215.

CAIRNS, R.C., Chemical Engineering Science, 1953, 2, 127.

CAIRNS, R.C. and ROPER, G.H., Chemical Engineering Science, 1955, 4, 22.

CAIRNS, R.C. and ROPER, G.H., Chemical Engineering Science, 1954, 3, 97.

CHAN, S.H., CHO, D.H. and CONDIFF, D.W., International Journal of Heat and Mass Transfer, 1980, 23 (1), 63.

CHATTERJEE, A., Ph.D. Thesis, University of London, 1970.

CHATTERJEE, A. and BRADSHAW, A.V., Journal of the Iron and Steel Institute, 1972, March, 179.

CHATTERJEE, A. and WAKELIN, D.H. and BRADSHAW, A.V., Metallurgical Transactions, 1972, 3 (12), 3168.

CHAUDHURI, K.R., RACHOR, F.E., WEBB, I.D. and SAUERT, F.A., Canadian Institution of Metallurgy Bulletin, 1980, June ,127.

CHESLAK, F.R., NICHOLLS, J.A. and SICHEL, M., Journal of Fluid Mechanics, 1969, 36 (1), 55.

COLBURN, A.P. and DREW, T.B., Transactions of the American Institute of Chemical Engineers, 1937, 33, 197.

COLBURN, A.P. and EDISON, A.G., Industrial and Engineering Chemistry, 1941, 33 (4), 457.

COLBURN, A.P. and HOUGEN, O.A., Industrial and Engineering Chemistry, 1934, 26, 1178.

COLLINS, R.D. and LUBANSKA, H., British Journal of Applied Physics, 1954, 5 (1), 22.

CONOCHIE, D.S. and GRAY, N.B., Transactions of the Institution of Mining and Metallurgy, 1979, March, C14.

COUGHANOWR, D.R. and STENSHOLT, E.O., Industrial and Engineering Chemistry Process Design and Development, 1964, 3 (4), 369.

CROXFORD, N.J.W. and JEPHCOTT, S., Proceedings of the AUS.I.M.M., 1972, 243, 1.

DAANE, R.A. and HAN, S.T., Institute of Paper Chemistry: TAPPI, 1961, 44 (1), 73.

DAI, X., "Gas Phase Mass Transfer on Top-Blown Liquid Surfaces", Unpublished Qualifying Masters Thesis, School of Chemical Engineering, University of Birmingham, 1990.

DANCKWERTS, P.V., American Institute of Chemical Engineering Journal, 1955, 1 (4), 456.

DAVENPORT, W.G., WAKELIN, D.H. and BRADSHAW, A.V., Heat and Mass Transfer in Process Metallurgy, 1966, Hills (Ed)., 207.

DAVEY, T.R.A., Vacuum, 1962, 12, 83.

DAVEY, T.R.A. and WILLIAMS, K.C., Proceedings of the Australian I.M.M., 1956, 180, 207.

DAVEY, T.R.A., Trans. A.I.M.E., Journal of Metals, 1953, 197, 991.

DAWSON, R.D., Australian I.M.M. Non-Ferrous Smelting Symposium, Port Pirie, South Australia, September, 1989, Proceeding, p. 1.

DENNY, V.E., MILLS, A.F. and JUSIONIS, V.J., Transactions of the American Society of Mechanical Engineers Journal of Heat Transfer, 1971, August, 297.

DMYTRYSEYN, M. Ph.D. Thesis, St. Louis, Missouri, Washington University, 1957.

DUBRAWKA, E., Open Hearth Processing, 1961, 44, 388.

ELLIOTT, J.F., Transactions of the Institution of Mining and Metallurgy, 1985, 94 (Dec), C171.

EMERSON, W.H., National Engineering Laboratory, Report No. 619, 1974.

EVANS, C.J.G. and GRAY, P.M.J., Advances in Extractive Metallurgy, Institution of Mining and Metallurgy, London, 1975, p. 565.

EVANS, J.W., American Institute of Metallurgical Engineering Symposium on Mathematical Modelling in Material Processing Operations, 1987, Proceedings, p. 9.

EVERSOLE, J.D. and BROIDA, H.P., Journal of Applied Physics, 1974, 45 (2), 596.

FAGELA-ALABASTRO, E.B. and HELLUMS, J.D., Industrial and Engineering Chemistry Fundamentals, 1967, 6 (4), 581.

FLINN, R.A., PEHLKE, R.D., GLASS, D.R. and HAYS, P.O., Transaction of the Metallurgical Society of the American Institute of Mechanical Engineering, 1967, 239 (11), 1776.

FORESTALL, W. and GAYLORD, E.W., Journal of Applied Mechanics, 1955, 22, 161.

FRANKS, R.G.E. and O'BRIEN, N.G., Chemical Engineering Progress Symposium Series, 1960, No. 31, 56, 37.

FRURIP, D.J. and BAUER, S.H., Journal of Physical Chemistry, 1977, 81 (10), 1001.

GAMMON, M., Imperial Smelting Limited, Avonmouth, Personal Correspondence, August 1989.

GAMMON, M., Unpublished Report, Imperial Smelting Ltd., Avonmouth, 1970.

GARDNER, C.G., British Chemical Engineering, 1957, 2 (6), 296.

GIRALT, F., CHIA, C. AND TRASS, O., Industrial and Engineering Chemistry Fundamentals, 1977, 16 (1), 21.

GOLDSTEIN, R.J. and TIMMERS, J.F., International Journal of Heat Mass Transfer, 1982, 25 (12), 1857.

GREEN, H.L. and LANE, W.R., Particulate Clouds: Dusts, Smokes and Mists, 2nd Edition, London, Spon Ltd., 1964.

GUTHRIE, R.I.L., American Institute of Metallurgical Engineering Symposium on Mathematical Modelling in Material Processing Operations, 1987, Proceedings, p. 447.

HAMPSON, H. and FURMAN, T., National Engineering Laboratory, Heat Division, Paper No. 50, Sept. 1953.

HANDBOOK OF PHYSICS AND CHEMISTRY, 52nd Edition (Ed.) R.C. Weast, Rubber Publishing Company, 1971-1972.

HARRIS, R. and ALLAIRE, A., Extraction Metallurgy '89, London, p. 91, 1989.

HARRIS, R., Canadian Metallurgical Quarterly, 1988, 27 (3), 169.

HASIMOTO, H.A., Tetsu-to-Hagane, 1958, 44, 222.

HAYASHI, Y., TAKIMOTO, A. and KANBE, M., Transactions of the American Society of Mechanical Engineers, Journal of Heat Transfer, 1976, February, 114.

HERBERTSON, J.G., Ph.D. Thesis, University of London, 1978.

HERBERTSON, J.G., ROBERTSON, D.G.C. and BRADSHAW, A.V., Canadian Metallurgical Quarterly, 1983, 22, (1) 1.

HERBERTSON, J.G. and WARNER, N.A., Transactions of the Institution of Mining and Metallurgy, Section C, 1973, 82, 16 and 1974, 83, 126.

HIGBIE, R., Transactions of the American Institute of Chemical Engineers, 1935, 31, 365.

HILLS, A.W.D. and SZEKELY, J., International Journal of Heat Mass Transfer, 1969, 12, 111.

HILLS, A.W.D. and SZEKELY, J., Chemical Engineering Science, 1964, 19, 79.

HOGG, E.A. and SILBERNAGE, B.G., Journal of Applied Physics, 1974, 45 (2), 593.

HOLDEN, C. and HOGG, A., Journal of the Iron and Steel Institute, 1960, November, 318.

HOLMES, B.S. and THRING, M.W., Journal of the Iron and Steel Institute, 1960, November, 259.

HUANG, G.C., Journal of Heat Transfer, Trans. ASME, 1963, August, p. 237.

HUANG, Y.S., Ph.D. Thesis, Case Western Reserve University, 1971.

HUANG, Y.S., LYMAN, F.A. and LICK, W.J., International Journal of Heat Mass Transfer, 1972, 15, 742.

HUTCHINSON, P., HEWITT, G.F. and DUKLER, A.E., Chemical Engineering Science, 1971, 26, 419.

ITO, R., HIRATA, Y., MA, F. and YOSHIDA, Y., International Chemical Enginering, 1981, 21 (2), 259.

IVANOV, M.E., International Chemical Engineering, 1962, 2 (2), 282.

JOHNSTONE, H.F., KELLEY, M.D. and McKINLEY, D.L., Industrial and Engineering Chemistry, 1950, 42 (11), 2298.

JONES, T., PH.D. Thesis, Birmingham University, 1986.

JONES, T. and WARNER, N.A., Proceedings of Pyrometallurgy 1987, Institution of Mining and Metallurgy Conference, London, p. 605.

KIRKBRIDE, C.G., Industrial and Engineering Chemistry, 1933, 25, 1324.

KORIA, S.C. and LANGE, L.W., Steel Research, 1987, 58 (9), 421.

KOTAKE, S., International Journal of Heat Mass Transfer, 1985, 28 (2), 407.

KRISHNA, R. and PANCHAL, C.B., Chemical Engineering Science, 1971, 32, 741.

KROLL, W.J., Vacuum, 1951, 1 (3), 163.

KUBASCHEWSKI, O. and ALCOCK, C.B., Metallurgical Thermochemistry, 5th Edition, Pergamon Press, London, 1979.

KUSAK, L.J., Ph.D. Thesis, Cornell University, Ithaca, New York, 1958.

VAN LANGEN, J.M., Journal of the Iron and Steel Institute, 1960, November, 262.

LEKAE, V.M., KUTNETSOV, V.M. and MYAGKOV, L.V., Chemische Technik (Leipzig), 1981, 33 (4), 179.

LEVINE, D.G. and FRIEDLANDER, S.K., Chemical Engineering Science, 1960, 13 (2), 49.

LEWIN, S.W. and DALIN, G.A., Journal of Chemical Education, 1965, 42 (1), A5.

LI, J., ARMITAGE, J.W. and WARNER, N.A., "Computer Prediction of Condensing Processes in the Ternary System $Zn_{(g)}/Pb_{(g)}$/Inert Gas Under Reduced Pressure Conditions", Technical Note Submitted to the Transactions of the Institution of Mining and Metallurgy, Section C, 1990.

LI, K., Journal of the Iron and Steel Institute, 1960, November, 275.

LÖHE, H., Chemical-Ingenieur Techn., 1966, 38, 309.

LOPINTO, L., Chemical Engineering, 1982, 89, May 17, 111.

MALAKFAM, F. and MALONE, L., Unpublished Project Report, Department of Minerals Engineering, University of Birmingham, 1983.

MARTIN, A.J., Metal Industry, 1956, 8 June, 473.

MARTIN, H., Advances in Heat Transfer, 1977, 13, 1.

MATHIEU, F., Revue Universelle des Mines de la Metallurgie, 1960, 16, 309.

MATHIEU, F., Revue Universelle des Mines de la Metallurgie, 1962, 18, 482.

MEISENBURG, S.J., BOARTS, R.M. and BADGER, W.L., Transactions of the American Institute of Chemical Engineers, 1935, 31, 622.

MICKLEY, H.S., Chemical Engineering Progress, 1949, 45 (12), 739.

MINKOWYCZ, W.J. and SPARROW, E.M., International Journal of Heat Mass Transfer, 1966, 9, 1125.

MISRA, B. and BONILLA, C.F., Chemical Engineering Progress Symposium Series, Heat Transfer, 1956, 52 (18), 7.

MIZUSHINA, T., HASHIMOTO, N. and NAKAJIMA, M., Chemical Engineering Science, 1959, 9, 195.

MOLLOY, N., Journal of the Iron and Steel Institute, 1970, October, 943.

MORGAN, S.W.K., Transactions of the Institution of Mining and Metallurgy, 1957, 66, 553.

MORI, Y., HIJIKATA, K. and UTSUNOMIYA, K., Transactions of the American Society of Mechanical Engineers, Journal of Heat Transfer, 1977, 99, May, 257.

MORI, K. and SANO, M., Tetsu-tu-Hagane, 1974, 60, 1432.

NICHOLAON, G., COOKE, D.D., DAVIS, E.J., KERKER, M. and MATIJEVIC, E., Journal of Colloid and Interface Science, 1971, 35 (3), 490.

NUSSELT, W., Zeitschrift Ver. Deut. Ing., 1916, 60, 541, 569.

OLANDER, D.R., Industrial and Engineering Chemistry, 1961, 53 (2), 121.

OLMSTEAD, W.E. and RAYNOR, S., Journal of Fluid Mechanics, 1984, 4 (4), 561.

OTHMER, D.F., Industrial and Engineering Chemistry, 1929, 21 (6), 576.

PARTINGTON, P., Broken Hill Associated Smelters, Port Pirie, South Australia, Personal Correspondence, October 1989.

PASKALL, H.G., "Sulphur Condenser Function and Problem Areas", Sulphur Recovery Seminar, Amsterdam, November 1981.

PERRY, R.H. and GREEN, D.W., (Ed.), Chemical Engineers' Handbook, 6th Edition, McGraw Hill, 1984.

PHYSICAL PROPERTIES OF HYDROCARBONS, 1966, Ch. 14, p. 124.

PORTER, K.E. and JEFFREYS, G.V., Transactions of the Institute of Chemical Engineers, 1963, 41, 126.

RANKIN, W.J., Australasian Institute of Mining and Metallurgy Symposium on Extractive Metallurgy, Melbourne, 1984, Proceedings, p. 233.

RANKIN, W.J. and BATTERHAM, R.J., Australasian Institute of Mining and Metallurgy Symposium on Extractive Metallurgy, Melbourne, 1984, Proceedings, p. 261.

RICHARDSON, F.D., Canadian Metallurgical Quarterly, 1982, 21(2), 111.

RICHARDSON, F.D., Transaction of the Institute of Mining and Metallurgy, 1973, 82, C128.

RICOU, F.P. and SPALDING, D.B., Journal of Fluid Mechancis, 1961, 11, 21.

ROSLER, R.S. and STEWART, G.J., Journal of Fluid Mechanics, 1968, 31 (1), 163.

ROSNER, D.E., International Journal of Heat Mass Transfer, 1967, 10, 1267.

ROSNER, D.E. and EPSTEIN, M., Journal of Colloid and Interface Science, 1968, 28 (1), 60.

ROTTMANN, G. and WUTH, W., Copper Metallurgy Practice and Theory (Ed)., M.J. Jones, 1975, p. 49.

SADOMOTO, S., British Chemical Engineering, 1964, 9, (11), 740.

St-DENIS, C.E. and FELL, C.J.D., Canadian Journal of Chemical Engineering, 1971, 49, 885.

SCHMITT, P. and WUTH, W., Heat and Mass Transfer in Metallurgical Systems, (Eds), A.B. Spalding and N. Afgan, Hemisphere, 1981, p. 271.

SCHOTTE, W., Industrial and Engineering Chemistry Research, 1987, 26, pp. 134-139 and pp. 300-306.

SCHRAGE, R.W., A Theoretical Study of Interphase Mass Transfer, Columbia University Press, New York, 1953.

SCHRODT, J.T., American Institute of Chemical Engineering Journal, 1973, 19 (4), 753.

SCHRODT, J.T. and GERHARD, E.R., Industrial and Engineering Chemistry Fundamentals, 1965, 4(1), 46.

SCHULER, R.W. and ABELL, J.B., Chemical Engineering Progress Symposium Series, Heat Transfer, 1956, 52(18), 51.

SHRIVASTAVA, U.S., MUKHOPADHYAY, B.N. and MALHOTRA, S.L., Indian Journal of Technology, 1976, 14(1), 13.

SHUMSKII, K.P., Soviet Physics-Technical Physics, 1962, 6(8), 720.

SHUMSKII, K.P., International Chemical Engineering, 1962, 2(1), 73.

SIKCHI, K.K.G., Ph.D. Thesis, Carnegie Institute of Technology College of Engineering and Science, 1956.

SILVER, L., Transactions of the Institute of Chemical Engineering, 1947, 25, 30.

SPARROW, E.M., MINKOWYCZ, W.J. and SADDY, M., International Journal of Heat Mass Transfer, 1967, 10, 1829.

STEINMEYER, D.E., Monsanto Company, Missouri, U.S.A., Personal Correspondence, April and July 1989.

STEINMEYER, D.E., Chemical Engineering Progress, 1972, 68(7), 64.

STERN, F. and VOTTA, F., American Institute of Chemical Engineering Journal, 1968, November, 928.

STRUCK, H.G., N.A.S.A. Report, TM X-53214, 1965, "Jet Penetration Into a Liquid".

SUKHATME, S.P. and ROHSENOW, W.M., Transactions of the American Society of Mechanical Engineers, Journal of Heat Transfer, 1966, February, 19.

SZEKELY, J. and ASAI, S., Metallurgical Transactions, 1974, 5 (2), 463.

THEMELIS, N.J., Transactions of the Institution of Mining and Metallurgy, 1987, 96 (Dec.), C179.

TOOR, H.L., American Institute of Chemical Engineering Journal, 1971, 17(1), 5.

TOOR, H.L., Industrial and Engineering Chemistry Fundamentals, 1971, 10(1), 121.

TURKDOGAN, E.T., Transactions of the Metallurgical Society of the American Institute of Mechanical Engineers, 1964, 230 (6), 740.

TURKDOGAN, E.T. and MILLS, K.C., Transactions of the Metallurgical Society of the American Institute of Mechanical Engineers, 1964, 230 (6), 750.

TURNER, R.H., Ph.D. Thesis, University of California, Los Angeles, 1971.

TURNER, R.H., MILLS, A.F. and DENNY, V.E., Transactions of the American Society of Mechanical Engineering. Journal of Heat Transfer, 1973, February, 6.

TUVE, G.L., American Society of Heating and Ventilating Engineers, 1953, 25(1), 181.

WAKELIN, D.H., Ph.D. Thesis, the University of London, 1966.

WARNER, N.A., "Advanced Technology for Smelting McArthur River Ore", Minerals Engineering, 1989, 2 (1), 3.

WARNER, N.A., American Institute of Metallurgical Engineering Symposium on Complex Sulphides, San Diego, 1985, Proceedings, p. 847.

WARNER, N.A., Transactions of the Institution of Mining and Metallurgy, Section C, 1983, 92, C147.

WARNER, N.A., Extraction and Refining, Institution of Metallurgists Review Course, Nov. 1970, Series 2, Number 4, 3.2.

WARNER, N.A., Advances in Extractive Metallurgy Symposium, London, 1968, IMM, 317.

WHITMAN, W.G., Chemical and Metallurgical Engineering, 1923, 29, 147.

WHITMAN, W.G. and LEWIS, W.K., Industrial and Engineering Chemistry, 1924, 16, 1215.

WINKLER, O. and BAKISH, R., Vacuum Metallurgy, Elsevier Publishing Company, London, 1971.

WRIGHT, J.K. and MORRISON, A.L., SEASI Q, Jan, 1985, 51.

ZETTLEMOYER, A.C. (ED.), Nucleation, New York, Marcel Dekker Inc., 1969.

ZINC THERMODYNAMIC DATA by KELLEY, U.S. Bureau of Mines Bulletin No. 383, 1935.